Thiophene-Containing Organic Semiconducting Heteroacenes for Electronic Applications

Dissertation

zur Erlangung des Grades
'Doktor der Naturwissenschaften'

am Fachbereich Chemie und Pharmazie der
Johannes Gutenberg-Universität in Mainz

Peng Gao
Geboren in Shanxi Province / China
Mainz 2009

Dekan:

1. Berichterstatter:

2. Berichterstatter:

Tag der mündlichen Prüfung: 17, Feb. 2010

Dedicated to my family

Table of Contents

List of Figures ····· vi

List of Schemes ····· xv

List of Tables ····· xvii

Glossary of Abbreviations ····· xviii

Chapter 1 Introduction and Motivation ····· 1

1.1 Semiconducting materials for organic field-effect transistors (OFETs) ····· 1

1.1.1 Oligoacenes vs. conjugated polymers ····· 4

1.1.2 PAH acenes and heteroacenes ····· 5

1.1.2.1 Why heteroacenes? ····· 5

1.1.2.2 *p*-Channel heteroacenes ····· 7

1.1.2.3 *n*-Channel heteroacenes ····· 8

1.2 Design principles of high performance oligoacenes ····· 9

1.2.1 Energy levels of organic semiconductors ····· 9

1.2.2 Tuning the HOMO level of *p*-channel oligoacenes ····· 11

1.2.3 Tuning the LUMO level of *n*-channel oligoacenes ····· 12

1.3 A summary of synthetic methods toward thiophene containing heteroacenes ····· 13

1.3.1 Synthesis of thiophene containing heteroacenes by sulfur-bridge formation ····· 14

1.3.1.1 Formation of sulfur-bridges by triflic acid induced electrophilic substitution ····· 14

1.3.1.2 Introducation of thiophene rings by aromatic nucleophilic substitution (S_NAr) reaction ····· 17

1.3.1.3 Introduction of thiophene rings by electrophilic cyclization reaction ···· 19

1.3.1.4 Introduction of thiophene ring by Hinsburg thiophene synthesis ····· 20

1.3.2 Synthesis of thiophene containing heteroacenes by direct annulation of thiophene units ····· 21

1.3.2.1 Friedel-Crafts-type alkylation and acylation reactions ····· 21

1.3.2.2 Cadogan reductive cyclization on thiophene units ····· 23
1.4 Solid-state structure of full ladder oligoacenes ····· 24
1.5 Solution processed organic thin film field-effect transistors ····· 26
1.5.1 Solution processing techniques ····· 26
1.5.2 Basic operation ····· 28
1.6 Motivation for the present work ····· 29
1.6.1 Development of novel pentacene analogues: the sulfur approach ····· 29
1.6.1.1 What benefit can sulfur substitution bring to us? ····· 29
1.6.1.2 Extended π-systems in conjugated oligomers for molecular electronics-the longer, the better? ····· 31
1.6.2 Our approach toward design and synthesis of new thiophene fused heteroacenes ····· 34
1.7 References ····· 36
Chapter 2 Conjugated Sulfur Containing Heteropentacene Analogues for *p*-Channel Organic Field-effect Transistors (OFETs) ····· 43
2.1 Introduction ····· 43
2.2 Synthesis and characterization of benzo[1,2-*b*:4,5-*b′*]bis[*b*]benzo-thiophene (BBBT) as pentacene analogues ····· 45
2.2.1 Synthesis of benzo[1,2-*b*:4,5-*b′*]bis[*b*]benzothiophene (BBBT) derivatives ····· 45
2.2.2 Solid-state crystal structure and packing ····· 47
2.2.3 Powder X-ray diffraction (PXRD) analyses of BBBT films ····· 50
2.2.4 Photophysical properties ····· 52
2.2.5 Electrochemical properties ····· 53
2.2.6 OFETs device fabrication based on BBBT derivatives ····· 55
2.3 Synthesis and characterization of dithieno[2,3-*d*;2′,3′-*d′*]benzo[1,2-*b*;4,5-*b′*]di-thphene (DTBDT) as pentacene analogues ····· 58
2.3.1 Synthesis of dithieno[2,3-*d*;2′,3′-*d′*]benzo[1,2-*b*;4,5-*b′*]dithiophene (DTBDT) derivatives ····· 58
2.3.2 Solid-state crystal structure and packing ····· 60

2.3.3 Powder X-ray diffraction (PXRD) analyses of DTBDT films 63
2.3.4 Photophysical properties 65
2.3.5 Electrochemical properties 67
2.3.6 OFET device fabrication based on DTBDT derivatives 68
2.3.6.1 Application of **2b** for the semiconducting channels in OFETs from solution 68
2.3.6.2 Device fabrication of **2c** by controlled dip-coating technique 72
2.4 Electronic structure computation 75
2.5 Conclusion 79
2.6 References 80
Chapter 3 Sulfur and Nitrogen-bridged Heteroheptacenes and Their Application for *p*-Channel Organic Thin Film Transistors 84
3.1 Introduction 84
3.1.1 Ladder-type heteroheptacenes 85
3.1.2 Reactivity of carbazole under the condition of electrophilic substitution reaction 86
3.1.3 How to solve the problem when carbazole was used as the nucleophilic core to construct the new molecules? 88
3.2 Synthesis and characterization of sulfur and nitrogen-bridged heptacenes with carbazole (Cz) as the central π system 89
3.2.1 Synthesis of dibenzo[*b*,*b*']thieno[2,3-*f*:5,4-*f*']-carbazole (DBTCz) derivatives 89
3.2.2 Synthesis of bisthieno[3,2-*b*]thieno[2,3-*f*:5,4-*f*']-carbazoles (BTTCz) 93
3.2.3 Synthesis of diindolo[3,2-*b*:2',3'-*h*]benzo[1,2-*b*:4,5-*b*']bis[1]benzothiophene (DIBBBT) 94
3.2.4 Structure proof of the heteroacenes by ^{1}H NMR spectroscopy 95
3.2.5 Solid-state crystal structure and packing properties revealing the alkyl substituting effect on the solid structure 96
3.2.6 Powder X-ray diffraction (PXRD) analyses and film microstructure for compounds DBTCz and BTTCz 105

3.2.7 Scanning electron microscopy (SEM): morphological characterization of compounds DBTCz and BTTCz 108
3.2.8 Photophysical properties 110
3.2.9 Electrochemical properties 113
3.2.10 OFET fabrication based on DBTCz derivatives 115
3.3 Conclusion 119
3.4 References 120
Chapter 4 Study of Structure-Property Relationship of Sulfur and (or) Nitrogen-Bridged Heptacenes 122
4.1 Introduction 122
4.1.1 New electronically active organic molecular building blocks 123
4.1.2 Single crystal to single crystal phase transition 125
4.1.3 Sulfur-extrusion reaction in dibenzo- or dithieno[1,2]dithiin 127
4.2 Synthesis and characterization of sulfur and (or) nitrogen-bridged heptacenes with dithienopyrrole (DTP) and cyclopenta[2,1-*b*: 3,4-*b*']dithiophene (CPDT) as the central π system 129
4.2.1 Synthesis of bisbenzo[*b*,*b*']thienodithieno[3,2-*b*:2',3'-*d*]pyrrole (27) and bisbenzo[*b*,*b*']thienocyclopenta [2,1-*b*:3,4-*b*']dithiophene (32) 129
4.2.2 Structure proof of the heteroacenes by ^{1}H NMR spectroscopy 131
4.2.3 Solid-state crystal structure and packing of the new heteroheptacenes and the unexpected single-crystal-to-single-crystal (SCSC) phase transition in the crystal structure of BBTCPDT 132
4.2.3.1 Solid-state crystal structure and packing of compound BBTDP 133
4.2.3.2 Single-crystal-to-single-crystal (SCSC) phase transition in the crystal structure of compound BBTCPDT 134
4.2.3.3 Temperature dependant study of the crystal structures 137
4.2.4 Powder X-ray diffraction (PXRD) analyses and film microstructure for compounds BBTDP and BBTCPDT 142
4.2.5 Scanning electron microscopy morphological characterization of compounds BBTDP and BBTCPDT 143

4.2.6 Photophysical properties 144
4.2.7 Electrochemical Properties 147
4.3 Synthesis of thieno[2',3':4,5]thieno[3,2-*b*]thieno[2'',3'':4',5']thieno[2',3':4,5] thieno [3,2-*f*][1]benzothiophene (TTTTTBT) and dibenzo[*b*,*b'*] thieno-[2,3-*f*:,4-*f'*]bis[1] benzothiophene (DBTBT) 149
4.3.1 Synthesis of thieno[2',3':4,5]thieno[3,2-*b*]thieno[2'',3'':4',5']thieno[2',3': 4,5]thieno[3,2-*f*] [1]benzothiophene (TTTTTBT) 149
4.3.2 Synthesis and characterization of dibenzo[*b*,*b'*]thieno[2,3-*f*:,4-*f'*]bis[1]-benzo thiophene (DBTBT) via sulfur-extrusion reaction 150
4.4 MO calculation and electronic structure of heptacenes by varying the heteroatoms 153
4.5 Conclusion 157
4.6 References 158
Chapter 5 Summary and Outlook 163
6.1 General procedures 169
6.1.1 Chemicals and solvents 169
6.1.2 Chromatography 169
6.1.3 Inert atmosphere 169
6.1.4 Apparatus for analysis 170
6.1.5 OFET devices 172
6.2. Synthetic procedures 174
6.3. Reference 208
Appendix Single Crystal Structures 209
Acknowledgements 254
List of Publications 256
Curriculum Vitae 258

List of Figures

Figure 1.1. Examples of applications (a) radio-frequency ID tags; (b), (c) flexable electronic papers ····· 2

Figure 1.2. Evolution of OFETs performance with time for various *p*-channel (pentacene, rubrene, other small molecules, and polymers) and n-channel organic semiconductors. (v): vacuum deposition; (s) solution deposition; (sc): single crystal. A range of mobilities for hydrogenated amorphous silicon (a-Si:H) is shown as reference. ····· 2

Figure 1.3. Classification of organic semiconducting materials in terms of their structure characteristics and the boxes in orange color showing the train of thought of this thesis. ····· 3

Figure 1.4. Examples of conjugated polymers for OFETs application ····· 4

Figure 1.5. Examples of conjugated oligomers for OFETs application ····· 5

Figure 1.6. Structure of benchmark oligoacenes for organic semiconductors. ····· 6

Figure 1.7. Examples of heteroacenes for organic semiconductors. ····· 6

Figure 1.8. Representative heteroacenes as *p*-channel OFET materials. ····· 8

Figure 1.9. Representative heteroacenes as *n*-channel OFET materials. ····· 8

Figure 1.10. Energy levels of organic semiconductors. ····· 10

Figure 1.11. Empirical rationalization of energy levels of organic semiconductors. (Left) Range of LUMO levels of typical *n*-type materials and HOMO levels of typical *p*-type materials. (Right) First reduction potential (E_{R1}) windows for modified *n*-type materials with both stable electron conduction and low doping levels. ····· 11

Figure 1.12. Examples of crystal structures showing the effect of planarization induced by ring fusion. (a) 5,5′′-diperfluorophenyl-2,2′:5′,2′′:5′′,2′′′-quarter-thiophene showing inter-ring torsional angles (Reproduced from ref [55]. Copyright 2006 American Chemical Society.); (b) dibenzo[*d*,*d*′]thieno[3,2-*b*;4,5-*b*′]dithiophene showing planar structure. (Reproduced from ref [37g]. Copyright 2005 American Chemical Society.) · 14

Figure 1.13. Herringbone (top) and π-stacking (bottom) arrangements of acenes, showing HOMO orbital interactions (Spartan '04, Wavefunction, Inc.). (Reproduced from Anthony.) ····· 25

Figure 1.14. Schematic presentation of a) drop-casting, b) spin-coating, c) dipcoating, and d) zone-casting. ····· 26

Figure 1.15. Layouts of organic field-effect transistors (OFETs) (left: top-contact; right: botom-contact) ····· 28

Figure 1.16. Packing diagram of compounds perylo[1,12-*b*,*c*,*d*]thiophene and fluorinated benzobisbenzothiophene, viewed from the direction showing inter-molecular contacts. (Reproduced from (a) Sun et al.[a] and (b) Wang et al.[b]) ····· 30

Figure 1.17. Thiophene fused heteroacenes with increasing conjugation and their band gaps ····· 33

Figure 1.18. General structure of new thiophene fused heteroacenes ····· 34

Figure 1.19. Precursors designed for the symmetrically fused thiophene containing heteroacenes ····· 34

Figure 1.20. Precursor designed for the higher heteroacenes ····· 35

Figure 2.1. Five-ring fused heteroacenes as the pentacene analogues ····· 44

Figure 2.2. Expanded aromatic region of ^{1}H NMR spectra of compounds (a) **1a** (500 MHz, 413 K, d_2-1,1,2,2-tetrachloroethane); (b) **1b** (250 MHz, 300 K, d_2-dichloromethane).····· 46

Figure 2.3. (a) Pitch angle (P) describing intermolecular slipping along the long molecular axis (view down short molecular axis). (b) Roll angle (R) describing intermolecular slipping along the short molecular axis (view down long molecular axis). (c) Long and short molecular axes of **1**.····· 47

Figure 2.4. Thermal ellipsoid plot of **1a** and **1b**. The hydrogen atoms are omitted for clarity. Thermal ellipsoids are drawn at 50% probability. (a) Crystal stacking of **1a**. View down the long molecular axis. (b) View down the b axis of the stacking molecules of **1a**. Dashed line illustrates short contact distance (ca. 3.5 Å). (c) Crystal packing of **1b**. Dashed lines illustrate short

intra-column distances (ca. 3.42 Å). (d) View down the stacking axis of cofacial molecules of **1b**. ····· 49

Figure 2.5. X-ray scattering in reflection of (a) BBBT (**1a**) film on a silicon wafer. (b) Organization of **1a** in the solution processed thin layer on the substrate. (c) BBBT-C4 (**1b**) film on a silicon wafer. (d) Organization of **1b** in the solution processed thin layer on the substrate. ····· 51

Figure 2.6. Absorption (solid) and photoluminescence (PL) (dash-dotted) spectra of **5a**, **1a** (a) and **5b**, **1b** (b) in THF (1.0×10^{-6}M). ····· 52

Figure 2.7. Cyclic voltamograms of **1a** (left) and **1b** (right) in dry CH_2Cl_2. Measurement conditions: 1 mM in CH_2Cl_2 for all compounds with Bu_4NPF_6 (0.10 M); scan rate = 50 mV s^{-1}. ····· 54

Figure 2.8. FET characteristics of BBBT (**1a**)-based OFET on PTES-treated substrate: (a) transfer characteristics at a source-drain bias of V_{SD} = -60V; (b) output characteristics for various gate voltages ····· 55

Figure 2.9. FET characteristics of BBBT–C4 (**1b**)-based OFET on PTES-treated substrate: (a) transfer characteristics at a source-drain bias of V_{SD} = -60V; (b) output characteristics for various gate voltages. ····· 56

Figure 2.10. Film formation by polarized optical microscopy: (a) spotlike film formation of BBBT (**1a**) on a PTES treated bottom contact device; (b) film formation of BBBT-C4 (**1b**) on a 1-octanethiol treated bottom contact device ····· 57

Figure 2.11. Expanded aromatic region of ^{1}H NMR spectra of compound **2b** (250 MHz, 300 K, d_2-dichloromethane). ····· 60

Figure 2.12. Long and short molecular axes of **2**. ····· 60

Figure 2.13. Thermal ellipsoid plot of **2b** and **2c**. The hydrogen atoms are omitted for clarity. Thermal ellipsoids are drawn at 50% probability. (a) Crystal stacking of **2b**. View down the *b* axis showing the lamella packing structures. (b) View along long molecular axis. Dashed line illustrate intra(inter)-column short contact distances (ca. 3.6 Å). (c) Crystal packing of **2c**. View down the *b* axis showing the lamella packing structures. (d) view along long

molecular axis. Dashed line illustrates intra-column short contact distance (ca. 3.6 Å). ····· 61

Figure 2.14. a), c), e), g) X-ray diffraction in reflection mode for the spin-coated films of **2a-2d**. The reflections for the dip-coated film are assigned by the Miller's indexes, b), d), f), h) Supposed organization of **2a-2d** in the solution processed thin layer on the substrate. ····· 64

Figure 2.15. Absorption (solid) and photoluminescence (PL) (dash-dotted) spectra of DTBDTs **2a–d** in THF (1.0×10-6M). ····· 65

Figure 2.16. UV-vis absorption of **2a–d** as solid film on quartz substrate ····· 66

Figure 2.17. Cyclic voltammograms of **2a** to **2d**. ····· 67

Figure 2.18. FET transfer characteristics and output curves at various gate voltages V_G of the a) and b) spin-coated; c) and d) dip-coated compound **2b**. ····· 69

Figure 2.19. Film formation of the spin-coated (a) and dip-coated (b) DTBDT-C6 (**2b**) on SiO_2 bottom gate, top contact devices (polarized optical microscopy). ····· 71

Figure 2.20. AFM and optical microscopy image of DTBDT-C9 single layers. (a) AFM image; (b) Large-area optical image; (c) section analysis ····· 73

Figure 2.21. AFM and optical microscopy image of **2b** double layers. (a) AFM image; (b) Large-area optical image; (c) section analysis ····· 74

Figure 2.22. AFM and optical microscopy image of DTBDT-C9 double layers. (a) AFM image; (b) Large-area optical image; (c) section analysis ····· 75

Figure 2.23. HOMO and LUMO of (a) **BBBT** (**1**), (b) **DTBDT** (**2**), (c) Pentacene and (d) pentathienoacene (**PTA**) at the B3LYP-6-31G(d) level ····· 77

Figure 3.1. Ladder-type π-conjugated heteroacenes with thiophene or pyrrole ring units. ····· 85

Figure 3.2. Ladder-type π-conjugated heteroheptacenes examined in this study.86

Figure 3.3. Structure of carbazole ring system versus dibenzothiophene ····· 86

Figure 3.4. Expended aromatic region of ^{1}H NMR spectra of compounds (a) **8c** (700 MHz, 420 K, d_2-1, 1, 2, 2-tetrachloroethane); (b) **8e** (250 MHz, 300 K,

d_2-dichloromethane); (c) **16** (250 MHz, 300 K, d_2-dichloromethane) and (d) **21** (250 MHz, 300 K, d_2-dichloromethane). ····· 95

Figure 3.5. Packing diagrams of **8b** in solid state. a) Thermal ellipsoid of **8b**. The hydrogen atoms were omitted for clarity. Thermal ellipsoids are drawn at 50% probability. b) views along the *a* axis. (Dashed lines illustrate the short contacts between each two molecules in the unit cell. Green lines indicate C-C contacts: 3.35 Å. Red lines indicate S-C contacts: 3.23~3.41 Å) c) Two different kinds of conformation of the butyl groups present in the two close contacted molecules respectively. (Dashed rectangular indicating the two different kinds of butyl groups). d) View down the projection direction of two almost head-to-tail cofacial molecules. ····· 97

Figure 3.6. Packing diagrams of **8c** and chloroform molecules in solid state. (Thermal ellipsoids are drawn at 50% probability) a) Short interactions between each molecule of **8c** and four chloroform molecules. b) views along the *a* axis. The anti-parallel pairs carrying their interacted chloroform molecules further stacked into slipped columns. c) Herringbone structures from the view in the long molecular axis. Dashed red lines indicating the short S-C contacts (ca. 3.44 Å). d) View down the projection direction of two cofacial molecules. ····· 98

Figure 3.7. Packing diagrams of **8c** in solid state. a) Thermal ellipsoid of **8c**. The hydrogen atoms were omitted for clarity. Thermal ellipsoids are drawn at 50% probability. b) views along the *a* axis. (Dashed rectangular illustrate the antiparallels pairs) c) Crystal stacking of 8c in one of the four antiparallel pair columns. Dashed red lines indicating the short S-C contacts (ca. 3.41 and 3.46 Å). Dashed green line indicating the interplanar distance (ca. 3.47 Å). d) View down the projection direction of two cofacial molecules (arrow shown in c)). ····· 100

Figure 3.8. Packing diagrams of **8e**. a) Thermal ellipsoid of **8e**. The hydrogen atoms were omitted for clarity. Thermal ellipsoids are drawn at 50% probability. b) Views along the short molecular axis. (c) View down the

stacking axis of dimers. (Dashed rectangular illustrate the dimmers of the molecules) (d) View along the long molecular axis showing sandwiched herringbone structure. (Dashed rectangular illustrate the dimmers of the molecules. Dashed lines illustrate intermolecular close-contacts within and between the dimers)····· 101

Figure 3.9. Packing diagrams of **8d** (isomer 2). (a) Thermal ellipsoid of **8d**. The hydrogen atoms were omitted for clarity. Thermal ellipsoids are drawn at 50% probability. b) Sandwiched herringbone structure formed by the anti-parallel pairs. (Dashed blue rectangular illustrate the pairs; dashed red line indicates the interplanar distance inside the pairs; dashed green lines indicate the short C-C interaction between the pairs) (c) View down the short axis of the molecule showing the large dihedral angle of 8.8°. (d) View down the projection direction of two cofacial molecules in one pair. ····· 103

Figure 3.10. X-ray diffractogram of the drop-cast thin films (40 mg/ml 1,2-dichlorobenzene solution) on an untreated Si/SiO_2 substrate. (a) **8c**; (b) Certain kind of lamellar packing of **8c** on the substrate; (c) **8e**. The reflections are assigned by the Miller's indices; (d) Supposed organization of **8e** in the solution processed thin layer on the substrate; (e) **16**. (f) Approximated organization of **16** in the solution processed thin layer on the substrate. ··· 106

Figure 3.11. Theoretical geometry optimization of using SPARTAN '04 at B3LYP/6-31G** level ····· 107

Figure 3.12. X-ray diffractogram of the drop-cast thin films (40 mg/ml 1,2-dichlorobenzene solution) on an untreated Si/SiO_2 substrate. (a) **8a**; (b) **8b**; (c) **8d**. ····· 108

Figure 3.13. Scanning electron micrographs of dropcasted films on untreated Si/SiO2 substrates of (a) & (b) DBTCz-C_6H_{13} (**8c**), 25 °C; (c) & (d) DBTCz-dibutyl (**8e**), 25 °C; (e) & (f) BTTCz-dihexyl (**16**) 25 °C. ····· 109

Figure 3.14. Normalized UV-vis absorption, PL spectra (a) and ormalized UV-vis absorption, PL spectra (b) of compounds **8c**, **8e**, **16** and **21** in THF (10^{-6} M). ·····111

Figure 3.15. Cyclic voltammogram of **8c**, **16** and **21**. Conditions: glassy carbon as working electrode (diameter 1mm); solution (ca.10^{-3} M) in CH_2Cl_2 with NBu_4PF_6 as supporting electrolyte (0.1 M); scan rate 50 mVs^{-1}; potentials are referred to an Ag/AgCl electrode. ····· 113

Figure 3.16. POM image between cross-polarizers of drop-cast **8c** from a 40 mg/ml 1,2-dichlorobenzene solution on an untreated SiO_2 substrate with source and drain electrodes. ····· 115

Figure 3.17. FET characteristics of **8c**-based OFET: (a) output characteristics at various gate biases V_G and (b) transfer characteristics at V_{SD} = -60 V.····· 116

Figure 3.18. Chemical and crystal structure of bis(4-(phenylthio)phenyl)amine (a) & (c) (reproduced from Leuninger et al.) and **8b** (b) & (d).····· 118

Figure 4.1. Carbazole versus dithienopyrrole versus cyclopentadithiophene versus fluorine ····· 123

Figure 4.2. Model of potential application of SCSC transformations. (a) Illustrations of rack-and-pinion gear; (b) schematic of one thermo-controlled molecular machine. (Reproduced from Sokolvo et al.[b]) ····· 126

Figure 4.3. Structures of 1,2-dithiin **H**, dibenzodithiin **I** and dithienodithiin **J**. · 128

Figure 4.4. New ladder-type π-conjugated heteroheptacenes ····· 129

Figure 4.5. Expanded aromatic region of ^1H NMR spectra of compounds (a) BBTDP and (b) BBTCPDT (250 MHz, 300 K, d_2-dichloromethane). ····· 132

Figure 4.6. Packing diagram of **27**. (a) Thermal ellipsoid of **27**. The hydrogen atoms were omitted for clarity. Thermal ellipsoids are drawn at 50% probability. (b) Views along the short molecular axis. (c) View down the stacking axis of head-to-head column pairs. (Dashed rectangular illustrate the head-to-head pairs, Dashed lines illustrate intermolecular close-contacts within and between the columns) (d) View along the long molecular axis showing "lamella herringbone" structure formed by antiparallel column pairs. (Dashed rectangular illustrate the antiparallel lamella structure. The hydrogen atoms are omitted for clarity. ····· 133

Figure 4.7. Packing diagram of **32** at room temperature (Phase A) (a) View down

the *b*-axis of the unit cell (Dashed rectangular illustrate the head-to-head pairs). (b) View along the long molecular axis showing the perpendicularly oriented alkyl chain (Dashed lines illustrate cofacial distance). Packing diagram of **32** at 120 K. (Phase B) (c) Crystal packing showing vertical trasnsitions of neighboring molecules. (d) View along the long molecular axis showing the two different conformations of the alkyl chain (Dashed rectangular illustrate two different kinds of alkyl conformation). The hydrogen atoms are omitted for clarity. ····· 136

Figure 4.8. Superposition in the *ab* plane of the crystalline cell at 140 K (blue rectangular) with unit cells belonging to the structure at room temperature (black rectangular) and 160 K (red rectangular). Black circles represent common inversion centers for all structures. In the structure at room temperature there is only one independent molecule and the number of inversion centers is 2 times higher than in the structure at 160 K. ····· 137

Figure 4.9. Temperature dependence of the equivalent cell parameters *a'*, *a* and *b* (left *y* axis). Error bars are negligible for *a* and *c* parameters with respect to the drawing scale. The two vertical dotted lines indicate the phase transition temperature ····· 138

Figure 4.10. Packing diagram of **32** at 160 K (Phase I) ····· 139

Figure 4.11. X-ray diffractogram of the drop-cast thin films (40 mg/ml 1,2-dichlorobenzene solution). (a) **27** on an untreated SiO_2 substrate. (b) unknown complicated lamellar packing on the substrate. (c) **32** on an untreated SiO_2 substrate. The reflections are assigned by the Miller's indices. (d) Supposed organization of **32** in the solution processed thin layer on the substrate. ····· 142

Figure 4.12. Scanning electron micrographs of dropcasted films from *o*-dichlorobenzene on untreated Si/SiO_2 substrates of (a) & (b) BBTDP (**27**), 25 °C; (c) & (d) BBTCPDT (**32**), 25 °C. ····· 143

Figure 4.13. (a) Normalized UV-vis absorption, PL spectra of compounds **27** and **32** in THF (10^{-6} M). (b) Normalized UV-vis absorption, PL spectra of

compounds **27** and **32** as thin film. ····· 145

Figure 4.14. Cyclic voltammogram of **27** and **32**. Conditions: glassy carbon as working electrode (diameter 1 mm); solution (ca.10^{-3} M) in CH_2Cl_2 with NBu_4PF_6 as supporting electrolyte (0.1 M); scan rate 50 mVs^{-1}; potentials are referred to an Ag/AgCl electrode. ····· 147

Figure 4.15. Normalized absorption spectra of solution of **45** in THF (10^{-6} M) ·· 151

Figure 4.16. FD-Mass spectroscopy of compound **45** ····· 152

Figure 4.17. Schematic representation of the HOMOs and LUMOs of **8**, **16**, **27**, **32** and **45** as well as **DIoCz, DIeCz, PTP** for comparison (DFT//B3LYP/6-31G**) ····· 156

Figure 5.1. Schematic of derivation of sulfur containing heteropentacenes and the "kinked" structure outlined by the blue bar. ····· 164

Figure 5.2. Structures of new *p*-channel heteroacenes for the future ····· 164

Figure 5.3. Structural evolution of heptacenes ····· 166

Figure 5.4. Structures of new *n*-channel heteroacenes for the future ····· 167

Figure 6.1. Schematic of (a) the *bottom-gate* organic field-effect transistors (OFETs) with *bottom contact* (coplanar) structures. (b) The *bottom-gate* organic field-effect transistors (OFETs) with *top contact* (staggered) structures. ····· 172

Figure 6.2. Schematic presentation of dip-coating. ····· 173

List of Schemes

Scheme 1.1. Synthesize PPS via soluble (polysulfonium cation) intermediate in acid ····· 14

Scheme 1.2. Mechanism of the super acid induced electrophilic substitution ··· 15

Scheme 1.3. Two examples of the electrophilic substitution towards thiophene fused heteroacenes ····· 16

Scheme 1.4. Synthesis of benzodichalcogenophenes ····· 17

Scheme 1.5. Intramolecular triple cyclization reaction by *nucleophilic* substitution ····· 18

Scheme 1.6. Synthesis of multithiophene fused-aromatic compounds ····· 18

Scheme 1.7. Mechanism of the nucleophilic reaction induced cyclization reaction ····· 19

Scheme 1.8. Introduction of sulfur-bridge via nucleophilic aromatic substitution in highly fluorinated aromatic system ····· 19

Scheme 1.9. Intramolecular electrophilic cyclization reaction ····· 20

Scheme 1.10. Synthesis of DNTT and DNSS via intramolecular electrophilic cyclization ····· 20

Scheme 1.11. Introduction of thiophene ring by Hinsburg thiophene synthesis 21

Scheme 1.12. Synthesis of ladder-type polymers via Friedel-Crafts alkylation ·· 22

Scheme 1.13. Example of thiophene unit containing heteroacenes by Friedel-Crafts alkylation ····· 22

Scheme 1.14. Wang's synthesis of ladder-type oligoacenes ····· 23

Scheme 1.15. Synthesis of thiophene containing heteroacenes ····· 23

Scheme 1.16. Example of the Cadogan reductive cyclization ····· 24

Scheme 1.17. Photogeneration of acenes from the diketones by Strating-Zwanenburg reaction and their decreasing band gaps with extended conjugation ····· 32

Scheme 2.1. Synthesis of BBBT derivatives **1a** and **1b**. ····· 45

Scheme 2.2. Synthesis of DTBDT derivatives **2a** to **2d**. ····· 59

Scheme 3.1. Reported synthesis of DBTBT isomers via double intramolecular electrophilic coupling reaction ····· 87

Scheme 3.2. Model reactions of the electrophilic substitution on thioanisole and diphenylamine ····· 88

Scheme 3.3. Two possible precursors **11** and **15** for the synthesis of **8** ····· 89

Scheme 3.4. Possible precursors **20** and **25** for the synthesis of **16** and **22** ····· 89

Scheme 3.5. Synthesis of DBTCz (**8**) through triflic acid induced ring-closure reaction ····· 91

Scheme 3.6. Test reaction of on precursor **11d** to DBTCz (**8d**) at 60°C ····· 92

Scheme 3.7. Synthesis of bisthieno[3,2-*b*]thieno[2,3-*f*:5,4-*f'*]-carbazoles (BTTCz, **16**) ····· 93

Scheme 4.1. Synthesis of soluble dithieno[3,2-*b*:2',3'-*d*]pyrroles. ····· 124

Scheme 4.2. Synthetic route to cyclopenta[2,1-*b*:3,4-*b'*]dithiophene ····· 125

Scheme 4.3. Proposed sulfur extrusion reaction to give S bridge instead of S-S bridge ····· 127

Scheme 4.4. Sulfur extrusion reaction of annulated 1,2-dithiins. ····· 128

Scheme 4.5. Synthesis of bisbenzo[*b*,*b'*]thienodithieno[3,2-*b*:2',3'-*d*]pyrrole (**27**) 130

Scheme 4.6. Synthesis of bisbenzo[*b*,*b'*]thienocyclopenta[2,1-*b*:3,4-*b'*]dithiophene (**32**) ····· 131

Scheme 4.7. Synthesis of TTTTTBT (**37**) through triflic acid induced ring-closure reaction ····· 150

Scheme 4.8. Resynthesis of DBTBT via sulfur-extrusion reaction ····· 151

List of Tables

Table 2.1. Crystallographic Parameters of 1a and 1b ····· 50

Table 2.2. Electrochemical, UV-Vis data and estimated HOMO and LUMO levels of 1a and 1b. ····· 54

Table 2.3. FET characteristics of 1a and 1b ····· 57

Table 2.4. Crystallographic parameters of 2b and 2c ····· 62

Table 2.5. Electrochemical, UV-Vis data and estimated HOMO and LUMO levels of 2a to 2d. ····· 68

Table 2.6. FET performance of DTBDT series[a] ····· 71

Table 2.7. Collection of reported HOMO levels and optical bandgaps of pentacene and its analogues in a sequence of increasing number of S atoms substitution. ····· 78

Table 3.1. Ratio of isomers under different conditions of test reactions[a] ····· 90

Table 3.2. Crystallographic parameters of 8b to 8e ····· 104

Table 3.3. UV-Vis Absorption and PL Data for 8c, 8e, 16 and 21 ····· 112

Table 3.4. Electrochemical data and estimated HOMO, optical band gap and LUMO levels of 8c, 16 and 21. ····· 114

Table 3.5. FET Performance of DBTCz series [a,b] ····· 117

Table 4.1. Crystallographic parameters of 27 and 32 ····· 141

Table 4.2. UV-Vis absorption and PL data for 27 and 32 ····· 145

Table 4.3. Electrochemical data for 27 and 32 in dry CH_2Cl_2 under nitrogen ··· 148

Table 4.4. Comparison of electrochemical, optical, and calculated HOMO-LUMO energy gaps (E_g) and absolute HOMO and LUMO energies for the studied heteroheptacenes. ····· 154

Glossary of Abbreviations

ABT	Anthra[2,3-*b*]benzo[*d*]thiophene
ADT	Anthra[2,3-*b*:6,7-*b′*]dithiophene
AFM	Atomic force microscopy
BADT	Bent anthradithiophene
BBBT	Benzo[1,2-*b*;4,5-*b'*]bis[*b*]benzodithiophene
BBTCPDT	Bisbenzo[*b*,*b'*]thienocyclopenta[2,1-*b*:3,4-*b'*]dithiophene
BBTDP	Bisbenzo[*b*,*b'*]thienodithieno[3,2-*b*:2',3'-*d*]pyrrol
BINAP	2,20-bis(diphenylphosphino)-1,10-binaphthyl
BTBT	[1]Benzothieno[3,2-*b*]benzothiophene
BTTCz	Bisthieno[3,2-*b*]thieno[2,3-*f*:5,4-*f'*]- carbazoles
CPDT	Cyclopenta-[2,1-*b*:3,4-*b'*]dithiophene
CV	Cyclic voltammetry
Cz	Carbazole
DBTBT	Dibenzo[*b*,*b′*]thieno[2,3-*f*:5,4-*f′*]bis[1]benzothiophene
DBTCz	Dibenzo[*b*,*b'*]thieno[2,3-*f*:5,4-*f'*]carbazole
DBTDT	Dibenzo[*d*,*d'*]thieno[3,2-*b*;4,5-*b'*]dithiophene
DCB	Dichlorobenzene
DFT	Density functional theory
DIBBBT	Diindolo[3,2-*b*:2',3'-*h*]benzo[1,2-*b*:4,5-*b'*]bis[1]benzothiophene
DieCz	Diindenocarbzole
DioCz	Diindolocarbazole
DMF	*N*,*N*-dimethylformamide
DMSO	Dimethylsulfoxide
DNSS	Dinaphtho[2,3-*b*:2′,3′-*f*]seleno[3,2-*b*]selenophene
DNTT	Dinaphtho[2,3-*b*:2′,3′-*f*]thieno[3,2-*b*]thiephene
DSC	Differential scanning calorimetry
DTBDT	Dithieno[2,3-*d*;2',3'-*d'*]benzo[1,2-*b*;4,5-*b'*]dithiophene

DTP	Dithieno[3,2-*b*:2',3'-*d*]pyrrole
EA	Electron affinity
FD-MS	Field desorption mass spectrometry
FDT	Perfluorodecanethiol
HOMO	Highest occupied molecular orbital
IP	Ionization potential
LADT	Linear anthradithiophenes
LTP	ladder-type tetraphenylene
LUMO	Lowest unoccupied molecular orbital
MO	Molecular orbital
MOSFET	Metal-oxide-semiconductor field-effect transistor
MS	Mass spectroscopy
NBS	*N*-bromosuccinimide
NBT	4-Nitrobenzenethiol
NMP	*N*-methyl-2-pyrrolidone
NMR	Nuclear magnetic resonance
NT-CDI	Naphthalene tetracarboxy dianhydride
OFET	Organic field-effect transistors
OLED	Organic light emitting diode
OT	1-Octanethiol
PAH	Polycyclic aromatic hydrocarbon
PBI	Perylene bisimide
PL	Photoluminescence
POM	Polarized optical microscopy
PPS	Poly(phenylene sulfide)
PPSA	Poly(phenylene sulfide-phenylene amine)
PPS-AA	Poly(phenylene sulfide phenylene amine-phenylene amine)
PTA	Pentathienoacene
PTCDI	Perylene tetracarboxy dianhydride

PTES	Phenyltriethoxysilane
PVD	Physical vapour deposition
PXRD	Powder X-ray diffraction
SCE	Saturated calomel electrode
SCSC	Single-crystal-to-single-crystal
SCXRD	Single crystal X-ray diffraction
TBBT	Thieno[*f,f'*]bis[1]benzothiophene
TCT	Tetraceno[2,3-*b*]thiophene
TFA	Trifluoroacetic acid
THF	Tetrahydrofuran
TLC	Thin layer chromatography
TTTTTBT	Thieno[2',3':4,5]thieno[3,2-*b*]thieno[2'',3'':4',5']thieno[2',3':4,5]thieno[3,2-*f*][1]benzothiophene
UPS	Ultraviolet photoelectron spectroscopy
UV-vis	Ultraviolet-visible
α-5T	α-Quinquethiophene

Chapter 1
Introduction and Motivation

1.1 Semiconducting materials for organic field-effect transistors (OFETs)

Organic semiconductors have been studied since the late 1940s,[1] but organic materials had not been considered as the active semiconductor layer until 1986, when Koezuka and coworkers demonstrated a polythiophene-based field-effect transistor.[2] While long before that, the metal-oxide-semiconductor field-effect transistor (MOSFET) based on inorganic materials has been the crucial building block in the electronics industry, since the first discovery by Julius Edgar Lilienfeld nearly a hundred years ago.[3],[4] These inorganic devices have proven to be reliable, highly efficient, and with performance increasing regularly according to Moore's law.[5]

Although the device performances based on organic materials still can not compete with conventional Si/GaAs technologies, OFETs have already shown the potential to be a powerful competitor of the inorganic counterparts. The advantages of organic systems include simple, solution-based processing which allows for unconventional deposition methods,[6] such as inkjet,[7] screen,[8] and microcontact printing.[9] The low temperature in comparison to high temperature vapour deposition required for these methods, combined with the mechanical flexibility of organic materials, offers compatibility with plastic substrates,[10] leading to the possibility of flexible integrated circuits,[11] electronic paper,[10] and roll-up displays.[12] (**Figure 1.1**) The opportunities for structural tailoring gave rise to a broad family of species with different superiorities.[13]

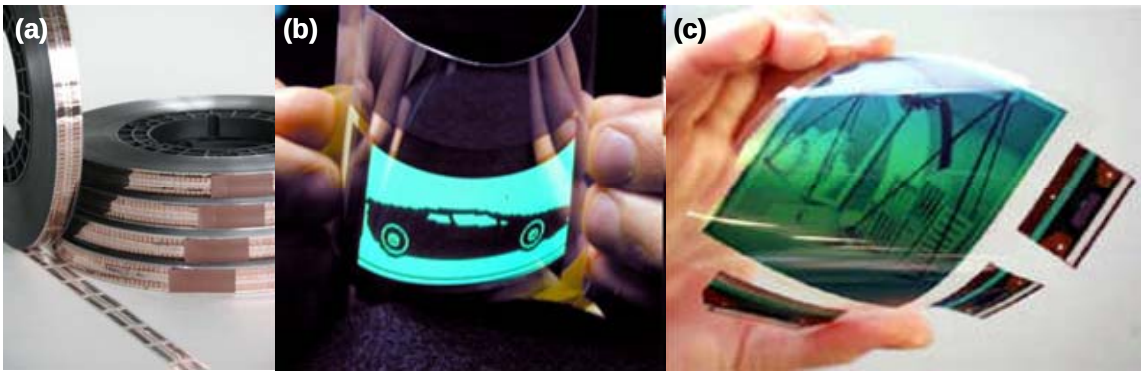

Figure 1.1. Examples of applications (a) radio-frequency ID tags; (b), (c) flexable electronic papers

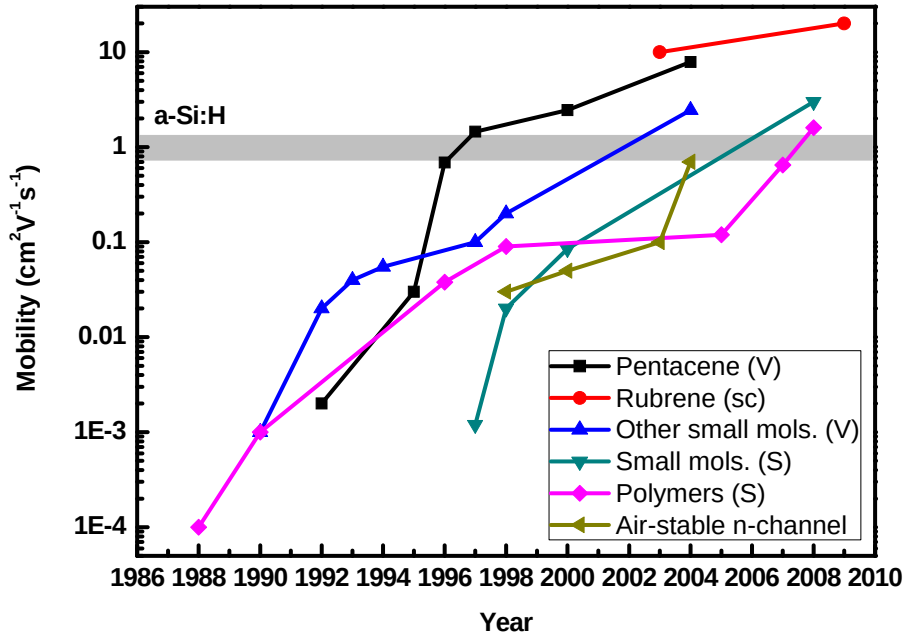

Figure 1.2. Evolution of OFETs performance with time for various *p*-channel (pentacene, rubrene, other small molecules, and polymers) and n-channel organic semiconductors. (v): vacuum deposition; (s) solution deposition; (sc): single crystal. A range of mobilities for hydrogenated amorphous silicon (a-Si:H) is shown as reference.

As one of the critical materials, the organic semiconductors have a dominant influence on the FET performance of OFETs. Organic semiconductors are commonly classified as either *p*-channel (hole-conducting) or *n*-channel (electron-conducting) depending on which type of charge carrier is more efficiently transported through

the material. In theory, all organic semiconductors should be able to conduct both holes and electrons, but the differences in internal reorganization energies[14] or work functions[15] of the electrodes relative to the HOMO (highest occupied molecular orbital) and LUMO (lowest unoccupied molecular orbital) energies of the material in the transistor can favour one type of charge transport.[16] (**Figure 1.2-1.8**) Over the past twenty years, thousands of organic semiconducting materials were designed and synthesized for the applications including both oligomeric and polymeric materials. The impressive growth is evident in **Figure 1.2**, which shows a logarithmic plot depicting the evolution of reported field-effect mobility values for *p*- and *n*-channel organic semiconductors over the past 20 years.

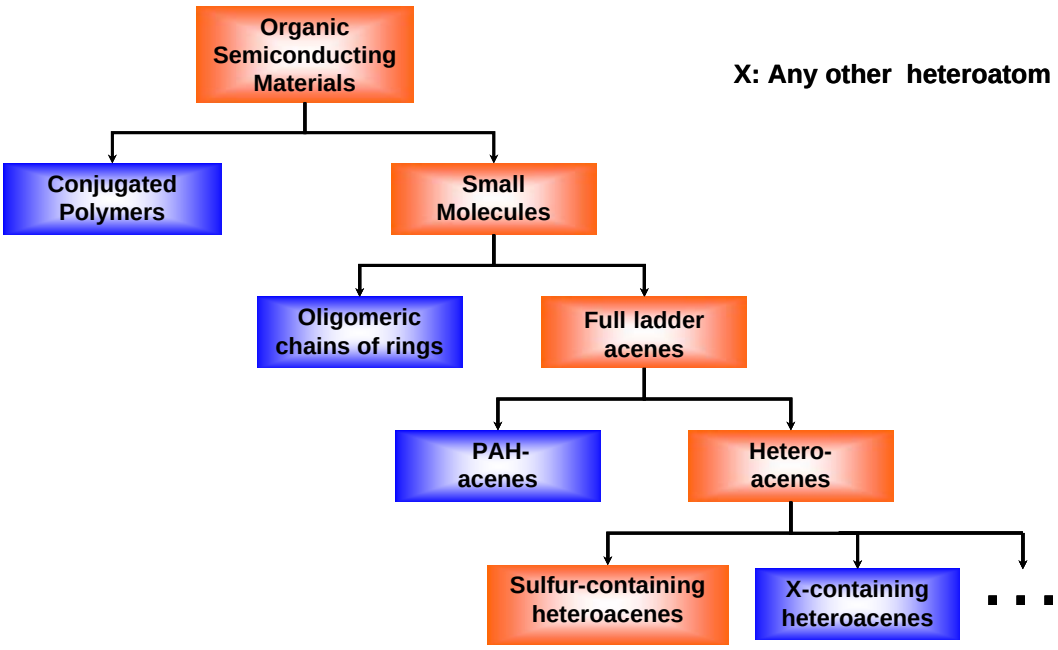

Figure 1.3. Classification of organic semiconducting materials in terms of their structure characteristics and the boxes in orange color showing the train of thought of this thesis.

On the other hand, there are two distinct classes of solution processible organic semiconductors – conjugated polymers and small molecules, in view of their structures, each offering its own advantages in realizing high performance devices. (**Figure 1.3**) In this Chapter, a general introduction following the divisions of small

molecular semiconducting materials will be shown. Attention will be put on the principles behind the development of soluble and air stable conjugated oligoacenes as semiconducting channels in OFETs (synthetic protocol, basic chemical/physical properties, mechanism, applications, etc.). Even though conjugated polymers have also been widely used for OFET applications as mentioned above, they are only briefly described since the main focus of this work is the synthesis and characterization of thiophene containing conjugated oligomers for use in OFETs. Finally, the motivation and framework of this thesis are presented.

1.1.1 Oligoacenes vs. conjugated polymers

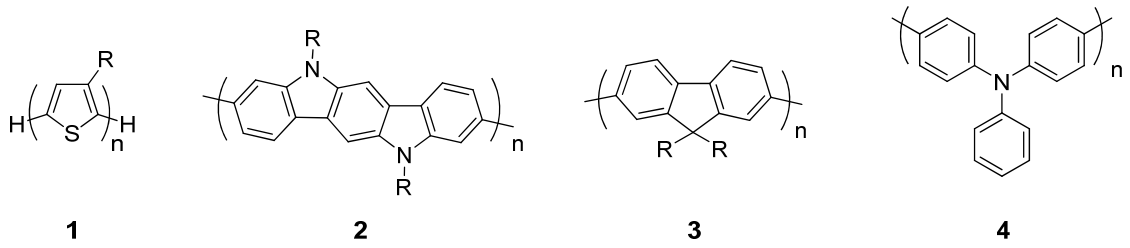

Figure 1.4. Examples of conjugated polymers for OFETs application

Conjugated polymers such as derivatives of poly(thiophene)s (**1**),[17] polyindolocarbazoles (**2**),[18] poly(fluorene)s (**3**),[19] and poly(arylamine)s (**4**)[20] have been shown to be promising semiconductor candidates for OFETs, offering good mechanical strength, adhesion, and plasticity, intrinsic rheological properties for ink formulations, and a wide tolerance for film-processing conditions. (**Figure 1.4**)

On the other hand, the concept of "oligomer approach" generated more than ten years ago by Müllen et al.,[21] demonstrated that monodisperse oligomers allow people to determine structure-propertity relationship more precisely and further extrapolate these relationships toward those expected for polymers. The parallel fast development of the family of well-defined oligomers, such as α,ω-substituted sexithiophenes (**5**),[22] substituted pentacenes (**6**),[23] and substituted phenylene thiophene co-oligomers (**7**),[24] has proved this assumption. (**Figure 1.5**) Two key advantages of the oligomer approach to polymeric materials are that firstly they are

more amenable to scale-up while maintaining high purity and reproducible quality and secondly their controllable and rigorously defined structure allows correlation of properties with chain and conjugation length. In addition, oligomers can provide more flexibility in the formation of the thin films needed for most devices. The oligomers' lower molecular weights allow deposition via vacuum sublimation and, providing the oligomers have significant solubility, can also be solvent cast in the same manner as the polymeric analogues.[25],[26] To this end, with the inherent polydispersity of polymers and limited purification methods for them on a commercial scale seen as drawbacks, we have chosen to develop the small-molecule class extensively. And among the several divisions of the small-molecules, fully ladderized oligoacenes are of extreme interest for many groups.

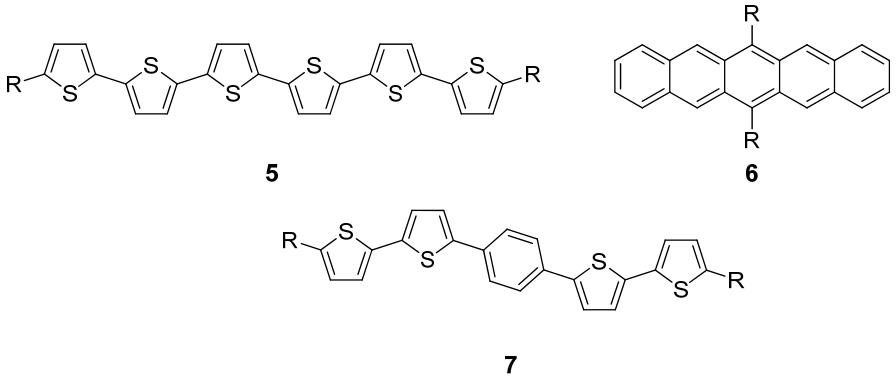

Figure 1.5. Examples of conjugated oligomers for OFETs application

1.1.2 PAH acenes and heteroacenes

1.1.2.1 Why heteroacenes?

Among the ladder-type oligoacenes ever reported, pentacene (**8**) and rubrene (**9**) (**Figure 1.6)** as two examples of polycyclic aromatic hydrocarbons (PAH), have recorded two of the highest mobilities (7 $cm^2V^{-1}s^{-1}$ and 20 $cm^2V^{-1}s^{-1}$), far exceeding that of amorphous silicon (~ 1 $cm^2V^{-1}s^{-1}$).[27],[28] Such high mobilities of oligoacenes over that of α,ω-substituted sexithiophenes[29] should originate from the highly ordered and close molecular packing which increase the π-π interaction between the adjacent molecules.[30] However, pure hydrocarbon ladder-type oligoacenes have

some drawbacks for a practical application to organic devices. For example, their high-lying HOMOs and narrow band gaps leave them sensitive to photooxidation, resulting in the deterioration of semiconductor performance under ambient conditions.[31] Therefore, it is important to develop new organic semiconducting materials which achieve both high charge carrier mobility and high stability under ambient conditions.

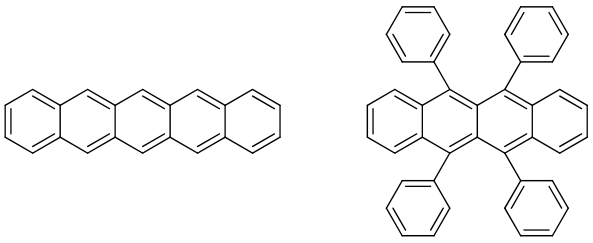

8 **9**

Figure 1.6. Structure of benchmark oligoacenes for organic semiconductors.

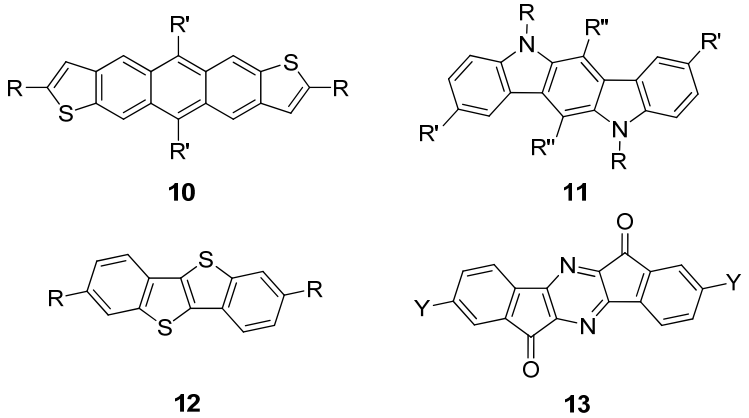

10 **11**

12 **13**

Figure 1.7. Examples of heteroacenes for organic semiconductors.

Introduction of heteroatoms (e.g. sulfur, nitrogen or oxygen) in the fused-ring system (namely heteroacenes) has been one of the major approaches to modify physical and chemical properties of ladder-type acene molecules. As shown in **Figure 1.7**, anthradithiophene (**10**) [32], indolo[3,2-*b*]carbazole (**11**) [33]-[34] and [1]benzo-thieno[3,2-*b*] benzothiophene (**12**) [35] were synthesized, giving oxidative stability higher than that of pentacene because of their lower lying HOMOs and larger band gaps. These heteroacene molecules form π-stacking arrangements in the solid states and show relatively high hole mobility (0.14~2.9 $cm^2V^{-1}s^{-1}$). The OFET

devices based on the diindenopyrazinedione (**13**) also showed high electron mobility of 0.17 $cm^2V^{-1}s^{-1}$.[36] These properties would allow heteroacene molecules to be promising candidates for OFET materials. Thus, facile and diverse synthetic approaches are necessary for the rapid improvement of heteroacene-based OFET materials.[37]

1.1.2.2 *p*-Channel heteroacenes

The number of research groups devoting significant effort to the synthesis of semiconducting heteroacenes has grown from just a few in the late 1990s to many dozens at the present time. There are now hundreds of compounds that have been demonstrated as *p*-channel (hole-transporting) semiconductors in organic field-effect transistors (OFETs). The preference for holes is determined by the HOMO energy levels relative to contact work functions and environmental quenchers. It would be futile to list all the compounds individually because new ones are reported each month. Many exhibit field-effect mobilities in the order of 0.1 to 2 $cm^2\ V^{-1}s^{-1}$, at or exceeding the value generally associated with amorphous silicon (which is an electron transporter used as a relatively inexpensive semiconductor for display applications). The main classes of hole-carrying heteroacenes include thiophene fused heteroacenes (such as dibenzothienobisbenzothiophene, pentathieacene, dithienobenzothiophene and dinaphthothienothiophene) (**14**-**17**), pyrrole fused heteroacenes (such as indolocarbazole and diindolocarbazole) (**11**, **18**), and multi-fused selenophenes (**19**). A few such structures are shown in **Figure 1.8**. In some cases, side chains (R) provide additional morphology, processing, and reliability control.[38] Some very recent examples of *p*-channel heteroacenes are cited here[39]; these are intended as the most recent practical entrances into the literature and only hint at the variety of organic structures now being considered. In particular, [1]benzothieno[3,2-*b*]benzothiophene (**12**) shows as high *p*-channel mobility (2.75 $cm^2\ V^{-1}\ s^{-1}$) as pentacene from solution procession.

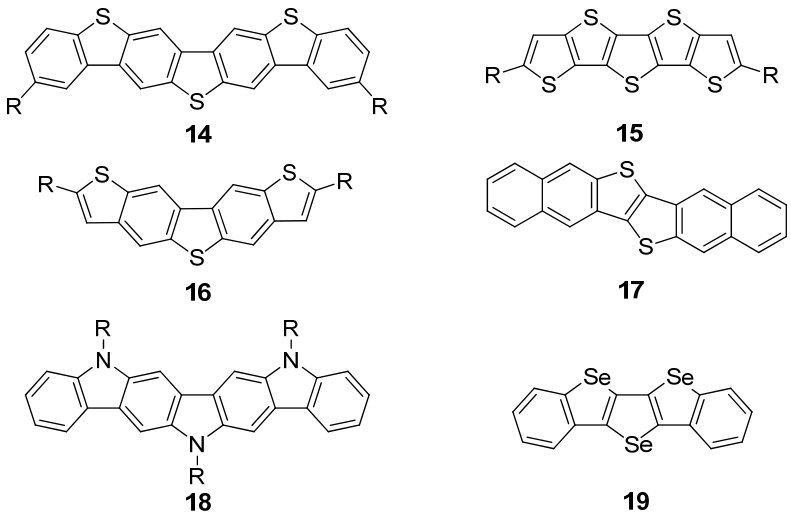

Figure 1.8. Representative heteroacenes as *p*-channel OFET materials.

1.1.2.3 *n*-Channel heteroacenes

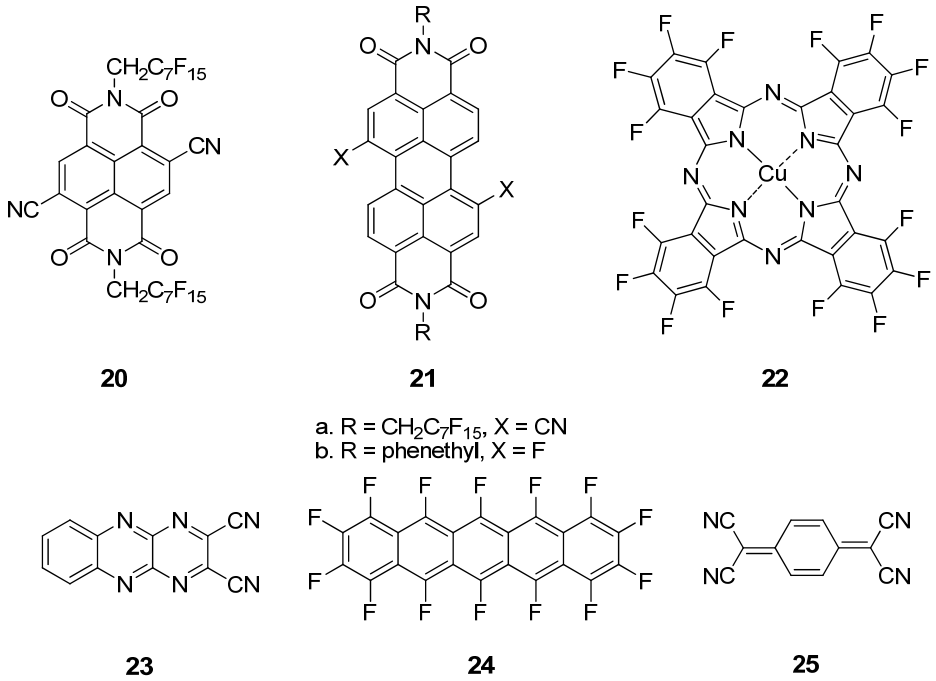

Figure 1.9. Representative heteroacenes as *n*-channel FET materials.

There are considerably fewer molecular structures that have been identified as preferential *n*-channel (electron-carrying) transistor semiconductors, although the list has grown rapidly in the past two years and now approaches 100 compounds in total, two thirds of which are heteroacenes.[40] *n*-Channel semiconductors are needed to

take advantage of the greater power efficiency of complementary transistor circuits, as well as to develop devices that rely on *p*-*n* junctions, such as thermoelectric modules and solar cells. Representative *n*-channel FET materials are depicted in **Figure 1.9**.

Perylene and naphthalene tetracarboxy dianhydride derivatives (PTCDI **20** and NTCDI **21**) and metallophthalocyanines (eg. F16 CuPc, **22**) are well known *n*-channel OFET semiconductors. A series of PTCDIs with small substituents such as core-cyano, *N*-heptafluorobutyl (**21a**) and core-fluoro, *N*-phenethyl (**21b**) showed mobilities of 0.1 - 0.7 $cm^2\ V^{-1}s^{-1}$, with some retaining most of the mobility in air.[41],[42],[43] In addition, a variety of fluoro and trifluoromethyl compounds are known to show *n*-channel performance. Perfluoropentacene (**24**) showed an electron mobility of 0.22 $cm^2\ V^{-1}s^{-1}$. TCNQ (tetracyanoquinodimethane **25**) gave an *n*-channel OFET.[44] Although the reported mobility (3×10^{-5} $cm^2\ V^{-1}\ s^{-1}$) is not very high, the OFET worked in air even after air exposure of several ten days.

1.2 Design principles of high performance oligoacenes

1.2.1 Energy levels of organic semiconductors

Energy levels of some organic semiconductors are depicted in **Figure 1.10** and compared with the work function of popular metals. The ionization potential (*IP*) of organic semiconductors, which is regarded as corresponding to the energy level of the HOMO,[45] could be directly measured by ultraviolet photoelectron spectroscopy (UPS), where ultraviolet light of frequency ν is used to irradiate the molecule in vacuum, and the kinetic energy E_K of the escaped electron is analyzed, so that the binding energy E_B is estimated from $h\nu = E_K + E_B$. Molecular solids and gaseous molecules afford different E_B values owing to the relaxation in the solids. The ionization energy of the usual electron donor molecule is around 5 eV in the solids, whereas it is 7 eV in the gas phase. We use the former values for the discussion of devices.

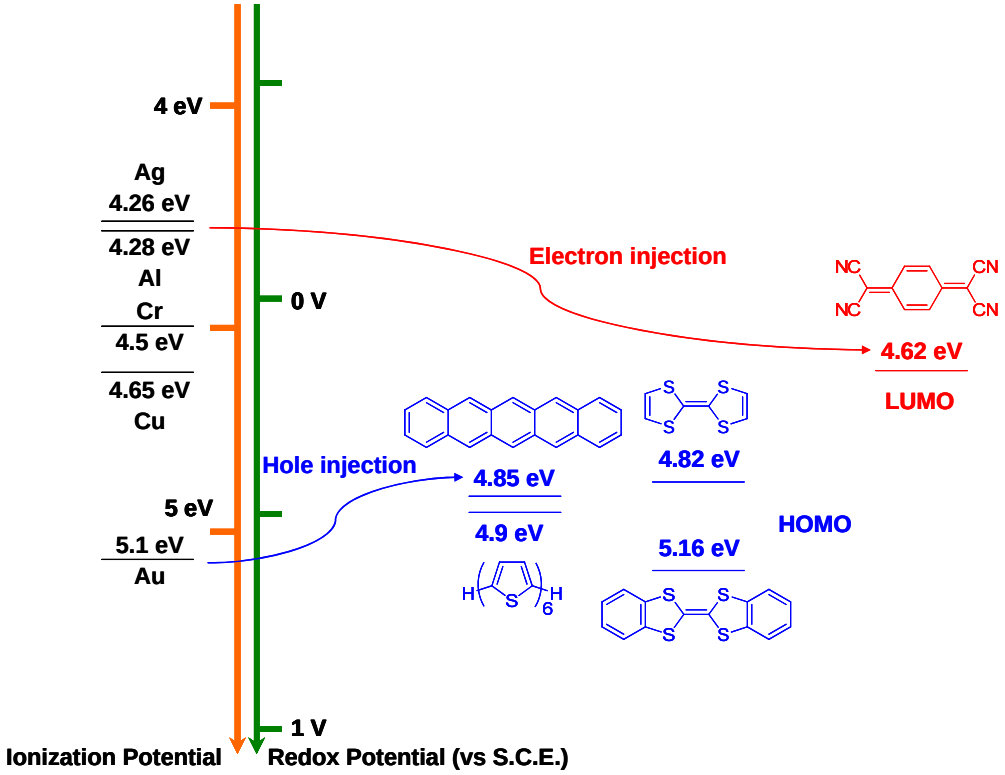

Figure 1.10. Energy levels of organic semiconductors.

We can compare these ionization potentials with work functions of metals, which are the positions of the Fermi levels.[46] For example, the work function of Au (5.1 eV) is located lower than the ionization potential of pentacene (4.85 eV), and hole injection from Au S/D electrodes to pentacene is expected. It is, however, not always easy to measure the ionization potentials by photoelectron spectroscopy. Instead, redox potentials E_{red} (versus SCE) are easily measured in solutions by cyclic voltammetry (CV), and they are converted to the ionization potentials E_P via $E_P = E_{red} + 4.34$ eV[47]. Although this is a very rough estimation, this relation is conveniently used to estimate the energy levels of new materials. The tuning of the energy levels is very important because the mismatch between the semiconducting materials and the electrodes could lead to large injection barriers or contact resistances at the S/D electrodes. The contact resistance is, however, not solely energetic in origin and also related to film morphology. This text will not go too much into detail, because the device physics is not at the focus of this study.

1.2.2 Tuning the HOMO level of *p*-channel oligoacenes

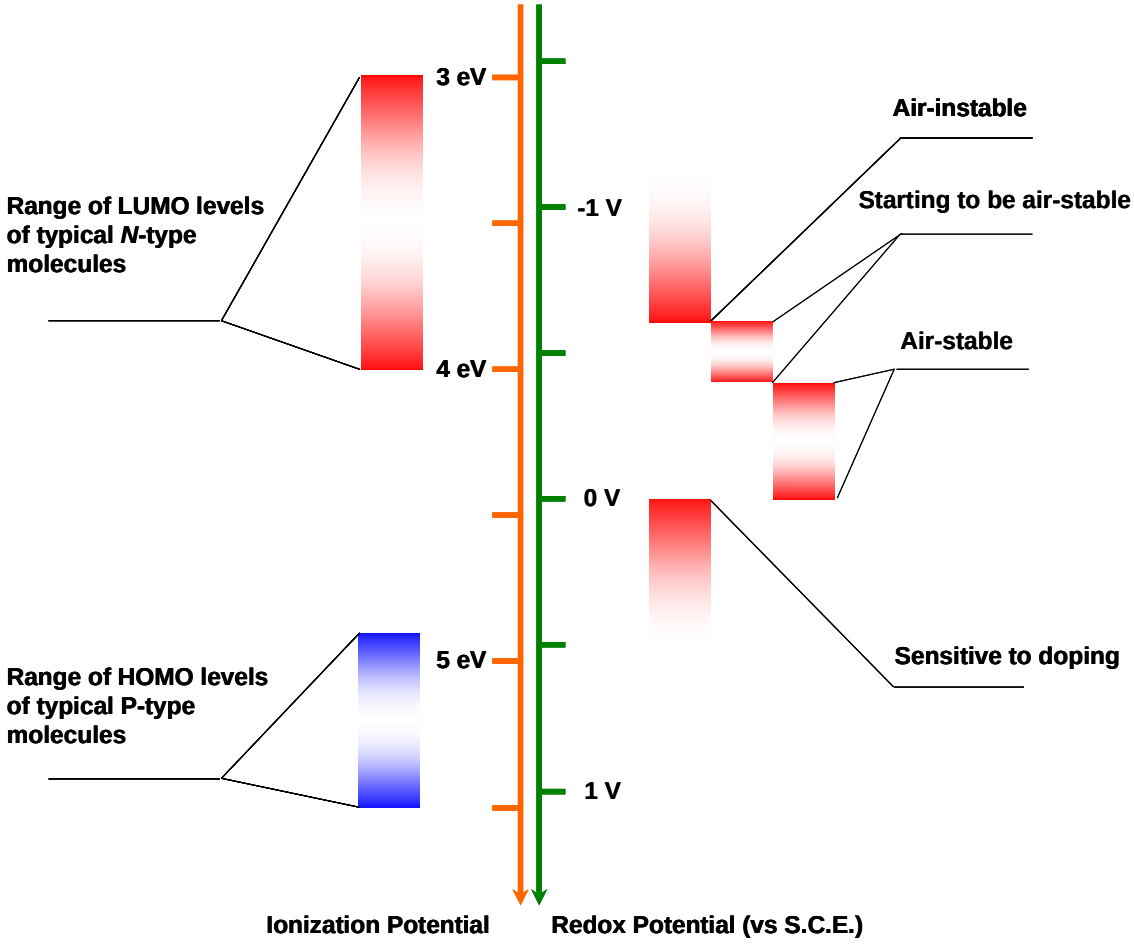

Figure 1.11. Empirical rationalization of energy levels of organic semiconductors. (Left) Range of LUMO levels of typical *n*-type materials and HOMO levels of typical *p*-type materials. (Right) First reduction potential (E_{R1}) windows for modified *n*-type materials with both stable electron conduction and low doping levels.

Stable *p*-channel organic semiconductors typically have HOMO levels between -4.9 and -5.5 eV, resulting in Ohmic contact with high work-function metals such as gold (5.1 eV) and platinum (5.6 eV).[48] (**Figure 1.11** left) Take pentacene as an example, besides the low band gap, its HOMO level (-4.85 eV) is so high that it makes pentacene suffer from rapid degradation in ambient conditions and formation of dimeric Diels–Alder adducts on the electron-rich central ring.[49] Therefore, the instability (oxidation sensitivity) of the compounds often lies in the low ionization potential, that is, a high-lying HOMO energy level. Meanwhile, the higher the

ionization potential, the more stable the radical cation, which is an important factor in achieving high mobilities.[50]

The HOMO energy is correlated among others with the π electron topology and the effective conjugation length of the compounds. Within a particular class of compounds (e.g. PAH-acenes and oligothiophenes) an increased effective conjugation length leads to energy-rich HOMO levels and thus to an increased susceptibility towards oxidation. Meanwhile, electron-rich substituents (e.g. alkoxy groups) normally result in a further increase in the HOMO energy levels. Tetramethoxy substituted diphenylpentacene shows an increased HOMO level of -4.78 eV compared with that of pentacene (-4.85 eV). In contrast, electron-deficient substituents on oligoacenes (e.g. fluoro) bring about electronic stabilization. For example, perfluoropentacene shows a much decreased HOMO level at -5.39 eV,[51] which however turns to *n*-channel materials.

1.2.3 Tuning the LUMO level of *n*-channel oligoacenes

n-Channel materials typically have LUMO levels between -3 and -4 eV, which therefore have a large electron injection barrier with respect to the Fermi level of the metal electrodes (5.1 eV for gold) and more importantly are normally air-instable. (**Figure 1.11** left) To solve the problem, chemists synthesized molecules with strong electron-withdrawing groups in the periphery of π conjugated molecules. This has been done successfully with several semiconductor core systems. These groups increase the electron affinity (*EA*) and stabilize the anionic form of the molecule, allowing for the possibility of efficient electron injection and transport.[52]

At the same time, however, the large electron affinities of known air-stable *n*-channel cores which prevent electron trapping also enhance sensitivity to electron-doping from the metal contacts and/or donor sites in the dielectric. An empirical first reduction potential (E_{R1}) window for both stable FET electron conduction and low doping levels is derived by analyzing the redox properties of several rylene/oligothiophene-based *n*-channel semiconductors developed in Mark's

group.[52f],[53] (**Figure 1.11** right) When E_{R1} ≤ -0.6 V (vs SCE), the material may be an *n*-channel semiconductor but not air-stable. When E_{R1} = -0.6 to -0.4 V, the onset of *n*-channel stability begins. However, for E_{R1} = > 0.0 V, significant doping becomes evident and device current modulation is difficult to control. Therefore, semiconductors with an E_{R1} ranging from -0.4 to 0.0 V should result in FETs exhibiting both stable electron transport in air and minimal doping (low I_{off}).

The stability problem motivated people to rationalize the design principle of these molecules. In general, there are three approaches to stabilize the electrons inside the semiconducting materials[54]: (a) use strongly electron-deficient π-conjugated cores; (b) employ *p*-channel materials but eliminate deep electron trapping sites by passivating the dielectric surface; (c) functionalize conventional *p*-channel cores with powerful electron-withdrawing and/or hydrophobic substituents. Indeed, high mobility *n*-channel semiconductors have recently been realized with these approaches.[52c,f] Some of these materials exhibit a combination of excellent FET performance both in vacuum (μ_e ≈ 0.3-0.6 cm^2 V^{-1} s^{-1}; I_{on}/I_{off} ≈ 10^7-10^9; V_{th} ≈ +30 to 50 V) and under ambient conditions (μ_e ≈ 0.1-0.6 cm^2 V^{-1} s^{-1}; I_{on}/I_{off} ≈ 10^4-10^5; V_{th} ≈ -30 to 15 V). Note that semiconductor film morphology optimization may also play a role in stabilization of FET transport.[41]

1.3 A summary of synthetic methods toward thiophene containing heteroacenes

As one of the most important families of semiconducting materials, thiophene containing heteroacenes have attracted tremendous attention. Such structures are believed to combine the stability of the thiophene ring with the planarity of the linear acenes such as pentacene. At the same time, these systems should retain the desirable properties of oligothiophenes, while limiting deviations from planarity that disrupt conjugation and potentially affect the band gap in the solid state. (**Figure 1.12**) To achieve this goal, many synthetic methods have been developed, which included generally two different strategies - insertion of sulfur atoms into the conjugated

skeleton and direct annulation of thiophene units.

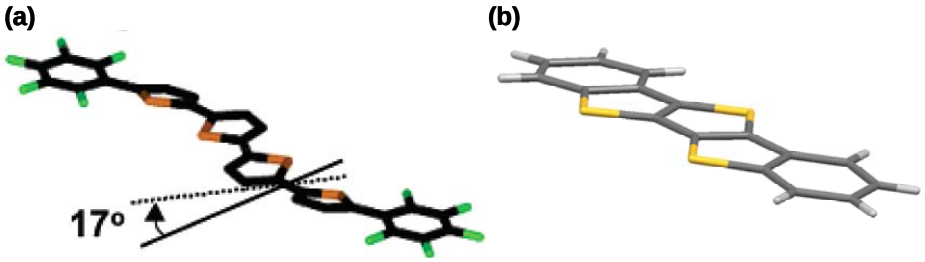

Figure 1.12. Examples of crystal structures showing the effect of planarization induced by ring fusion. (a) 5,5′′-diperfluorophenyl-2,2′:5′,2′′:5′′,2′′′-quaterthiophene showing inter-ring torsional angles[55] (Reproduced from ref [55]. Copyright 2006 American Chemical Society.); (b) dibenzo[*d*,*d'*]thieno[3,2-*b*;4,5-*b'*]dithiophene showing planar structure. (Reproduced from ref [37g]. Copyright 2005 American Chemical Society.)

1.3.1 Synthesis of thiophene containing heteroacenes by sulfur-bridge formation

1.3.1.1 Formation of sulfur-bridges by triflic acid induced electrophilic substitution

16 Years ago, Yamamoto et al. reported the intermolecular coupling reaction of aromatic methyl sulfoxides with activated aromatic building blocks in the presence of strong acids for the preparation of high-molecular weight polymers, such as poly(phenylene sulfide) (PPS, **26**),[56],[57] poly(phenylene sulfide-phenylene amine) (PPSA, **27a**) [58],[59] and poly(phenylene sulfide phenylene amine-phenylene amine) (PPS-AA, **27b**).[60] (**Scheme 1.1**)

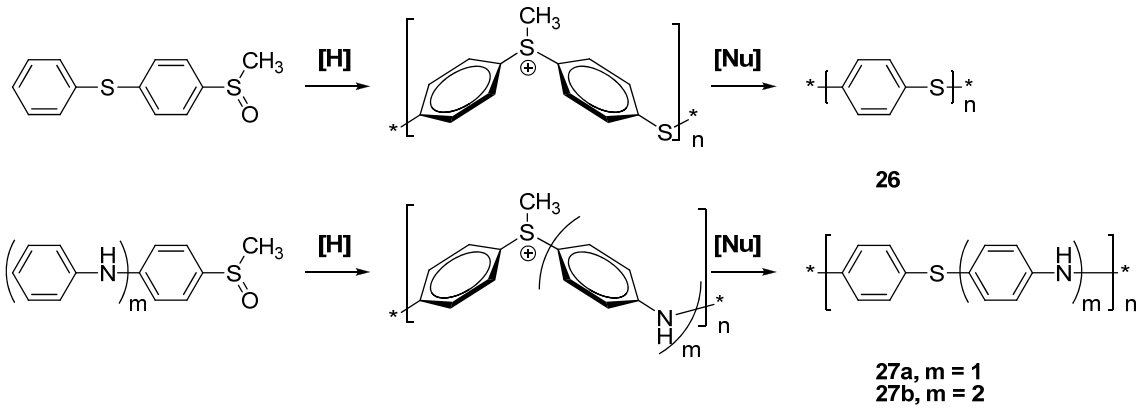

Scheme 1.1. Synthesize PPS via soluble (polysulfonium cation) intermediate in acid

The mechanism of the reaction is demonstrated in **Scheme 1.2**. In a sulfoxide structure (**28**), the S=O bond is polarized as $S^{+}O^{-}$ due to the presence of the *d* empty orbital. In the presence of trifluoromethanesulfonic acid (triflic acid), the electrophilic attack occurred at the negatively charged oxygen atom to give methyl(4-phenyl-thio)phenylsulfonium cation (**29**) as an active species, as shown in ***eq1*, Scheme 1.2**. The formed sulfonium cation could be isolated quantitatively as a stable salt.[59] The activated sulfoxide is well-known as an electrophile (Swern method).[61] Then the active species electrophilically attracks on the benzene ring (**30**) to eliminate water as a byproduct. (***eq2*, Scheme 1.2**.) The reaction was therefore influenced by the acidity of the mixture. Triflic acid, which is the strongest protic acid, is most efficient for the formation of the sulfonium cation. In weak acids such as CH_3COOH and CF_3COOH, the electrophilic reaction scarcely proceeds.[57] Sometimes the reaction is promoted in the presence of phosphorus pentoxide due to the dehydration effect of phosphorus pentoxide. In the end, the demethylation proceeded quantitatively using pyridine as a nucleophile (***eq3*, Scheme 1.2**.).

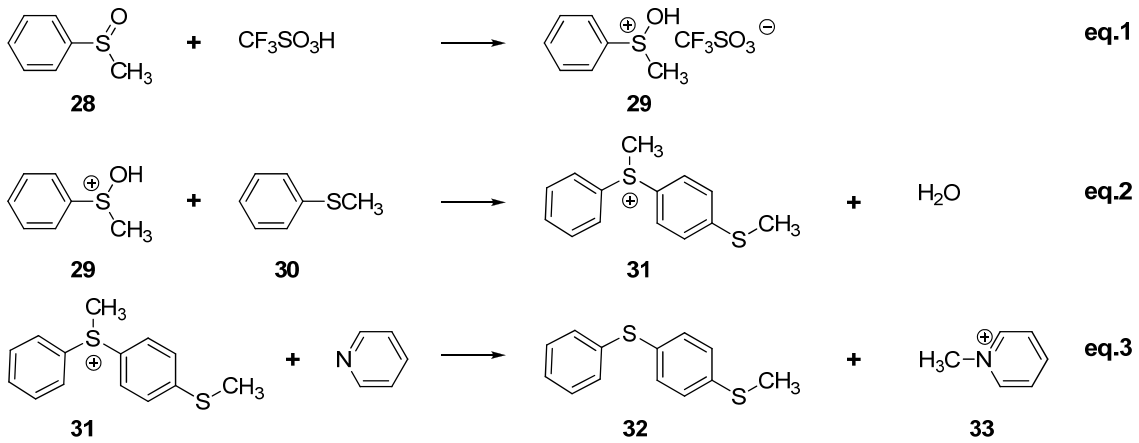

Scheme 1.2. Mechanism of the super acid induced electrophilic substitution

When the intermolecular substitution is applied to intramolecular reactions, a sulfur bridge is formed between two adjacent aromatic rings. Due to the easy availability of the Ar-methylsulfoxide (**28**) and the straightforwardness of the reaction, it has been a powerful tool to construct sulfur containing ladder type polymers and oligoacenes.[62] In 1999, our group first reported the triflic acid induced

intramolecular ring closure, from which were obtained oligoheteroacene dibenzo[*b*,*b'*]thieno[2,3-*f*:5,4-*f'*]bis[1]benzothiophene (**DBTBT**) as a high performance OFETs material.[37m] But due to the nature of the precursor, three isomers (**35**-**37**) were present in the final product. (**Scheme 1.3a**) Another recently reported heteroacene synthesized using this strategy for OLED application is shown in **Scheme 1.3b**.[63]

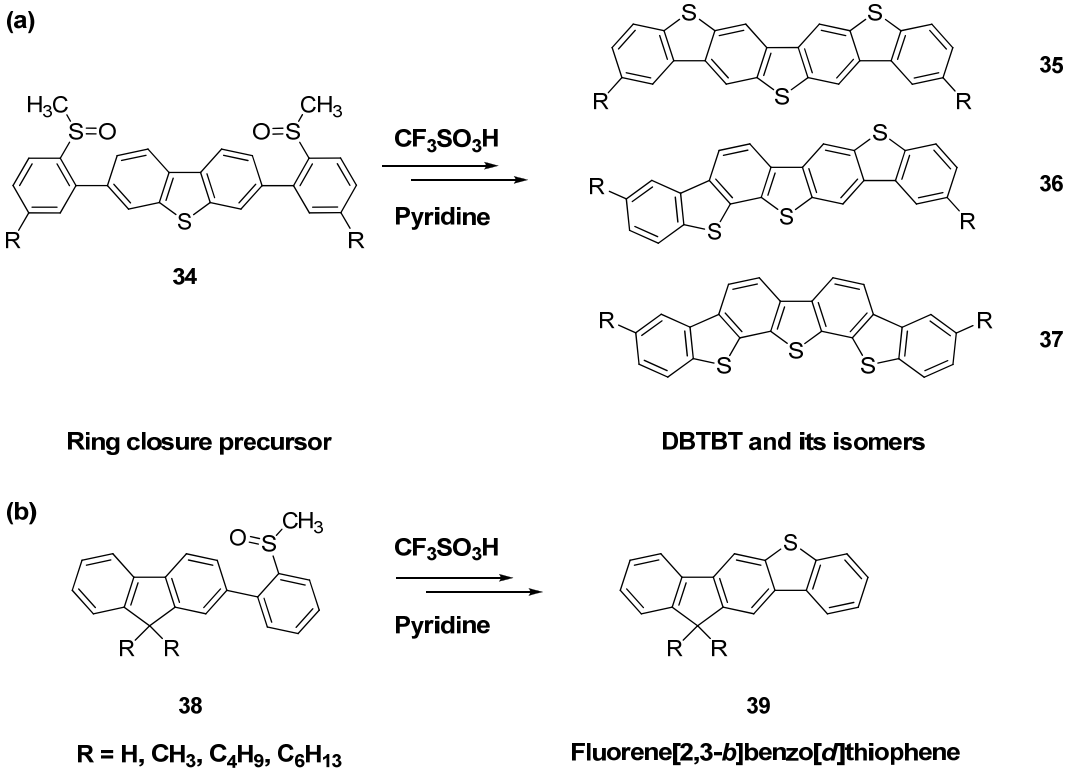

Scheme 1.3. Two examples of the electrophilic substitution towards thiophene fused heteroacenes

During our study, we found that there are two disadvantages with this method. The first one is the low functional group tolerance. Functional groups like halogen atoms (Br or I), trimethylsily, carbonyl groups and α-H of thiophene etc can react with triflic acid activated sulfoxide and lead to significant side reactions. The second drawback is that longer alkyl groups (C_nH_{2n+1}, n > 10) will degrade in the triflic acid. This means that under some conditions, we can not achieve enough solubility due to the limited length of the alkyl groups.

1.3.1.2 Introducation of thiophene rings by aromatic nucleophilic substitution (S_NAr) reaction

Benzo[*b*]thiophene and its related fused-aromatic compounds are attracting current interest as promising electronic materials. For the further development of new materials based on benzo[*b*]thiophenes, it is of primary importance to devise effective synthetic methods. To this end, much work has been done to develop new and convenient synthetic approaches to benzo[*b*]thiophenes. In particular, the use of phenylacetylene-based precursors in cyclization reactions affording fused-thiophene or selenophene moieties has emerged: Sashida et al. first reported that o-alkynylbromobenzenes (**40**) react with elemental chalcogene (sulfur, selenium, or tellurium) upon lithium-halogen exchange to afford benzo[*b*]chalcogenophenes in good yields.[64] Later on, Takimiya et al. employed the same method and successfully applied it to 2-fold cyclization reactions to give benzo[1,2-*b*:4,5-*b'*]dithiophenes and benzo[1,2-*b*:5,4-*b'*]diselenophenes (**43**).[65] (**Scheme 1.4**)

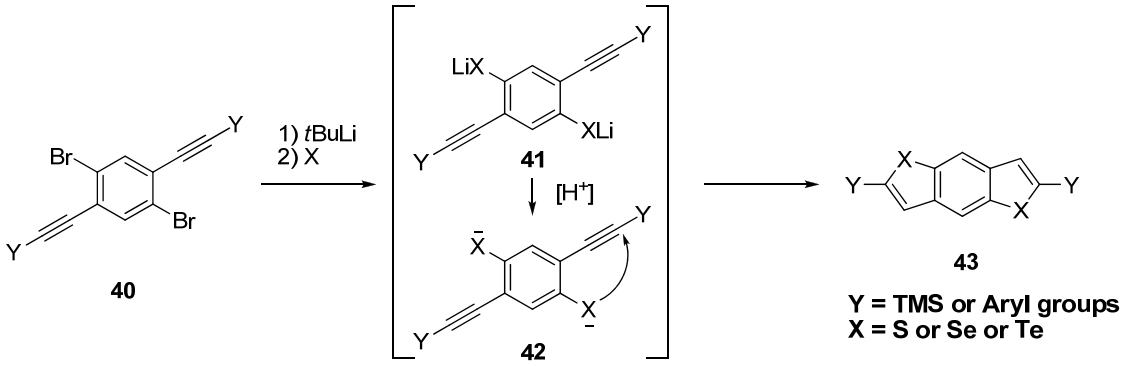

Scheme 1.4. Synthesis of benzodichalcogenophenes

Furthermore, Yamaguchi et al. developed the intramolecular triple cyclization of bis(o-haloaryl)-diacetylenes (**44**) to produce heterole-1,2-dichalcogenin-heterole (**45**) fused tricyclic skeletons. Then the subsequent dechalcogenation with copper metal affords a series of thiophene- and selenophene-based heteroacenes (**46**).[37b,g] (**Scheme 1.5**)

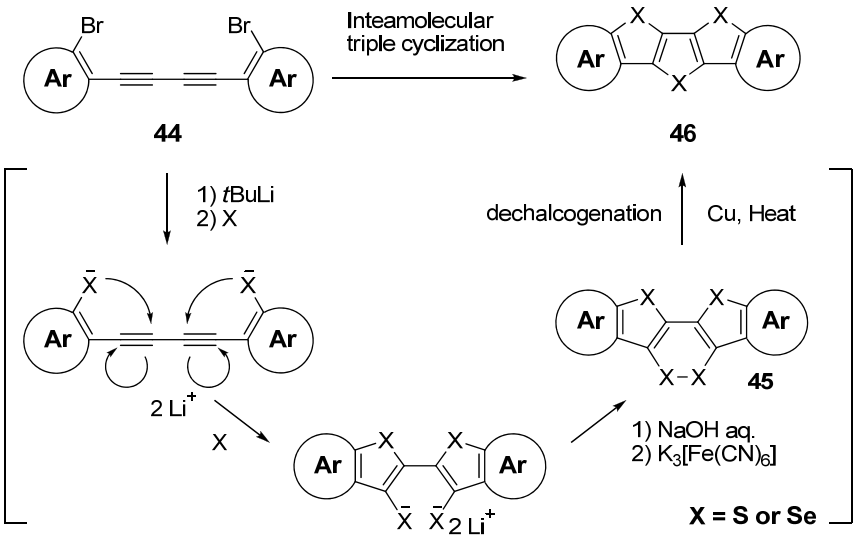

Scheme 1.5. Intramolecular triple cyclization reaction by *nucleophilic* substitution

Very recently, based on the result of Shvartsberg et al.[66], Takimiya and his colleagues further developed the nucleophilic cyclization reaction using inorganic sulfur sources, such as sodium sulfide (Na_2S), as reagent and o-alkynylbromobenzenes (**47**), from which they realized a 3-fold cyclization reaction to get benzo[1,2-*b*:3,4-*b'*:5,6-*b''*]trithiophenes (**48**) in one pot procedure. Owing to the accessibility of the precursors, the easy experimental operation, and the reasonable yields of the products, this method for the synthesis will be beneficial for developing new materials based on benzothiophenes. **(Scheme 1.6)**

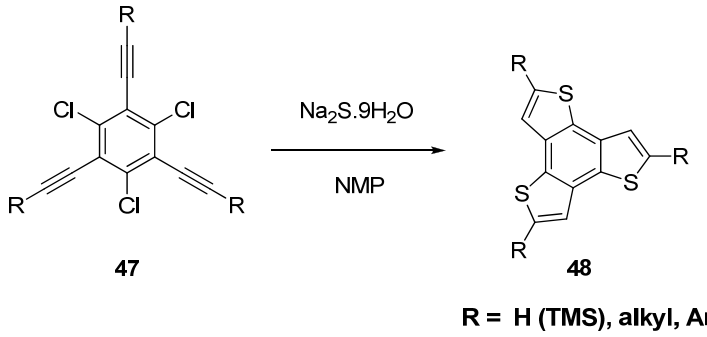

Scheme 1.6. Synthesis of multithiophene fused-aromatic compounds

Another important nucleophilic reaction with a cyclization step can lead to thienothiophenes. (**Scheme 1.7**) In the presence of base, the reaction started with a nucleophilic attack of the thioglycolate anion (**49**) on the bromo-substituted carbon

atom (**50**) and a concomitant intramolecular aldol condensation of the carbaldehyde with the CH_2 besides the ester to yield ethyl thieno[3,2-*b*]thiophene-2-carboxylate (**51**).

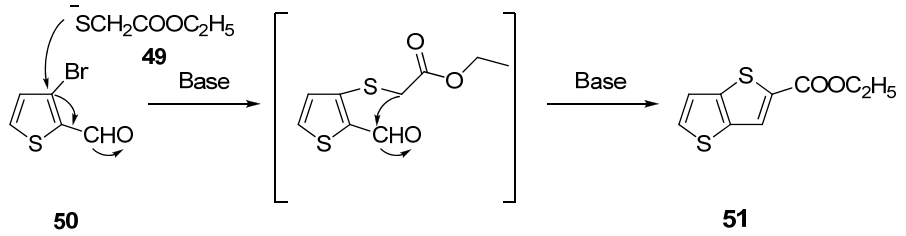

Scheme 1.7. Mechanism of the nucleophilic reaction induced cyclization reaction

In the end, Watson et al. employed a very clever route that involves nucleophilic aromatic substitution (S_NAr) to synthesize fluorinated benzobisbenzothiophenes (**53**).[67] The synthesis scheme is shown in **Scheme 1.8**. The reaction is so efficient that the dealkylation and ring closure are allowed to be finished in one-pot. The only limitation is that the reaction could only be performed efficiently in highly electron deficient systems which are also sustainable in strong base.

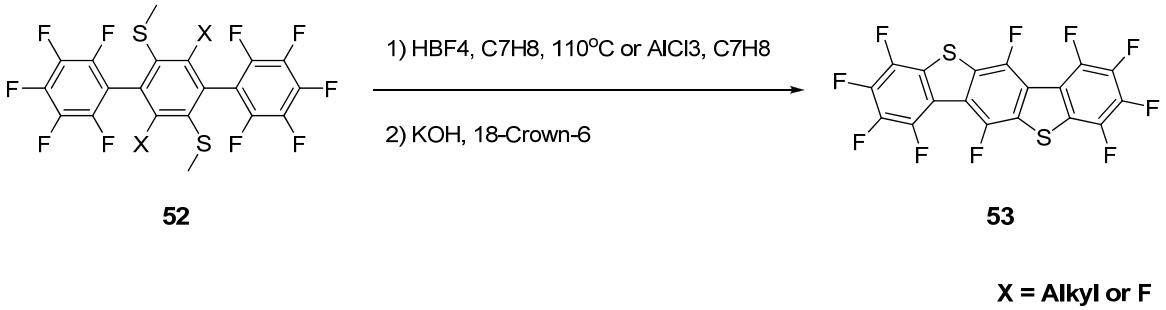

Scheme 1.8. Introduction of sulfur-bridge via nucleophilic aromatic substitution in highly fluorinated aromatic system

1.3.1.3 Introduction of thiophene rings by electrophilic cyclization reaction

Larock et al. has developed a very efficient synthesis of 2,3-disubstituted benzo[*b*]thiophenes (**55**) involving *electrophilic* cyclization of o-alkynylthioanisol (**54**) catalysed by I_2, Br_2, NBS, and sulfur and selenium electrophiles.[68] (**Scheme 1.9**) The high yield of this reaction is quite attractive to other chemists. Pei and his colleagues used this method in a two fold structure to construct C_2-symmetric ladder-type

heteroacenes.[73a]

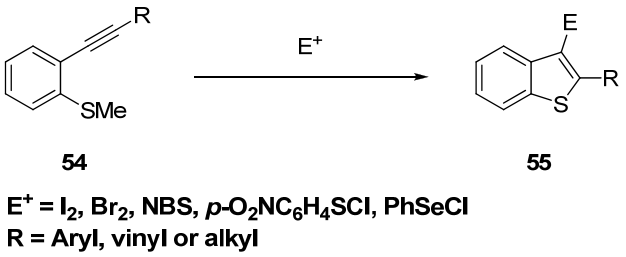

Scheme 1.9. Intramolecular electrophilic cyclization reaction

Recently, Takimiya et al. designed and synthesized dinaphtho[2,3-*b*:2′,3′-*f*]-chalcoge[3,2-*b*]chalcogenophenes (**57**) (**Scheme 1.10**) with six fused aromatic rings. In the presence of excess iodine (Lewis acid), the olefin intermediates (**56**) forms the thienothiophene (**57a**) or selenophenoselenophene (**57b**) moieties in good yields. It should be noted that the present method is much shorter than the previously reported one [37d] and is a versatile tool to obtain various novel heteroacenes.

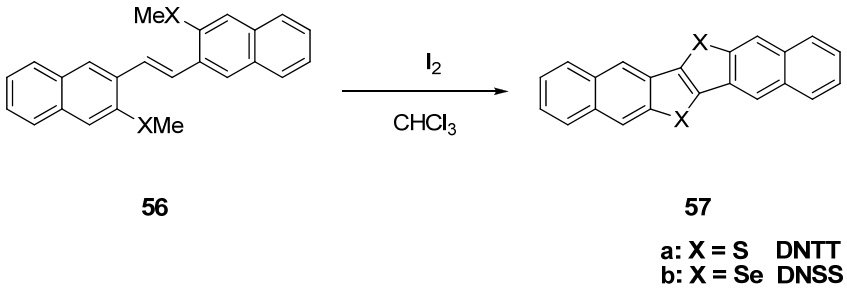

Scheme 1.10. Synthesis of DNTT and DNSS via intramolecular electrophilic cyclization

All the results based on these *electrophilic* cyclization reactions showed the advantages of high yields and the tolerance for various substituents.

1.3.1.4 Introduction of thiophene ring by Hinsburg thiophene synthesis

Hinsburg thiophene synthesis was named after Hinsburg, since he described in 1910 the reaction between benzyl and diethylthiodiacetate to give thiophene ring system.[69] The mechanism of the reaction, which was corrected by Wynberg and Kooreman in 1965, is shown in **Scheme 1.11a**. The reaction involves the condensation of the enolate of diethyl thiodiglycolate (**58**) with benzyl (**59**), and spontaneous

lactonization to provide **61.** Base-induced ring fragmentation in the elimination of the carboxylate and a subsequent Knoevenagel-type cyclization provides the mono-ester **63.** Reaction conditions must allow for the isomerization of the newly formed alkene via reversible conjugate addition reactions since only the *Z*-alkene geometry permits cyclization via a Claisen/elimination process to form the thiophene ring. Upon hydrolysis of **63** under acidic conditions, the thiophene dicarboxylic acid product **64** is obtained. It should be noticed that one O atom is transferred from benzyl (**58**) to the carboxylate end product.[70]

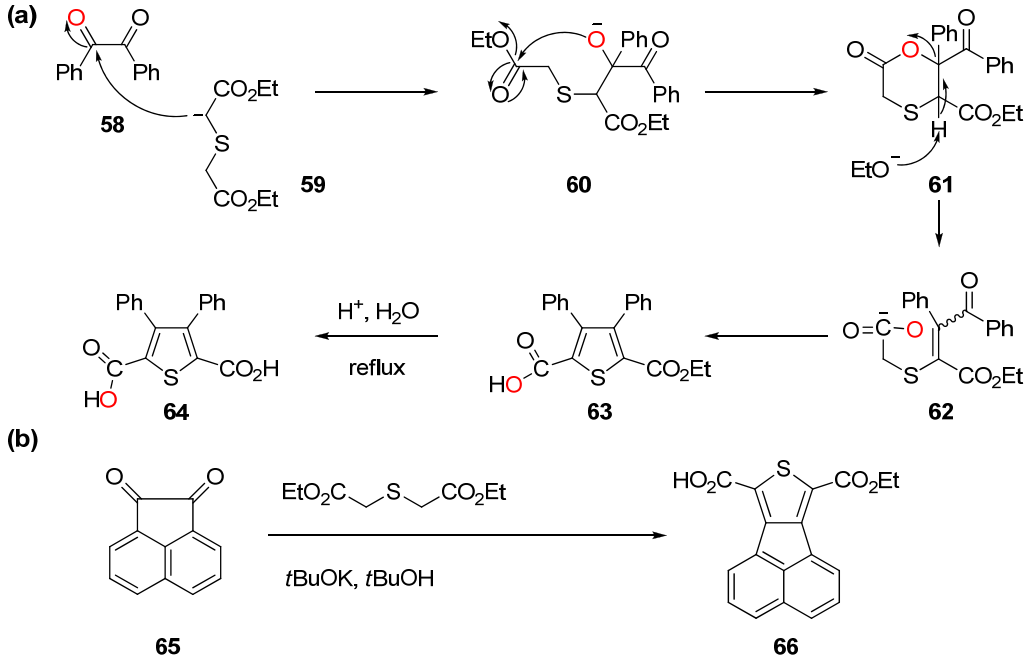

Scheme 1.11. Introduction of thiophene ring by Hinsburg thiophene synthesis

A very recent example of using Hinsburg reaction to condensed thiophene ring on the naphthylene-*α*-dione (**65**) is shown in **Scheme 1.11b**.[71]

1.3.2 Synthesis of thiophene containing heteroacenes by direct annulation of thiophene units

1.3.2.1 Friedel-Crafts-type alkylation and acylation reactions

Intramolecular Friedel-Crafts alkylation has been used firstly by Müllen and colleagues 18 years ago in the synthesis of ladder-type conjugated polymers.[72] The

reaction involved two key steps: reduction of α-ketone (**67**) to benzyl alcohol (**68**) and boron trifluoride etherate catalyzed Friedel-Crafts cyclization. (**Scheme 1.12**) This method is a versatile way to construct ladder-type or spiro-bridged structures and has been widely applied.[73]

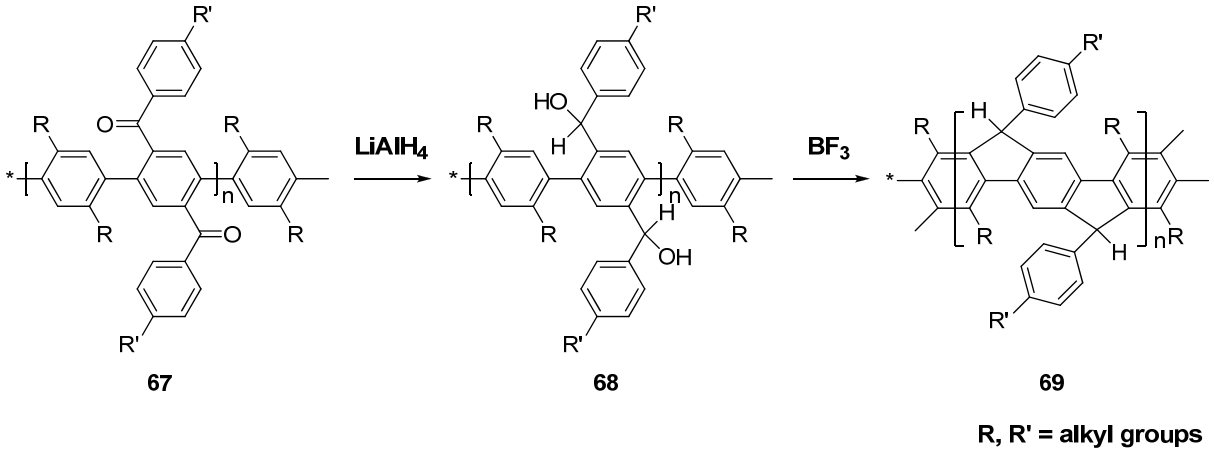

Scheme 1.12. Synthesis of ladder-type polymers via Friedel-Crafts alkylation

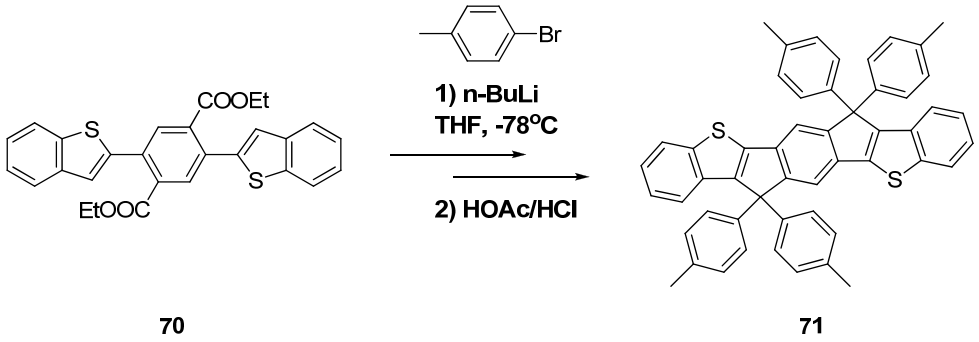

Scheme 1.13. Example of thiophene unit containing heteroacenes by Friedel-Crafts alkylation

With regard to the thiophene containing heteroacenes, thiophene ring is readily fused by this method, but the boron trifluoride etherate should be replaced by a mixture of acetic acid and hydrochloride acid.[74] One example is given in **Scheme 1.13.**

Intramolecular Friedel-Crafts *acylation* is on the other hand a convenient way to construct n-channel semiconducting materials. Wang et al. resynthesized indeno[1,2-*b*]fluorine-6,12-dione (**73**) using sulfuric acid induced Friedel-Crafts

acylation in high yield.[75] The reaction was performed much more easily than the alkylation reaction and left two electron withdrawing ketone groups. (**Scheme 1.14**) Based on the ketone functional groups, spiro-bridged oligomer for OLED application[76] and malononitrile substituted compound for *n*-channel OFET could be developed.[77]

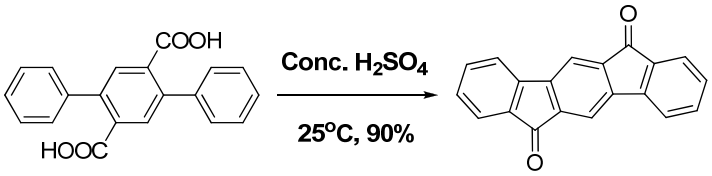

72 **73**

Scheme 1.14. Wang's synthesis of ladder-type oligoacenes

If one wants to combine thiophene rings into the conjugated system through the Friedel-Crafts *acylation*, the reaction condition should be modified in order not to destroy the thiophene system.[78] One example is given in **Scheme 1.15.**

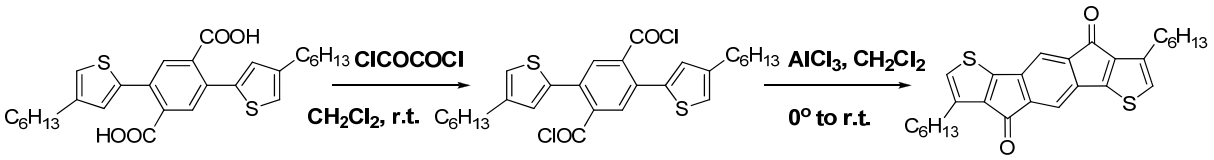

74 **75** **76**

Scheme 1.15. Synthesis of thiophene containing heteroacenes

1.3.2.2 Cadogan reductive cyclization on thiophene units

Cadogan and coworkers developed reductive cyclization of nitro groups, the mechanisms of which have not been established, and it may be that there is not a common mechanistic pathway.[79] A notable feature of the reduction is its success when applied to the synthesis of five-membered rings containing nitrogen (e.g. carbazole).[80] In the synthesis of higher conjugated heteroacenes in the presence of thiophene units, the same reaction as the synthesis of carbazole is used. An example is given in **Scheme 1.16**.

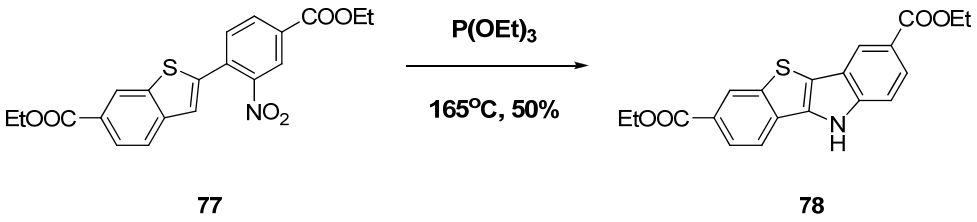

77 **78**

Scheme 1.16. Example of the Cadogan reductive cyclization

One advantage of the Cadogan ring closure reaction over those of electrophilic Friedel-Crafts reaction is that it is not influenced by the electronic state of the substrate. Therefore the Cadogan cyclization occurs at both electron rich and poor system. In a very extreme condition, the ring closure reaction can be done on the famous electron acceptor benzothiadiazole.[81] On the other hand, this "advantage" can lead to much lower regioselectivity than Friedel-Crafts reaction in some cases.[37k]

1.4 Solid-state structure of full ladder oligoacenes

Organic semiconductors that are composed of oligoacenes typically produce polycrystalline or disordered films. The individual molecules inside the film are only weakly interacting through van der Waals, hydrogen bonding, and π-π interactions. Charge delocalization can only occur along the conjugated backbone of a single molecule or between the π-orbitals of adjacent molecules. Therefore, charge transport in organic materials is thought to rely on intermolecular order adopted by the individual molecules in the solid state and charge hopping from these localized states, which can be thought of as an electron transfer between a charged oligomer and an adjacent neutral oligomer.

In general, good electronic performance requires strong electronic coupling between adjacent molecules in the solid. As will be seen in the main text of this thesis, there are two common packing motifs adopted by heteroacenes in the solid state that may yield strong intermolecular overlap. In the classic "herringbone" arrangement, the aromatic edge-to-face interaction dominates, yielding two-dimensional electronic interactions in the solid (**Figure 1.13**, top). Alternatively, the molecules can adopt a

coplanar arrangement and stack, typically with some degree of displacement along the long and short axes of the molecules (**Figure 1.13**, bottom).[82] The strong interaction between the π-electron-rich faces (π-faces) of the molecules in these π -stacked arrays yields strong electronic coupling, and further interactions with adjacent stacks can yield two dimensional electronic coupling in the solid.

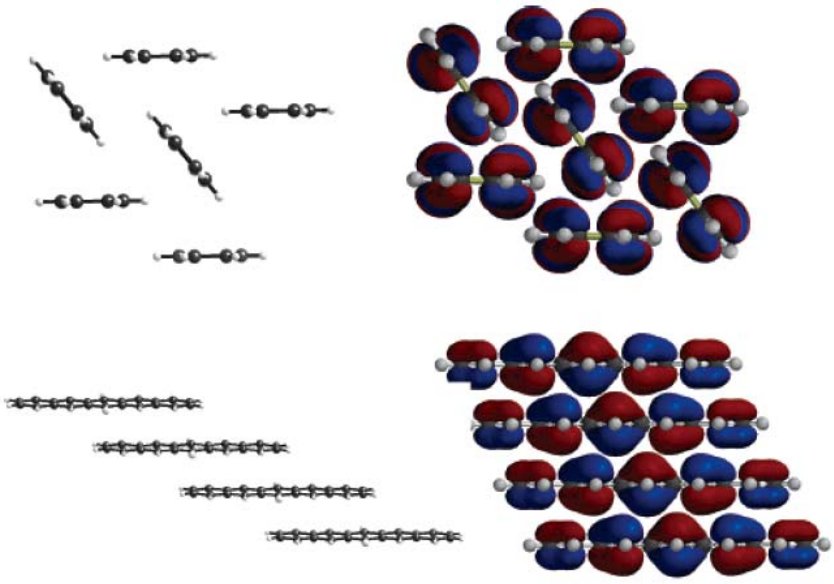

Figure 1.13. Herringbone (top) and π-stacking (bottom) arrangements of acenes, showing HOMO orbital interactions (Spartan '04, Wavefunction, Inc.). (Reproduced from Anthony.[83])

It is known that long-range molecular ordering is of paramount importance to obtain high charge mobilities in organic semiconductors, and in particular, the amount of π-orbital overlap is expected to have a strong influence on the mobility, as has been recently illustrated in structurally related pentacene derivatives.[84] To shed light on supramolecular organization a new oligoacene, single-crystal X-ray crystallography (SCXRD) is the most commonly used and powerful experimental technique. Although it is not an imaging technique, SCXRD allows the resolution of individual atoms and therefore a molecule as well as the solid packing structures. A combination of SCXRD and powder X-ray diffraction pattern (PXRD) could give us an insight into the exact film morphology made of the organic semiconducting materials.

1.5 Solution processed organic thin film field-effect transistors

Organic thin film field-effect transistors (OFETs) are particularly interesting as their fabrication processes are much less complex compared with conventional silicon technology, which involves high-temperature and high-vacuum deposition processes and sophisticated photolithographic patterning methods. In addition, the mechanical flexibility of organic materials makes them naturally compatible with plastic substrates for lightweight and foldable products. Since the report of the first organic field-effect transistor in 1986,[2] there has been great progress in both the materials' performance and development of new fabrication techniques. Especially, to meet the requirements of fabricating flexible, large area and low cost, several solution-processing techniques have been developed.

1.5.1 Solution processing techniques

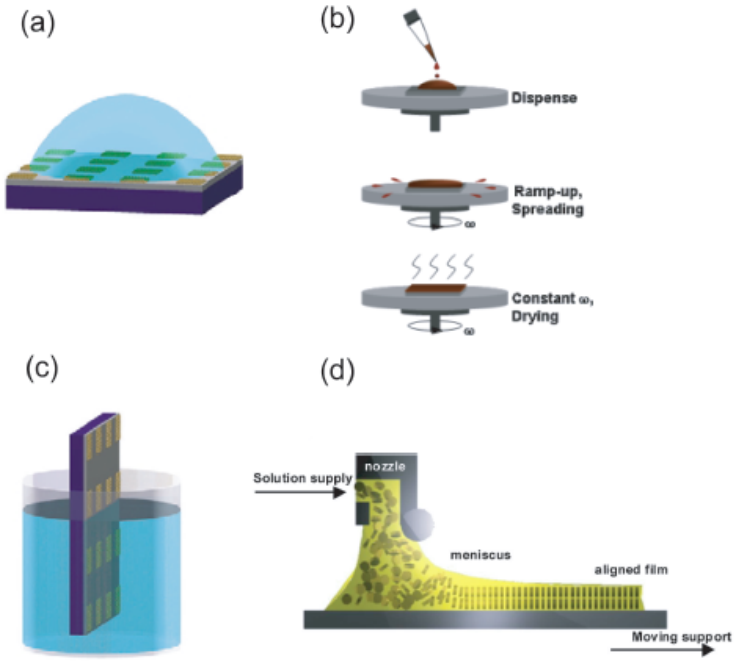

Figure 1.14. Schematic presentation of a) drop-casting, b) spin-coating, c) dipcoating, and d) zone-casting.

Solution-processing technique is more favourable to industrial application than

PVD due to its convenience and low cost in the large-area device fabrication. In the following, the most common solution deposition methods are presented.

The simplest method is drop-casting (**Figure 1.14a**). Here, the organic semiconductor is dissolved in an organic solvent. From this solution, drops are applied on the transistor substrate. During solvent evapour ation, the molecules form a thin film whose morphology depends on their tendency for self-assembly. Here, the rate of evapour ation can be controlled by the type of solvent used. However, the drawback of drop-casting is that the self-assembly cannot be controlled to take place in a specific direction but rather occurs randomly. This also holds for spin-coating. Here, the solution is deposited on the substrate and spun at a specific rate and time. During the spinning, the solvent evapour ates, leaving behind a thin film (**Figure 1.14b**). For this method, it is important to use a solvent with low boiling point such that it evapour ates fast enough during the rapid spinning process. Otherwise, the whole solution is spread away from the substrate without film formation. This technique is very simple and hence particularly interesting for producing cheap and large area plastic electronics. Nevertheless, like drop-casting, spin-coating also does not allow space for controlling film formation, that is, for directional alignment of the molecules.

To align the molecules in a thin film from solution, different methods exist. One simple technique is to immerse the substrate in a solution containing the dissolved compound and to take it out at a specific rate. More precisely, at the interface between the surface of the solution and the substrate, the solvent evapour ates, in this way enabling self-assembly and film formation of the compound. When the substrate is additionally moved out or dipped into the solution, the molecules in the best case align in the direction of this dipping direction. This method is hence termed dip-coating. (**Figure 1.14c**)[85],[86] Based on the same principle, another alternative to dip-coating is zone-casting (**Figure 1.14d**). Here, the advantage compared to dip-coating is that the substrate and solution temperature can be additionally changed together with the rate at which the solution is supplied to the substrate. These additional parameters facilitate the realization of a homogeneous ordered

film.[87]

1.5.2 Basic operation

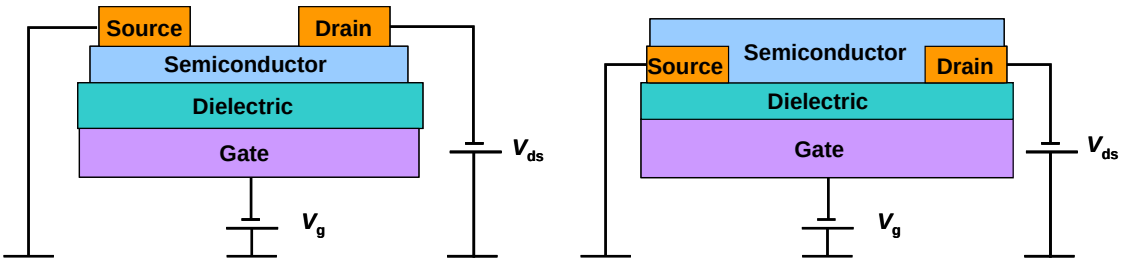

Figure 1.15. Layouts of organic field-effect transistors (OFETs) (left: top-contact; right: botom-contact)

An OFET is basically a capacitor, with a sandwich-like structure consisting of gate, dielectric, and semiconductor layers. Two metal contacts, the source and drain electrodes, are connected electrically to the semiconductor film, as shown schematically in **Figure 1.15**. This structure was initially developed for amorphous silicon transistors[88]. For testing purposes, a conductive substrate is used as mechanical support and also acts as gate electrode. Insulating oxide or polymeric insulators coated on the gate, with or without surface treatment, act as dielectric layers. OFETs are usually operated in accumulation mode, with the source always grounded. Without applied gate voltage V_g, the intrinsic conductivity of most organic semiconductors is low; when a source-drain voltage V_d is applied between two electrodes, very little current can flow through the semiconductor thin film, and the device is in the OFF state. When a gate voltage V_g is applied on the gate, a potential gradient is built in the capacitor structure, and charges then accumulate at the dielectric-semiconductor interface. Those charges are mostly mobile and lead to the formation of conducting channels between source and drain, charges move in response to the applied V_d, and the transistor is in the ON state.

Most organic semiconductors are not intentionally doped so that charges are actually injected and extracted from source and drain electrodes. As mentioned in section **1.2.1**, there is mismatch between the Fermi level of metal electrodes and

HOMO (LUMO) of *p*-channel (*n*-channel) semiconductors, which induces charge injection barriers. A nonzero V_g is required to shift the molecular orbital energy levels of semiconductors up or down so that the molecular orbitals become resonant with the Fermi level of metal electrodes and reduce the charge injection barriers. In addition, there are always trap states in the semiconductor film that are induced from impurities and defects (including grain boundaries), as well as molecules like H_2O and O_2 adsorbed from the environment. A nonzero V_g must be applied to fill these trap states before charges can be transported in semiconductor films. The threshold voltage V_t was defined to account for all those effects. In other words, V_t is the minimum gate voltage needed to turn on the organic thin-film transistor device.

1.6 Motivation for the present work

Along with their fast developing family members, organic semiconductors for FETs have long been particularly challenging to work with as most of them were either insoluble or very sensitive to air under ambient conditions. Insoluble materials preclude the use of solution deposition while air sensitivity requires manufacturing in an inert atmosphere; both of these restrictive requirements invariably lead to increased cost, thereby nullifying the fundamental economic advantage of OFETs. Therefore, how to develop new molecules to solve these problems will become part of the motivation of this thesis.

1.6.1 Development of novel pentacene analogues: the sulfur approach

1.6.1.1 What benefit can sulfur substitution bring to us?

Any progress in the design of new conjugated systems should be conducted by well-established structure-property relationships. As for the heteroacenes, much attention has been devoted to the combination of heavy chalcogen atoms (e.g. S, Se and Te) with organic π-conjugated cores.[89] In the designs of these systems, people have taken into account many molecular factors such as the expanded π-frameworks, the chalcogen effects, the frontier MO energy levels, high stability, and ready

accessibility.

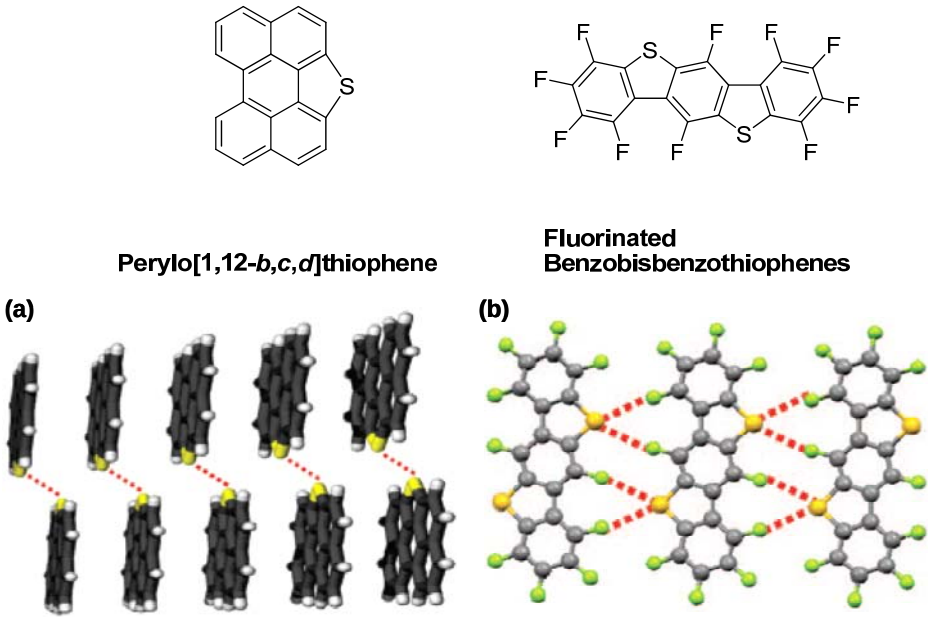

Figure 1.16. Packing diagram of compounds perylo[1,12-*b*,*c*,*d*]thiophene and fluorinated benzobisbenzothiophene, viewed from the direction showing inter-molecular contacts. (Reproduced from (a) Sun et al.[90a] and (b) Wang et al.[90b])

Chalcogen effects include short intermolecular contacts between chalcogens and other chalcogens or other heteroatoms which have been shown to influence molecular packing geometry in many structures of electroactive materials.[90] Hence the position and number of the chalcogen atom in the material can profoundly affect its properties. For example Sun et al.[90a] reported the X-ray crystal structure of compound perylo[1,12-*b*,*c*,*d*]thiophene (**Figure 1.16a**), a candidate for an organic field-effect transistor, showing the effect of inter-molecular S-S close contacts (marked in red dashed line) in the establishment of double-channel charge transport system. In another example reported by Wang et al,[90b] interactions between antiparallel, triangular F-S-F units along each side of the lath-shaped fluorinated benzobisbenzothiophene molecules, combined with face-to-face electrostatic attraction, preclude edge-to-face interactions. (**Figure 1.16b**) At the same time, the presence of polarizable chalcogen atoms could enhance intermolecular orbital overlap, which will facilitate intermolecular charge transfer. The synthetic chemist who can manipulate these interactions therefore has control over some fundamental

properties of the material.

Some others also reported that the terminal or internal thiophene rings of these heteroacenes help to form "*kinked*" substructure, which increase the benzenoid character of the conjugation systems, thus stabilizing the HOMO levels and increasing the HOMO–LUMO band gap.[37a],[91] As a consequence, such a chemical modification enhances the stability of the materials. In the end, the site-selective reactivity of thiophene makes these molecules amenable to derivatization, leading to improved solubility and processability.

1.6.1.2 Extended π-systems in conjugated oligomers for molecular electronics-the longer, the better?

People have recognized that the extension of π-systems in conjugated oligomers will naturally "create a contact between organic and macromolecular synthesis" and an intensive study of the physical properties of extended π-systems could make it "possible to control the optical, electrical and magnetic properties via the π-topology".[92] In 1993, Müllen raised the question "Extended π-systems in conjugated oligomers and polymers-the longer, the better?", and he has analyzed the question in four different approaches.[93] In this regards, in combination of my work, I have to continue thinking about the question in a similar situation: extended π-systems in conjugated oligomers for molecular electronics-the longer, the better?

For example, in the family of polycyclic aromatic hydrocarbons (PAH) acenes that is composed of linearly annulated benzene units, the energy gap decreases rapidly with the length of the conjugated π system, as seen in the bathochromic shift of the absorption spectra[94] and the decreasing singlet-triplet energy splitting.[95] This has two decisive and interrelated consequences: the acenes are turning from insulators to organic molecular *p-channel* semiconductors with increasing length, and at the same time they turn from prototypical stable aromatic compounds to reactive species.[96] The decrease in the reorganization energies,[97] the increase in the charge carrier mobilities, and the band widths make tetracene and the higher acenes potentially useful materials for organic electronic applications.[1c,d],[98],[99]

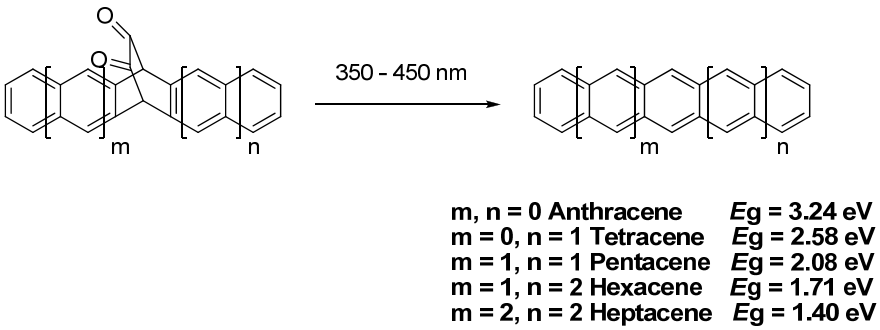

Scheme 1.17. Photogeneration of acenes from the diketones by Strating-Zwanenburg reaction and their decreasing band gaps with extended conjugation[100]

However, because of the quick increase of the reactivity of acenes, only the members up to the size of pentacene are characterized well. Hexacene already slowly decomposes in solution at room temperature.[101] The lack of experimental information on the thermal stability of heptacene led to several reinvestigations of the synthesis, and the common conclusion was that heptacene appears to be the limiting acene with respect to stability.[102] Though kinetically stabilized heptacene derivatives were obtained in 2005 by Payne et al.[103] and very recently by Chun et al.[104], Kaur et al.,[105] and Mondal et al.,[106] the synthesis of the parent heptacene was only reported recently by photochemical bisdecarbonylation, known as the Strating-Zwanenburg[107] reaction, of bridged α-diketones and should be stabilized by matrices.[108] (**Scheme 1.17**)

From the development of PAH acenes, we can see that besides the more and more tedious synthesis procedures, any meaningful gain in electronic properties (e.g. charge carrier mobilities) are totally undermined by the deterioration of solubility and environmental stability.

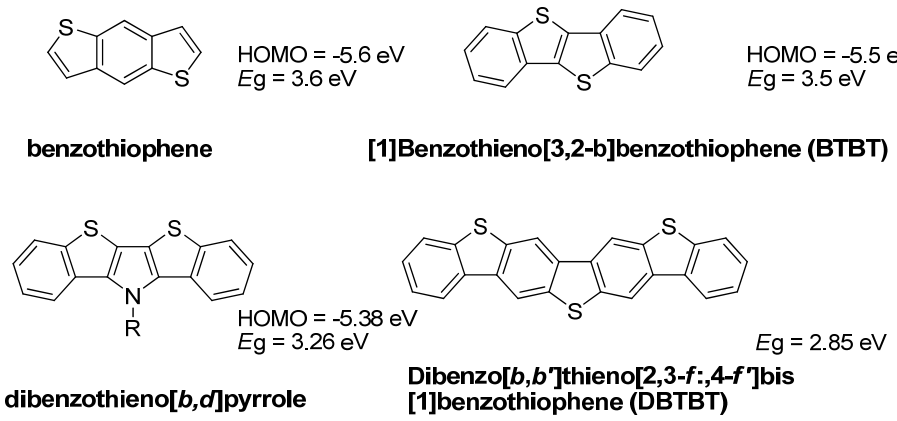

Figure 1.17. Thiophene fused heteroacenes with increasing conjugation and their band gaps

On the other hand, several groups have worked on the thiophene containing heteroacenes from benzodithiophene (two thiophenes out of three fused rings) to DBTBT (three thiophenes out of seven fused rings). [35],[37m],[65a],[109] (**Figure 1.17**) Upon comparison of the π-topology of these molecules, it appeared that despite the increase in the length of the conjugated π system, the energy gaps do not decrease so much as the case of PAH. One can see from **Figure 1.17** that the heteroheptacene dibenzo[*b,b'*]thieno[2,3-*f'*:,4-*f'*]bis[1]benzothiophene (**DBTBT**) first reported by Leuninger et al. showed an even larger band gap than that of PAH tetracene.[37m] The HOMO levels also increase very slowly with the extending skeleton.

It is obvious that the introduction of heteroatoms like sulfur could stabilize the highly conjugated acenes by widening their band gaps even up to seven fused rings. And this is in agreement with the observation by Matzger and Takimiya et al.. Taking the benefits of sulfur substitution, one can make use of both the advantage of a highly extended π-system and the S-S interaction to meet the requirements of the applications. So here the question arises: Extended π-systems in conjugated oligomers for molecular electronics-the longer, the more sulfur, the better?

1.6.2 Our approach toward design and synthesis of new thiophene fused heteroacenes

In our design principle of new thiophene fused heteropentacenes, we opted for symmetrically fused thiophene rings around a central benzene ring. (**Figure 1.18**) The number of thiophene rings could be adjusted depending on the choice of the precursor. Among the synthetic methods summarized in section 1.3, we found that the triflic acid induced electrophlic substitution (1.3.2.1) is the best choice to realize the desired structure, due to the easy availability of the methylsulfoxide containing precursor and much shorter synthetic route compared with other methods. Moreover, the advantage of using this ring-closing method is the possibility of introducing and varying solubilizing alkyl groups at the end of the molecules, which will facilitate most of the solution processing techniques.

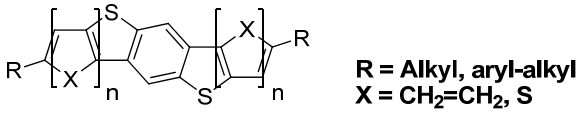

Figure 1.18. General structure of new thiophene fused heteroacenes

In view of the reaction condition of the chosen method, two possible precursors (**I** and **II**) are suggested as shown in **Figure 1.19**.

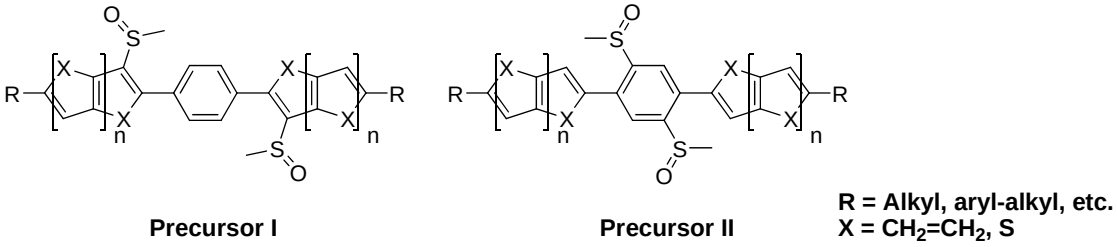

Figure 1.19. Precursors designed for the symmetrically fused thiophene containing heteroacenes

The precursor I was soon abandoned due to the possibility of giving isomers and incomplete ring-closing reaction. The presence of isomers raised the difficulty of purification, moreover, the partially ring-closed semi-finished products need to be reacted again. This could be due to the strong electron-withdrawing property of

the sulfonyl group bonded to the phenyl ring. The electrophilic substitution by the protonated sulfoxide (hydroxymethyl-phenylsulfonio) group to the electron-poor phenyl ring attached to a sulfonio group was hard to proceed.[110] Therefore, we chose precursor II for the synthesis of final heteroacenes.

Enlightened by the synthesis of **DBTBT**, precursor I is modified and employed to make further extended π-conjugated systems. (**Figure 1.20**) This is realized simply by changing the central π framework from a benzene ring to larger π systems, for example: carbazole, dithieno[3,2-*b*:2',3'-*d*]pyrrole (**DTP**) and cyclopenta-[2,1-*b*:3,4-*b*']dithiophene (**CPDT**). The attempt to expand the π-conjugated framework over seven rings, as opposed to the common heterotetracenes and heteropentacene, is expected to lead to improved intermolecular packing and better π-overlap. So far, only a few examples of further extended ladder-type molecules containing fused heterocycles (e.g. thiophene or/and pyrrole) have been reported,[37i,k],[111] presumably due to the difficulty in the establishment of efficient and practical synthetic protocols.

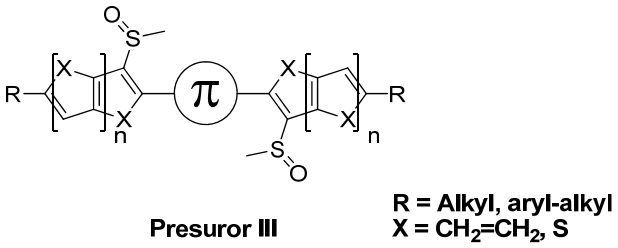

Figure 1.20. Precursor designed for the higher heteroacenes

Hereby, based on precursor III, the triflic acid induced electrophlic substitution reaction will be used to construct new heteroheptacenes, which have the same coplanar structure as PAH heptacene but much increased environmental stability and more tunable structural as well as optoelectronic-properties. The study may shed some light on both the advantage and limitation of the synthetic method as well as the structure-property relationship of the new heteroheptacenes.

1.7 References

[1] Pope, M.; Swenberg, C. E., Electronic Processes in Organic Crystals and Polymers, 2nd ed., *Oxford University Press*, New York, **1999**.

[2] Koezuka, H., Tsumura, A., and Ando, T., *Synth. Met.* **1987**, *18*, 699-704.

[3] Lilienfeld, J. E. Method and appara- tus for controlling electric currents, **1926**, US patent 1745175.

[4] Sze, S.M., Semiconductor Devices: Physics and Technology, Wiley, New York, **1985**, *6*, pp 216, 507.

[5] Moore, G. E., *IEEE IEDM Tech. Dig.* **1975**, 11.

[6] Bao, Z. N.; Rogers, J. A.; Katz, H. E., *J. Mater. Chem.* **1999**, *9*, 1895-1904.

[7] (a) Kawase, T.; Shimoda, T.; Newso- me, C.; Sirringhaus, H.; Friend, R. H. *Thin Solid Films* **2003**, *438*, 279-287. (b) Sirringhaus, H.; Kawase, T.; Friend, R. H.; Shimoda, T.; Inbasekaran, M.; Wu, W.; Woo, E. P. *Science* **2000**, *290*, 2123. (c) Kawase, T.; Sirringhaus, H.; Friend, R. H.; Shimoda, T. *Adv Mater* **2001**, *13*, 1601. (d) Arias, A. C.; Ready, S. E.; Lujan, R.; Wong, W. S.; Paul, K. E.; Salleo, A.; Chabinyc, M. L.; Apte, R.; Street, R. A.; Wu, Y.; Liu, P.; Ong, B. *Appl Phys Lett* **2004**, *85*, 3304-3306. (e) Chabinyc, M. L.; Salleo, A., *Chem. Mater.*, **2004**, *16*, 4509-4521.

[8] (a) Bao, Z. N.; Lovinger, A. J.; Dodabalapur, A., *Adv. Mater.*, **1997**, *9*, 42. (b) Garnier, F.; Hajlaoui, R.; Yassar, A.; Srivastava, P. *Science* **1994**, *265*, 1684-1686.

[9] (a) Gates, B. D.; Xu, Q. B.; Stewart, M.; Ryan, D.; Willson, C. G.; Whitesides, G. M. *Chem Rev* **2005**, *105*, 1171-1196. (b) Xia, Y. N.; Whitesides, G. M., *Angew. Chem. Int. Ed.*, **1998**, *37*, 551-575.

[10] (a) Rogers, J. A.; Bao, Z.; Baldwin, K.; Dodabalapur, A.; Crone, B.; Raju, V. R.; Kuck, V.; Katz, H.; Amundson, K.; Ewing, J.; Drzaic, P. *P Natl Acad Sci USA* **2001**, *98*, 4835-4840. (b) Wisnieff, R., *Nature* , **1998**, *394*, 225. (c) Comiskey, B.; Albert, J. D.; Yoshizawa, H.; Jacobson, J. *Nature* **1998**, *394*, 253-255. (d) Gelinck, G. H.; Huitema, H. E. A.; Van Veenendaal, E.; Cantatore, E.; Schrijnemakers, L.; Van der Putten, J. B. P. H.; Geuns, T. C. T.; Beenhakkers, M.; Giesbers, J. B.; Huisman, B. H.; Meijer, E. J.; Benito, E. M.; Touwslager, F. J.; Marsman, A. W.; Van Rens, B. J. E.; De Leeuw, D. M. *Nat Mater* **2004**, *3*, 106-110.

[11] (a) Dodabalapur, A.; Laquindanum, J.; Katz, H. E.; Bao Z. *Appl. Phys. Lett.*, **1996**, *69*, 4227-4229. (b) Crone, B. K.; Dodabalapur, A.; Sarpeshkar, R.; Filas, R. W.; Lin, Y. Y.; Bao, Z.; O'Neill, J. H.; Li, W.; Katz, H. E. *J Appl Phys* **2001**, *89*, 5125-5132. (c) Drury, C. J.; Mutsaers, C. M. J.; Hart, C. M.; Matters, M.; de Leeuw, D. M. *Appl Phys Lett* **1998**, *73*, 108-110.

[12] (a) Zhu, F. R.; Hao, X. T.; Soo, O. K.; Li, Y. Q.; Tan, L. W. *P Ieee* **2005**, *93*, 1440-1446. (b) Carts-Powell, Y. *Laser Focus World* **2005**, *41*, 40.

[13] (a) Yamaguchi, S.; Xu, C. H.; Okamoto, T. *PureAppl. Chem.* **2006**, *78*, 721-730; (b) Kunugi, Y.; Takimiya, K.; Yamane, K.; Yamashita, K.;

Aso, Y.; Otsubo, T. *Chem. Mater.* **2003**, *15*, 6-7; (c) Dimitrakopoulos, C. D.; Malenfant, P. R. L., *Adv. Mater.* **2002**, *14*, 99-117

[14] (a) Marcus. R. A. *J. Chem. Phys.* **1956**, *24*, 966-978. (b) Marcus. R. A. *Discuss. Faraday Soc.* **1960**, *29*, 21. (c) Marcus R. A.; Sutin. N. *Biochim. Biophys. Acta.* **1985**, *811*, 265-322.

[15] Lang, N. D.; Kohn, W. *Physical Review B* **1971**, *3*, 1215-1223.

[16] Hutchison, G. R.; Ratner, M. A.; Marks, T. J. *J. Am. Chem. Soc.* **2005**, *127*, 16866-16881.

[17] (a) Mcculloch, I.; Heeney, M.; Bailey, C.; Genevicius, K.; Macdonald, I.; Shkunov, M.; Sparrowe, D.; Tierney, S.; Wagner, R.; Zhang, W. M.; Chabinyc, M. L.; Kline, R. J.; Mcgehee, M. D.; Toney, M. F. *Nat. Mater.* **2006**, *5*, 328-333. (b) Bao, Z. N.; Lovinger, A. *J. Chem. Mater.* **1999**, *11*, 2607-2612. (c) Ong, B. S.; Wu, Y. L.; Liu, P. *Proc. IEEE* **2005**, *93*, 1412-1419.

[18] Li, Y.; Wu, Y.; Ong, B. S. *Macromolecules* **2006**, *39*, 6521 -6527.

[19] (a) Kim, Y. M.; Lim, E.; Kang, I. N.; Jung, B. J.; Lee, J.; Koo, B. W.; Do, L. M.; Shim, H. K. *Macromol.* **2006**, *39*, 4081-4085. (b) Chen, M. X.; Crispin, X.; Perzon, E.; Andersson, M. R.; Pullerits, T.; Andersson, M.; Inganas, O.; Berggren, M. *Appl. Phys. Lett.* **2005**, *87*, 52105.

[20] Veres, J.; Ogier, S. D.; Leeming, S. W.; Cupertino, D. C.; Khaffaf, S. M. *Adv. Funct. Mater.* **2003**, *13*, 199-204.

[21] Müllen, K.; Wegner, G. *Electronic Materials: The Oligomer Approach*, Wiley-VCH (**1998**).

[22] (a) Horowitz, G.; Peng, X.; Fichou, D.; Garnier, F. *Synth. Met.* **1992**, *51*, 419-424. (b) Servet, B.; Horowitz, G.; Ries, S.; Lagorsse, O.; Alnot, P.; Yassar, A.; Deloffre, F.; Srivastava, P.; Hajloui, R.; Lang, P.; Garnier, F.; *Chem. Mater.* **1994**, *6*, 1809-1815. (c) Dodabalapur, A.; Torsi, L.; Katz, H. E.; *Science* **1995**, *268*, 270-271. (d) Garnier, F.; Yassar, A.; Hajlaoui, R.; Horowitz, G.; Dellofre, F.; Servet, S.; Alnot, R. P. *J. Am. Chem. Soc.* **1993**, *115*, 8716-8721. (e) Katz, H. E.; Dodabalapur, A.; Torsi, L.; Elder, D. *Chem. Mater.* **1995**, *7*, 2238-2240. (f) Dimitrakopoulos, C. D.; Furman, B. K.; Graham, T.; Hegde, S.; Purushothaman, S. *Synth. Met.* **1998**, *92*, 47-52.

[23] (a) Schmidt, R.; Gottling, S.; Leusser, D.; Stalke, D.; Krause, A. M.; Wurthner, F. J. *Mater. Chem.* **2006**, *16*, 3708-3714. (b) Anthony, J. E.; Eaton, D. L.; Parkin, S. R. *Org. Lett.* **2002**, *4*, 15-18.

[24] (a) Mushrush, M.; Facchetti, A.; Lefenfeld, M.; Katz, H. E.; Marks, T. J. *J. Am. Chem. Soc.* **2003**, *125*, 9414-9423. (b) Facchetti, A.; Letizia, J.; Yoon, M. H.; Mushrush, M.; Katz, H. E.; Marks, T. J. *Chem. Mater.* **2004**, *16*, 4715-4727.

[25] Hadziioannou, G.; van Hutten, P. F. Semiconducting Polymers: Chemistry, Physics and Engineering, Wiley-VCH: Weinheim, **2000**.

[26] Roncali, J. In Handbook of Conducting Polymers, 2nd ed.; Skotheim, T. A., Elsenbaumer, R. L., Reynolds, J. R., Eds.; Marcel Dekker: New York, **1998**; Chapter 12.

[27] Kelley, T. W.; Boardman, L. D.; Dunbar, T. D.; Muyres, D. V.; Pellerite, M. J.; Smith, T. Y. P. *J. Phys. Chem. B* **2003**, *107*, 5877-5881.

[28] Klauk, H.; Halik, M.; Zschieschang, U.; Schmid, G.; Radlik, W.; Weber, W. *J. Appl. Phys*. **2002**, *92*, 5259-5263.

[29] Afzali, A.; Breen, T. L.; Kagan, C. R. *Chem. Mater*. **2002**, *14*, 1742-1746.

[30] (a) Moon, H.; Zeis, R.; Borkent, E. J.; Besnard, C.; Lovinger, A. J.; Siegrist, T.; Kloc, C.; Bao, Z. N. *J. Am. Chem. Soc*. **2004**, *126*, 15322-15323. (b) Curtis, M. D.; Cao, J.; Kampf, J. W. *J. Am. Chem. Soc*. **2004**, *126*, 4318-4328. (c) Brédas, J. L.; Calbert, J. P.; da Silva Filho, D. A.; Cornil, J. *Proc. Natl. Acad. Sci. U.S.A*. **2002**, *99*, 5804-5809. (d) Cornil, J.; Beljonne, D.; Calbert, J. P.; Brédas, J. L. *Adv. Mater*. **2001**, *13*, 1053-1067.

[31] Yamada, M.; Ikemoto, I.; Kuroda, H. *Bull. Chem. Soc. Jpn*. **1988**, *61*, 1057- 1062.

[32] (a) Payne, M. M.; Parkin, S. R.; Anthony, J. E.; Kuo, C. C.; Jackson, T. N. *J. Am. Chem. Soc*. **2005**, *127*, 4986-4987. (b) Gundlach, D. J.; Royer, J. E.; Park, S. K.; Subramanian, S.; Jurchescu, O. D.; Hamadani, B. H.; Moad, A. J.; Kline, R. J.; Teague, L. C.; Kirillov, O.; Richter, C. A.; Kushmerick, J. G.; Richter, L. J.; Parkin, S. R.; Jackson, T. N.; Anthony, J. E. *Nat. Mater*., **2008**, 7, 216-221. (c) Hamilton, R.; Smith, J.; Ogier, S.; Heeney, M.; Anthony, J. E.; McCulloch, I.; Veres, J.; Bradley, D. D. C.; Anthopoulos, T. D. *Adv. Mater*., **2009**, *21*, 1166-1171.

[33] Li, Y. N.; Wu, Y. L.; Gardner, S.; Ong, B. S. *Adv. Mater*. **2005**, *17*, 849-853.

[34] Wakim, S.; Bouchard, J.; Simard, M.; Drolet, N.; Tao, Y.; Leclerc, M. *Chem. Mater*. **2004**, *16*, 4386-4388.

[35] Ebata, H.; Izawa, T.; Miyazaki, E.; Takimiya, K.; Ikeda, M.; Kuwabara, H.; Yui, T. *J. Am. Chem. Soc*. **2007**, *129*, 15732-15733.

[36] Nakagawa, T.; Kumaki, D.; Nishida, J.; Tokito, S.; Yamashita, Y. *Chem. Mater*. **2008** *20*, 2615-2617.

[37] (a) Yamamoto, T.; Takimiya, K. *J. Am. Chem. Soc*. **2007**, *129*, 2224-2225. (b) Okamoto, T.; Kudoh, K.; Wakamiya, A.; Yamaguchi, S. *Chem. Eur. J*. **2007**, *13*, 548-556. c) Rong, G.; Ahmed, H.; Wim, D. *Synlett* **2006**, 1535-1538. (d) Takimiya, K.; Ebata, H.; Sakamoto, K.; Izawa, T.; Otsubo, T.; Kunugi, Y. *J. Am. Chem. Soc*. **2006**, *128*, 12604-12605. (e) Takimiya, K.; Kunugi, Y.; Konda, Y.; Ebata, H.; Toyoshima, Y.; Otsubo, T. *J. Am. Chem. Soc*. **2006**, *128*, 3044-3050. (f) Xiao, K.; Liu, Y. Q.; Qi, T.; Zhang, W.; Wang, F.; Gao, J. H.; Qiu, W. F.; Ma, Y. Q.; Cui, G. L.; Chen, S. Y.; Zhan, X. W.; Yu, G.; Qin, J. G.; Hu, W. P.; Zhu, D. B. *J. Am. Chem. Soc*. **2005**, *127*, 13281-13286. (g) Okamoto, T.; Kudoh, K.; Wakamiya, A.; Yamaguchi, S. *Org. Lett*. **2005**, *7*, 5301-5304. (h) Wu, Y. L.; Li, Y. N.; Gardner, S.; Ong, B. S. *J. Am. Chem. Soc*. **2005**, *127*, 614-618. (i) Wakim, S.; Bouchard, J.; Blouin, N.; Michaud, A.; Leclerc, M. *Org. Lett*. **2004**, *6*, 3413-3416. (j) Payne, M. M.; Odom, S. A.; Parkin, S. R.; Anthony, J. E. *Org. Lett*. **2004**, *6*, 3325-3328. (k) Bouchard, J.; Wakim, S.; Leclerc, M. *J. Org. Chem*. **2004**, *69*, 5705-5711. (l) Yudina, L. N.; Bergman, J. *Tetrahedron* **2003**, *59*, 1265-1275. (m) Sirringhaus, H.; Friend, R. H.; Wang, C.;

Leuninger, J.; Müllen, K. *J. Mater. Chem.* **1999**, *9*, 2095-2101. (n) Laquindanum, J. G.; Katz, H. E.; Lovinger, A. J. *J. Am. Chem.Soc.* **1998**, *120*, 664-672.

[38] (a) Naber, R. C. G.; Tanase, C.; Blom, P. W. M.; Gelinck, G. H.; Marsman, A. W. *Nat.Mater.* **2005**,*4*, 243-248. (b) Huang, C.; West, J. E.; Katz, H. E. *Adv. Funct. Mater.* **2007**, *17*, 142-153. (c) Crouch, D. J.; Skabara, P. J.; Heeney, M.; McCulloch, I.; Coles, S. J.; Hursthouse, M. B. *Chem. Commun.* **2005**, *11*, 1465-1467. (d) Mas-Torrent, M.; Hadley, P.; Bromley, S. T.; Crivillers, N.; Veciana, J.; Rovira, C. *Appl.Phys. Lett.* **2005**, *86*, 012110. (e) Mori, H.; Kamiya, M.; Haemori, N.; Suzuki, H.; Tanaka, S. *J. Am. Chem. Soc.* **2002**, *124*, 1251-1260. (f) Ponomarenko, S. A.; Kirchmeyer, S.; Halik, M.; Klauk, H.; Zschieschang, U. *Synth. Met.* **2005**, *149*, 231-235. (g) Takimiya, K.; Kunugi, Y.; Toyoshima, Y.; Otsubo, T. *J.Am.Chem.Soc.***2005**, *127*, 3605-3612.

[39] (a) Du, C. Y.; Guo, Y. L.; Liu, Y. Q. ; Qiu, W. F. ; Zhang, H. J. *Chem. Mater.* **2008**, *20*, 4188-4190. (b) Kashiki, T.; Miyazaki, E.; Takimiya, K. *Chem. Lett.*, **2008**, *37*, 284-285. (c) Mamada, M.; Nishida, J. I.; Kumaki, D.; Tokito, S.; Yamashita, Y. *J. Mater. Chem.* **2008**, *18*, 3442-3447. (d) Tang, M. L.; Reichardt, A. D.; Miyaki, N.; Stoltenberg, R. M.; Bao, Z. N. *J. Am. Chem. Soc.* **2008**, *130*, 6064-6065. (e) Tang, M. L.; Reichardt, A. D.; Okamoto, T.; Miyaki, N.; Bao, Z. A. *Adv. Funct. Mater.* **2008**, *18*, 1579-1585. (f) Tang, M. L.; Reichardt, A. D.; Siegrist, T.; Mannsfeld, S. C. B.; Bao, Z. N. *Chem. Mater.* **2008**, *20*, 4669-4676. (g) Yamada, T.; Hasegawa, T.; Hiraoka, M.; Matsui, H.; Tokura, Y.; Saito, G. *Appl. Phys. Lett.* **2008**, *92*, 233306.

[40] (a) Newman, C. R.; Friebie, C. D.; Da Silva Filho, D. A.; Brédas, J.; Ewbank, P. C.; Mann, K. R. *Chem. Mater.* **2004**, *46,* 4436-4451. (b) Zaumseil, J.; Sirringhaus, H. *Chem. Rev.* **2007**, *107*, 1296-1323.

[41] Ling, M. M.; Erk, P.; Gomez, M.; Koenemann, M.; Locklin, J.; Bao, Z. N. *Adv. Mater.* **2007**, *19*, 1123-1127

[42] Oh, J. H.; Liu, S.; Bao, Z. N.; Schmidt, R.; Wurthner, F. *Appl. Phys.Lett.* **2007**, *91*, 212107.

[43] Schmidt, R.; Ling, M. M.; Oh, J. H.; Winkler, M.; Konemann, M. *Adv. Mater.* **2007**, *19*, 3692-3695.

[44] Brown, A. R.; de Leeuw, D. M.; Lous, E. J.; Havinga, E. E. *Synth. Met.* **1994**. *66*, 257-261.

[45] (a) Seki, K.; Kanai, K. *Mol. Cryst. Liq. Cryst.* **2006**, *455*, 145-181. (b) Seki, K. *Mol. Cryst. Liq. Cryst.* **1989**, *171*, 255-270.

[46] Sze, S. M. (1964). *Physics of Semiconductor Devices*. Wiley.

[47] Meng, H.; Zheng, J.; Lovinger, A. J.; Wang, B.; Van Patten, P. G.; Bao, Z. N. *Chem. Mater.* **2003**, *15*, 1778-1787

[48] Fichou, D. *Handbook of Oligo- and Polythiophenes*; Wiley-VCH, New York, **1998**.

[49] Maliakal, A.; Raghavachari, K.; Katz, H. E.; Siegrist, C. T. *Chem. Mater.* **2004**, *16*, 4980-4986.

[50] Bromley, S. T.; Mas-torrent, M.; Hadley, P. *J. Am. Chem. Soc.* **2004**, *126*, 6544-6545.

[51] Sakamoto, Y.; Suzuki, T.; Kobayashi, M.; Gao, Y.; Inoue, Y.; Tokito, S. *Mol. Cryst. Liq. Cryst.* **2006**, *444*, 225-232.

[52] (a) Kuo, M. Y.; Chen, H. Y.; Cao, I. *Chem. Eur. J.* **2007**, *13*, 4750-4758. (b) Chen, H. Z.; Ling, M. M.; Mo, X.; Shi, M. M.; Wang, M.; Bao, Z. N. *Chem. Mater.* **2007**, *19*, 816-824. (c) Tang, Q.; Li, H.; Liu, Y.; Hu, W *J. Am. Chem. Soc.* **2006**, *128*, 14634-14639. (d) Anthopoulos, T. D.; Kooistra, F. B.; Wondergem, H. J.; Kronholm, D.; Hummelen, J. C.; de Leeuw, D. M. *Adv. Mater.* **2006**, *18*, 1679-1684. (e) Haddock, J. N.; Zhang, X.; Domercq, B.; Kippelen, B. *Org. Electron.* **2005**, *6*, 182-187. (f) Yoon, M. H.; DiBenedetto, S.; Facchetti, A.; Marks, T. J. *J. Am. Chem. Soc.* **2005**, *127*, 1348-1349. (g) Jones, B. A.; Ahrens, M. J.; Yoon, M. H.; Facchetti, A.; Marks, T. J.; Wasielewski, M. R. *Angew. Chem. Int. Ed.* **2004**, *43*, 6363-6366. (h) Chesterfield, R. J.; McKeen. J. C.; Newman, C. R.; Ewbank, P. C.; da Silva Filho, D. A.; Brédas, J. L.; Miller, L. L.; Mann, K. R.; Frisbie, C. D. *J. Phys. Chem. B* **2004**, *108*, 19281-19292.

[53] Wang, Z.; Kim, C.; Facchetti, A.; Marks, T. J. *J. Am. Chem. Soc.* **2007**, *129*, 13362-13363.

[54] (a) Yoon, M. H.; Kim, C.; Facchetti, A.; Marks, T. J. *J. Am. Chem. Soc.* **2006**, *128*, 12851-12869. (b) Chua, L. L.; Zaumseil, J.; Chang, J. F.; Ou, E. C. W.; Ho, P. K. H.; Sirringhaus, H.; Friend, R. H. *Nature* **2005**, *434*, 194-199

[55] Yoon, M. H.; Facchetti, A.; Stern, C. E.; Marks, T. J. *J. Am. Chem. Soc.* **2006**, *128*, 5792-5801.

[56] Yamamoto, K.; Shouji, E.; Nishide H.; Tsuchida, E. *J. Am. Chem. Soc.*, **1993**, *115*, 5819-5820.

[57] Tsuchida, E.; Shouji E.; Yamamoto, K. *Macromolecules*, **1993**, *26*, 4113-4117.

[58] Wang, L.; Soczka-Guth, T.; Havinga E.; Müllen, K. *Angew. Chem. Int. Ed.*, **1996**, *35*, 1495-1497.

[59] Leuninger, J.; Wang, C.; Soczka-Guth, T.; Enkelmann, V.; Pakula, T.; Müllen, K. *Macromolecules*, **1998**, *31*, 1720-1727.

[60] Leuninger, J.; Uebe, J.; Salbeck, J.; Gherghel, L.; Wang, C.; Müllen, K. *Synth. Met.*, **1999**, *101*, 681-684.

[61] Mancuso, A. J.; Swern, D. *Synthesis*, **1981**, 165-185.

[62] (a) Haryono, A.; Miyatake, K.; Natori, J.; Tsuchida, E. *Macromolecules*. **1999**, *32*, 3146-3149. (b) Miyatake, K.; Hay, A. S.; Mitsuhashi, F.; Tsuchida, E. *Macromolecules*. **2001**, *34*, 2385-2388. (c) Oyaizu, K.; Iwasaki, T.; Tsukahara, Y.; Tsuchida, E. *Macromolecules*. **2004**, *37*, 1257-1270.

[63] Du, C.; Ye, S.; Chen, J.; Guo, Y.; Liu, Y.; Lu, K.; Liu, Y.; Qi, T.; Gao, X.; Shuai, Z.; Yu, G. *Chem. Eur. J.* **2009**, *15*, 8275-8282.

[64] Sashida, H.; Sadamori, K.; Tsuchiya, T. *Synth. Commun.* **1998**, *28*, 713-727.

[65] (a) Takimiya, K.; Konda, Y.; Ebata, H.; Niihara, N.; Otsubo, T. *J. Org. Chem.* **2005**, *70*, 10569-10571. (b) Takimiya, K.; Konda, Y.; Ebata, H.; Otsubo, T.; Kunugi, Y. *Mol. Cryst. Liq. Cryst.* **2006**, *455*, 361-365.

[66] Ivanchikova, I. D.; Lebedeva, N. I.;

Shvartsberg, M. S. *Synthesis*, **2004**, 2131-2134.

[67] Wang, Y.; Parkin, S. R.; Gierschner, J.; Watson, M. D. *Org. Lett.* **2008**, *10*, 3307-3310.

[68] Yue, D.; Larock, R. C. *J. Org. Chem.* **2002**, *67*, 1905-1909.

[69] Hisburg, O. *Ber.* **1910**, *43*, 901.

[70] Wynberg, H.; Kooreman, H. *J. Am. Chem.Soc.* **1965**, *899*, 1739-1742.

[71] Jimenez, R. P.; Parvez, M.; Suther- land, T. C.; Viccars, J. *Eur. J. Org. Chem.* **2009**, ASAP.

[72] (a) Scherf, U.; Müllen, K. *Makromole. Chem. Rapid Commun.* **1991,** *12,* 489-497. (b) Freund, T.; Scherf, U.; Müllen, K. *Angew. Chem. Int. Ed.* **1995,** *33,* 2424-2426.

[73] (a) Ye, S.; Liu, Y.; Di, C. A.; Xi, H.; Wu, W.; Wen, Y.; Lu, K.; Du, C.; Liu , Y.; Yu, G. *Chem. Mater.* **2009**, *21*, 1333-1342. (b) Wu, Y.; Zhang, J.; Fei, Z.; Bo, Z. *J. Am. Chem. Soc.* **2008**, *130*, 7192-7193.

[74] (a) Pouchain, L.; Alévêque, O.; Nico las, Y.; Oger, A.; Le Régent, C.; Allain, M.; Blanchard, P.; Roncali, J. *J. Org. Chem.* **2009**, *74*, 1054-1064. (b) Wong, K.; Chao, T.; Chi, L.; Chu, Y.; Balaiah, A.; Chiu, S.; Liu, Y.; Wang, Y. *Org. lett.* **2006**, *8*, 5033-5036.

[75] Merlet, S.; Birau, M.; Wang, Z. Y. *Org. lett.* **2002**, *4*, 2157-2159.

[76] Mitschke, U.; Bäuerle, P. *J. Chem. Soc., Perkin Tran. 1* **2001**, 740-753.

[77] Usta, H.; Facchetti, A.; Marks, T. J. *Org. lett.* **2008**, *10*, 1385-1388.

[78] Zhao, C.; Zhang, Y.; Ng, M. *J. Org. Chem.* **2007**, *72*, 6364-6371.

[79] Cadogan, J. I. G.; Cameron-Wood, M.; Mackie, R. K.; Searle, R. J. G. *J. Chem. Soc.* **1965,** 4831-4837.

[80] Dierschke, F.; Grimsdale, A. C.; Müllen, K. *Synthesis*. **2003**, 2470-2472.

[81] Balaji, G.; Shim, W. L.; Parames- waran, M.; Valiyaveettil, S., *Org. lett.* **2009**, *11*, 4450-4453.

[82] For an excellent description of solid-state aromatic interactions, see: Ref. 30b

[83] Anthony, J. E. *Chem. Rev.* **2006**, *106*, 5028-5048.

[84] Sheraw, C. D.; Jackson, T. N.; Eaton, D. L.; Anthony, J. E. Adv. Mater. 2003, 15, 2009-2011.

[85] Kastler, M.; Pisula, W.; Wasserfallen, D.; Pakula, T.; Müllen, K. *J. Am. Chem. Soc.* **2005**, *127*, 4286-4296.

[86] Pal, B. N.; Trottman, P.; Sun, J.; Katz, H. E. *Adv. Funct. Mater.* **2008**, *18*, 1832-1839.

[87] Pisula, W.; Menon, A.; Stepputat, M.; Lieberwirth, I.; Kolb, U.; Tracz, A.; Sirringhaus, H.; Pakula, T.; Müllen, K. *Adv. Mater.* **2005**, *17*, 684-689.

[88] Weimer, P. *Proc. Inst. Radio Eng.* **1962**, *50*, 1462-1469.

[89] Takimiya, K.; Kunugi, Y.; Konda, Y.; Niihara, N.; Otsubo, T. *J. Am. Chem. Soc.* **2004**, *126*, 5084-5085.

[90] (a) Sun, Y.; Tan, L.; Jiang, S.; Qian, H.; Wang, Z.; Yan, D.; Di, C.; Wang, Y.; Wu, W.; Yu, G.; Yan, S.; Wang, C.; Hu, W.; Liu, Y.; Zhu, D. *J. Am. Chem. Soc.* **2007**, *129*, 1882-1883. (b) Subramanian, S.; Park, S. K.; Parkin, S. R.; Podzorov, V.; Jackson, T. N.; Anthony, J. E. *J. Am. Chem. Soc.* **2008**, *130*, 2706-2707.

[91] Zhang, X.; Matzger, A. J. *J. Org. Chem.* **2003**, *68*, 9813-9815.

[92] Müllen, K. *Pure and Applied Chem- istry*. **1993**, *65*, 89-96.

[93] ibid

[94] Clar, E. *Polycyclic Hydrocarbons*; Aca demic Press: New York, **1964**; Vol. 1.

[95] Hachmann, J.; Dorando, J. J.; Aviles, M.; Chan, G. K. L. *J. Chem. Phys*. **2007**, *127*, 134309.

[96] Biermann, D.; Schmidt, W. *J. Am. Chem. Soc*. **1980**, *102*, 3163-3173.

[97] Winkler, M.; Houk, K. N. *J. Am. Chem. Soc.* **2007**, *129*, 1805-1815.

[98] (a) Bendikov, M.; Wudl, F.; Perepi- chka, D. F. *Chem. Rev*. **2004**, *104*, 4891-4946. (b) Würthner, F.; Schmidt, R. *Chem. Phys. Chem.* **2006**, *7*, 793-797.

[99] (a) Würthner, F. *Angew. Chem., Int. Ed.* **2001**, *40*, 1037-1039. (b) Dimitrakopoulos, C. D.; Malenfant, P. R. L. *Adv. Mater.* **2002**, *14*, 99-117. (c) Kitamura, M.; Arakawa, Y. *J. Phys.: Condens. Matter* **2008**, *20*, 184011.

[100] Mondal, R. Dissertation, Bowling Green State University, **2007**.

[101] Mondal, R.; Adhikari, R. M.; Shah, B. K.; Neckers, D. C. *Org. Lett.* **2007**, *9*, 2505-2508.

[102] (a) Clar, E. *Chem. Ber.* **1942**, *75*, 1330. (b) Bailey, W. J.; Liao, C. W. *J. Am. Chem. Soc.* **1955**, *77*, 992-993. (c) Marschalk, C. *Bull. Soc. Chim.* **1943**, *10*, 511. (d) Boggiano, B.; Clar, E. *J. Chem. Soc*. **1957**, 2681-2689.

[103] Payne, M. M.; Parkin, S. R.; Anthony, J. E. *J. Am. Chem. Soc.* **2005**, *127*, 8028-8029.

[104] Chun, D.; Cheng, Y.; Wudl, F. *Angew. Chem., Int. Ed.* **2008**, *47*, 8380-8385.

[105] Kaur, I.; Stein, N. N.; Kopreski, R. P.; Miller, G. P. *J. Am. Chem.Soc.* **2009**, *131*, 3424-3425.

[106] Mondal, R.; Tönshoff, C.; Khon, D.; Neckers, D. C.; Bettinger, H. F. *J. Am. Chem.Soc.* **2009**, *131*, 14281-14289.

[107] Strating, J.; Zwanenburg, B.; Wagenaar, A.; Udding, A. C. *Tetrahedron Lett.* **1969**, 125-129.

[108] (a) Mondal, R.; Shah, B. K.; Neckers, D. C. *J. Am. Chem. Soc.* **2006**, *128*, 9612-9613. (b) Bettinger, H. F.; Mondal, R.; Neckers, D. C. *Chem. Comm.* **2007**, 5209-5211. (c) Yamada, H.; Yamashita, Y.; Kikuchi, M.; Watanabe, H.; Okujima, T.; Uno, H.; Ogawa, T.; Ohara, K.; Ono, N. *Chem. Eur. J.* **2005**, *11*, 6212-6220.

[109] Qi, T.; Guo, Y.; Liu, Y.; Xi, H.; Zhang, H.; Gao, X.; Liu, Y.; Lu, K.; Du, C.; Yu, G.; Zhu, D. *Chem. Commun.* **2008**, 6227-6229.

[110] Haryono, A.; Miyatake, K.; Natori, J.; Tsuchida, E. *Macromolecules*. **1999**, *32*, 3146-3149.

[111] Sonntag, M.; Strohriegl, P. *Tetra- hedron* **2006**, 62, 8103-8108.

Chapter 2
Conjugated Sulfur Containing Heteropentacene Analogues for *p*-Channel Organic Field-effect Transistors (OFETs)

2.1 Introduction

Linear thieno-fused oligomers composed of laterally fused benzene and thiophene rings are the most studied heteroatom containing π-conjugated materials, the molecular structures of which can be seen as an intermediate between pentacene and oligothienophenes.[1] (**Figure 2.1**) In particular, great attention has been given to five-ring fused heteroacenes as the pentacene analogues, such as tetraceno[2,3-*b*]thiophene (**TCT**)[1a],[2], anthra[2,3-*b*]benzo[*d*]thiophene (**ABT**)[1b], bent anthradithiophene (**BADT**)[1c,d], anthra[2,3-*b*:6,7-*b'*]dithiophene (**ADT**)[1e,f], benzo[1,2-*b*;4,5-*b'*]bis[*b*]benzodithiophene (**BBBT**)[1g,h], thieno[*f*,*f'*]bis[1]benzothiophene (**TBBT** *anti* and *syn*)[1i,j], dibenzo[*d*,*d'*]thieno[3,2-*b*;4,5-*b'*]dithiophene (**DBTDT**)[1k], dithieno[2,3-*d*;2',3'-*d'*]benzo[1,2-*b*;4,5-*b'*]dithiophene (**DTBDT**)[1l], and pentathienoacene (**PTA**)[1m], with a minor change of the rigid, linear and coplanar conjugated structure of pentacene were intensively studied. **Figure 2.1** shows some examples of known thiophene-based acenes and the target molecules **1** and **2** in this study as pentacene analogues.

However, most of the reported molecules encountered tedious synthesis, demanding purification processes and, more importantly devices based on heteroacenes have been mainly fabricated by the physical vapour deposition (PVD)

technique,[1a-g],[i-k,m] which further restricts their practical applications in large-area printable OFETs.

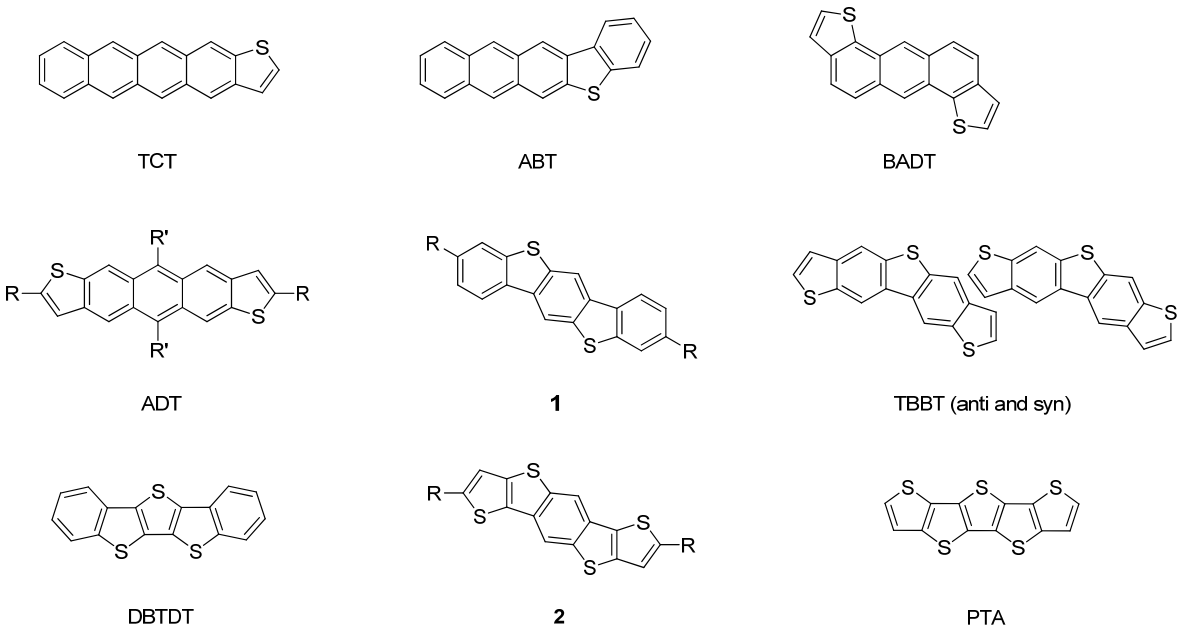

Figure 2.1. Five-ring fused heteroacenes as the pentacene analogues

In this chapter, we report the synthesis of benzo[1,2-*b*;4,5-*b'*]bis[*b*]benzo-dithiophene (**BBBT**) and dithieno[2,3-*d*;2',3'-*d'*]benzo-[1,2-*b*;4,5-*b'*]dithiophene (**DTBDT**) via triflic acid induced intramolecular electrophilic substitution. Then these new semiconducting materials were characterized by NMR, single crystal XRD, optical absorption and emission spectroscopy and cyclic voltammetry before the OFET devices based on highly crystalline **BBBT** and **DTBDT** derivatives were made via different solution processing techniques. The focus of this work was to examine whether the introduction of more sulfur substitution into the oligoacene frameworks would enhance the charge carrier mobility. In the end, we will show the qualitative relationship between DFT calculated frontier orbitals and the charge mobilities of the (hetero)pentacenes. It thus appears that the two new semi-conductive compounds are promising candidates for high performance OFETs applications.

2.2 Synthesis and characterization of benzo[1,2-*b*:4,5-*b'*]bis[*b*]benzothiophene (BBBT) as pentacene analogues

Benzo[1,2-*b*:4,5-*b'*]bis[*b*]benzothiophene (BBBT, **1**) is an analogue of pentacene with similarly rigid, linear conjugated structure and was first synthesized 40 years ago.[3] Very recently, during our preparation of this work, OFET properties of PVD fabricated BBBT films have been investigated by Takimiya et. al.[1g] and showed *p*-channel carrier mobility of 2.4×10^{-3} and on/off ratio of 10^6. Herein, we report a new synthesis of BBBT and its alkyl substituted derivative. The advantages of our synthesis are experimental ease and high yields.

2.2.1 Synthesis of benzo[1,2-*b*:4,5-*b'*]bis[*b*]benzothiophene (BBBT) derivatives

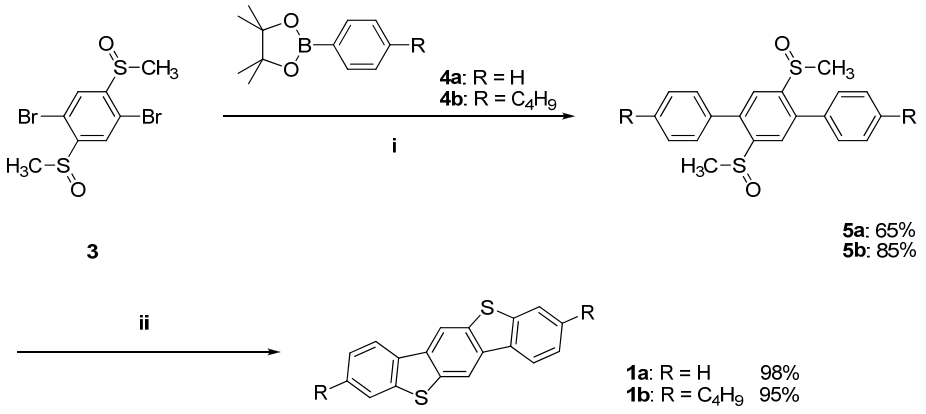

Scheme 2.1. Synthesis of BBBT derivatives **1a** and **1b**.

Scheme 2.1 illustrates the synthetic approach to BBBT **1a** and **1b**. Precursor **5** was readily obtained by following the procedure described in the literature.[4] The Suzuki coupling between **3** and the phenyl boronic ester affords **4a** and **4b** in 65% and 85% yields respectively. The quantitative intramolecular ring-closing condensation[5] of the dimethylsulfinyl benzene with the adjacent phenyl ring

proceeded slowly in the dark with an excess of pure triflic acid. After 72 hrs, the clear solution was poured into a water/ice mixture to give a yellowish powder which was filtered, dried and used directly in the next step without further purification. In the end, the powder was dissolved in pyridine and heated to reflux overnight. The product was purified by recrystalization from tetrachloroethane or by silica chromatography, giving pure BBBT **1a** and BBBT-C4 **1b** as colorless solids in 95% and 98% yields, respectively. The alkyl substituents in **1b** dramatically increased the solubility. It can be easily dissolved in common organic solvents at room temperature. To our best knowledge, no synthetic method has been reported for endcapping of BBBT by alkyl chains. In our modular approach, the peripheral "R" group can be easily altered with alkyl or aryl, and thus, the intermolecular interactions and electronic characteristics of target molecules can be precisely tuned.

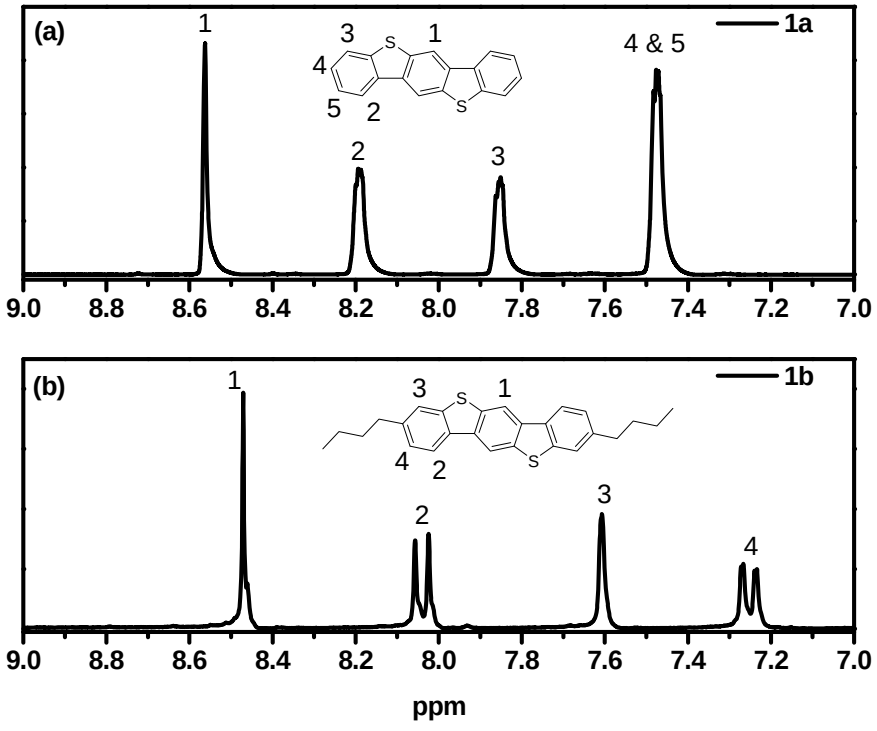

Figure 2.2. Expanded aromatic region of ^{1}H NMR spectra of compounds (a) **1a** (500 MHz, 413 K, d_2-1,1,2,2-tetrachloroethane); (b) **1b** (250 MHz, 300 K, d_2-dichloro-methane).

The NMR spectra of the two compounds are shown in **Figure 2.2**, from which one can see the highly symmetric structure. Due to the low solubility of compound **1a**, the measurement was done at 413 K.

2.2.2 Solid-state crystal structure and packing

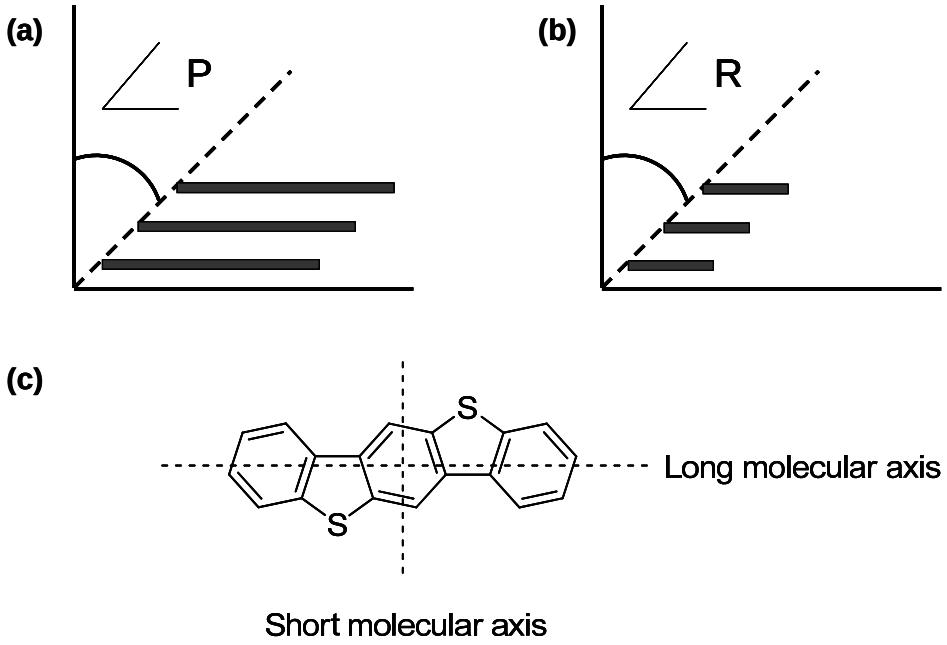

Figure 2.3. (a) Pitch angle (P) describing intermolecular slipping along the long molecular axis (view down short molecular axis). (b) Roll angle (R) describing intermolecular slipping along the short molecular axis (view down long molecular axis). (c) Long and short molecular axes of **1**.

Recent studies have shown that the solid-state morphology of conjugated materials plays an important role in the performance characteristics of electronic devices;[6] thus, X-ray diffraction studies were performed on crystals and thin films grown by drop-casting of **1a** and **1b** to determine their solid-state order and the effect of the side-chain substitution on the solid-state structures. For the BBBT derivatives that adopt a cofacial stacking arrangement translational displacements between adjacent molecules were quantified using a method developed by Curtis et. al. where slipping along the long and short molecular axis is described by pitch (**P**) and roll (**R**) angles (**Figure 2.3**).[7] Obviously, the smaller the angle, the higher the

degree of cofacial overlaps. The crystallographic parameters are collected in **Table 2.1**.

Single crystals of **1a** and **1b** suitable for single crystal XRD (SCXRD) analysis were obtained by recrystallization from tetrachloroethane and chloroform, respectively (**Figure 2.4**). X-Ray Crystallographic measurements were made by Dr. Enkelmann in Max-planck Institute for Polymer Research. Compound **1a** crystalllized in the monoclinic $P\ 2_1/n$ space group with two molecules in the unit cell. The rigid conjugated structure is planar and shows no prominent cofacial π-π interactions between adjacent molecules in comparison to the literature.[1g] (**Figure 2.4a**) In the solid state, **1a** adopts an edge-to-face herringbone packing motif similar to pentacene where the tilt angle between two mean planes of the BBBT framework is 57.3°, compared to 50.5° in the oxygen analog dibenzo[*d*,*d'*]benzo[1,2-*b*:4,5-*b'*]difuran[8] and 53° in pentacene.[9] There are four intermolecular close-contacts in these edge-to-face structures that link a molecule of **1a** with four others in the lattice. (**Figure 2.4b**) The closest intermolecular C-S distance is 3.50 Å which is shorter than the closest intermolecular C-C distances observed in dibenzo[*d*,*d'*]benzo[1,2-*b*:4,5-*b'*]difuran and pentacene,[9] and may lead to strong electronic coupling between adjacent molecules in the crystalline lattice. In this regard, we assume that there is a two-dimentional electronic structure in the solid of **1a**.

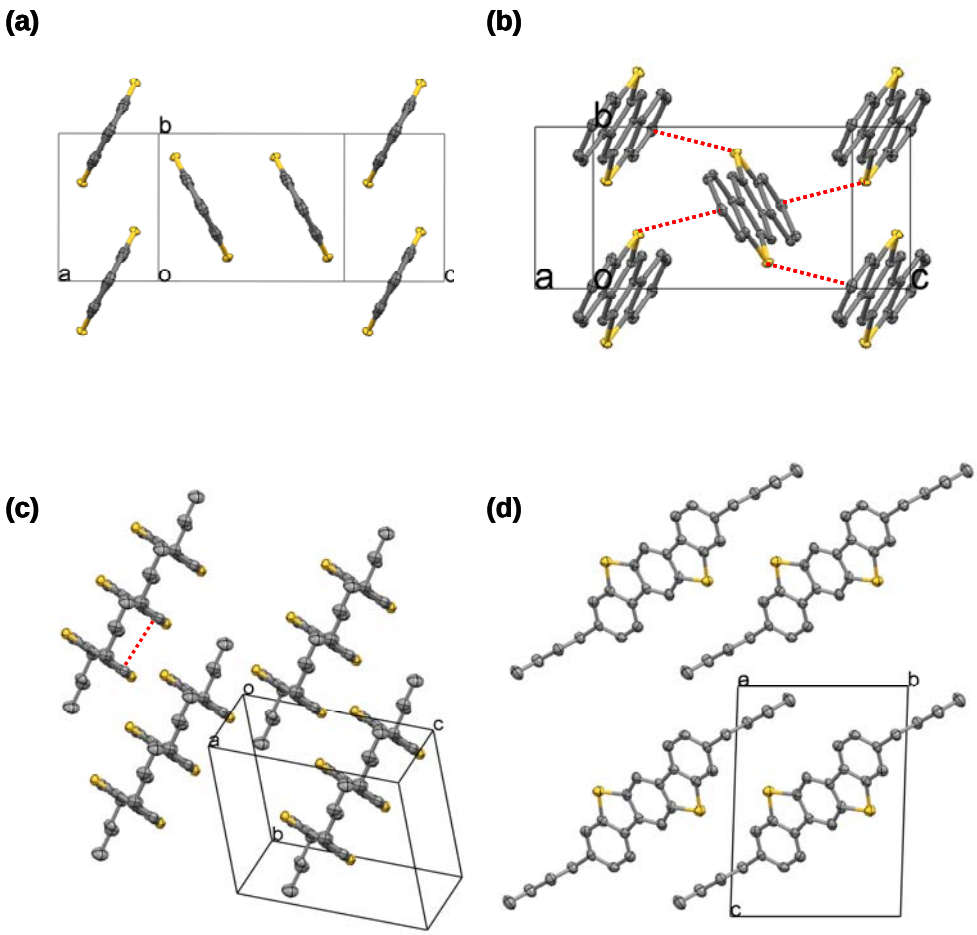

Figure 2.4. Thermal ellipsoid plot of **1a** and **1b**. The hydrogen atoms are omitted for clarity. Thermal ellipsoids are drawn at 50% probability. (a) Crystal stacking of **1a**. View down the long molecular axis. (b) View down the b axis of the stacking molecules of **1a**. Dashed line illustrates short contact distance (ca. 3.5 Å). (c) Crystal packing of **1b**. Dashed lines illustrate short intra-column distances (ca. 3.42 Å). (d) View down the stacking axis of cofacial molecules of **1b**.

The dibutyl derivatized **1b** crystallized into the triclinic *P*-1 space group with a single molecule in the unit cell. Functionalizing the terminal phenyl rings with butyl chains generates the cofacial stacking arrangement with pitch and roll angles of 42° and 5°. The molecular structure of **1b** is similar to **1a** except for the two terminal *n*-butyl groups, which lie in a conformation that extends above and below the lane of the skeleton at 45° angles. This all-anti conformation is adoped to minimize the steric energy in the packing of aliphatic chains and the

interplanar stacking distance of 3.42 Å is indicative of π–π interactions along the stacking axis. (**Figure 2.4c**) In the solid state, the stretched and doubly bent molecules of **1b** are organized into a slipped columnar structure and the columns further stack to form "lamellar" arrangement[7] with the columns separated by insulating butyl chains. (**Figure 2.4d**) The lack of short contacts between the π stacks suggests a one-dimentional electronic structure in the crystal, which may not favour charge transport as good as a two-dimentional electronic structure.

Table 2.1. Crystallographic parameters of **1a** and **1b**

	1a	**1b**
Empirical formula	$C_{18}H_{10}S_2$	$C_{26}H_{26}S_2$
Formula weight	290.40	402.61
Crystal color, habit	colorless, block	colorless, needle
Crystal system	monoclinic	triclinic
a, Å	9.4941(5)	4.5840(4)
b, Å	5.9036(4)	9.2230(5)
c, Å	11.5824(5)	12.4880(5)
β, deg	102.9379(13)	79.5940(13)
V, Å^3	632.71(6)	509.75(6)
ρ_{calc}, g/cm^3	1.524	1.311
space group	$P\,2_1/n1$	P -1
Z value	2	1
Temperature, K	120	120
No. of reflections measured	1831	2584
No. of variables	91	127
Residuals: *R*; wR^2	0.0307; 0.0387	0.0701; 0.0565

2.2.3 Powder X-ray diffraction (PXRD) analyses of BBBT films

The XRD pattern of a film of **1a** prepared by drop-casting of a 30 mg/ml solution of **1a** on to a silicon wafer, suggests that there are two phases present (**Figure 2.5a**). The two sharp reflections at 2θ = 8.44 and 16.9^o correspond to the (001) and (002) planes of the $P2_1/n$ space group. These assignments are supported by the SCXRD data and consistent with the diffraction pattern obtained from crystals of **1a**. The

molecules are inclined approximately 37.2° with respect to the (001) plane that is parallel to the substrate surface. (**Figure 2.5b**) The additional reflections observed at 2θ = 11 and 12° are corresponding to another two different kinds of crystallization orientation. Similar features have been observed in the XRD analysis of a pentacene thin-film grown onto a silica substrate using molecular beam deposition techniques.[10] These features have been attributed to the coexistence of two phases, a "thin-film" phase and a "single-crystal" phase that form under certain deposition conditions.

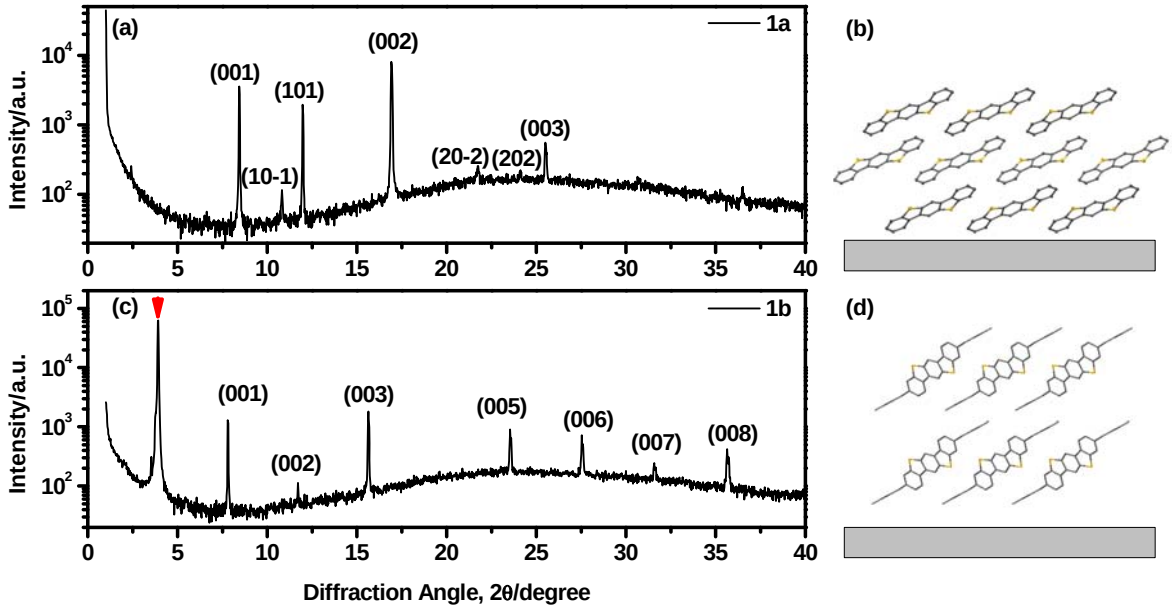

Figure 2.5. X-ray scattering in reflection of (a) BBBT (**1a**) film on a silicon wafer. (b) Organization of **1a** in the solution processed thin layer on the substrate. (c) BBBT-C4 (**1b**) film on a silicon wafer. (d) Organization of **1b** in the solution processed thin layer on the substrate.

The XRD pattern of a film of **1b** prepared by drop-casting of a 30 mg/ml solution on to a silicon wafer exhibits much regular film morphology than that of **1a** with nine strong reflections corresponding to the (001) through (007) planes (**Figure 2.5c**). The molecules are oriented with their long molecular axes inclined approximately 64° with respect to the (001) plane that is parallel to the substrate surface. At the same time, the derived *d*-spacings (11.33 Å) are practically identical to *c* axis length

observed in the crystal structure (12.49 Å), which again means that molecules of **1b** are oriented with the (001) plane parallel to the substrate surface. The arrow marked peaks (at 2θ = 3.92°) correspond to a higher order reflection. These reflections are consistent with those observed in films prepared from the didodecyl derivative of LADT reported by Katz et al,[1e] suggesting that this compound packed into a similar lamellar arrangement in the film. (**Figure 2.5d**) It has also been shown from the solution processed OFETs that devices with dialkyl substituted LADT as the semiconducting channel demonstrated mobilities around 0.01-0.02 $cm^2 V^{-1} s^{-1}$. Katz et al found that dihexyl and didodecyl derivatives showed higher charge carrier mobilities in OFET devices than the nonsubstituted LADT, although quite a large volume is occupied by insulating alkyl chains. Evidently, alkyl chains support better molecular organization and packing that favour charge transport in solid films.

2.2.4 Photophysical properties

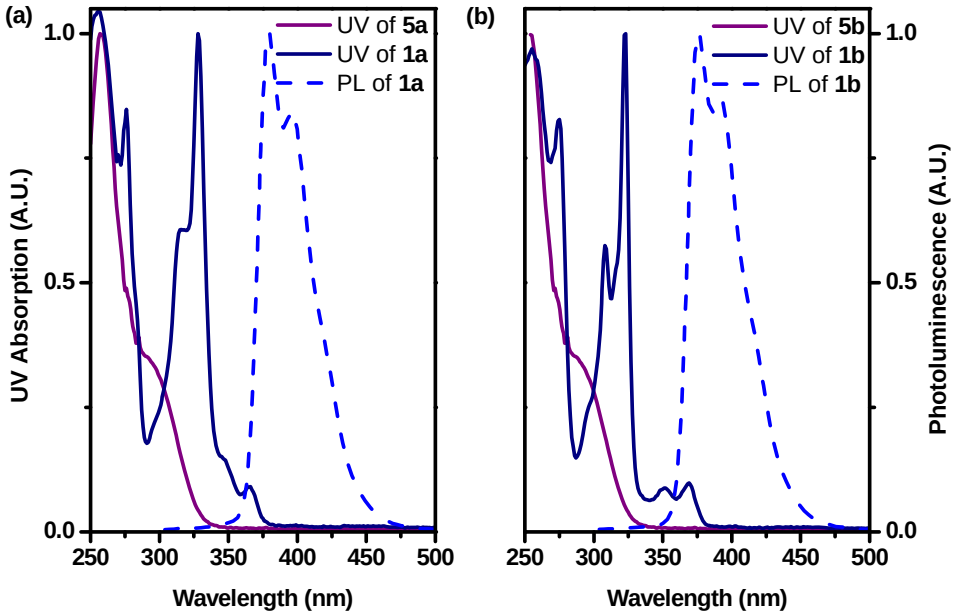

Figure 2.6. Absorption (solid) and photoluminescence (PL) (dash-dotted) spectra of **5a**, **1a** (a) and **5b**, **1b** (b) in THF (1.0×10^{-6}M).

UV absorption and photoluminescence spectra (PL) of conjugated acenes **1a** and **1b** are shown in **Figure 2.6**. UV absorption of **5a** and **5b** are also shown for

comparison. In the UV spectra, the absorption maxima of the ring fused derivatives **1a** and **1b** are obviously red-shifted respected to those of **5a** and **5b**, which could be attributed to the extended π-system after the ring closure (**Scheme 2.1**). In addition, the strong absorptions at 256 nm, 276 nm and 328 nm for **1a** as well as 255nm, 275nm, 308nm and 323 nm for **1b** are attributed to the *β* band of π-π* transitions of the BBBT backbones. On the other hand, the longer wavelength and weaker absorption observed at 350 – 380 nm for both compounds originate from the *a* and/or *p* band of π-π* transition.[11] The HOMO-LUMO energy gaps of **1a** and **1b** can be evaluated from the absorption edge (λ = 376 nm and 382 nm) of 3.30 eV and 3.24 eV, which are much larger than that of pentacene (2.15 eV),[12] indolo[3,2-*b*]carbazole (2.95 eV)[8] and smaller than that of dibenzo[*d*,*d'*]benzo[1,2-*b*:4,5-*b'*]difuran (3.50 eV)[8]. In the PL spectra, both compounds exhibit weak purple fluorescence with the emission maximum at 380.4 nm and 376.7 nm respectively. The small Stokes shift of around 14.0 nm or 7.7 nm is due to the rigid planar structure.[13] The similarity in the UV-vis absorption and photoluminescence spectra of **1b** to **1a** indicates no pronounced perturbation from the substitution of alkyl chains. The photophysical data are summarized in **Table 2.2**.

2.2.5 Electrochemical properties

Oxidation potentials of **1a** and **1b** were investigated by cyclic voltammetry (CV). Both oligomers **1a** and **1b** exhibited similar and quasireversible oxidation waves [oxidation peak potential (E_{ox} peak) vs Ag/Ag^+; 1.06 V for **1a**, 1.07 V for **1b**] at the scan rate of 50 mV s^{-1} as depicted in **Figure 2.7a** and **2.7b**. The HOMO energy levels (E_{HOMO}) of heteroacenes were estimated from the first oxidation onsets (E_{onset}^{ox}) to be -5.4 eV for **1a** and**1b**. (**Table 2.2**)

Based on the HOMO energy levels and the optical band gaps (E_g) evaluated from the onset wavelengths of UV-vis absorption spectra, LUMO energy levels (E_{LUMO}) of BBBT derivatives were calculated to be -2.1 eV for **1a**, -2.2 eV for **1b**. In these heteroacenes, the introduction of an electron-donating alkyl group in **1b** had little

influence on the HOMO and LUMO energy levels. The compounds practically have lower-lying HOMO energy levels than pentacene (E_{HOMO} = -4.60 eV)[14] and most oligothiophenes, but higher than dibenzo[*d*,*d'*]benzo-[1,2-*b*:4,5-*b'*]difuran (E_{HOMO} = -5.78 eV)[8], which are indicative of better stabilities than pentacene under ambient conditions.

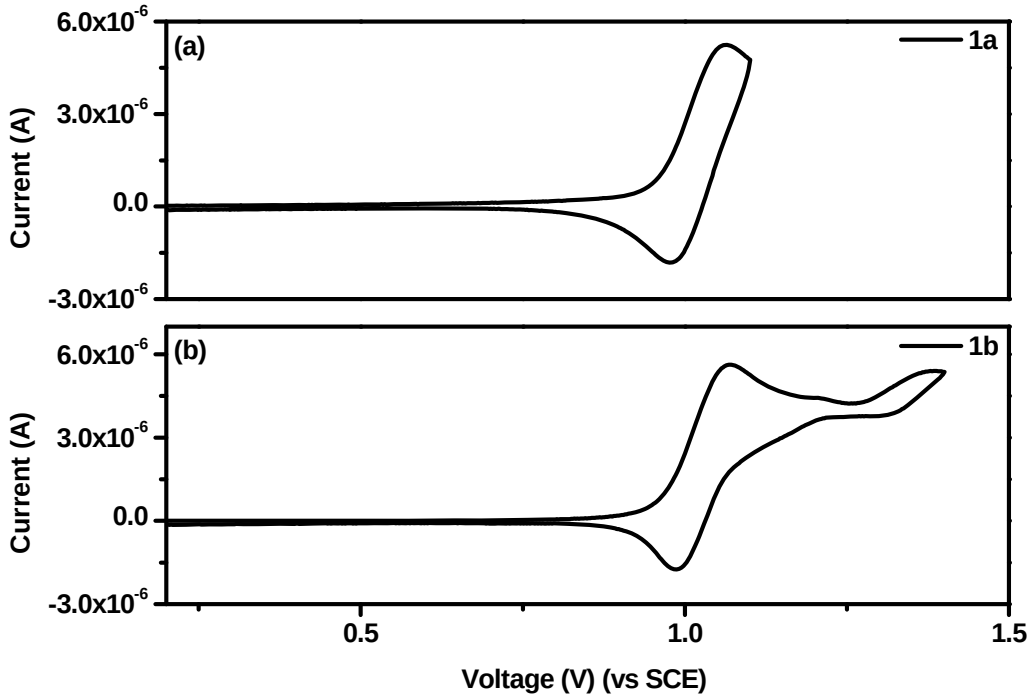

Figure 2.7. Cyclic voltamograms of **1a** (left) and **1b** (right) in dry CH_2Cl_2. Measurement conditions: 1 mM in CH_2Cl_2 for all compounds with Bu_4NPF_6 (0.10 M); scan rate = 50 mV s^{-1}.

Table 2.2. Electrochemical, UV-Vis data and estimated HOMO and LUMO levels of **1a** and **1b**.

Compound	E_{ox}[a]/V anodic/ onset	λ_{max}[b]/nm peak/edge	Emission λ_{max}/nm	HOMO[c]/eV	Band gap[d]/eV	LUMO[e]/ eV
1a	1.06/0.95	366/379	380	-5.4	3.30	-2.1
1b	1.07/0.96	369/375	377	-5.4	3.24	-2.2

[a] Versus. Ag/AgCl in CH_2Cl_2 with 0.1 M *n*-Bu_4NPF_6 as supporting electrolyte (scan speed = 50 mV/s). [b] Absorption spectra.
[c] Calculated based on HOMO = - (E_{ox}^{onset} + 4.34) eV. [d] Estimated from the absorption edge by E_g^{opt} (eV) = 1240.8/λ_{onset}.
[e] calculated from LUMO=HOMO+band gap.

2.2.6 OFETs device fabrication based on BBBT derivatives

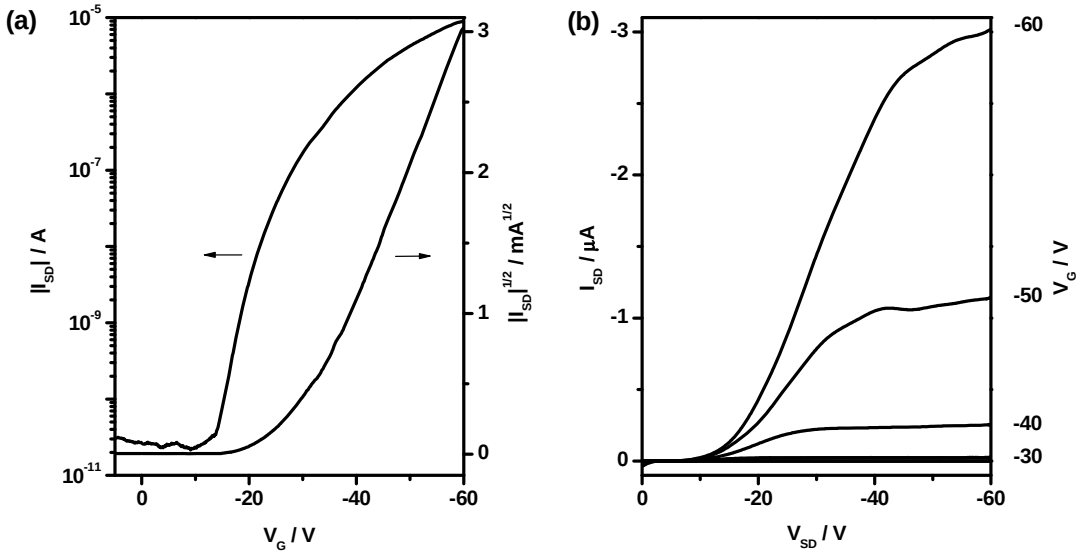

Figure 2.8. FET characteristics of BBBT (**1a**)-based OFET on PTES-treated substrate: (a) transfer characteristics at a source-drain bias of V_{SD} = -60V; (b) output characteristics for various gate voltages

Organic field-effect transistors (OFETs) were fabricated in our lab by Dr. Hoi Nok Tsao and Dirk Beckmann. Devices were made in a "bottom contact" configuration as follows: Oligomer **1a** was drop-cast from a 5 mg/ml 1,1,2,2-tetrachloroethane solution onto photolithographically defined transistor substrates, where the dielectric surface (SiO_2) was treated with phenyltriethoxysilane (PTES) in order to avoid interfacial trapping. **Figure 2.8a** illustrates the transfer characteristics after annealing the sample at 100 °C for 30 min. From these curves, a saturated hole mobility of 0.01 $cm^2\ V^{-1}\ s^{-1}$ which was applied to the real channel length in consideration of the spotlike film formation (**Figure 2.10a**) could be reached. Furthermore a threshold voltage V_T of -29 V and an on/off current ratio of 10^5 were extracted (**Table 2.3**). It is interesting to compare this charge carrier mobility with the value reported for vacuum deposited BBBT of 2.4×10^{-3} $cm^2\ V^{-1}\ s^{-1}$.[1g] However, the high threshold voltage together with the superlinear increase of the source-drain current in the output

curves (**Figure 2.8b**) suggest interface trapping and high contact resistances. We attributed these limiting factors to the rigidity of the crystals lying between the electrodes, which prevented sufficient contact to the interface and the metals. It is believed that the device fabrication can be further improved by trying different surface treatment reagents or film optimization methods.

Due to its low solubility, compound **1a** was difficult to process. To improve the solubility and thus the processibility, dibutylated **1b** was therefore synthesized, allowing film formation via drop-casting from a 20 mg/ml toluene solution on a transistor substrate held at 60°C. The bottom contact gold electrodes were treated with 1-octanethiol to reduce contact resistance.[15] Despite the high crystallinity and large domains (**Figure 2.9b**), compound **1b** revealed one order of magnitude *lower* charge carrier mobility than that of **1a** (**Table 2.3**), possibly due to the lack of interlayer contact inside the crystal lattices. This result is out of accord with the finding by Katz et al. where the dialkyl substituted derivatives showed higher charge carrier mobilities in OFET devices than the nonsubstituted ones.

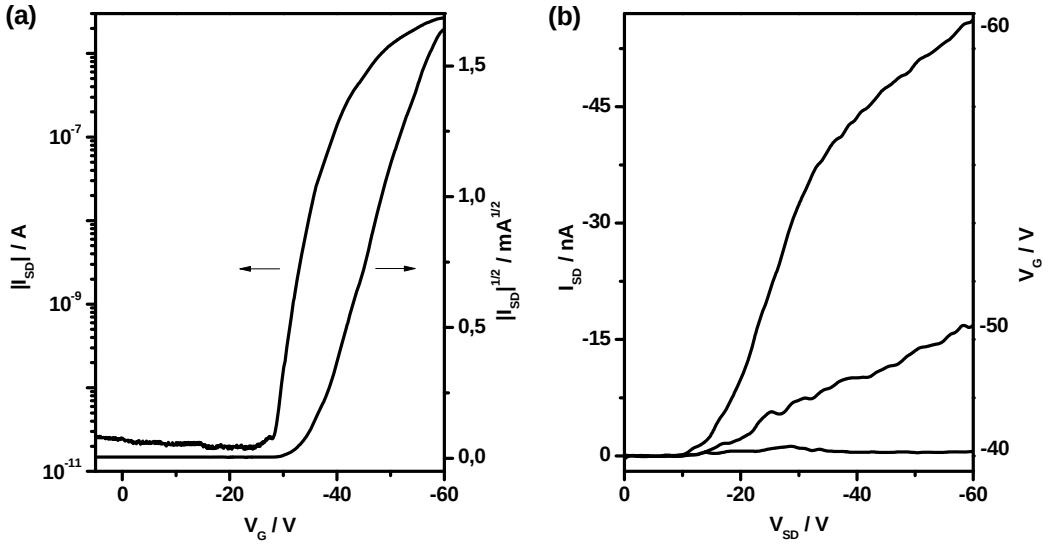

Figure 2.9. FET characteristics of BBBT–C4 (**1b**)-based OFET on PTES-treated substrate: (a) transfer characteristics at a source-drain bias of V_{SD} = -60V; (b) output characteristics for various gate voltages.

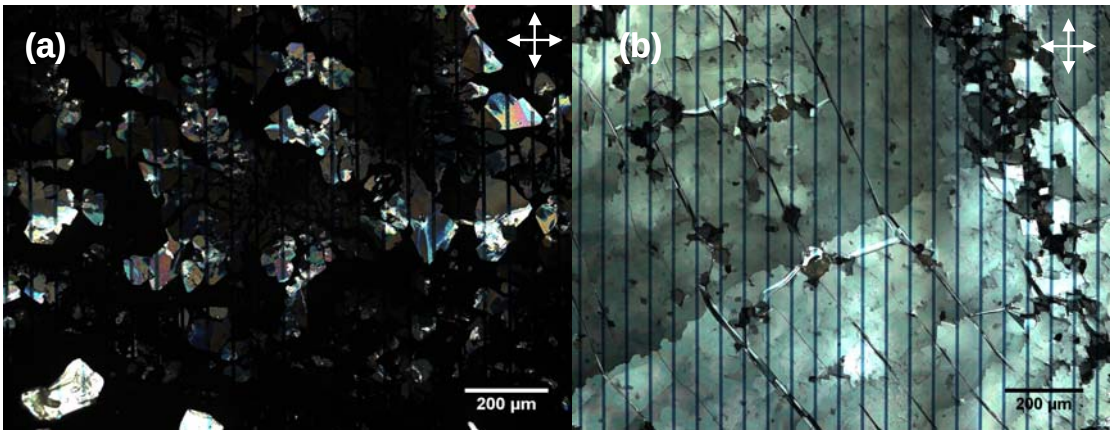

Figure 2.10. Film formation by polarized optical microscopy: (a) spotlike film formation of BBBT (**1a**) on a PTES treated bottom contact device; (b) film formation of BBBT-C4 (**1b**) on a treated bottom contact device, gold electrode was treated with 1-octanethiol

Table 2.3. FET characteristics of **1a** and **1b**

Compound	Surface-treatment reagent	Electrode-treatment reagent	T_{sub}/°C	μ_{sat}[b]/cm^{2}V^{-1}s^{-1}	I_{on}/I_{off}	V_{th}/V
1a	PTES	-	rt[a]	1.0×10^{-2}	10^5	-29 ± 5
1b	PTES	1-octanethiol	60	1.0×10^{-3}	10^5	-35 ± 2

[a] rt = room temperature. [b] Data from more than 20 devices.

The threshold voltage of **1b** increased to -35 V and the on/off ratio of 10^5 remained unchanged in comparison with **1a** (**Table 2.3**). However, poor output characteristics were observed, possibly due to severe charge trapping at the semiconductor-dielectric interface or at the macroscopic domain boundaries.[16] The presence of serious charge trapping was also supported by the increased threshold voltage of the device based on **1b**. Inspite of the improved film quality and enlarged domains the films of **1b** may contain more defects compared to that of **1a**, which formed much smaller crystal domain. To solve this problem, high boiling point solvents will be employed to cast the film. The highly crystalline molecules would therefore have enough time to pack with each other and give give films with least defects. At the same time, various surface-treatment reagents

will be tested to modify the surface properties of the dielectric material (silicon dioxide). In the end, there is still room for other solution processing techniqes. Therefore, for further FET optimization, various solution processing techniques (e.g. spin-coating and dip-coating) are in the focus of our interest.

It has to be admitted that two examples (**1a** and **1b**) can not fully reflect the real semiconducting properties of compound BBBT. Therefore more data from a variety of more different alkyl substituted BBBT are needed to find the proper alkyl group that give the best device performance. At the same time, from the chemical structure's point of view, it is also interesting to add more sulfur atoms into the molecule backbone, which may also help the improvement of charge transfer efficiency. To this end, the heteropentacene **2** (**Figure 2.1**) was designed and will described in next section.

2.3 Synthesis and characterization of dithieno[2,3-*d*;2′,3′-*d*′]benzo-[1,2-*b*;4,5-*b*′]dithiophene (DTBDT) as pentacene analogues

In accord with the consideration at the beginning of this chapter, we focused our attention on heteroacenes with more thiophene units. In this regard, thiophene rings are used in place of the benzene ring in compound **5**, therefore another new heteropentacene (**2**) with four thiophene ring symmetrically fused outside a benzene ring was achieved with the same ring closure method.

2.3.1 Synthesis of dithieno[2,3-*d*;2′,3′-*d*′]benzo[1,2-*b*;4,5-*b*′]dithiophene (DTBDT) derivatives

As demonstrated in **Scheme 2.2**, a series of **DTBDT** derivatives with two alkyl chains (linear or branched) in the molecular *long-axis* direction were synthesized via two-step reactions. Stille coupling between 1,4-dibromo-2,5-bis(methyl-sulfinyl)benzene (**3**) and corresponding (5-alkylthiophen-2-yl)trimethylstannane afforded precursors **7a–d** in good yields. Subsequent intramolecular ring-closure was performed in an excess of pure triflic acid, where the as-formed clear solution

was poured into water to give a yellowish powder as precipitate, followed by filtering, drying, and reflux in pyridine. The final **DTBDT** derivatives **2a–d** were achieved in an overall yield of ca. 75% after purification by flash column chromatography. Their chemical structures were fully characterized by ^{1}H NMR, ^{13}C NMR, mass spectroscopy (MS), and elemental analysis.

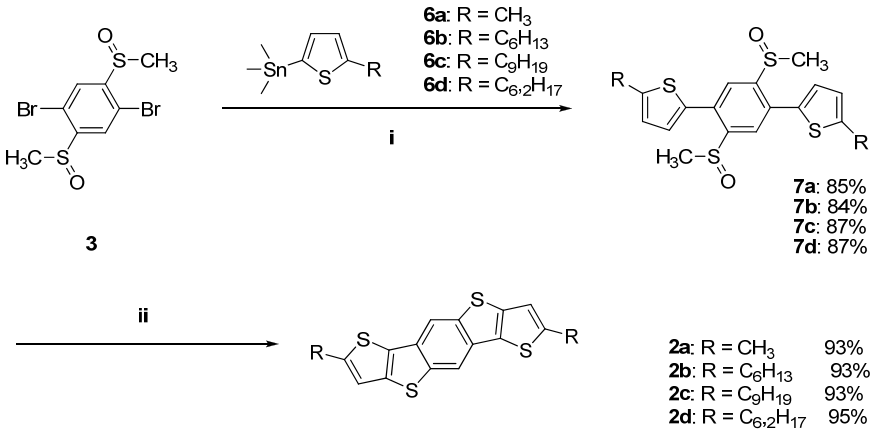

Reagens and conditions:

(i) $Pd(PPh_3)_4$, DMF, 85°C, 24 h; (ii) a. CF_3SO_3H, P_2O_5, rt.; b. Pyridine, reflux.

Scheme 2.2. Synthesis of DTBDT derivatives **2a** to **2d**.

DTBDT derivatives **2a–d** are off-white flakes that are readily soluble in common organic solvents. *It is interesting to notice that the attempt to extend the length of alkyl substitution up to C12 totally failed, due to the degradation of the alkyl groups in the presence of triflic acid. Since alkyl chains longer than C12 also degraded, we assume that the reaction could only tolerate alkyl groups shorter than C10.* This phenomenon has not been reported before and the reason is still unclear yet. Therefore all the oligomers achieved by this method have alkyl chains shorter than C10. One example of the NMR proof of the structure of **2b** is shown in **Figure 2.11**. These air- and moisture-stable materials are soluble in a variety of organic solvents, so solution processing for fabrication of OFET devices may be possible. Moreover, differential scanning calorimetry (DSC) studies on **2a-2d** showed significant thermal stability for all the compounds, which decompose only at temperatures above 350 °C and have a much lower melting/sublimation point, which potentially would also allow

vapour phase deposition onto OFET devices.

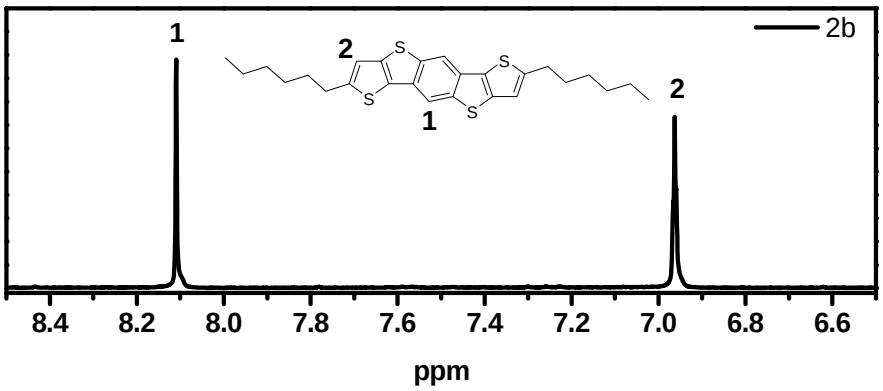

Figure 2.11. Expanded aromatic region of ^{1}H NMR spectra of compound **2b** (250 MHz, 300 K, d_2-dichloromethane).

2.3.2 Solid-state crystal structure and packing

Since solid state packing properties and molecular interactions have a major impact on potential performance in OFET devices, the single crystal structures of heteropentacenes **2b** and **2c** were investigated. The long and short molecular axes of **DTBDT** derivatives are shown in **Figure 2.12**. The crystallographic parameters are collected in **Table 2.4**.

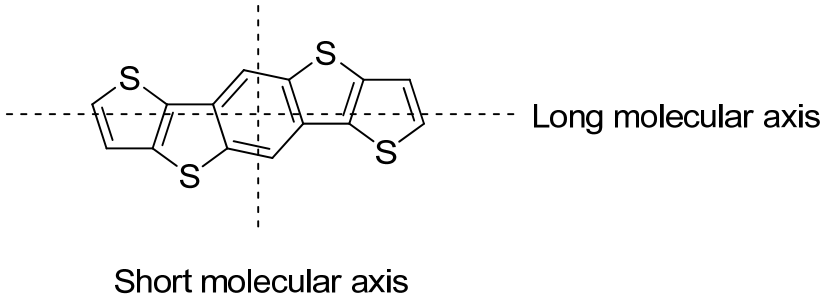

Figure 2.12. Long and short molecular axes of **2**.

Single crystals of heteropentacene **DTBDT 2b** and **2c** that were suitable for an X-ray diffraction study were obtained from a concentrated solution of them in chloroform at room temperature. Compound **2b** crystallized into the triclinic *P*-1 space group with a single molecule in the unit cell (**Figure 2.13a** and **b**). The **DTBDT**

core showed almost planar structures like pentacene, while the hexyl chain on the thienyl *a*-position was located outside the plane of the skeleton, taking an all-*anti* conformation that minimizes the steric energy in the aliphatic chains. The stretched, doubly bent molecules formed a layer-by-layer structure consisting of alternately stacked aliphatic layers and the **DTBDT** core (**Figure 2.13a**). In each layer, the molecules were promoted to pack in a shifted cofacial arrangement with pitch and roll angles of 47° and 9°, respectively. An interplanar separation of 3.6 Å was measured, which was indicative of π-π interactions along the stacking axis (**Figure 2.13b**); a side-by-side interaction of 3.73 Å through the S-S contact was also observed. This contact distance was close to those observed between close-carbon contacts in adjacent molecules of pentacene (3.6-3.8 Å), and suggested that a single crystal of **2b** may have two-dimensional electronic structure.

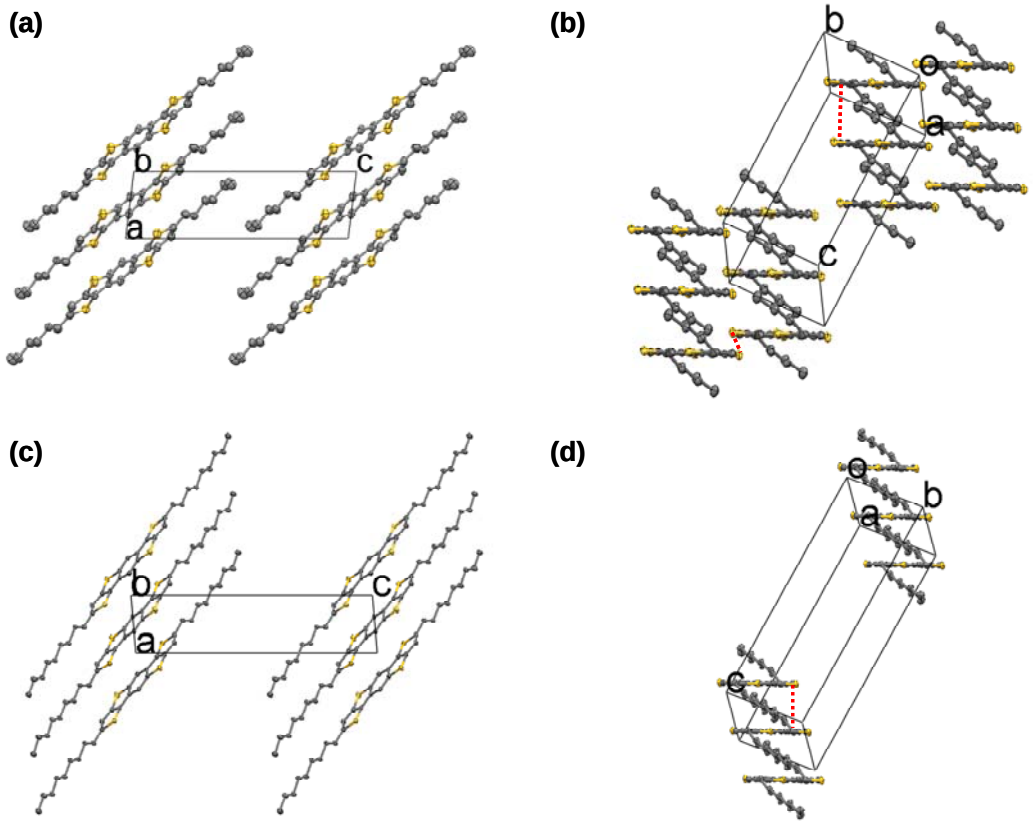

Figure 2.13. Thermal ellipsoid plot of **2b** and **2c**. The hydrogen atoms are omitted for clarity. Thermal ellipsoids are drawn at 50% probability. (a) Crystal stacking of **2b**. View down the *b* axis showing the lamella packing structures. (b) View along long molecular axis. Dashed line illustrate intra(inter)-column short contact distances (ca.

3.6 Å). (c) Crystal packing of **2c**. View down the *b* axis showing the lamella packing structures. (d) view along long molecular axis. Dashed line illustrates intra-column short contact distance (ca. 3.6 Å).

Compound **2c** crystallized into the triclinic *P*-1 space group with two molecules in the unit cell (**Figure 2.13 c** and **d**). In the crystal lattice, both nonyl chains were in a all-*anti* conformation that extended above and below the aromatic plane of the **DTBDT** framework at 23° angles (**Figure 2.13d**). The same as **2b**, the stretched, doubly bent molecules formed a layer-by-layer structure consisting of alternately stacked aliphatic layers and the **DTBDT** core and in each layer, the molecules were promoted to pack in a shifted cofacial arrangement with pitch and roll angles of 45° and 2°, respectively. An interplanar separation of 3.6 Å was measured, which was indicative of π-π interactions along the stacking axis (**Figure 2.13d**). However, unlike **2b**, there was no side-by-side interaction between the columns. This could be due to steric effects imparted by the nonyl substituents. The lack of contact between the π-stacks suggested a one-dimensional electronic structure in the crystal.

Table 2.4. Crystallographic parameters of **2b** and **2c**

	2b	**2c**
empirical formula	$C_{26}H_{30}S_4$	$C_{32}H_{42}S_4$
formula weight	470.78	554.94
crystal color, habit	colorless, needle	colorless, needle
crystal system	triclinic	triclinic
a, Å	5.3344(2)	5.2764(1)
b, Å	6.3989(4)	6.4925(2)
c, Å	17.6924(9)	21.4725(7)
β, deg	95.789(3)	84.7774(16)
V, Å^3	587.87(5)	720.65(4)
ρ_{calc}, g/cm^3	1.330	1.279
space group	*P* -1	*P* -1
Z value	1	1
temperature, K	120	120
no. of reflections measured	3289	4035
no. of variables	136	163
residuals: *R*; *wR*^{2}	0.0430; 0.0930	0.0387; 0.0456

2.3.3 Powder X-ray diffraction (PXRD) analyses of DTBDT films

Thin film X-ray diffraction (XRD) patterns in reflection mode for spin-coated films of **2a**-**2d** were shown in **Figure 2.14**. The *d*-spacing was calculated according to Bragg's law and correlated with the unit-cell parameters of the single crystal if available.

As can be seen from **Figure 2.14c**, the XRD pattern of compound **2b** showed five sharp reflections at 2θ = 4.7, 9.62, 14.54, 19.5 and 24.52° corresponding to the (001) to (005) planes of the *P*-1 space group. These assignments were supported by the SCXRD data and consistent with the diffraction pattern obtained from crystals of **2b**. The lamella packed molecules were inclined approximately 47° with respect to the (00*l*) plane that was parallel to the substrate surface. (**Figure 2.14d**) A calculated *d*-spacing of 18.8 Å was in line with the length of the *c*-axis (17.7 Å), which further confirmed the molecular orientation on the surface.

Similarly, the XRD pattern of compound **2c** (**Figure 2.14e**) showed sharp reflections at 2θ = 3.78, 7.8, 15.86, 19.94 and 24.02°, which corresponded to the (00*l*) planes of the *P*-1 space group. The calculated diffraction pattern from SCXRD data suggested that the lamella packed molecules were inclined approximately 46° with respect to the (00*l*) plane that was parallel to the substrate surface. (**Figure 2.14f**) The calculated *d*-spacing of 23.36 Å was also in line with the length of the *c*-axis (21.5 Å), which further confirmed the molecular orientation on the surface.

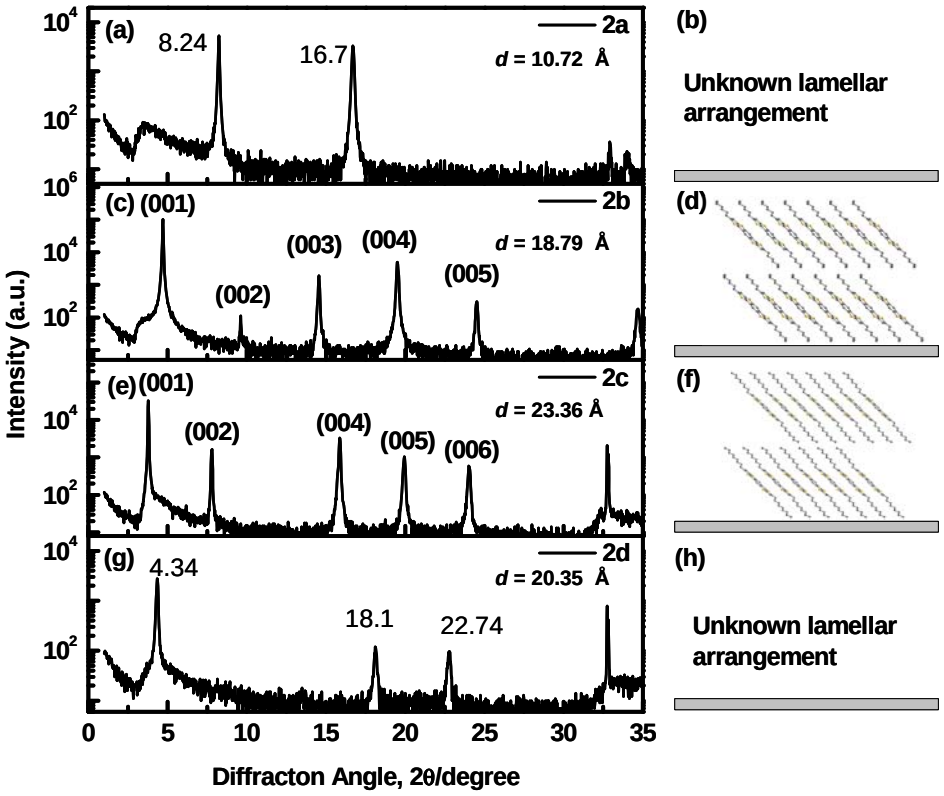

Figure 2.14. a), c), e), g) X-ray diffraction in reflection mode for the spin-coated films of **2a-2d**. The reflections for the dip-coated film are assigned by the Miller's indexes, b), d), f), h) Supposed organization of **2a-2d** in the solution processed thin layer on the substrate.

Unfortunately, we did not get decent single crystals from **2a** and **2d**; therefore it was not possible to draw exactly the arrangement of molecules on the surface. However, from their XRD patterns (**Figure 2.14a** and **g**), we could conclude that these two molecules also adopt certain lamella type packing arrangement. The calculated *d*-spacing are 10.7 Å and 20.35 Å respectively. From the *d*-spacing values of the four molecules, we can see the increase of *d*-spacing with the length of the alkyl groups.

2.3.4 Photophysical properties

The photophysical properties of **DTBDT**s **2a–d** were shown in **Figure 2.15** and **Table 2.5**. For the series of **DTBDT**s, the variations in the absorption spectrum in a dilute solution were much less pronounced, thus indicating that the length of the alkyl chains had no significant effect on the absorption spectrum. The **DTBDT**s all exhibited purple fluorescence both in solution and in the solid state.

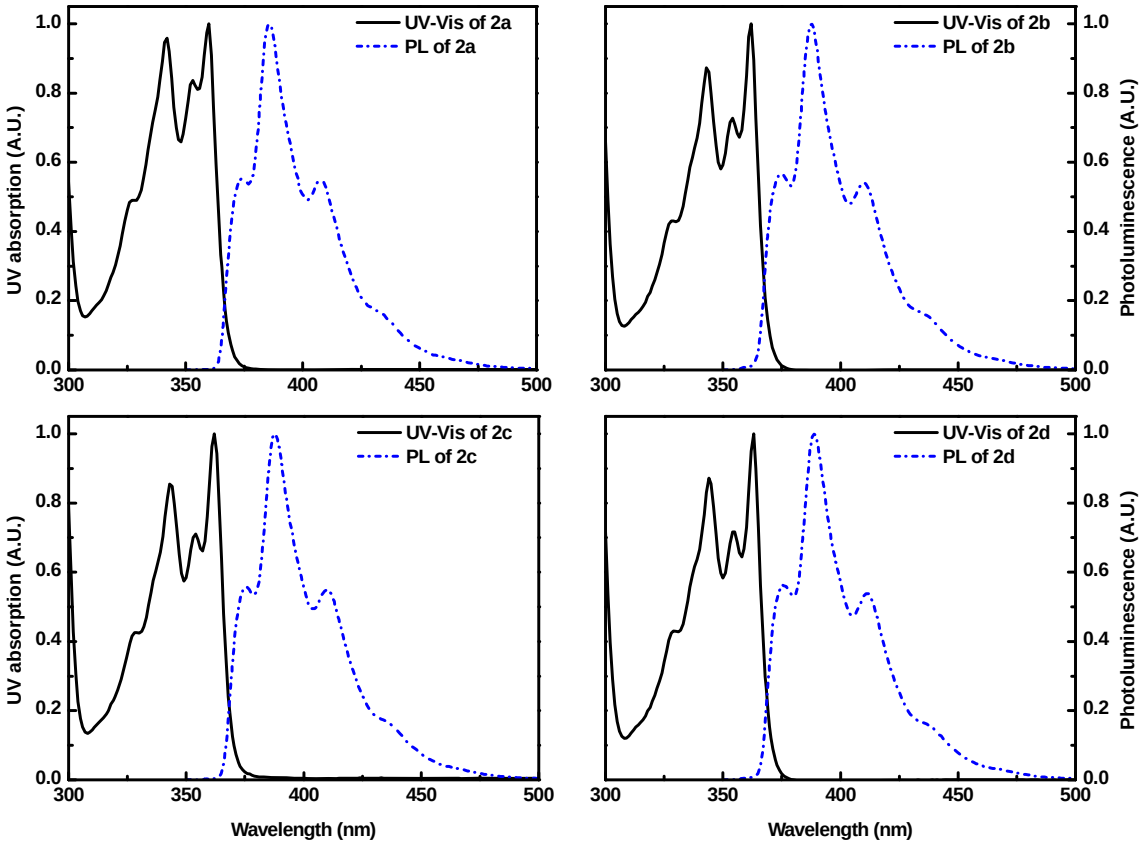

Figure 2.15. Absorption (solid) and photoluminescence (PL) (dash-dotted) spectra of DTBDTs **2a–d** in THF (1.0×10-6M).

As seen from **Figure 2.15**, compounds **2a-d** exhibited similar fluorescence spectra in solution with the wavelength maxima at λ_{max} = 375, 389, and 411 nm, respectively. Relative to pentacene, the absorption spectrum wavelength maximum of **2** showed a blue shift of δ_λ = 208 nm from λ_{max} = 570 nm of pentacene[14] to 362 nm, and the optical gap estimated from the absorption edges of the solution spectra for **2** is 3.36

eV, which was much wider than that of pentacene (2.15 eV) and pentathienoacene (3.20 eV)[1m] (**Figure 2.1**). The structural difference between **2** and pentacene was that four periphery benzene rings in pentacene were changed to four thiophene units in **2**, thus resulting in spectral changes and demonstrating that the introduction of the π-electron-rich thiophene moiety impacts greatly on the optical properties.

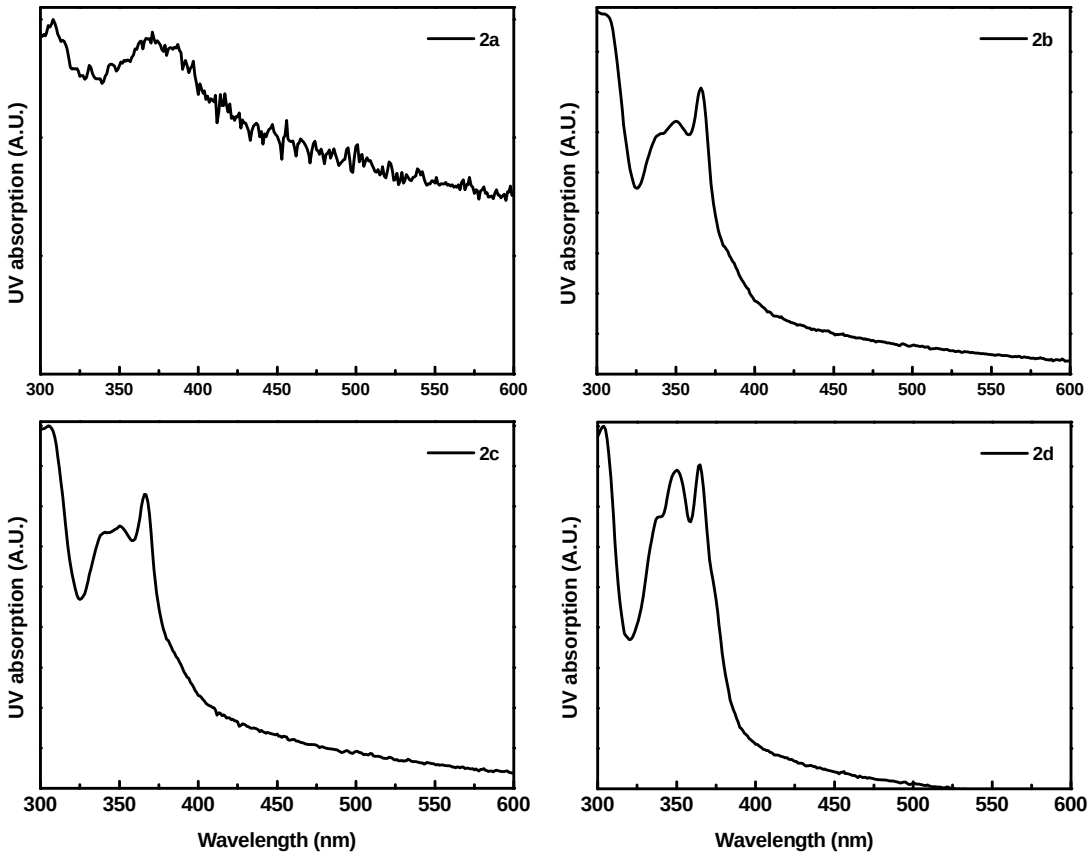

Figure 2.16. UV-vis absorption of **2a–d** as solid film on quartz substrate

The solid-state UV-vis absorption spectra of drop-cast films of **2a-d** on quartz substrates exhibited nearly identical features with λ_{max} ranging between 365 and 371 nm. Spectra of **2a** to **2d** were shown in **Figure 2.16**. The high energy peaks in the solid-state emission spectrum of **2a** to **2d** were similar to those found in the solution spectrum. At longer wavelengths, however, the emission intensity from the thin film was greater. In comparison to the spectra recorded in solution, red shifts of 4 ~ 9 nm in the absorption maxima for annealed films of **2a-d**, were observed, thus suggesting

that moderate intermolecular interactions were present in the solid-state, eg. π–π stacking.

2.3.5 Electrochemical properties

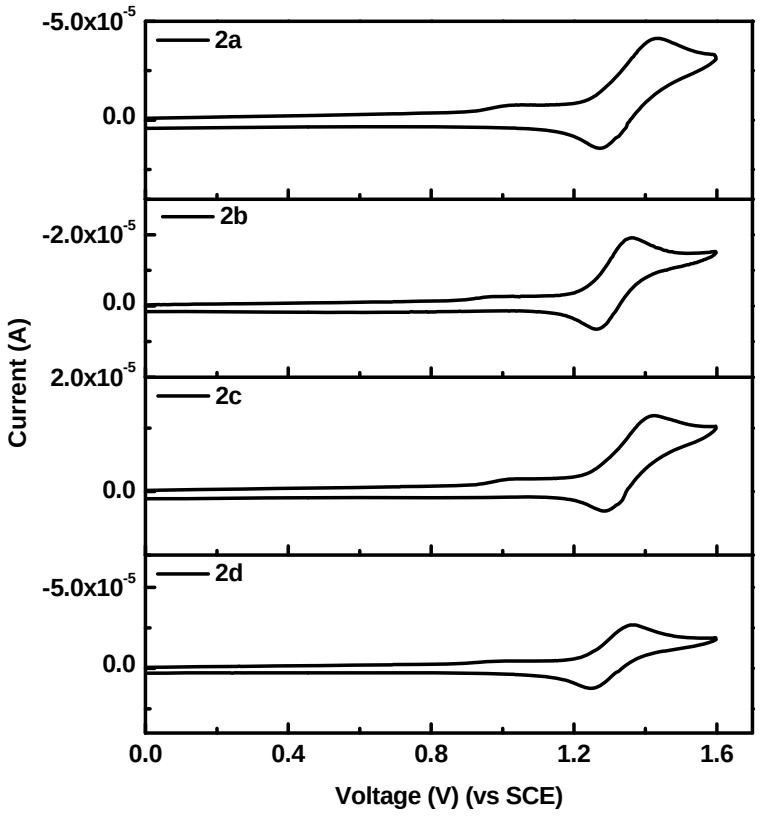

Figure 2.17. Cyclic voltammograms of **2a** to **2d**.

The cyclic voltammograms of **DTBDT** series **2a-d** in methylene chloride showed a reversible oxidation peak at $E_{1/2}$ = +1.36 V (Ag/AgCl as reference. **Figure 2.17**), indicating the good stability of the **DTBDT** radical. (The stability of the radical is an important factor in achieving high mobility.)[17] Surprisingly, the HOMO energy levels (E_{HOMO}) of the heteroacenes estimated from the first oxidation onsets (E_{onset}^{ox}) were around -5.56 eV, about 0.42 eV and 0.16 eV lower than those of pentacene[14] and pentathienoacene[1m] respectively. (**Table 2.5**) This is one of the lowest values for OFET organic semicondutors.[18] The comparison of the relatively low HOMO level and larger band gap of **2** to other heteroacenes (**Table 2.7**) suggested **DTBDT** as one of the most stable oligoacene semiconductors, which was qualitatively consistent

with the results obtained by molecular orbital (MO) calculations (**Figure 2.20**).

Table 2.5. Electrochemical, UV-Vis data and estimated HOMO and LUMO levels of **2a** to **2d.**

Compound	E_{ox}[a]/V anodic/onset	λ_{max}[b]/nm peak/edge	Emission λ_{max}/nm	λ_{max}[b]/nm peak (film)	HOMO[c] /eV	Band gap[d] /eV	LUMO[e] /eV
2a	1.44/1.23	360/367	374	365	-5.56	3.38	2.18
2b	1.37/1.22	362/369	375	366	-5.55	3.36	2.19
2c	1.43/1.23	362/370	375	366	-5.56	3.35	2.21
2d	1.37/1.22	362/370	375	365	-5.55	3.35	2.20

[a] Versus. Ag/AgCl in CH_2Cl_2 with 0.1 M *n*-Bu_4NPF_6 as supporting electrolyte (scan speed = 50 mVs). [b] Absorption spectra.
[c] Calculated based on HOMO = - (E_{ox}^{onset} + 4.34) eV. [d] Estimated from the absorption edge by E_g^{opt} (eV) = 1240.8/λ_{onset}.
[e] calculated from LUMO=HOMO+band gap.

2.3.6 OFET device fabrication based on DTBDT derivatives

2.3.6.1 Application of **2b** for the semiconducting channels in OFETs from solution

FET devices with the "top-contact" configuration were fabricated by deposition of gold source and drain electrodes (80 nm) under vacuum on top of the semiconductive thin films through a shadow mask that defined the channel length and width of 50 μm and 1.5 mm, respectively. All the devices showed typical *p*-channel FET responses under ambient conditions (**Figure 2.18**). The extracted FET parameters are summarized in **Table 2.6**.

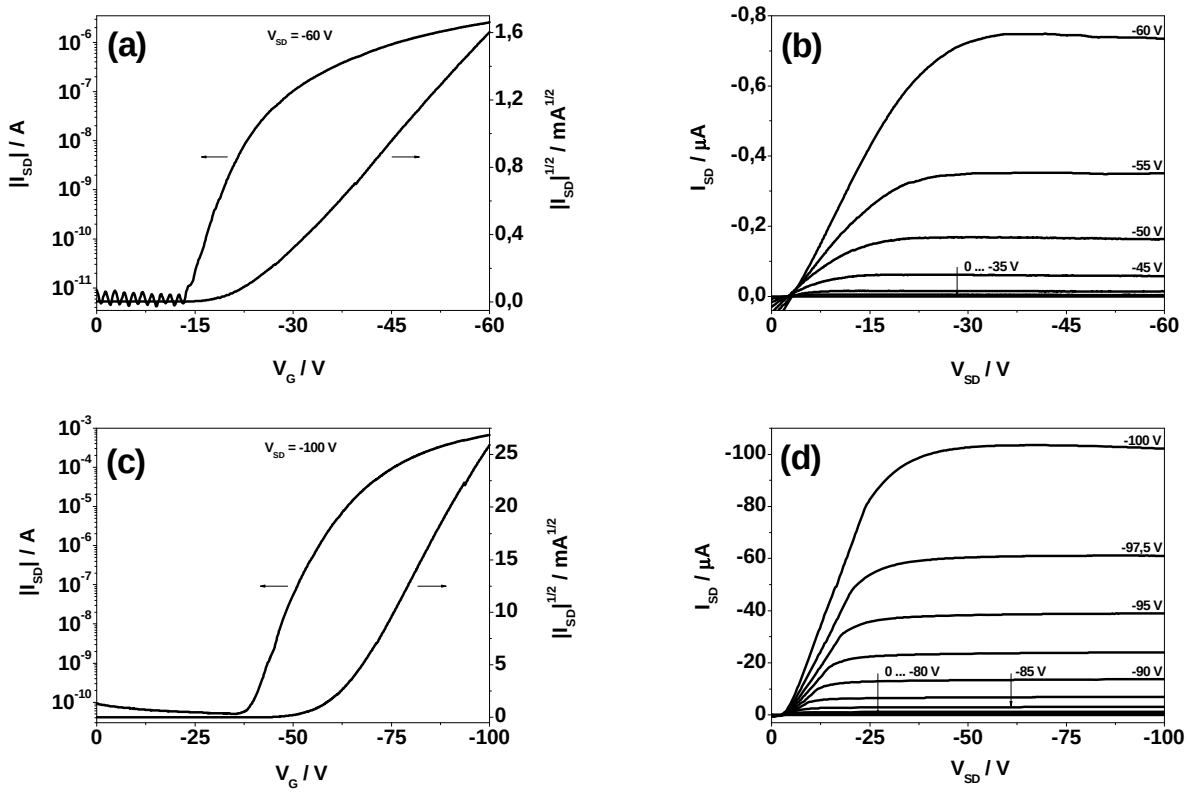

Figure 2.18. FET transfer characteristics and output curves at various gate voltages V_G of the a) and b) spin-coated; c) and d) dip-coated compound **2b**.

As a representive, OFETs based on **2b** were prepared by spin-coating a 10 mg mL^{-1} chloroform solution on plain silicon dioxide wafers. The resulting film was contacted by evapour ated source and drain gold electrodes, in this way establishing a bottom-gate, top-contact OFET geometry. This kind of device exhibits typical *p*-type transistor behavior with hole mobility of $(1.2 \pm 0.8) \times 10^{-2}$ $cm^2V^{-1}s^{-1}$ (90 % confidence region) and on/off ratios as high as 10^5 (**Figure 2.18a,b**). Notably, these mobility results were obtained for an untreated SiO_2 insulator surface and spin-coated films with only small crystalline domains, as evidenced by polarized optical microscopy (POM, **Figure 2.18a**), possibly hindering the charge transport by numerous grain boundaries.[19]

Motivated by this good transistor performance, we aimed for extending the crystal-domain sizes and minimizing the limiting influence of the grain boundaries on device performance. This was achieved by dip-coating of a 1 mg ml^{-1} toluene

solution of **2b** on an untreated SiO_2 bottom-gate, top-contact device. In contrast to spin-coating, this method allows control of solvent evapour ation, and thus film formation via the dipping rate. The obtained dip-coated layer was highly crystalline, with large domains extending over several millimeters and exhibiting optical anisotropy (**Figure 2.19b**). OFETs based on this morphology resulted in average hole mobilities of 0.6 $cm^2\ V^{-1}\ s^{-1}$ and on/off ratios of 10^6. In addition, layers with similar morphologies were achieved by dip-coating untreated SiO_2 substrates from a 2 mg ml^{-1} toluene solution, yielding even further improved device performance. Excellent hole mobilities of 1.0 ± 0.2 (90 % confidence region) $cm^2\ V^{-1}\ s^{-1}$, on/off ratios of 9 ± 3 $\times 10^6$ and threshold voltages of -39 ± 3 V were obtained as averaged from ten devices. The best device exhibited a hole mobility of 1.7 $cm^2\ V^{-1}\ s^{-1}$ as highlighted in **Figure 2.18** c and d. However, all these transistors suffered from high threshold voltages V_T of -22 ± 9 V for the spin-coated and -39 ± 6 V for the dip-coated devices. The high mobility transistor illustrated in **Figure 2.18** c and d even resulted in a V_T of -56 V. High threshold voltages are generally caused by charge trapping, that is, at the organic/insulator interface or within the semiconductor layer itself.[20] Since identical dielectrics were employed (untreated SiO_2) for both the spin-coated and dip-coated cases, interface trapping does not seem to explain the elevated threshold voltage observed for the dip-coated transistors in comparison to the spin-coated ones. Considering that the impurities inside the semiconducting compound are also an important reason for the charge trapping, which could induce high threshold voltages, the purification of the compound and the device fabrication have been done with extreme care. Compounds from the same batch of reaction were used in both the spin-coated and dip-coated devices and the observed difference in the threshold voltages V_T seemed to preclude the influence of impurities.

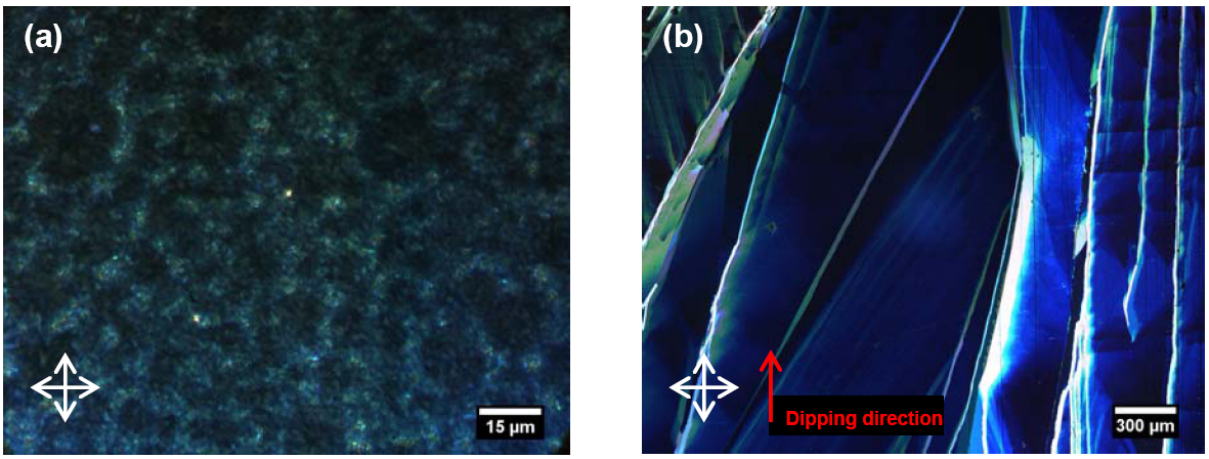

Figure 2.19. Film formation of the spin-coated (a) and dip-coated (b) DTBDT-C6 (**2b**) on SiO_2 bottom gate, top contact devices (polarized optical microscopy).

Table 2.6. FET performance of DTBDT series[a]

Organic layer	compounds	Electrode treatment reagent	μ_{FET}/cm^2 V^{-1} s^{-1}	I_{on}/I_{off}	V_{th}/V
Spin-coated film	DTBDT-C_1[b]	Pentafluorobenzenethiol (F_5BT)	7.0 ± 4.4 ×10^{-4}	1.7 × 10^3	4.7
	DTBDT-C_6	-	1.2 ± 0.8	10^5	-22 ± 9
	DTBDT-C_9[b]	Pentafluorobenzenethiol (F_5BT)	1.6 ± 0.4 ×10^{-3}	6.3 × 10^2	-3.9
	DTBDT-$C_{6.2}$[b]	Pentafluorobenzenethiol (F_5BT)	1.1 ± 0.4 ×10^{-3}	2.6 × 10^5	-36 ± 9
Dip-coated film	DTBDT-C_1	-	-	-	-
	DTBDT-C_6	-	1.0 ± 0.7	9 ± 3 ×10^6	-39 ± 6
	DTBDT-C_9	-	0.18 ± 0.15	3.2 × 10^5	-20 ± 10
	DTBDT-$C_{6,2}$	-	-	-	-

[a] More than 10 devices for each category were tested to confirm reproducibility and parameters were extracted from typical devices.
[b] Bottom contact configuration.

The superior mobilities and on/off ratios of the dip-coated devices in comparison to the spin-coated ones (**Table 2.6**) could be explained by the pronounced long-range order, which was reflected by a larger number of reflections with high scattering intensity. Based on this finding, less charge-trapping sites and hence lower threshold voltages are expected for the dip-coated than for the

spin-coated samples. However, higher threshold voltage values for the better-aligned dip-coated transistors were measured. The effects causing the increased threshold voltage are still unknown, and are currently under investigation.

It has been reported that bias stress could lead to increasing mobility and threshold voltage shifts in *p*- as well as *n*-type organic field-effect transistors. In general, the bias stress shifts are not fully understood but have been ascribed to several possible mechanisms as to why charge trapping occurs and where this charge is located, including (a) trapping in near-surface defects of the dielectric; (b) trapping in localized states at the dielectric/semiconductor interface; (c) trapping in the semiconductor; (e) ion migration in the dielectric or in the semiconductor; and (f) structural changes in the semiconductor. Stressed devices based on solution-processed compound **2** even led to mobilities up to 4.2 $cm^2V^{-1}s^{-1}$ but also to threshold voltages down to -75 V. These performance characteristic shifts could be addressed to charge carrier traps inside the semiconductor layer (c) as revealed by the use of different interface modifications, impedance spectroscopy and scanning Kelvin probe microscopy. The reason is still an open question to be investigated.

2.3.6.2 Device fabrication of **2c** by controlled dip-coating technique

In this study, the dip-coating technique was systematically studied and used to fabricate thin films transistors with DTBDT-C9 as the semiconducting channel. Through the careful control of dipping rate and solution concentration, the thickness of the film was readily adjusted. **Figure 2.20** shows an atomic force microscopy (AFM) image of the DTBDT-C9 *single* layers from dip-coating. According to the AFM image of the thin films, the thickness of the single layer thin film (1.745 nm) is in line with the reflection angle from powder XRD measurements (2.2 nm), which indicated that like the thick films from spin-coating, the molecules are packed with their *001* plane parallel to the substrate plane. By following the same dip-coating technique, double layers of the same compound were also made succesfully and shown in **Figure 2.21**.

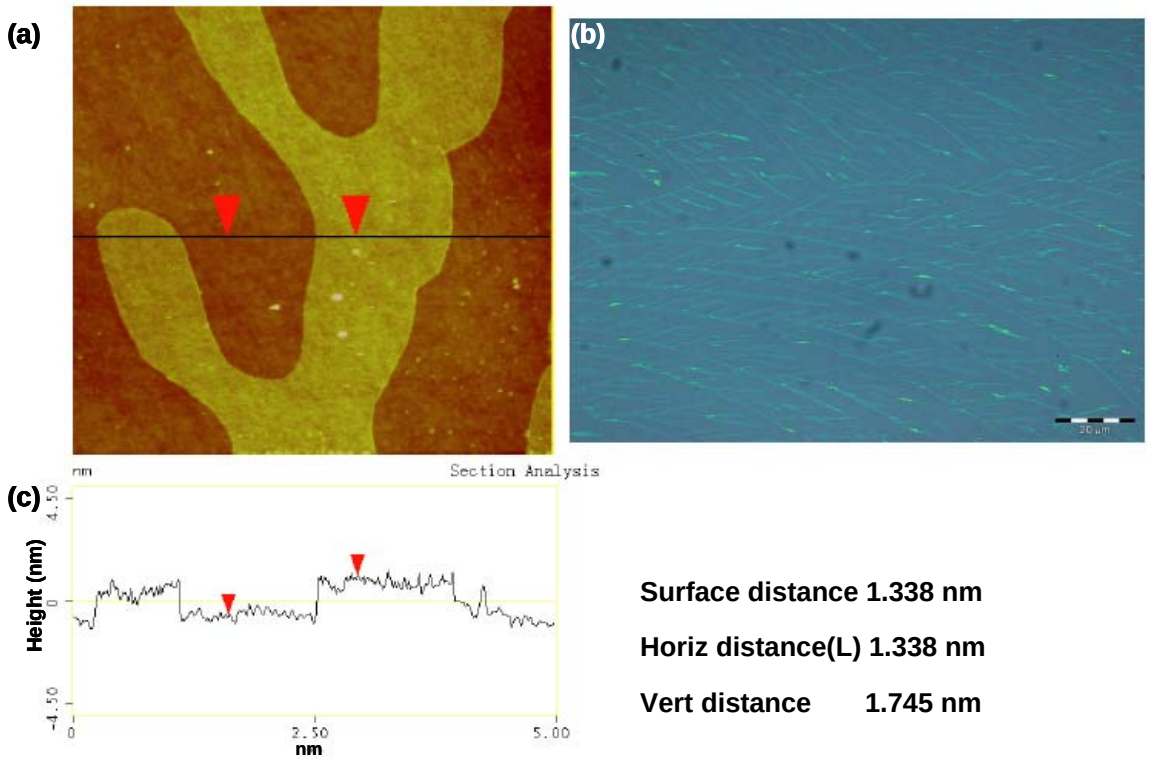

Figure 2.20. AFM and optical microscopy image of DTBDT-C9 single layers. (a) AFM image; (b) Large-area optical image; (c) section analysis

The formation of the double layers was supported by the thickness revealed by AFM section analysis (3.647 nm). The successful manipulation of the film formation makes it possible to fully understand the relationship between film morphology and charge transport properties.

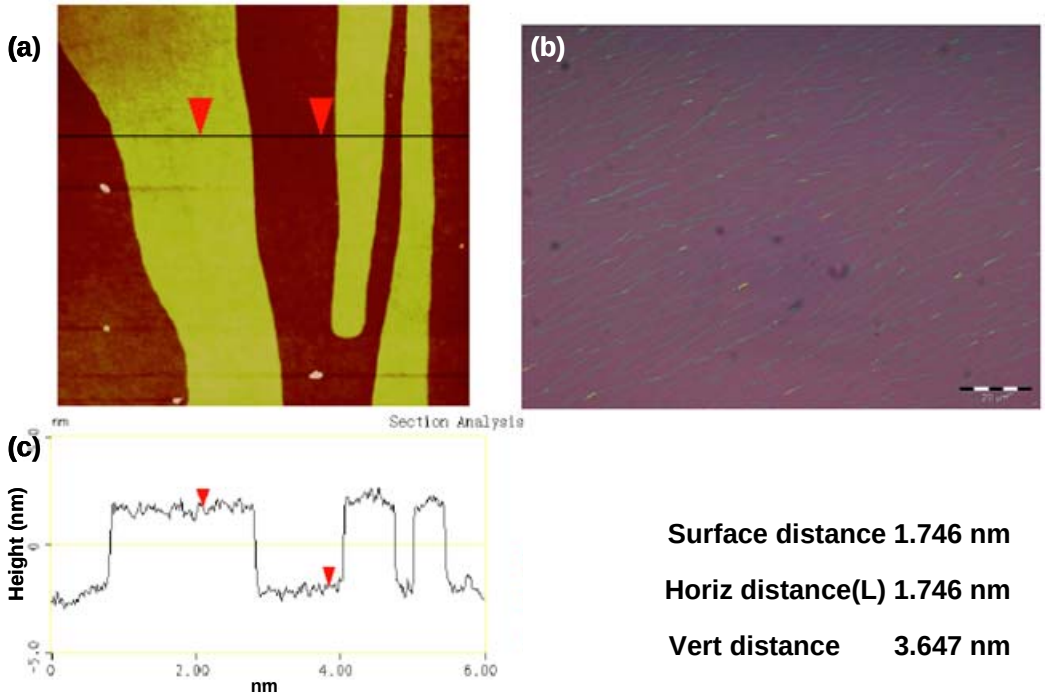

Figure 2.21. AFM and optical microscopy image of **2b** double layers. (a) AFM image; (b) Large-area optical image; (c) section analysis

After the successful fabrication of the semiconducting channel with a double layer thickness, a top contact device was made based on the same substrate. Gold electrodes were deposited via the vapour deposition method. A shadow mask was used to give a 20 μm channel (**Figure 2.22a**). **Figure 2.22b** showed the typical output characteristics (I_D-V_D) at different gate voltages (V_G) of OFETs based on **2b** thin films. They are typical of *p*-type semiconductors, with well-resolved current linear regimes (Ohmic region) in the low drain-source voltage range (V_{DS} < -5 V) and a saturation current near 16 μA at V_G = -40 V. (**Figure 2.22c**) By using the transfer characteristics of the transistors shown in **Figure 2.22c**, the average field-effect mobility (0.2 $cm^2 V^{-1}s^{-1}$) was calculated in the saturation regime (V_{DS} = -40 V) under ambient conditions. At the same time, an on/off ratio of 10^6 and V_{th} = -18 V were also derived. These results were comparable to the devices based on thick films made of the same compound and confirmed that the charge carrier movement happened in the first few monolayers adjacent to the interface.[21] A complete study of a series of devices with different precisely controlled film thickness is underway in the lab of Prof.

Lifeng Chi from Uni-Münster.

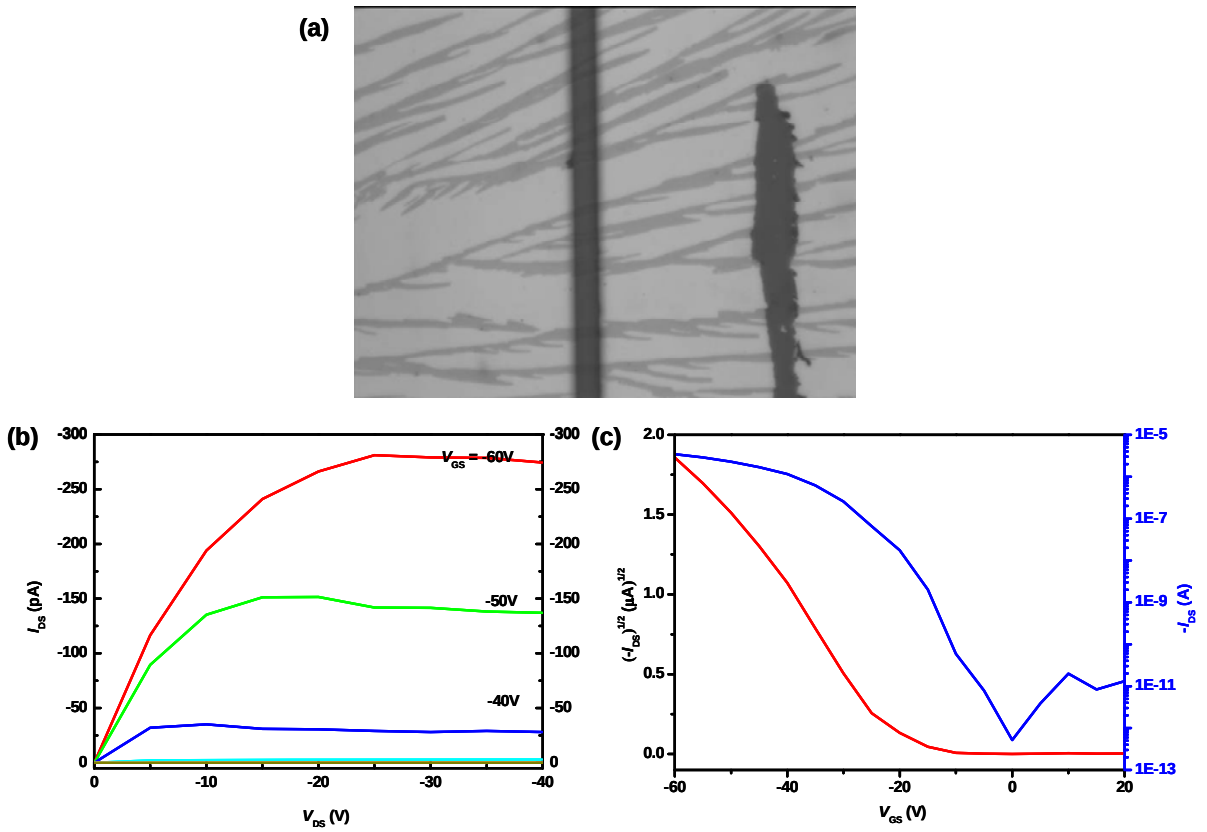

Figure 2.22. AFM and optical microscopy image of DTBDT-C9 double layers. (a) AFM image; (b) Large-area optical image; (c) section analysis

2.4 Electronic structure computation

A number of effects are important for describing charge carrier transport in thin films of semiconducting molecules at both molecular and intermolecular levels.[22] Although it is very difficult to predict such intermolecular effects as molecular packing and phonon energies from a molecular structure itself, it is believed that polycyclic heteroaromatics with large orbital coefficients on heteroatoms are especially promising as organic semiconductors, because such molecules can enhance the overlap of frontier molecular orbitals between adjacent molecules through strong heteroatomic interactions. To obtain insight into the effect of sulfur substitution on the orbital coefficients of BBBT (**1**) and DTBDT (**2**), MO calculations were carried out by Dr. Martin Baumgarten using the DFT method at the

B3LYP-6-31G(d) level with the Gaussian 03 program.[23] The HOMO and LUMO energy levels of **1** and **2** were summarized in **Table 2.7**, together with those of other sulfur-based five-ring-fused *p*-type semiconductors that were previously studied (**Figure 2.1**),[1] for comparison.

It should be noted that the two sulfur-containing molecules (**1** and **2**) have quite different orbital coefficients on sulfur atoms in the HOMOs, as depicted in orbital contour plots. (**Figure 2.23 a** and **b**) For comperision, the orbital contour plots of pentacene[12] and pentathenoacene (PTA)[24] are also shown. (**Figure 2.23 c** and **d**) In the HOMOs of **1** and **2**, the orbital spread over the whole molecule and there are large coefficients on sulfur atoms, suggesting an effective contribution of polarizable sulfur atoms to the intermolecular interactions for charge migration. In contrast, the HOMO of PTA has virtually no coefficients on sulfur atoms, thus explaining the fact that PTA-based OFETs showed relatively low hole mobility (0.045 $cm^2\ V^{-1}\ s^{-1}$),[1m] comparable to that of α-quinquethiophene (*α*-5T) (0.025 $cm^2\ V^{-1}\ s^{-1}$).[25] Actually, this assumption has already been corroborated by the fact that FET devices made of BBBT (**1**) and DTBDT (**2**) showed much higher hole mobility (0.1 $cm^2\ V^{-1}\ s^{-1}$ and 1.7 $cm^2\ V^{-1}\ s^{-1}$). On the other hand, although no sulfur atom involved, the HOMO of pentacene shows strong contributions from the carbon $2p_p$ orbitals and is fully delocalized along the whole molecule as indicated from DFT calculations, which is assumed to give rise to the high charge transport of pentacene (~ 1.0 $cm^2\ V^{-1}\ s^{-1}$).[26]

In addition, **table 2.7** indicates that **1** and **2** have lower HOMO energy levels and larger HOMO-LUMO gaps than pentacene (no sulfur-substitution) and **PTA** (five sulfur-substitutions). Although lowering of the HOMO levels may be disadvantageous to charge carrier injection, both the experiment and MO calculations suggest that **1** and **2** can behave as air-stable semiconductors.

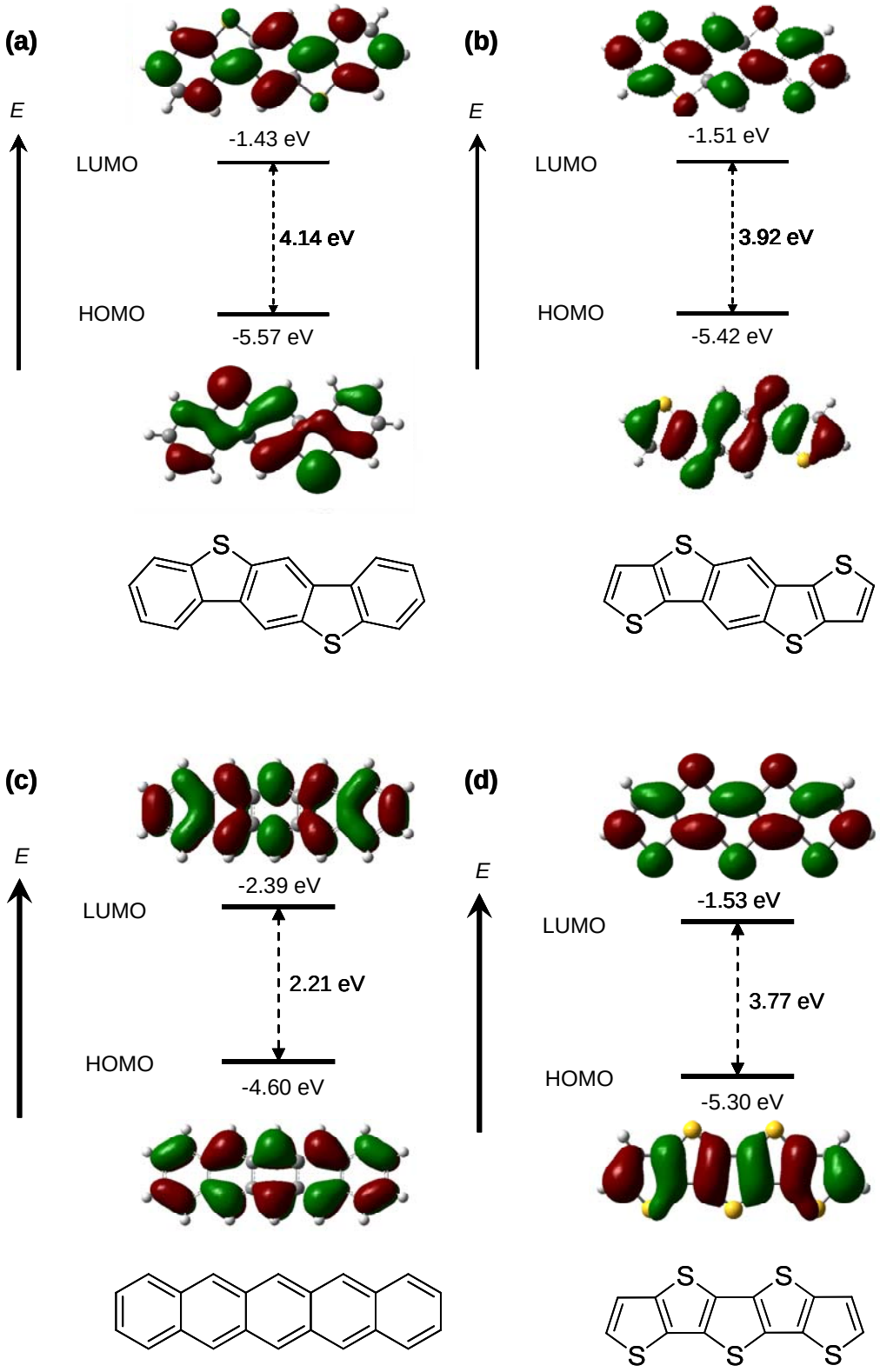

Figure 2.23. HOMO and LUMO of (a) **BBBT** (**1**), (b) **DTBDT** (**2**), (c) Pentacene and (d) pentathienoacene (**PTA**) at the B3LYP-6-31G(d) level

Table 2.7. Collection of reported HOMO levels and optical bandgaps of pentacene and its analogues in a sequence of increasing number of S atoms substitution.

		Pentacene[a]	picene[b]	TCT	ABT	ADT	BADT	**BBBT**	TBBT	DBTDT	**DTBDT**	PTA
	Number of Sulfur atoms	0	0	1	1	2	2	**2**	3	3	**4**	5
Experimental	HOMO[c]/eV	5.14	5.5	5.17	5.35	-[f]	-	**5.4**	5.6	5.6	**5.56**	5.33
Experimental	E_g/eV	2.14[e]	3.3	1.96[d]	2.5[d]	2.46[d]	-	**3.28[e]**	3.1(*anti*)[e] 3.3(*syn*)[e]	3.46[e]	**3.36**[e]	3.20[e]
Theory[g]	HOMO/eV	-4.56	-	-	-	-	-	**-5.57**	-	-5.545	**-5.42**	-5.30
Theory[g]	LUMO/eV	-2.39	-	-	-	-	-	**-1.43**	-	-1.497	**-1.51**	-1.53
Theory[g]	E_g/eV	2.17	-	-	-	-	-	**4.14**	-	4.048	**3.92**	3.77

[a] see ref. [1a. b]. [b] see ref. [27]. [c] from CV measurement. [d] thin film. [e] Solution. [f] Not reported. [g] DFT calculation

In conclusion, the efficient charge transport of the new molecules in this study can be attributed to the common structural features shared by **BBBT** (**1**), **DTBDT** (**2**) and pentacene, including molecular shape (flat molecule with a large aspect ratio), closed packing in crystals, and a delocalized HOMO with an energy level accessible for charge injection. This is in agreement with the reported results that in general, a more delocalized HOMO would allow better intermolecular orbitals overlap which would in turn lead to easier hole-transport by hopping.[28] It was found that semiconducting materials with a delocalized distribution of the highest occupied molecular orbital (HOMO) tend to have smaller reorganization energy (λ).[29] On the basis of Marcus theory[30], the λ is directly related to the charge carrier mobility. This study gives a clear guideline for the theoretical design of useful materials, and could open a way to the engineering of organic devices.

2.5 Conclusion

In efforts to develop pentacene analogues, two series of new heteropentacenes benzo[1,2-*b*:4,5-*b'*]bis[*b*]benzothiophene (**BBBT**, **1a-b**) and dithieno[2,3-*d*;2',3'-*d'*]-benzo[1,2-*b*;4,5-*b'*]dithiophene (**DTBDT**, **2a-d**) have been prepared by triflic acid induced intramolecular electrophilic substitution. Single-crystal XRD studies demonstrated that non-substituted **BBBT**, **1a** adopted an edge-to-face herringbone packing motif similar to pentacene, while other alkyl-substituted heteroacenes (**1b**, **2a-2d**) all gave rise to slipped cofacial π-π stacking motifs. Their crystal structures showed that the size of substituents and the degree of sulfur substitution had effects on the solid-state packing, and the S-S interactions enhanced the electronic transport between molecules. As deduced from optical properties and electrochemical redox measurements, both BBBT and DTBDT series exhibited low-lying HOMO energy levels (-5.4 eV and -5.56 eV) and large band gaps (3.28 eV and 3.36 eV) compared with that of pentacene (-5.14 eV and 2.14 eV), which was indicative of good stabilities against oxygen under ambient conditions.

OFETs fabricated with **BBBT** series showed mobilities as high as 0.1 $cm^2V^{-1}s^{-1}$ at

room temperature by solution drop-casting, which facilitated the use of any type of plastic substrates. Interestingly, our preliminary studies revealed better performance of solution processed OFETs in comparison to devices prepared by PVD. On the other hand, OFETs based on DTBDT series were fabricated by the dip-coating technique. Especially, devices employing the hexyl-substituted **DTBDT** (**2b**) as the semiconducting channel produced mobilities as high as 1.7 $cm^2V^{-1}s^{-1}$, and on/off ratios of 10^7. On the other hand, devices based on nonanyl-substituted **DTBDT** (**2c**) were fabricated by a controlled dip-coating technique. The thickness of the thin film is exactly tuned to give mono- and double-layered films. Preliminary study of the OFETs characteristics with double-layers revealed outstanding mobility of 0.2 $cm^2 V^{-1}s^{-1}$ under ambient conditions, which confirmed that the charge carrier movement took place in the first few monolayers adjacent to the interface. These results indicate that small heteroacene molecules possessing an extended aromatic core and solubilizing alkyl chains are extremely promising candidates for solution-processed organic–electronics devices.

In the end, DFT calculation of the frontier orbital topology of the new heteropentacenes was performed and compared with pentacene and pentathiacenes. The results revealed the reason for the high mobility of these new heteropentacenes in the molecular orbital level.

2.6 References

[1] (a) Tang, M. L.; Okamoto, T.; Bao, Z. *J. Am. Chem. Soc.* **2006**, *128*, 16002-16003. (b) Du, C.; Guo, Y.; Liu, Y.; Qiu, W.; Zhang, H.; Gao, X.; Liu, Y.; Qi, T.; Lu, K.; Yu, G. *Chem. Mater.* **2008**, *20*, 4188-4190. (c) Pietrangelo, A.; MacLachlan, M. J.; Wolf, M. O.; Patrick, B. O. *Org. Lett.* **2007**, *9*, 3571-3573. (d) Pietrangelo, A.; Patrick, B. O.; MacLachlan, M. J.; Wolf M. O. *J. Org. Chem.* **2009**, *74*, 4918-4926. (e) Laquindanum, J. G.; Katz, H. E.; Lovinger, A. J. *J. Am. Chem. Soc.* **1998**, *120*, 664-672. (f) Chen, M. C.; Kim, C.; Chen, S. Y.; Chiang, Y. J.; Chung, M. C.; Facchetti A.; Marks, T. J. *J. Mater. Chem.*, **2008**, *18*, 1029-1036. (g) Ebata, H.; Miyazaki, E.; Yamamoto, T.; Takimiya, K. *Org. Lett.* **2007**, *9*, 4499-4502. (h) Gao, P.; Beckmann, D.; Tsao, H. N.; Feng, X.; Enkelmann, V.; Pisula, W.; Müllen, K. *Chem. Commun.*, **2008**, 1548-1550. (i) Wex, B.; Kaafarani, B. R.; Kirschbaum, K.; Neckers, D. C. *J. Org. Chem.* **2005**, *70*, 4502-4505. (j) Wex, B.; Kaafarani, B. R.;

Schroeder, R.; Majewski, L. A.; Burckel, P.; Grell, M.; Neckers, D. C. *J. Mater. Chem.*, **2006**, *16*, 1121-1124. (k) Gao, J.; Li, R.; Li, L.; Meng, Q.; Jiang, H.; Li, H.; Hu, W. *Adv. Mater.* **2007**, *19*, 3008-3011. (l) Gao, P.; Beckmann, D.; Tsao, H. N.; Feng, X.; Enkelmann, V.; Pisula, W.; Müllen, K. *Adv. Mater.* **2009**, *21*, 213-216. (m) Xiao, K.; Liu, Y.; Qi, T.; Zhang, W.; Wang, F.; Gao, J.; Qiu, W.; Ma, Y.; Cui, G.; Chen, S.; Zhan, X.; Yu, G.; Qin, J.; Hu, W.; Zhu, D. *J. Am. Chem. Soc.* **2005**, *127*, 13281-13286.

[2] Valiyev, F.; Hu, W.-S.; Chen, H.-Y.; Kuo, M.-Y.; Chao, I.; Tao, Y.-T. *Chem. Mater.* **2007**, *19*, 3018-3026.

[3] (a) Pandya, L. J.; Pillai, B. D.; Tilak *J. Sci. Ind. Res.* **1959**, *18B*, 198-202. (b) Ahmed, J.; Ashby; Ayad, M.; Meth-Cohn, O. *J. Chem. Soc., Perkin Trans. I*, **1973**, 1099-1103.

[4] Haryono, A.; Miyatake, K.; Natori J.; Tsuchida, E. *Macromolecules*, **1999**, *32*, 3146-3149.

[5] (a) Sirringhaus, H.; Friend, R. H.; Wang, C.; Leuninger J.; Müllen, K. *J. Mater. Chem.*, **1999**, *9*, 2095-2101; (b) Leuninger, J.; Trimpin, S.; Räder H. J.; Müllen, K. *Macromol. Chem. Phys.*, **2001**, *202*, 2832-2842.

[6] (a) Anthony, J. E. *Chem. Rev.* **2006**, *106*, 5028-5048; (b) Anthony, J. E. *Angew. Chem.* **2008**, *120*, 460-492; *Angew. Chem. Int. Ed.* **2008**, *47*, 452-483.

[7] Curtis, M. D.; Cao, J.; Kampf, J. W. *J. Am. Chem. Soc.* **2004**, *126*, 4318-4328.

[8] Kawaguchi, K.; Nakano, K. ; Nozaki, K. *J. Org. Chem.* **2007**, *72*, 5119-5128

[9] (a) Campbell, R. B.; Robertson, J. M.; Trotter, J. *Acta Crystallogr.* **1962**, *15*, 289-290. (b) Holmes, D.; Kumaraswamy, S.; Matzger, A. J.; Vollhardt, K. P. C. *Chem. Eur. J.* **1999**, *5*, 3399-3412. (c) Siegrist, T.; Kloc, C.; Schön, J. H.; Batlogg, B.; Haddon, R. C.; Berg, S.; Thomas, G. A. *Angew. Chem., Int. Ed.* **2001**, *40*, 1732-1736. (d) Mattheus, C. C.; Dros, A. B.; Baas, J.; Meetsma, A.; de Boer, J. L.; Palstra, T. T. M. *Acta Cryst., Sect. C: Cryst. Struct. Commun.* **2001**, *C57*, 939-941. (e) Cornil, J.; Calbert, J. P.; Bredas, J. L. *J. Am. Chem. Soc.* **2001**, *123*, 1250-1251.

[10] Dimitrakopoulos, C. D.; Brown, A. R.; Pomp, A. *J. Appl. Phys.* **1996**, *80*, 2501-2508.

[11] Fogel, Y.; Kastler, M.; Wang, Z.; Andrienko, D.; Bodwell, G. J.; Mullen, K. *J. Am. Chem. Soc.* **2007**, *129*, 11743-11749.

[12] Maliakal, A.; Raghavachari, K.; Katz, H.; Chandross, E.; Siegrist, T. *Chem. Mater.* **2004,** *16,* 4980-4986.

[13] Scherf, U. *J. Mater. Chem.* **1999**, *9*, 1853-1864.

[14] Meng, H.; Bendikov, M.; Mitchell, G.; Helgeson, R.; Wudl, F.; Bao, Z.; Siegrist, T.; Kloc, C.; Chen, C. H. *Adv. Mater.* **2003**, *15*, 1090-1093.

[15] Wang, W.; Lee, T.; Reed, M. A., *Phys. Rev. B,* **2003**, *68*, 035416.

[16] Horowitz, G. *Adv. Funct. Mater.*, **2003**, *13*, 53-60.

[17] Bromley, S. T.; Mas-Torrent, M.; Hadley, P.; Rovira, C. *J. Am. Chem. Soc.* **2004**, *126*, 6544-6545.

[18] Locklin, J.; Ling, M. M.; Sung, A.; Roberts, M. E.; Bao, Z. *Adv. Mater.* **2006**, *18*, 2989-2992.

[19] (a) Bourguiga, R. ; Horowitz, G.; Garnier, F. ; Hajlaoui, R. ; Jemai, S. ; Bouchriha, H. *Eur. Phys. J. Appl. Phys.* **2002**, *19*, 117-122; (b) Di Carlo, A.; Piacenza, F.; Bolognesi, A.; Stadlober, B.; Maresch, H. *Appl. Phys. Lett.* **2005**, 86, 263501-263503.

[20] Scheinert, S.; Paasch, G.; Schrödner, M.; Roth, H. K.; Sensfuß, S.; Toll, Th. *J. Appl. Phys*. **2002**, 92, 330-337.

[21] a) Schreck, E.; Läuger, K.; Dransfeld, K. *Zeitschrift für Physik B Condensed Matter* **1986,** *62,* 331-334. b) Huang, J.; Sun, J.; Katz, H. E. *Advanced Materials* **2008,** *20,* 2567-2572.

[22] (a) Cornil, J.; Beljonne, D.; Calbert, J.-P.; Brédas, J.-L. *Adv. Mater*. **2001**, *13*, 1053-1066. (b) Brédas, J.-L.; Calbert, J. P.; da Silva Filho, D. A.; Cornil, J. *Proc. Natl. Acad. Sci. U.S.A*. **2002**, *99*, 5804-5809. (c) Brédas, J.-L.; Beljonne, D.; Coropceanu, V.; Jérôme, C. *Chem. Rev.* **2004**, *104*, 4971-5003. (d) Newman, C. R.; Frisbie, C. D.; da Silva Filho, D. A.; Brédas, J.-L.; Ewbank, P. C.; Mann, K. R. *Chem. Mater.* **2004**, *16*, 4436-4451.

[23] Gaussian 03, Revision B.04, M. J. Frisch, G. W. Trucks, H. B. Schlegel, G. E. Scuseria, M. A. Robb, J. R. Cheeseman, J. A. Montgomery, Jr., T. Vreven, K. N. Kudin, J. C. Burant, J. M. Millam, S. S. Iyengar, J. Tomasi, V. Barone, B. Mennucci, M. Cossi, G. Scalmani, N. Rega, G. A. Petersson, H. Nakatsuji, M. Hada, M. Ehara, K. Toyota, R. Fukuda, J. Hasegawa, M. Ishida, T. Nakajima, Y. Honda, O. Kitao, H. Nakai, M. Klene, X. Li, J. E. Knox, H. P. Hratchian, J. B. Cross, V. Bakken, C. Adamo, J. Jaramillo, R. Gomperts, R. E. Stratmann, O. Yazyev, A. J. Austin, R. Cammi, C. Pomelli, J. W. Ochterski, P. Y. Ayala, K. Morokuma, G. A. Voth, P. Salvador, J. J. Dannenberg, V. G. Zakrzewski, S. Dapprich, A. D. Daniels, M. C. Strain, O. Farkas, D. K. Malick, A. D. Rabuck, K. Raghavachari, J. B. Foresman, J. V. Ortiz, Q. Cui, A. G. Baboul, S. Clifford, J. Cioslowski, B. B. Stefanov, G. Liu, A. Liashenko, P. Piskorz, I. Komaromi, R. L. Martin, D. J. Fox, T. Keith, M. A. Al-Laham, C. Y. Peng, A. Nanayakkara, M. Challacombe, P. M. W. Gill, B. Johnson, W. Chen, M. W. Wong, C. Gonzalez, J. A. Pople, Gaussian, Inc., Wallingford, CT, **2004**.

[24] Osuna, R. M.; Zhang, X.; Matzger, A. J.; Juan, Victor H.； Navarrete T. L. *J. Phys. Chem. A* **2006,** *110,* 5058-5065.

[25] Rost, C.; Karg, S.; Riess, W.; Loi, M. A.; Murgia, M.; Muccini, M. *Appl. Phys. Lett.* **2004**, *85*, 1613-1615.

[26] (a) Klauk, H.; Halik, M.; Zshieschang, U.; Schmid, G.; Radlik, W.; Weber, W. *J. Appl. Phys.* **2002**, *92*, 5259-5263. (b) Sheraw, C. D.; Zhou, L.; Huang, J. R.; Gundlach, D. J.; Jackson, T. N.; Kane, M. G.; Hill, I. G.; Hammond, M. S.; Campi, J.; Greening, B. K.; Francl, J.; West, J. *Appl. Phys. Lett.* **2002**, *80*, 1088-1090. (c) Gundlach, D. J.; Lin, Y. Y.; Jackson, T. N.; Nelson, S. F.; Schlom, D. G. *IEEE Electron Device Lett.* **1997**, *18*, 87.

[27] Okamoto, H.; Kawasaki, N.; Kaji, Y.; Kubozono, Y.; Fujiwara A.; Yamaji, M. *J. Am.*

Chem. Soc., **2008**, *130*, 10470-10471.

[28] Chu, T.; Ho, M.; Chen, J.; Chen, C. *Chem. Phy. Lett.* **2005,** *415,* 137-140.

[29] Tokunaga, T.; Kawabata, H.; Matsushige, K. *Jpn. J. Appl. Phys.* **2008**, *47*, 3638-3642.

[30] Marcus, R.A., *Rev. Mod. Phys.* **1993**, *65*, 599.

Chapter 3
Sulfur and Nitrogen-bridged Hetero-heptacenes and Their Application for *p*-Channel Organic Thin Film Transistors

3.1 Introduction

In this chapter, ladder-type heteroacenes containing pyrrole and thiophene rings, dibenzo[*b*,*b*']thieno[2,3-*f*:5,4-*f*']carbazoles (DBTCz), bisthieno[3,2-*b*]thieno[2,3-*f*:5,4-*f*']- carbazoles (BTTCz) and diindolo[3,2-*b*:2',3'-*h*]benzo[1,2-*b*:4,5-*b*']bis[1]benzothio- phene (DIBBBT), were facilely synthesized through precursors (**11**, **15**, **20** and **25**) respectively. The key step was again a triflic acid induced intramolecular electrophilic coupling reaction of corresponding aromatic methyl sulfoxides with activated aromatic building blocks, which was performed at 0 ^{o}C to enable regioselective ring closure. Under the optimized reaction conditions, all the precursors gave the symmetrical products and with solubilizing alkyl chains in two different fashions. DIBBBT was synthesized as the extended ladder-type heteroacene with defined structure. These obtained heteroacenes were fully characterized by a combination of NMR, XRD, optical spectroscopic (UV/Vis and photoluminescence) and electrochemical (cyclic voltammetry) techniques. OFETs devices were fabricated with DBTCz series as the semiconducting channel.

3.1.1 Ladder-type heteroheptacenes

In marked contrast to the enormous study on heterotetraacenes and heteropentacenes, very few have been reported about the synthesis and application of heteroheptacenes in organic electronics.[1],[2],[3] In 1999, dibenzothienobisbenzo-thiophene (**DBTBT**) (**Figure 3.1**a) was first synthesized by Leuninger et al. as a hardly soluble solid with three different isomers.[1] During the same time, Bouchard et al. have tried several methods to get symmetrical ladder oligo(*p*-aniline) (diindolocarbazole DioCz) as a fully nitrogen atom bridged *p*-quaterphenyl (**Figure 3.1**b), and finally they found that the intramolecular Ullmann reaction instead of an unregioselective Cadogan ring closure was the most effective pathway.[2] In contrast, Sonntag et al. successfully synthesized diindenocarbzole (DieCz) via the Friedel-Crafts type alkylation ring closure which occurred exclusively at the 3 and 6 position of the carbazole (**Figure 3.1**c).[3] Moreover, only the first case, the purified isomer-free **DBTBT** was used as the active semiconducting layer in OFETs devices by PVD technique, the results of which turned out to be one of the best at that time (μ = 0.15 $cm^2V^{-1}s^{-1}$ and I_{on}/I_{off} >10^6).

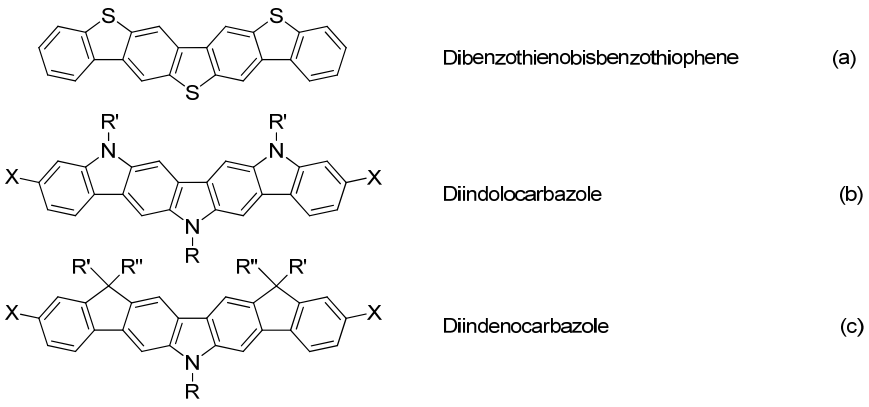

Figure 3.1. Ladder-type π-conjugated heteroacenes with thiophene or pyrrole ring units.

Based on the known examples and encouraged by work of Leuninger et al., we tried to further broaden the family of π-extended heteroheptacences, especially with the combination of electron rich thiophene and pyrrole ring units. For example, carbazole instead of dibenzothiophene as a stronger nucleophilic core will be used to construct the new molecules. (**Figure 3.2**)

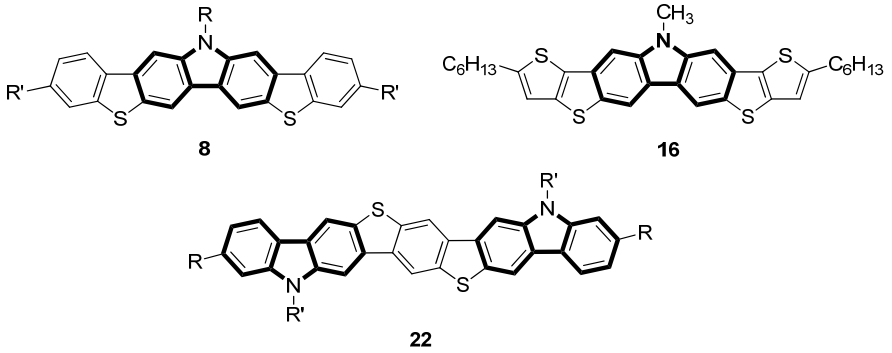

Figure 3.2. Ladder-type π-conjugated heteroheptacenes examined in this study.

3.1.2 Reactivity of carbazole under the condition of electrophilic substitution reaction

In the context of organic electronics, carbazoles have received considerable attention in the literature, as an important building block for both small-molecule and polymericoptoelectronic materials because of their desirable electronic and charge transport properties, as well as their high thermal stability. [2],[3] The ability to tune the carbazole's properties and incorporate them into more complex molecular structures requires either the chemical functionalization of the parent carbazole skeleton or its construction from simple, readily available synthons.[4],[5]

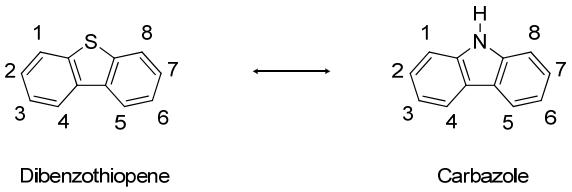

Figure 3.3. Structure of carbazole ring system versus dibenzothiophene

Owing to its highly electron-rich nature, the carbazole skeleton (**Figure 3.3**) is a modest nucleophile that can be readily derivatized with a wide variety of electrophiles (tertiary alkyl, acyl, nitro, halogen, etc.).[6] While commonly employed, such methods are limited in the position(s) on the ring system to which electrophiles can be introduced. The most reactive positions for electrophilic substitution are the 3 and 6 position, "para" to the nitrogen atom, and to a lesser extent, the 1 and 8 positions, which often require more drastic reaction conditions. The reported Friedel-Crafts type acylation/alkylation reaction and nitration reaction proceeded exclusively on the 3 and 6 position when exactly two equivalents of carbonyl chloride or nitration reagent were used, which firmly proved the pronounced difference in reactivity of these different positions.[7]

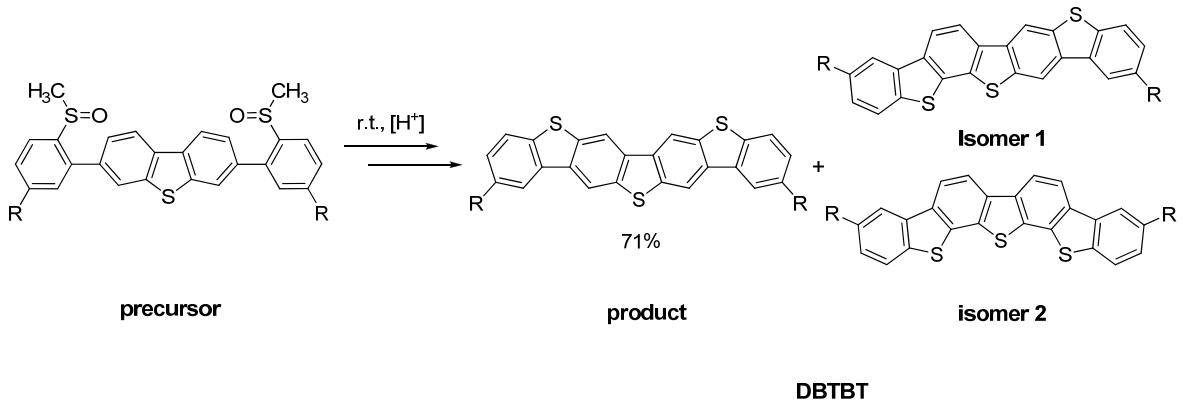

Scheme 3.1. Reported synthesis of DBTBT isomers via double intramolecular electrophilic coupling reaction [1]

We know from **Chapter 1** that the triflic acid activated aromatic methyl sulfoxides are utilized as electrophiles,[8] and the intramolecular electrophilic coupling reaction can form thiophene ring units easily. The electrophile species formed by methylsulfoxide and trifluoromethanesulfonic acid are attacking the most nucleophilic positions. Further, the reactions on dibenzothiophene failed to give regioselectivity although the 3 and 6 positions are the most reactive positions on the skeleton and yielded DBTBT as an inseparable mixture of three different regioisomers and the desired product in a ratio of 71%.[1] (**Scheme 3.1**)

3.1.3 How to solve the problem when carbazole was used as the nucleophilic core to construct the new molecules?

Although the differences in reactivity of carbazole, the possibility of isomerization is still present if the reactions are performed improperly. We learned from the literatures that in a similar reaction the para-selectivity was drastically influenced by the reaction temperature (**Scheme 3.2**).[9] The *ortho*-substituted thioanisole was not detected below 40 °C. At 100 °C, 1.3% of the *ortho*-substituted product (methyl-(2-(methylthio)-phenyl)phenylsulfoniumtrifluoro-methane-sulfonate) was observed.[9a] (**Scheme 3.2a**) On the other hand, the coupling reaction on diphenylamine performed at 0 °C occured only in the position *para* to the amino group.[9b] (**Scheme 3.2b**)

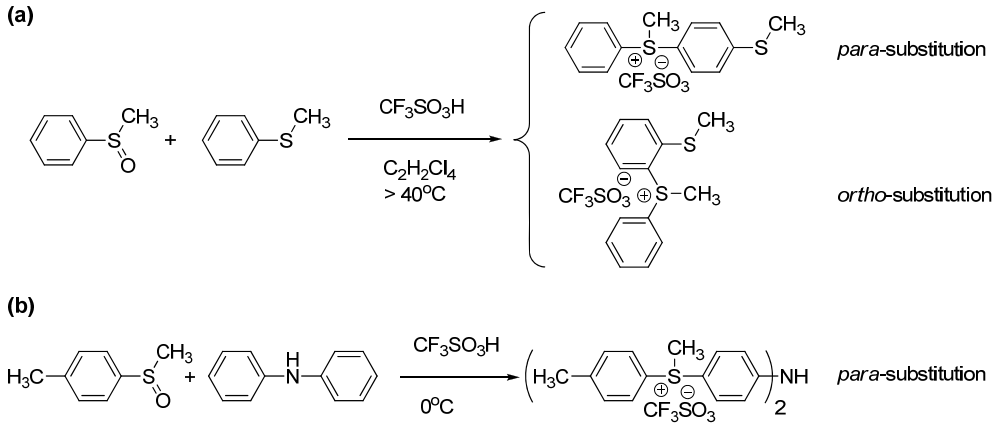

Scheme 3.2. Model reactions of the electrophilic substitution on thioanisole and diphenylamine

Therefore, the reaction temperature played an important role in the regioselectivity of the triflic acid induced electrophilic substitution reaction. Besides the low temperature that will be used in the reaction, two precursors **11** and **15** were designed for target molecule **8** (**Scheme 3.3**) to avoid the generation of unwanted isomers. It is obvious that precursor **11** is similiar to the one for DBTBT and can give compound **8** with alkyl chains lying on one side of the central rings, whereas precursor **15** hardly gives isomers and allows the facile introduction of two alkyl substituents in the *long-axis* of the molecular skeleton. The synthesis of precursor **15**

is possible due to the ultra reactive nature of the 3 and 6 position on carbazole, which offers the chance to introduce methylsulfoxide groups without perturbing the periphery aromatic systems.

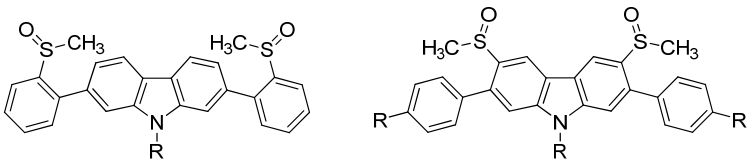

11 **15**

Scheme 3.3. Two possible precursors **11** and **15** for the synthesis of **8**

For compound **16**, precursor **20** was used due to the difficulty in the introduction of methylsulfoxide into the *β*-position of thiophene ring. And for the π extended compound **22**, we chose the same strategy as the synthesis of heteropentacene **1** and therefore precursor **25** was designed. (**Scheme 3.4**)

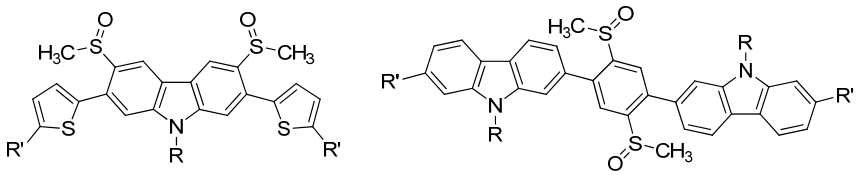

20 **25**

Scheme 3.4. Possible precursors **20** and **25** for the synthesis of **16** and **22**

3.2 Synthesis and characterization of sulfur and nitrogen-bridged heptacenes with carbazole (Cz) as the central π system

3.2.1 Synthesis of dibenzo[*b*,*b*']thieno[2,3-*f*:5,4-*f*']-carbazole (DBTCz) derivatives

The total synthetic route towards **8** via these two different precursors is therefore described in **Scheme 3.5**. Obviously, the shortest synthetic route towards **8** is via the synthesis of precursor **11**. Starting from 2,7-dibromocarbazole, compounds **9a-d** were made by introducing different alkyl side chains.[7] Subsequently, compounds **9** were treated with *n*-BuLi in hexane at -78 °C and quenched with

2-isopropoxy-4,4,5,5-tetramethyl-1,3,2-dioxaborolane to yield *N*-alkyl-2,7-bis(4,4,5,5-tetramethyl-1,3,2-dioxaborolane-2-yl)carbazole (**10a-d**).[10] Suzuki coupling of **10a-d** with 1-bromo-2-(methylsulfinyl)benzene[1] gave precursors **11a-d** in good yields.

The final ring-closure reaction was crucial to determine the isomeric purity. Before all the precursors were put into the triflic acid for the ring closure, test reactions were performed to find the optimized reaction conditions. Precusor **11d** was chosen for the test. The temperature effect in the coupling reaction was studied in triflic acid as both the solvent and reagent, at 0, 30 and 60 °C. (**Table 3.1**) One example reaction peformed at 60 °C is shown in **Scheme 3.6**. The isomers were isolated after nucleophilic demethylation of sulfonium salt by pyridine at reflux temperature, and calculated as {isomer X}/{[product] + [isomer 1] + [isomer 2] + [starting material]}

Table 3.1. Ratio of isomers under different conditions of test reactions[a]

Entry	Temperature /°C	Time/hour	Starting Material/%	Product /%	Isomer 1 /%	Isomer 2 /%
1	0	168	0	100	0	0
2	0[b]	72	0	100	0	0
3	30	72	5	90	5	0
4	30[b]	72	0	92	8	0
5	60	24	0	83	17	0

[a.] The disappearance of starting material is checked by FD-Mass. [b.] Phosphorus pentoxide added.

It can be seen from the table above that by lowering the reaction temperature the ratio of unwanted isomers can be reduced to zero and the presence of phosphorus pentoxide can effectively speed up the reaction by dehydrating the reaction system. What is surprising is that at all high temperature conditions only one kind of isomer was found as proven by SCXRD characterizations. (**Figure 3.9**) The alkyl group on the nitrogen atom probably hindered the ortho-substitution.

Therefore, instead of following exactly the procedure described in the synthesis of DBTBT (**scheme 3.1**), precursors **11a-d** were treated with trifluoromethanesulfonic acid (triflic acid) in the presence of phosphorus pentoxide at 0 °C and reacted for 72 h in the dark. Then the as-formed clear mixture was poured into ice/water to give a

yellowish powder as precipitate, followed by filtration, drying and reflux in pyridine for 12 h. After normal workup, only one spot was observed on thin layer chromatography (TLC) plates, which was supposed to be the desired product of DBTCz. After column chromatography, the yellow powder of DBTCz was achieved in good yield (85% to 95%). The further determination of isomeric purity by ^{1}H NMR spectroscopy (**Figure 3.4a**) and the single crystal structure (**Figure 3.5, 3.6, 3.7**) indicated that the symmetrical ladder-type oligoacene DBTCz (**8**) was the sole product. (**Scheme 3.5**) We ascribe this high regioselectivity to two reasons: firstly, the *3*- and *6*- positions on carbazole are the most reactive positions for electrophilic substitution and secondly, the reactions were all conducted near 0 ^{o}C since the regioselectivity of the thermodynamically controlled reaction is strongly influenced by reaction temperature and steric hindrance.

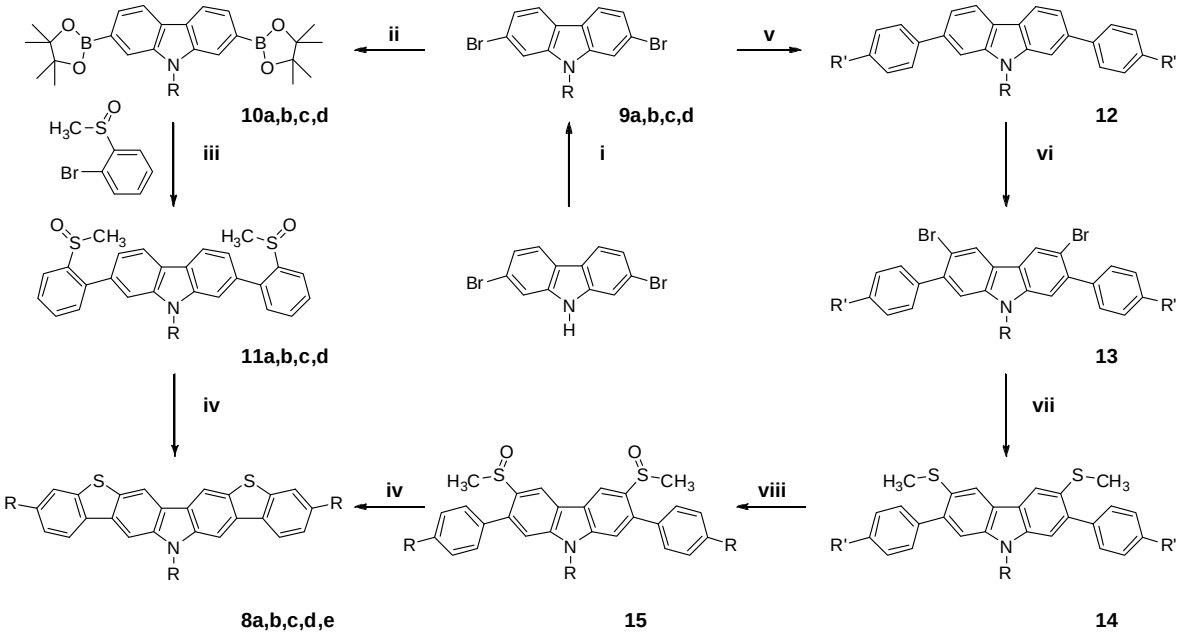

Reagents and conditions: i) NaH, alkyl bromide, dry DMF, rt; ii) THF, n-BuLi, -78 ^{o}C, 2-isopropoxy-4,4,5,5-tetramethyl -1,3,2-dioxaborolane; iii) Toluene, 2M K_2CO_3, 1-bromo-2-(methylsulfinyl)benzene, $Pd(PPh_3)_4$, 90 ^{o}C, 65 %; iv) a.CF_3SO_3H. rt., b. pyridine, reflux. 95 %; v) **4b**, $Pd(Ph_3)_4$, K_2CO_3, Toluene, 80^{o}C; vi) NBS, AcOH, $CHCl_3$, 86 %; vii) THF, n-BuLi, -78 ^{o}C, CH_3SSCH_3, 70 %; viii) AcOH, H_2O_2, 0 ^{o}C, 72 %.

a: R = CH_3; R' = H
b: R = C_4H_9; R' = H
c: R = C_6H_{13}; R' = H
d: R = C_8H_{17}; R' = H
e: R = CH_3; R' = C_4H_9

Scheme 3.5. Synthesis of DBTCz (**8**) through triflic acid induced ring-closure reaction

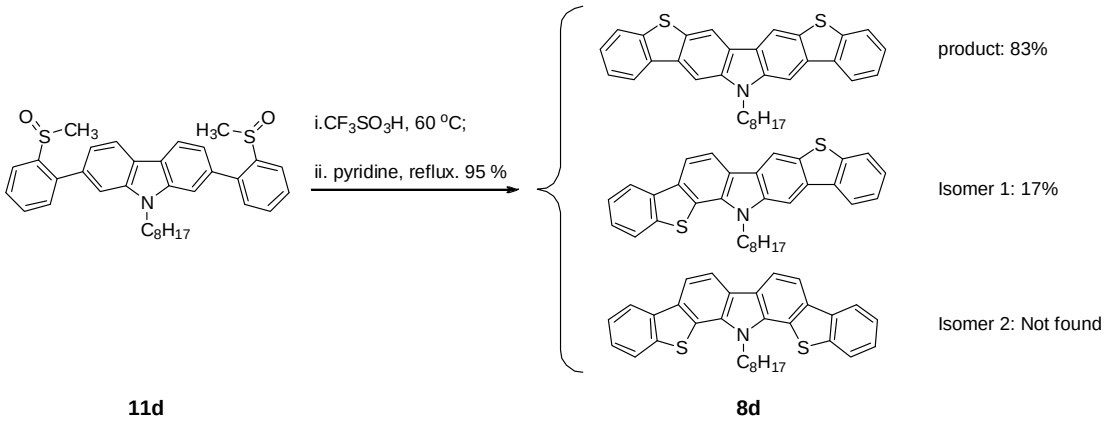

Scheme 3.6. Test reaction of on precursor **11d** to DBTCz (**8d**) at 60°C

Apart from the success in synthesizing **8a-d** from precursors **11a-d**, we followed the second route via precursor **15** towards **8e** which opened the opportunity to introduce additional two alkyl chains in the molecular *long-axis* direction. A Suzuki coupling reaction between **9a** and **4b** was carried out in a two-phase system of toluene and aqueous potassium carbonate, with $Pd(PPh_3)_4$ as catalyst and gave **12** in good yield. Afterwards, with two equivalent of *N*-bromosuccinimide in acetic acid, it was possible to regioselectively introduce two bromine groups at the *3*- and *6*-positions on the carbazole unit of compound **12**. Compound **13** was obtained after a simple column chromatography and further reacted with two equivalents of *n*-BuLi to form the corresponding 3,6-dilithiated species which was then quenched by dimethyl disulfide to afford compound **14** in 70 % isolated yield. Oxidation of **14** with hydrogen peroxide in acetic acid gave precursor **15** in 72 % yield. Finally, by following the same procedure as for precursor **11**, compound **8e** was received as yellow flakes in 96 % yield. *Again, when the N-alkyl groups are longer than C10, degradation was detected.* Therefore, we never achieve an oligomer with long alkyl chain groups.

3.2.2 Synthesis of bisthieno[3,2-*b*]thieno[2,3-*f*:5,4-*f*']-carbazoles (BTTCz)

The synthesis of BTTCz (**16**) is outlined in **Scheme 3.7**. The Stille coupling reaction between 2,7-dibromo-9-methyl-9H-carbazole (**9a**) and (5-hexylthiophen-2-yl) trimethylstannane (**6b**) was carried out in DMF as the solvent with $Pd(PPh_3)_4$ as the catalyst to give **17** in good yield. Afterwards, regioselective bromination on the *3*- and *6*- positions on the carbazole core of compound **17** was achieved using two equivalents of *N*-bromosuccinimide in a 1:1 mixture of chloroform and acetic acid. Compound **18** was obtained after a simple column chromatography and further reacted with two equivalents of *n*-BuLi to form the corresponding 3,6-dilithiated species which was then quenched with dimethyl disulfide to afford compound **19** in 50 % isolated yield. Oxidation of **19** with hydrogen peroxide in acetic acid gave precursor **20** in 72 % yield. By following the same ring-closure procedure as for precursor **11**, BTTCz (**16**) was received in 95% yield as a light yellow solid.

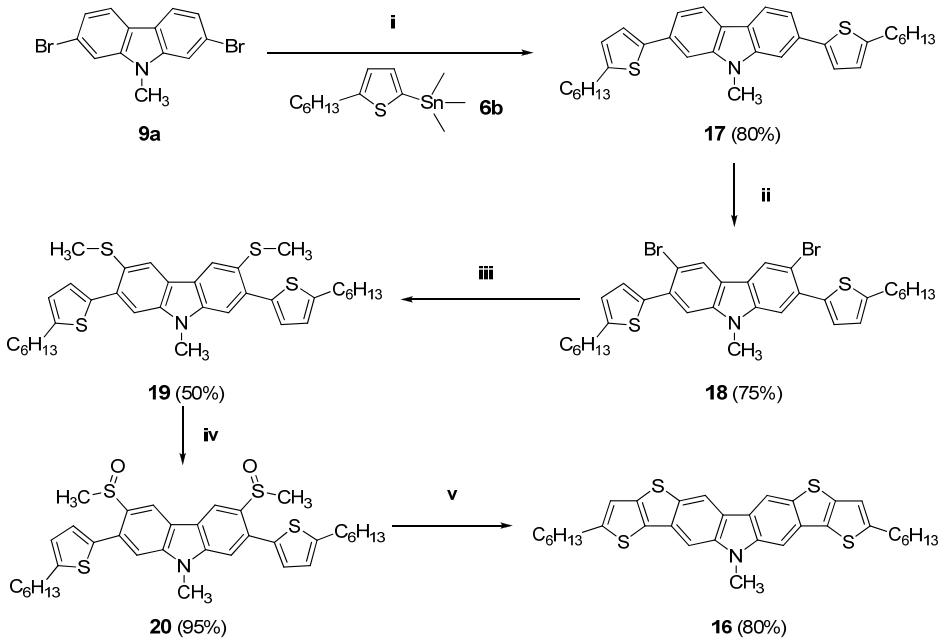

Reagents and conditions: i) $Pd(PPh_3)_4$, DMF, 85°C; ii) NBS, AcOH, $CHCl_3$, rt; iii) THF, *n*-BuLi, -78 °C, CH_3SSCH_3; iv) AcOH, H_2O_2, 0 °C; v) a. CF_3SO_3H, 0°C; b. Pyridine, reflux.

Scheme 3.7. Synthesis of bisthieno[3,2-*b*]thieno[2,3-*f*:5,4-*f*']-carbazoles (BTTCz, **16**)

3.2.3 Synthesis of diindolo[3,2-*b*:2',3'-*h*]benzo[1,2-*b*:4,5-*b'*]bis[1]benzothiophene (DIBBBT)

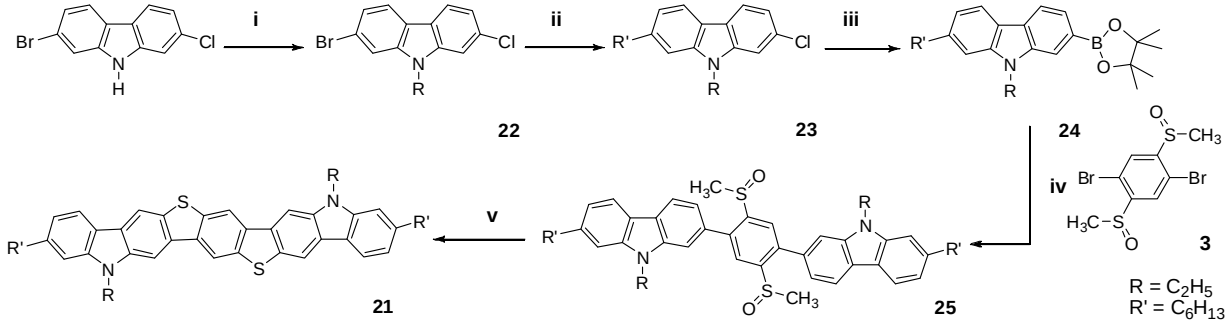

Reagents and conditions: i) NaH, ethyl bromide, dry DMF, rt; ii) THF, *n*-BuLi, -78^{o}C, hexyl iodide, 65 %; iii) $Pd_2(dba)_3$, 2-dicyclohexylphosphino-2',4',6'-triisopropylbiphenyl, bis(pinacolato)diboron, KOAc, 110 ^{o}C, 90 %; iv) Toluene, 2M K_2CO_3, **3**, $Pd(PPh_3)_4$, 90 ^{o}C, 72 %; v) a.CF_3SO_3H. rt., b. pyridine, reflux. 95 %.

Scheme 3.8. Synthesis of DIBBBT (**21**) through triflic acid induced ring-closure reaction

By following the similar strategy as described above, we synthesized another precursor **25** which allowed the final triflic acid induced ring closure towards further extended but soluble oligoacene **21**. (**Scheme 3.8**). The easily available 2-bromo-7-chloro-carbazole[11] was alkylated with an ethyl group on the nitrogen atom to give **22**, which was then reacted with one equivalent of *n*-BuLi at -78 ^{o}C. The monolithiated species was then quenched with hexyl iodide to generate the 2-chloro-7-hexyl-9-ethyl-carbazole (**23**). Monoboronic ester **24** from **23** was made in high yield by using a mixture of $Pd_2(dba)_3$ and 2-dicyclohexylphosphino-2',4',6'-triisopropylbiphenyl as catalyst system.[12] A double Suzuki cross-coupling reaction between **24** and **3** using $Pd(PPh_3)_4$ as catalyst afforded precursor **25** in 72 % yield. Subsequent treatment of **25** with trifluoromethanesulfonic acid at 0 ^{o}C for 72 h induced double intramolecular ring closure. Later on, the intermediate was refluxed in pyridine to afford target **21** in 95% yield as yellow solid. The ^{1}H NMR spectrum of **21** confirmed the pure product formation and indicated the high regioselectivity of the electrophilic ring closure reaction (**Figure 3.4d**)

3.2.4 Structure proof of the heteroacenes by ^{1}H NMR spectroscopy

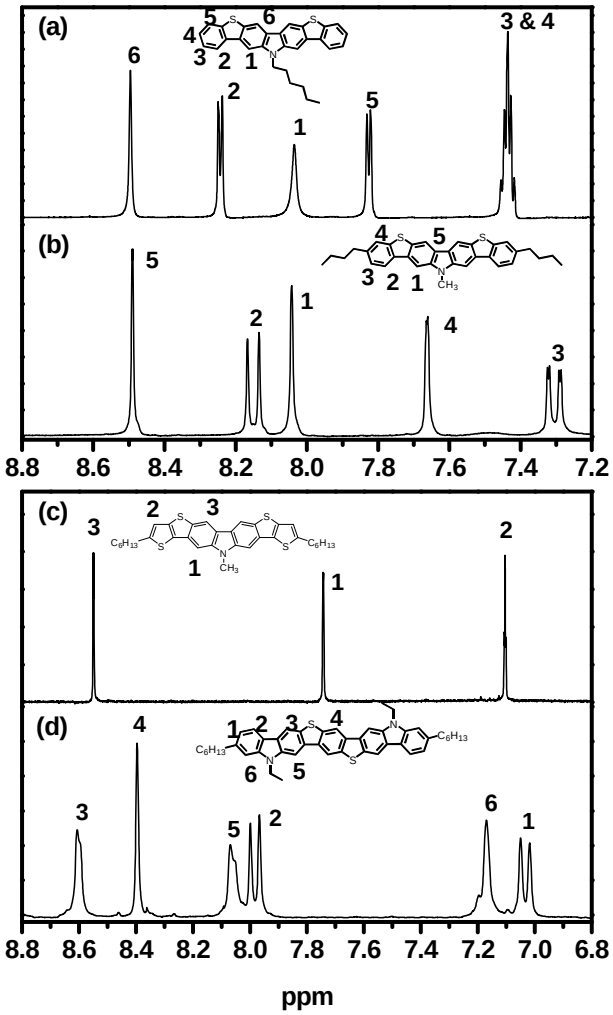

Figure 3.4. Expended aromatic region of ^{1}H NMR spectra of compounds (a) **8c** (700 MHz, 420 K, d_2-1, 1, 2, 2-tetrachloroethane); (b) **8e** (250 MHz, 300 K, d_2-dichloromethane); (c) **16** (250 MHz, 300 K, d_2-dichloromethane) and (d) **21** (250 MHz, 300 K, d_2-dichloromethane).

As depicted in **Figure 3.4**, the ^{1}H NMR spectra provide evidence for the regioselectivity of the ring-closure reaction, since all the typical singlets can be assigned to the corresponding aromatic protons in the molecules. No isomers could be discerned from the spectra. The signals of aromatic protons of **8c** (proton 2, 3 and 5) (**Figure 3.4a**) shift to high field in the case of **8e** (aromatic protons 2, 3 and 4 (**Figure 3.4b**), owing to the electron donating effects of the substituted alkyl chain.

Due to the symmetry of compound **16**, only 3 singlets in the aromatic region of the spectrum were expected and were assigned accordingly (**Figure 3.4c**). In **Figure 3.4d**, all the aromatic proton signals were in good agreement with the highly symmetrical structure of compound **21**.

3.2.5 Solid-state crystal structure and packing properties revealing the alkyl substituting effect on the solid structure

It has been shown in the literature and in **Chapter 2** that the solid-state morphology of conjugated materials plays an important role in the performance characteristics of electronic devices;[13] thus, X-ray diffraction studies were performed on crystals of **8b, 8c, 8d** (isomer 1) and **8e** to determine their solid-state order and the effect of the side-chain substitution on the solid-state structures. For **8a**, **8d**, **16** and **21**, however, no suitably sized crystals for single-crystal X-ray analysis could be obtained from different solvents. The crystallographic parameters are collected in **Table 3.2**.

Compound **8b** has two independent molecules in one unit cell and each molecule possesses a symmetrical geometry with the *n*-butyl substituents arranged out of the backbone at one side (**see Figure 3.5c**). Interestingly, the *n*-butyl substituents in each molecule were arranged in a different manner with the four carbon atoms of one n-butyl substituent adopting a mean 'anti' geometry with a torsion angle of 177° and the other a tangled geometry with a torsion angle of -147°. (**Figure 3.5c**) This arrangement may be because of the steric hindrance of the two molecules in one unit cell. From the stacking structure shown in **Figure 3.5b**, we can see that two independent molecules closely interacted via C-C short interaction (3.35 Å) in a face-to-face fashion to construct an anti-parallel pair. (**Figure 3.5d**, marked in green lines) Several short C-H···π contacts are also found inside the crystal structures. Then the anti-parallel pairs interact with two adjacent pairs with short C-S interactions (3.23~3.41 Å) to form a herringbone structure. (**Figure 3.5d**, marked in red lines) As for the pendant *n*-butyl chains, different short C-H···π contacts exist between the two

n-butyl chains and the adjacent π system. This may explain why the two n-butyl chains adopt different arrangements.

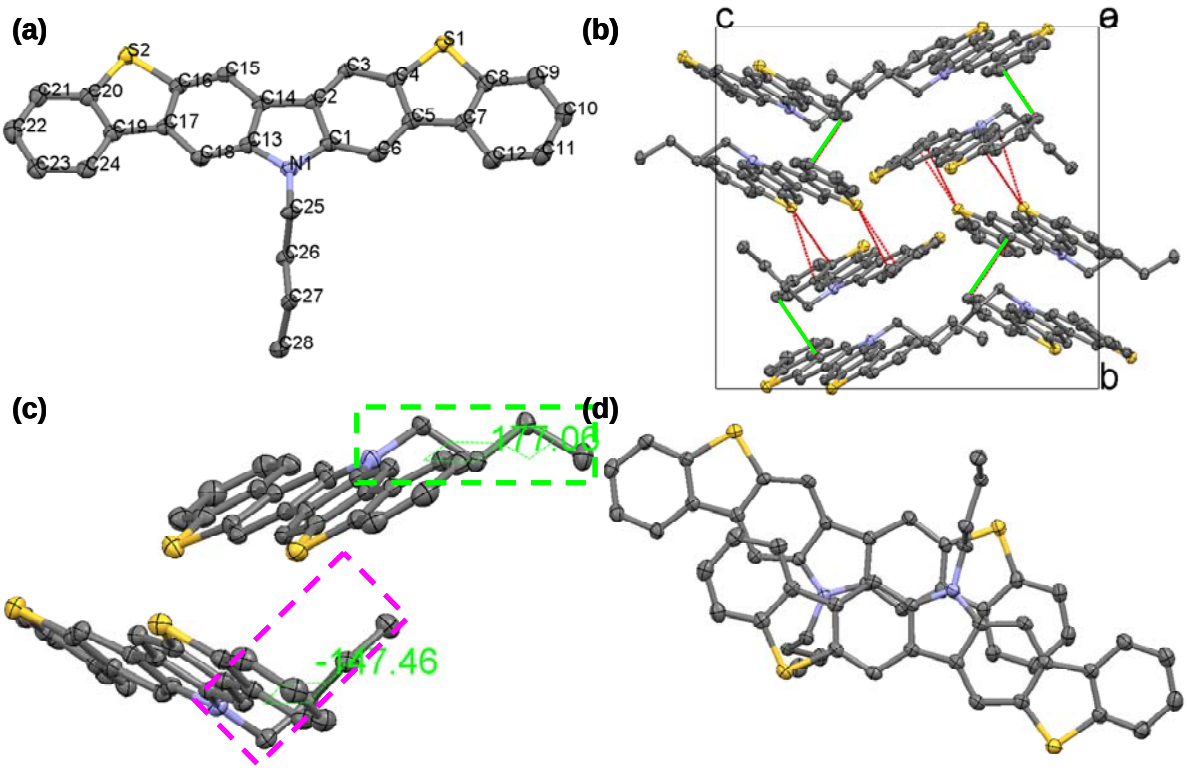

Figure 3.5. Packing diagrams of **8b** in solid state. a) Thermal ellipsoid of **8b**. The hydrogen atoms were omitted for clarity. Thermal ellipsoids are drawn at 50% probability. b) views along the *a* axis. (Dashed lines illustrate the short contacts between each two molecules in the unit cell. Green lines indicate C-C contacts: 3.35 Å. Red lines indicate S-C contacts: 3.23~3.41 Å) c) Two different kinds of conformation of the butyl groups present in the two close contacted molecules respectively. (Dashed rectangular indicating the two different kinds of butyl groups). d) View down the projection direction of two almost head-to-tail cofacial molecules.

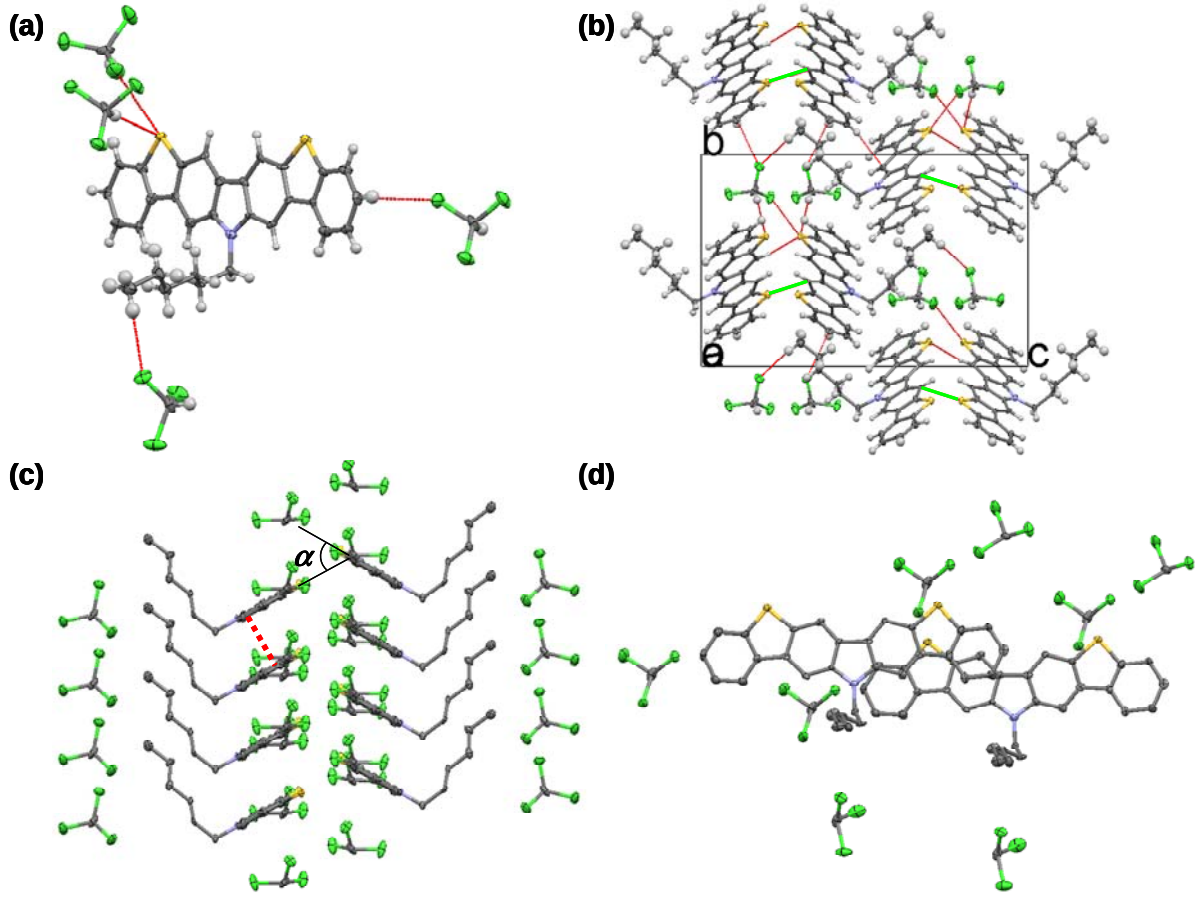

Figure 3.6. Packing diagrams of **8c** and chloroform molecules in solid state. (Thermal ellipsoids are drawn at 50% probability) a) Short interactions between each molecule of **8c** and four chloroform molecules. b) views along the *a* axis. The anti-parallel pairs carrying their interacted chloroform molecules further stacked into slipped columns. c) Herringbone structures from the view in the long molecular axis. Dashed red lines indicating the short S-C contacts (ca. 3.44 Å). d) View down the projection direction of two cofacial molecules.

Crystals of **8c** suitable for single-crystal X-ray diffraction (XRD) studies were grown from cold chloroform. The first SC XRD analysis showed crystals of **8c** with chloroform molecules as guest molecules inside the crystal lattice. As shown from **Figure 3.6**a, the planar and highly symmetric molecule of 8c interacts with four chloroform molecules via close S-Cl, S-H and Cl-H interactions as indicated by red lines. The molecules of **8c** and chloroform co-crystallized in the orthorhombic *P* n 2_1/a space group with eight independent molecules in the unit cell (four **8c** and four

chloroform molecules). In one unit cell, the four molecules of **8c** assembled into two anti-parallel pairs which were surrounded by chloroform molecules. An extended example is illustrated in **Figure 3.6**b, from which one can see the short interactions among the molecules marked with red lines. Close S-C distances shorter than the sum of their van der Waals radii (3.55 Å) were measured (3.44 Å) within the pairs and highlighted with green lines. The anti-parallel pairs carrying their interacted chloroform molecules further stacked into slipped columns. In **Figure 3.6**c, we see herringbone structures from the view in the long molecular axis, where the tilt angle (*a*) between two mean planes of the **8c** framework is 60°. The presence of π-π overlapping is confirmed by the measured interplanar distance as 3.33 Å. (Marked in red dash line) A top view of the first two molecules from the stacking direction of the columns is shown in **Figure 3.6**d.

Several days later, the totally dried crystals were analyzed again by SC XRD. It was surprising to see the transformation of the crystal structure from orthorhombic to triclinic upon the losing of all the chloroforms molecules. The structure of dried **8c** is shown in **Figure 3.7a**, which kept the same planar structure. However the crystal packing property changed dramatically. As can be seen in **Figure 3.7b**, in one unit cell, four independent molecules lie with the long molecular axis perpendicular to the adjacent molecules. Each of the four molecules couples with another molecule from surrounding unit cells to form a pair with antiparallel structure (indicated by the dashed rectangular) with the tilt angle between two mean planes close to 0°. The antiparallel pairs further stack along the *a* axis into a tilted "double-column", the side view of which is shown in **Figure 3.7c**. Interestingly, there is no overlap between the adjacent molecules inside each semi-column, but the molecules are interacting through two S-C short interactions. The short distances (3.41 and 3.46 Å) are much shorter than the sum of their van der Waals radii (3.55 Å). These same distances are observed between the S1 and S2 atoms of each molecule and the C12 and C24 atoms of additional molecule inside the semi-columns (Marked in red dash line). However, partial head-to-head overlap is found between two molecules from two semi-columns respectively and an interplanar distance of 3.47 Å indicates the

presence of π-π interactions between the molecules (Marked in green dash line). This contact distance is shorter than those observed between close-carbon contacts in adjacent molecules of pentacene (3.6-3.8 Å).[14] This structure seems like an intermediate state between herringbone structure and cofacial stacking structure. Only weak C-H···π contacts[15] were found between the independent antiparallel columns.

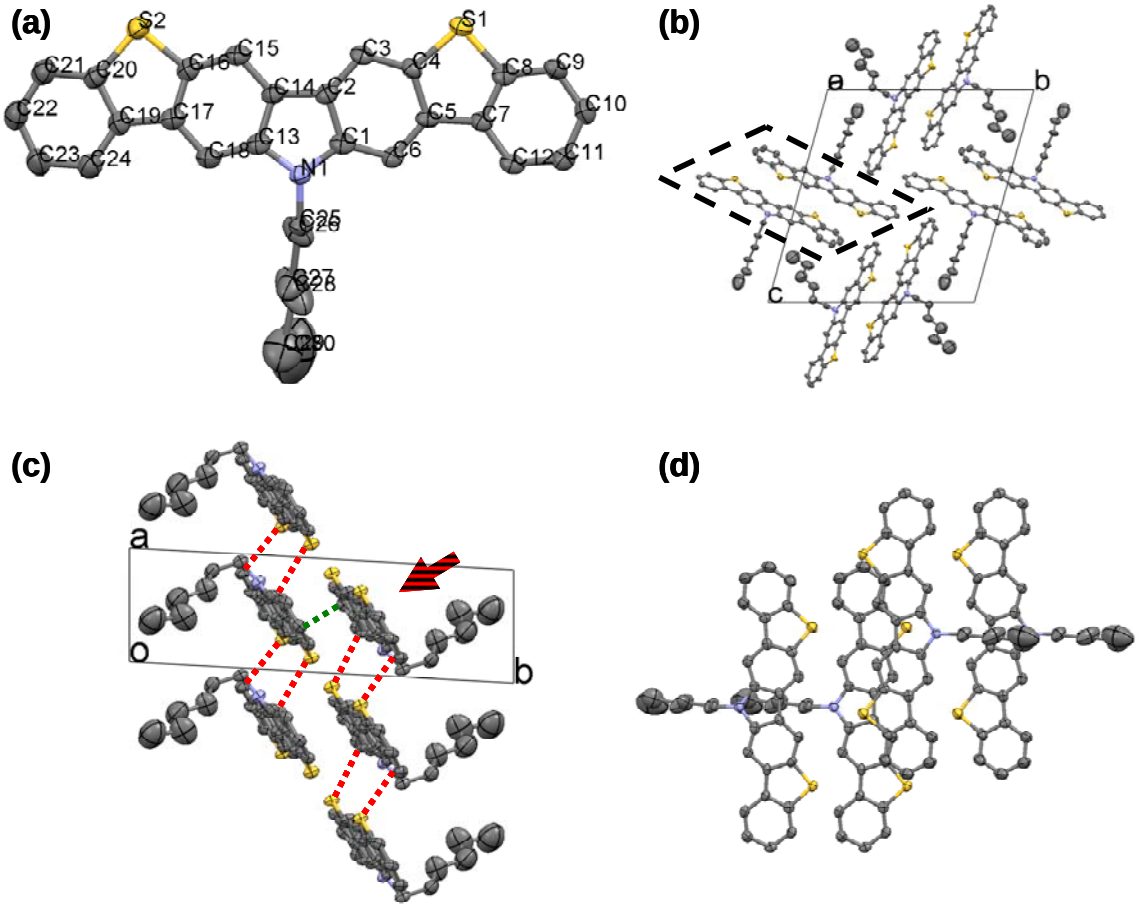

Figure 3.7. Packing diagrams of **8c** in solid state. a) Thermal ellipsoid of **8c**. The hydrogen atoms were omitted for clarity. Thermal ellipsoids are drawn at 50% probability. b) views along the *a* axis. (Dashed rectangular illustrate the antiparallels pairs) c) Crystal stacking of 8c in one of the four antiparallel pair columns. Dashed red lines indicating the short S-C contacts (ca. 3.41 and 3.46 Å). Dashed green line indicating the interplanar distance (ca. 3.47 Å). d) View down the projection direction of two cofacial molecules (arrow shown in c)).

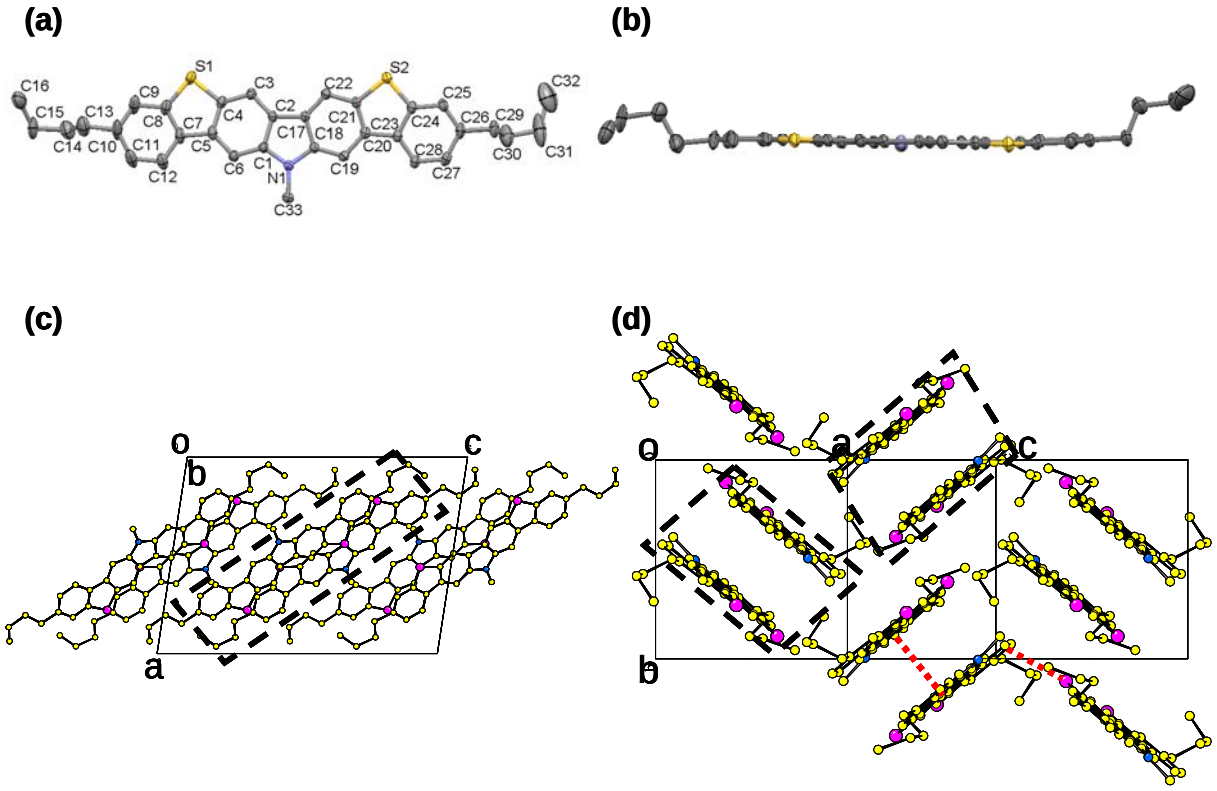

Figure 3.8. Packing diagrams of **8e**. a) Thermal ellipsoid of **8e**. The hydrogen atoms were omitted for clarity. Thermal ellipsoids are drawn at 50% probability. b) Views along the short molecular axis. (c) View down the stacking axis of dimers. (Dashed rectangular illustrate the dimmers of the molecules) (d) View along the long molecular axis showing sandwiched herringbone structure. (Dashed rectangular illustrate the dimmers of the molecules. Dashed lines illustrate intermolecular close-contacts within and between the dimers)

The main structural difference between **8e** and all other DBTCz molecules is the position of the long alkyl substitution with **8a-d** on the *short-axis* direction and **8e** on the *long-axis* direction. What will this difference induce in the solid structure? Single crystal X-ray analysis shows that compound **8e** crystallizes in the monoclinic $P\,2_1/c$ space group with four molecules in the unit cell. As seen from **Figure 3.8a**, **b**, compared with that of **8c**, the aromatic skeleton of **8e** is exactly the same, while the packing characteristics are dramatically changed by altering the position of alkyl substituents. The crystal structure of **8e** is based on a sandwiched herringbone

structure in which its dimers are packed tightly in the crystal (**Figure 3.8c**, marked in dashed rectangular). These dimers are formed by two inversely packed molecules in an anti-parallel fashion to the direction of short molecular axis. The plane-to-plane distance is ca. 3.45 Å (suggesting π-π overlapping), and short C-S contacts (3.49 Å) also exist in a face-to-edge manner between the dimers, indicative of the two-dimensional electronic structure of the crystal (marked in dashed line).

In the end, as shown in **Figure 3.9**, there comes the crystal structure of **8d** (isomer 1). The molecules crystallize in the monoclinic $P\ 2_1/a$ space group with four independent molecules in the unit cell and each molecule possesses an asymmetrical geometry due to the ortho-electrophilic attack on the bottom of the carbazole. The *n*-octyl lies with only the C25 in the plane of the aromatic skeleton and all the others out of the backbone at one side (see **Figure 3.9a**). Interestingly, unlike the other wanted isomers, the skeleton of **8d**-isomer 2 has a large dihedral angle between the mean planes of the two outside benzene rings ≈ 8.8°, comparing to 4.8° of **8b**, 3.5° of **8c** and 3.2° of **8e**. (**Figure 3.9c**) This could be due to the high strain induced by the isomerization and indicates that more energy is needed to form such distorted structures. From the stacking structure shown in **Figure 3.9b**, we can see that, like all the other three molecules above, two independent molecules construct one anti-parallel pair in a face-to-face fashion with an interplanar distance of 3.38 Å which indicates the presence of π-π interactions. (Marked in red dash line) Meanwhile, each of the two molecules in the pair interacts with another molecule in two adjacent pairs respectively with short C-C interactions (3.4 Å), based on which the anti-parallel pairs form a sandwiched herringbone structure. Several short C-H$\cdots\pi$ contacts are also found inside the crystal structures.

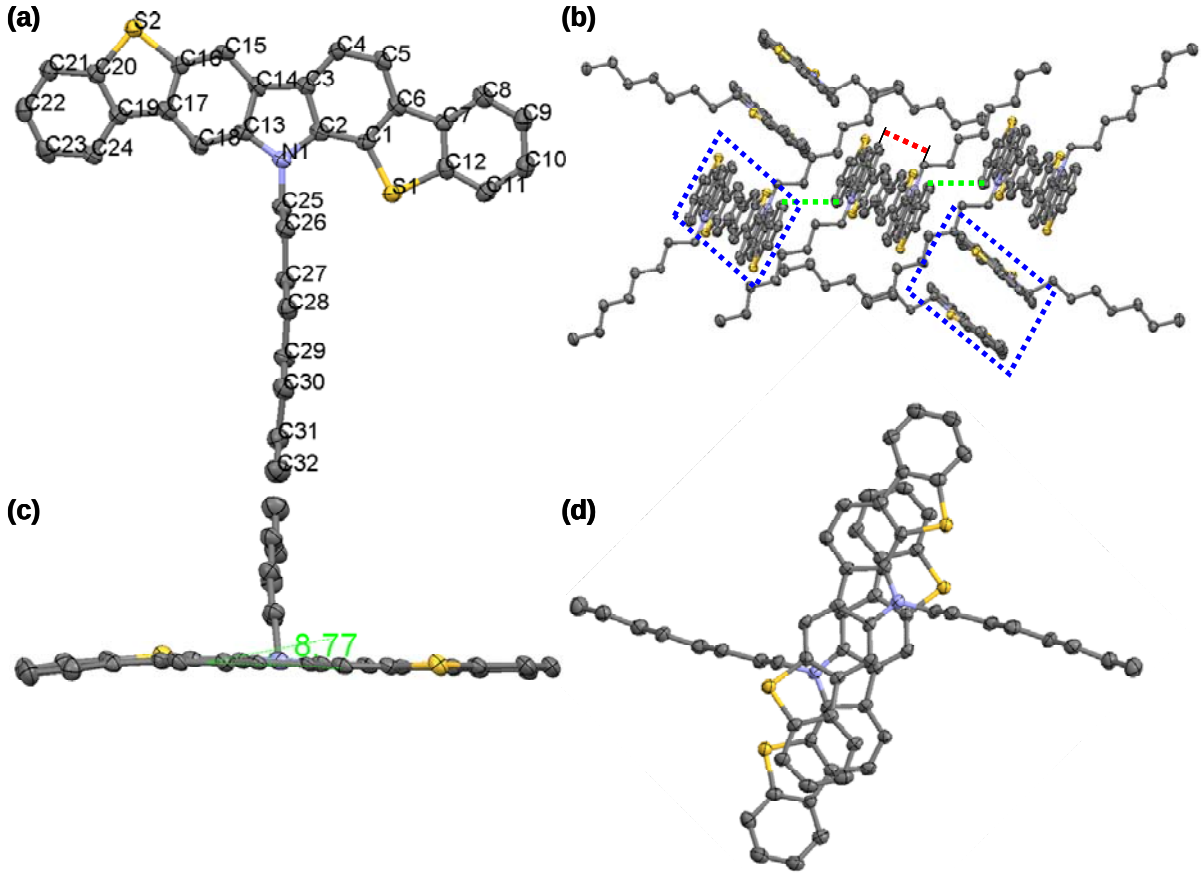

Figure 3.9. Packing diagrams of **8d** (isomer 2). (a) Thermal ellipsoid of **8d**. The hydrogen atoms were omitted for clarity. Thermal ellipsoids are drawn at 50% probability. b) Sandwiched herringbone structure formed by the anti-parallel pairs. (Dashed blue rectangular illustrate the pairs; dashed red line indicates the interplanar distance inside the pairs; dashed green lines indicate the short C-C interaction between the pairs) (c) View down the short axis of the molecule showing the large dihedral angle of 8.8°. (d) View down the projection direction of two cofacial molecules in one pair.

Table 3.2. Crystallographic Parameters of **8b** to **8e**

	8b	**8c**		**8d** (isomer 1)	**8e**
		With guest	Without guest		
Empirical formula	$C_{28}H_{21}N_1S_2$	$C_{31}H_{26}Cl_3NS_2$	$C_{30}H_{25}NS_2$	$C_{32}H_{29}NS_2$	$C_{33}H_{31}N_1S_2$
Formula weight	435.61	583.04	463.66	491.72	505.75
Crystal color, habit	light yellow, needle	light yellow, needle	light yellow, needle	light yellow, block	light yellow, needle
Crystal system	monoclinic	orthorhombic	triclinic	monoclinic	monoclinic
a, Å	15.8914(4)	8.9981(4)	5.8528(4)	10.6776(8)	14.6050(4)
b, Å	15.8283(5)	13.9190(5)	20.2829(9)	12.8920(9)	8.6960(2)
c, Å	17.4615(4)	21.4328(8)	21.9207(9)	18.3570(9)	20.5770(6)
β, deg	106.84(0)	90	97.41(0)	94.967(4)°	98.72(0)
V, Å^3	4203.73(192)	2684.34(18)	2484.46(93)	2517.45(92)	2583.16(45)
ρ_{calc}, g/cm^3	1.3765	1.44259	1.23954	1.2973	1.300
Space group	*P* 1 2_1/n1 (14)	*P* n 2_1/a (33)	*P* -1 (2)	*P* 1 2_1/a1 (14)	*P* 1 2_1/c1 (14)
Z value	8	4	4	4	4
Temperature, K	120	120	120	120	120
No. of reflections measured	12270	5006	7664	4229	7888
No. of variables	559	334	595	316	325
Residuals: *R*; *wR*^{2}	0.0377; 0.0437	0.0303; 0.0345	0.0435; 0.0497	0.0826; 0.0710	0.0715; 0.0834

The single crystal data show that the new heteroheptacenes with alkyl substitutions in the short molecular axis direction form peculiar crystal structures. The short interactions between the aromatic planes lead to the generation of anti-parallel pairs. Then depending on the length of the alkyl groups the molecules adopted different kinds of herringbone structures. By including the guest solvent molecules, crystals of **8c** showed higher symmetry than without guest molecules. The isomeration of the main backbone (**8d**-isomer 1) does not change the packing diagram so much, but give a highly strained molecular structure with the highest dihedral angle among the series. This finding in the molecular structure further proved the difficulity in production of isomers. In the end, by changing the alkyl substitution from the short molecular axis (**8b**, **8c**, **8d**) to long molecular axis (**8e**), the packing motif of the compound can change from a highly slipped herringbone structure to a densely packed π– π stacking structure.

3.2.6 Powder X-ray diffraction (PXRD) analyses and film microstructure for compounds DBTCz and BTTCz

X-ray diffraction (XRD) measurements were recorded on a Siemens D-500 powder diffractometer (Cu-Ka: 1.541 Å) with scan rate of 0.1°/20 s. The XRD pattern of DBTCz and BTTCz with different alkyl length and substituting position are shown in **Figure 3.10** and **Figure 3.12**.

In **Figure 3.10**, the XRD patterns are corresponding with their SCXRD results respectively and a schematic molecular model on the surface is drawn accordingly. The XRD patterns of a thin film of **8c** prepared by drop-casting exhibits six strong reflections at 2θ = 4.9, 9.84, 14.78, 19.7, 24.7 and 29.74^{o} (**Figure 3.10**a). These reflections are inconsistent with those calculated from the SCXRD data suggesting that the *N*-hexyl-derivated **8c** adopts a different packing motif in the drop-cast film. Interestingly, this diffraction pattern is very similar to that obtained from a film of **1b** (see Chapter 2, **Figure 2.4c**). The similarities between the diffraction patterns suggest that, like the dibutyl substituated **1b**, the **8c** also adopts a lamella packing

arrangement in the film, with a *d*-spacing of 18.03 Å. This unassignable *d*-spacing may correspond to the so-called previously dentifed "thin film" phase.[16]

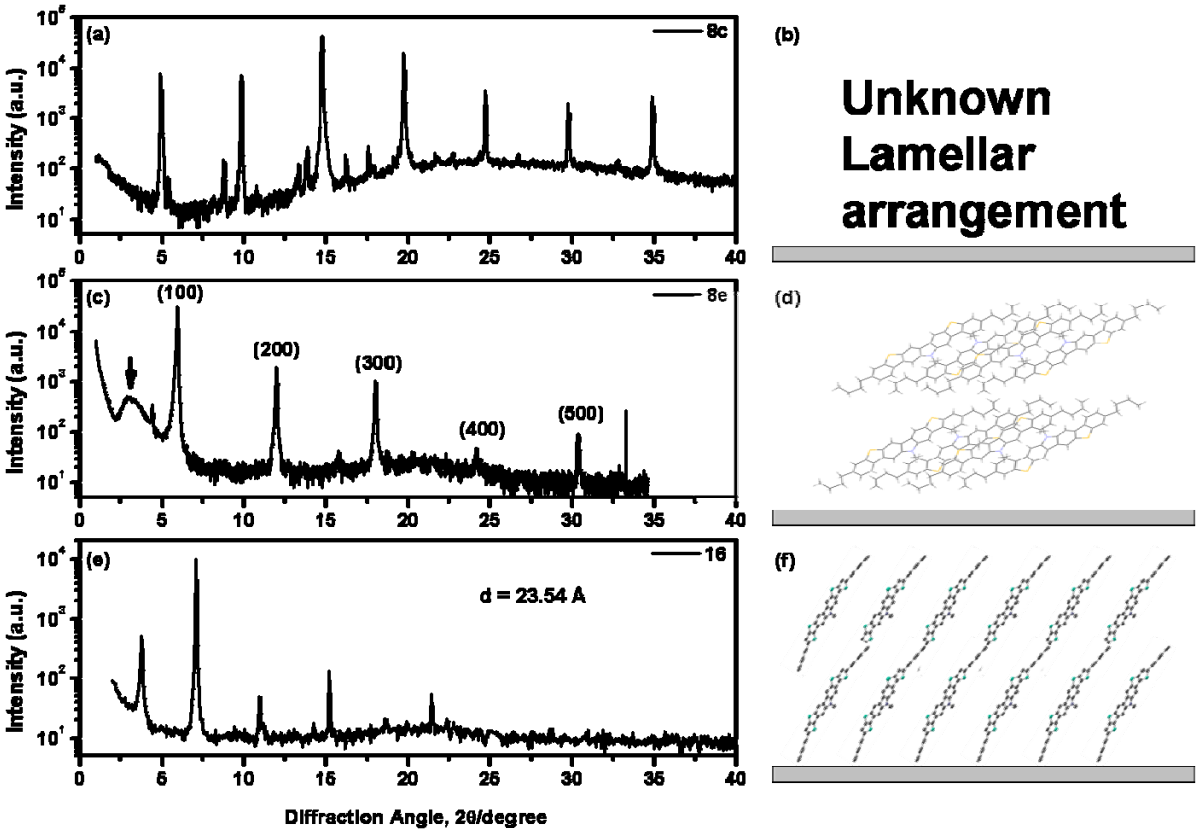

Figure 3.10. X-ray diffractogram of the drop-cast thin films (40 mg/ml 1,2-dichlorobenzene solution) on an untreated Si/SiO_2 substrate. (a) **8c**; (b) Certain kind of lamellar packing of **8c** on the substrate; (c) **8e**. The reflections are assigned by the Miller's indices; (d) Supposed organization of **8e** in the solution processed thin layer on the substrate; (e) **16**. (f) Approximated organization of **16** in the solution processed thin layer on the substrate.

The diffraction pattern of a film of **8e** prepared by drop-casting of a 30mg/ml solution on to a silicon wafer exhibits three sharp reflections at 2θ = 5.92, 11.96, 18.04, 24.16 and 30.36 ° corresponding to the (100) through (500) planes of the $P_1\ 2_1/c$ group (**Figure 3.10c**). These reflections are consistent with those calculated from the SCXRD data suggesting that the dibutyl-substituted DBTCz molecules are oriented with their long molecular axes inclined approximately 60.5° with respect to the (100) plane that is parallel to the substrate surface. (**Figure 3.10d**) At the same time, the derived

d-spacings (14.92 Å) are pratically identical to the *a* axis length obeserved in the crystal structure (14.61 Å), which again means that molecules of **8e** are oriented with the (100) plane parallel to the substrate surface. The arrow marked peaks at (at 2θ = 2.92°) correspond to the other five higher order reflections. These reflections are similar to those observed in films prepared from the didodecyl derivative of LADT,[17] suggesting that this compound packs into a lamellar arrangement in the film.

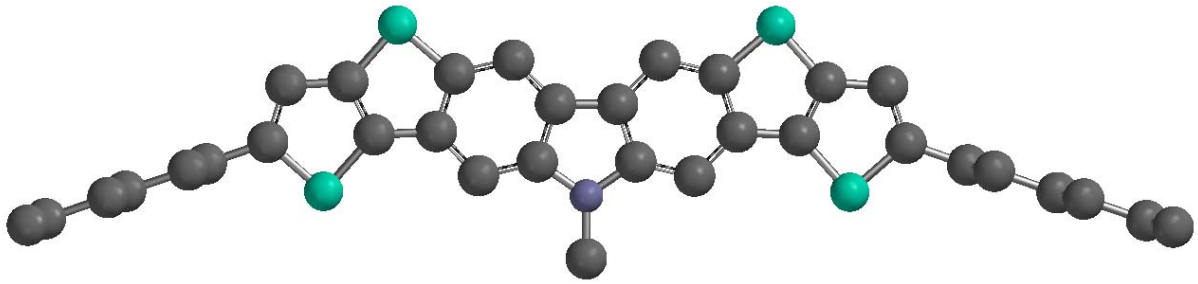

Figure 3.11. Theoretical geometry optimization of using SPARTAN '04 at B3LYP/6-31G** level

Like films of **8e**, thin film of compound **16** shows high degrees of crystallite orientation when cast from solution on to silicon wafers. (**Figure 3.10**e) Because of the lack of SCXRD supporting results, no unit cell parameters could be used to define the reflection peaks. Therefore a theoretical geometry was simulated using SPARTAN 04 at B3LYP/6-31G** level, from which the optimized molecular length was calculated to be 26.4 Å. (**Figure 3.11**) Therefore the approximate tilt angle (θ) with respect to the substrate surface was calculated from the molecular length (l) and the film d spacing ($d = l \sin\theta$) to be 63°. (**Figure 3.10f**)

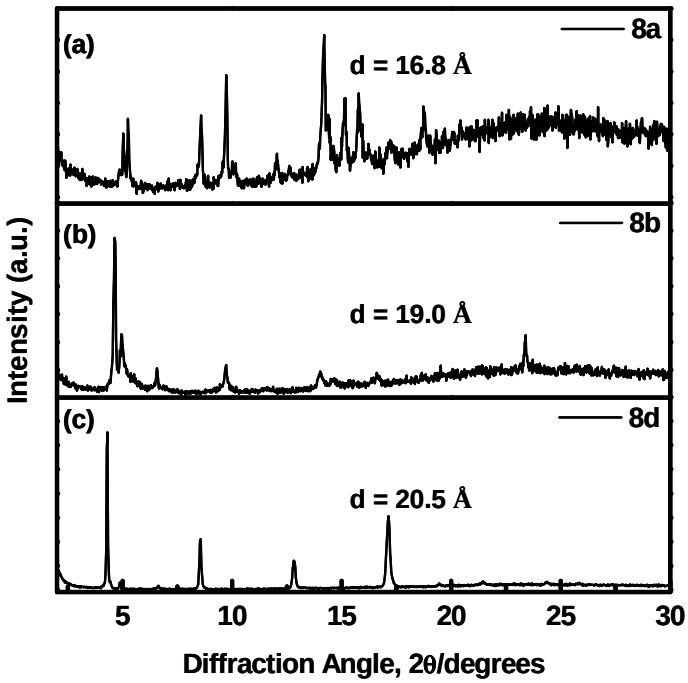

Figure 3.12. X-ray diffractogram of the drop-cast thin films (40 mg/ml 1,2-dichlorobenzene solution) on an untreated Si/SiO_2 substrate. (a) **8a**; (b) **8b**; (c) **8d**.

In **Figure 3.12**, the XRD patterns of compounds **8a** , **8b** and **8d** are included. Generally, they showed lamellar packing diagram and the calculated *d*-spacings are also shown. It is obvious to see that the *d*-spacing values of the *N*-alkylated molecules (**8a-d**) increase with the length of the alkyl groups indicating that the molecules are aligned with their alkyl chains extended in the normal direction of the substrate. At the same time, the crystalline films become more and more ordered with the increase of alkyl chain length.

3.2.7 Scanning electron microscopy (SEM): morphological characterization of compounds DBTCz and BTTCz

Films of compounds **8c**, **8e** and **16** display a variety of morphological features, such as isolated vertical ridges and interconnected rodlike crystallites. **Figure 3.13** shows scanning electron micrographs of films from **8c** deposited at 25 ^{o}C from saturated hexane solution (a and b), **8e** deposited at 25 ^{o}C from dichlorobenzene (c and d) and **16** deposited at 25 ^{o}C from dichlorobenzene (e and f).

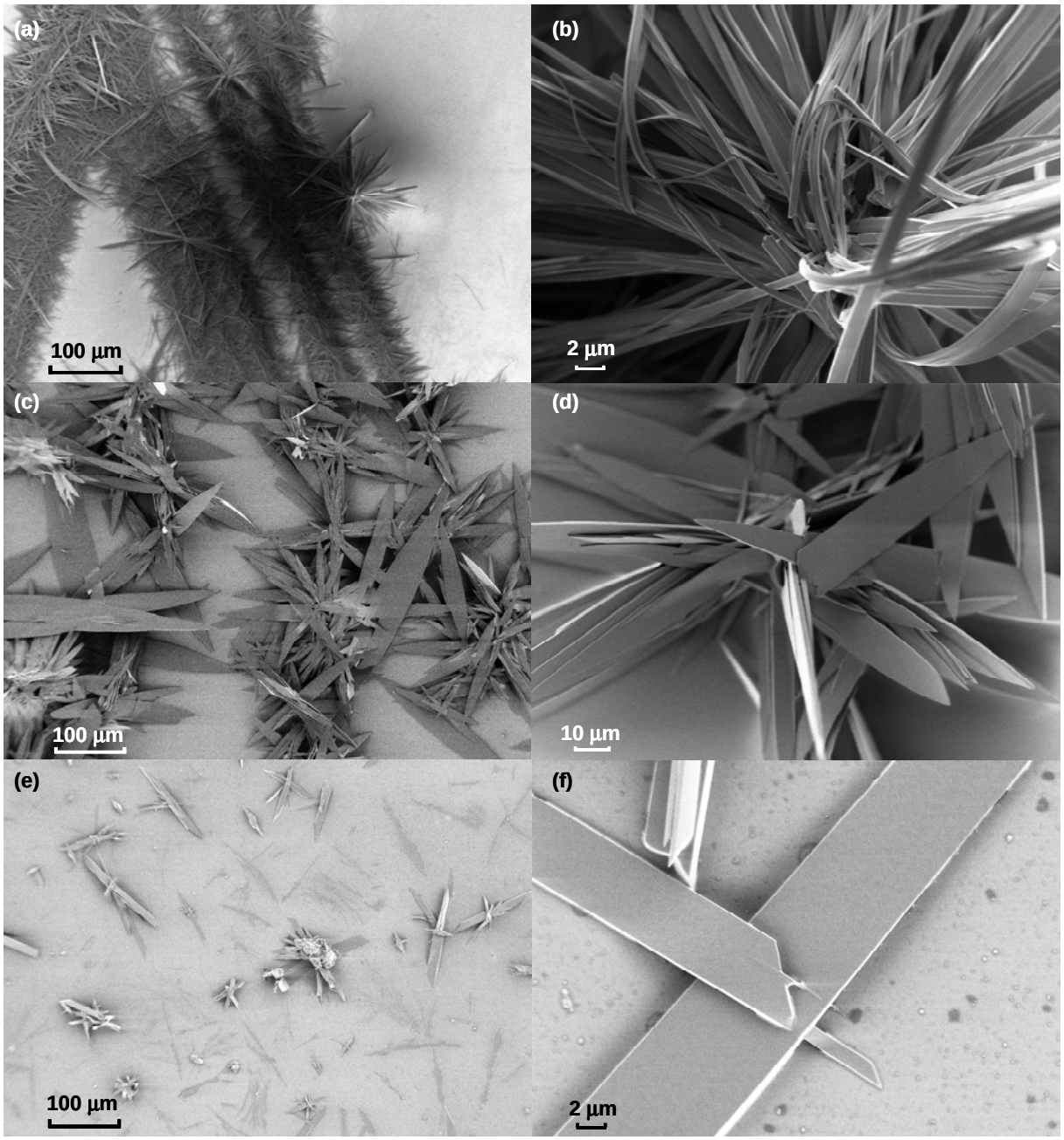

Figure 3.13. Scanning electron micrographs of dropcasted films on untreated Si/SiO2 substrates of (a) & (b) DBTCz-C_6H_{13} (**8c**), 25 °C; (c) & (d) DBTCz-dibutyl (**8e**), 25 °C; (e) & (f) BTTCz-dihexyl (**16**) 25 °C.

Interestingly, films of **8c** appear as belt-like crystallites protruding from a self-assembled ribbon. The ribbons made of small crystallites are on the order of a few millimeters (long axes of the rods) and the small crystallites look like bent belts in a scale of 2 μm. From the PXRD pattern of the same sample, we could know that it

is highly crystalline inside the belt. Therefore, this structure characteristics provide the possibility of using these microbelts to construct semiconducting channels in OFET devices.[18] However, as seen in the SEM image, the film surface is not smooth and the crystallites on the surface are not interconnected as well, which may lead to low mobilities when the films are directly used as semiconducting channels.

Films of DBTCz-dibutyl (**8e**) (**Figure 3.13** c,d) adopt a morphology different from those of DBTCz-CH_3 films when deposited at 25 °C. Swordlike crystals with much increased size are found on the substrate surface. These microstructural features may be attributed to the dialkyl substitution along the long molecular axis, which favours the molecular packing to form large crystal domains.

An image of a BTTCz-dihexyl (**16**) film deposited at 25 °C is shown in **Figure 3.13**e,f. It displays a similar morphology to that of DBTCz-dibutyl (**8e**) films, which is in agreement with X-ray diffraction studies. In this case, however, the swordlike crystals are extremely small and not well interconnected. The poorer solubility of the compound is supposed to be the reason for the small crystal domains.

3.2.8 Photophysical properties

UV absorption and photoluminescence spectra (PL) of heteroheptacene **8c**, **8e**, **16** and **22** were measured in both solution and as drop-casted thin films to assess the effect of heteroatom and alkyl substitution on the heteroheptacene absorption/emission maxima and the optical energy gap as shown in **Figure 3.14**. **Table 3.3** collects the UV/Vis and PL data for all compounds in THF solution. In the UV/Vis absorption spectra of all the compounds, the strong structured absorption bands below 400 nm are attributed to the *β* (Platt's ^1B_b band), and *p*-band of the π-π* transitions. At the same time, one can also see one or two weak *a* (Platt's ^1L_b band) and/or *p*-band in the visible region (**Figure 3.14a**).[19] Similar UV absorption bands have been observed in the case of diindolocarbazoles.[2b] Little difference is found in the absorption bands of **8c** and **8e**, indicating that the type of alkyl substitution has no prominent influence on the absorption spectra. When two more sulfur atoms are

incorporated in the skeleton, compound **16** shows a red shifted *β* band (from 363 to 374 nm) and a blue shifted *a* band (from 432 to 413 nm) compared with that of **8**. Surprisingly, although compound **22** has a more extended π system, the absorption spectrum shows only a slight bathchromic shift (387 nm) for the *β* band and the *a* band at 425 nm.

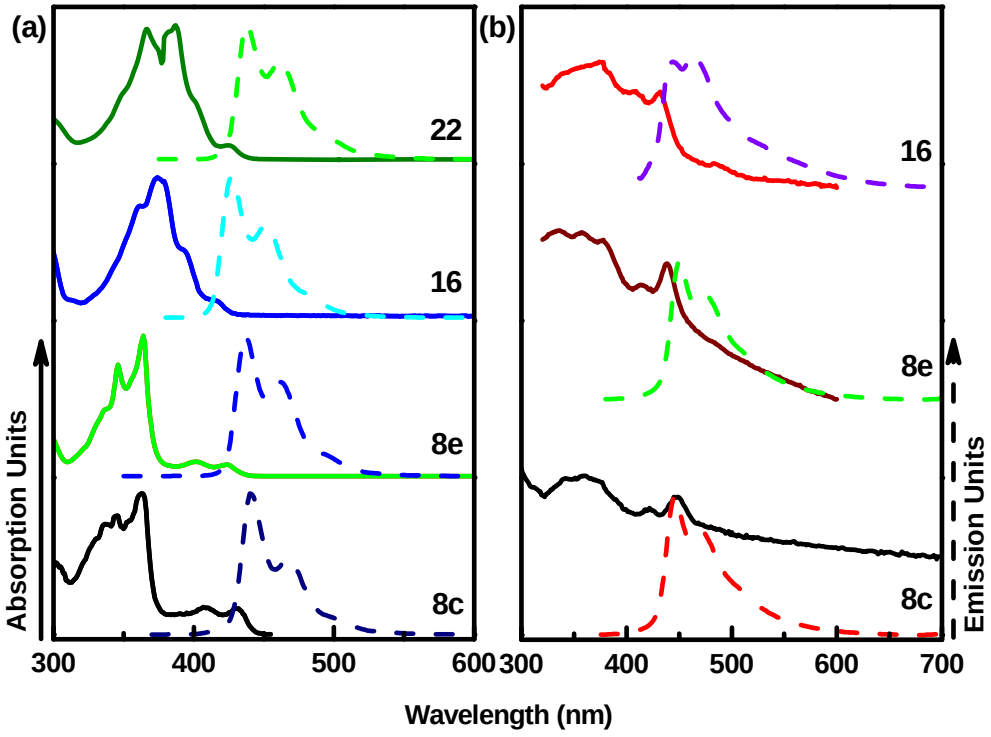

Figure 3.14. Normalized UV-vis absorption, PL spectra in THF (10^{-6} M) (a) and normalized UV-vis absorption, PL spectra on quatz plates (b) of compounds **8c**, **8e**, **16** and **21**.

Solution optical band gaps (E_g^{op}) of compounds **8c**, **8e**, **16** and **21**, defined by the 0-0 transition energies, were estimated based on the λ_{max} absorption edge and listed in **Table 3.3**. All compounds have significantly larger band gaps than that of hydrocarbon-heptacene (1.5 eV),[20] pentacene (2.15 eV),[21] diindolocarbazole (2.59 eV)[2b] and smaller than that of diindenocarbazole (3.2 eV)[3], indicating that in planarized aromatic systems, the increased thiophene incorperation widens the HOMO- LUMO gap.[22]

In the PL spectra, recorded in THF solution, compounds **8c**, **8e**, **16** and **21** exhibit weak purple emissions with the maxima at 440 nm, 437 nm, 426 nm and 438 nm, respectively. Relative photoluminescence quantum yields (Φ_f) of these heteroheptacenes were determined using diphenyl anthracene in cyclohexane as the standard,[23] and the PL data were also collected in **Table 3.3**. The quantum yield Φ_f can be described by the relative rates of the radiative and non-radiative pathways, which deactivate the excited state. In this study, the results show that Φ_f increases with the sulfur substitution and when long alkyl chains are substituted in the short molecular axis direction (in the case of **8c**), the Φ_f increases dramatically. The small Stokes shift of 8 or 15 nm is similar to that of bisindenocarbazoles due to the rigid planar structure.[24] The UV-vis absorption and photoluminescence spectra of other derivatives of **8** do not show obvious differences compared to **8c**.

Table 3.3. UV-Vis Absorption and PL Data for **8c, 8e, 16** and **21**

	Solution[a]			Film	
compound	Absorption λ_{max} [b] /nm peak/edge	PL λ_f /nm	Quantum yield[c] (Φ_f)	Solid-state absorption λ_{max}/nm	Solid-state PL λ_f /nm
8c	432/443	440	0.16	445	446
8e	423/438	437	0.03	438	450
16	413/427	426	0.12	432	444
21	424/436	438	-	-	-

[a] In THF 10^{-6} M. η = 1.4070. [b] λ_{max} as π-π^* HOMO-LUMO transition. [c] Quantum yield relative to diphenyl anthracene (10^{-7} M, cyclohexane solution), excitation at 365 nm.

The solid-state optical absorption/PL data for molecules **8c**, **8e** and **16** are collected in **Table 3.3**. In general, the film absorption spectra exhibit characteristic transitions that are bathochromically shifted compared to their solution values, which is indicative of the presence of π-π stacking in the solid state. In the UV/Vis thin film absorption spectrum of **8c**, **8e** and **16**, the absorption *p*-bands at the long wavelength are much more intense than those in solution. In analogy to previous oligothiophene results,[25] the weak unresolved absorption at the longest wavelengths-a low energy tail of the intense band (500 nm), can be attributed to the *p*-bands of isolated molecules, either located in disordered domains or at grain

boundaries, where molecular misalignment can lead to weak intermolecular coupling and minimal splitting of the excited levels. Thin film photoluminescence spectra were obtained by λ_{max} excitation, and data are compiled in **Table 3.3**. All the spectral maxima exhibit red shifts relative to the emission maxima in solution, which again suggests the existence of strong inter-molecular interaction.

3.2.9 Electrochemical properties

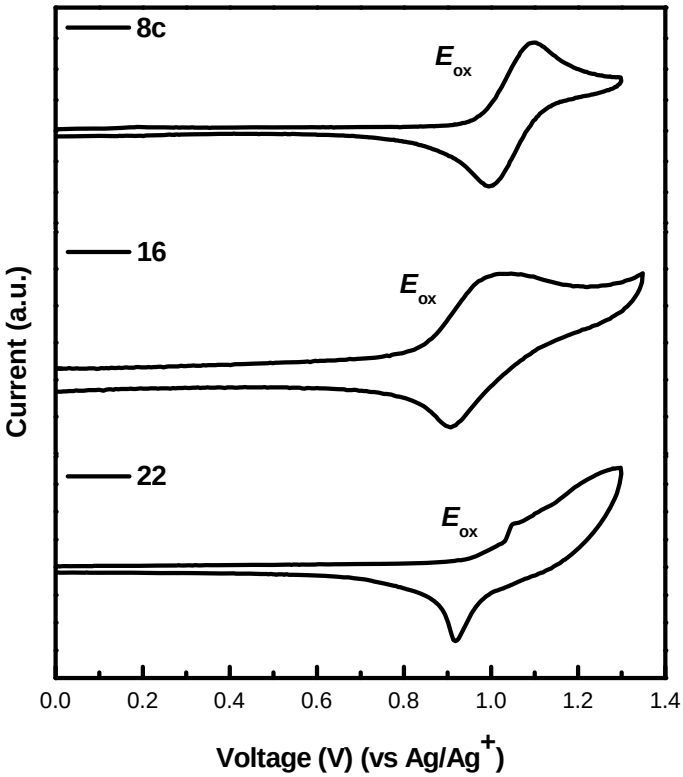

Figure 3.15. Cyclic voltammogram of **8c**, **16** and **21**. Conditions: glassy carbon as working electrode (diameter 1mm); solution (ca.10^{-3} M) in CH_2Cl_2 with NBu_4PF_6 as supporting electrolyte (0.1 M); scan rate 50 mVs^{-1}; potentials are referred to an Ag/AgCl electrode.

To investigate the redox potentials of the new heteroheptacenes, cyclic voltammetry (CV) measurements were performed in dry CH_2Cl_2 (with 0.1 M tetrabutylammonium hexafluorophosphate) by using Au as the working electrode and Ag/Ag^+ as the reference electrode. **Figure 3.15** shows voltammograms of compounds **8c**, **16** and **21** and the electrochemical data are summarized in **Table 3.4**

below. Single-electron oxidations (versus SCE) are obtained at 1.1 V for **8c**, at 1.05 V for **16**, and at 1.05 V for **21**. However, due to the reduction part of the compounds are out of the range of our experimental setup, we can not observe the reduction in the CV data. The electrochemical studies on heteroheptacenes **8**, **16** and **21** indicate that they are intrinsically electron-donor molecules. According to E_{HOMO}=-(E^{ox}_{onset}+4.34) eV,[26] the HOMO levels of these heteroheptacenes could be estimated and listed in **Table 3.4**.

Table 3.4. Electrochemical data and estimated HOMO, optical band gap and LUMO levels of **8c, 16** and **21.**

Compound	E_{ox}[a]/V anodic		cathodic	Half	HOMO[c]/eV	E_g^{opt} [d]/eV	LUMO[e]/eV
	E^{onset}	E_a	E_c	$E_1^{1/2}$			
8c	0.98	1.1	0.99	1.05	-5.32	2.80	-2.52
16	0.82	1.05	0.91	0.98	-5.16	2.90	-2.26
21	0.98	-	0.92	-	-5.32	2.85	-2.47

[a] Versus. Ag/AgCl in CH_2Cl_2 with 0.1 M *n*-Bu_4NPF_6 as supporting electrolyte (scan speed = 50 mVs). [b] Absorption spectra. [c] Calculated based on HOMO = - (E_{ox}^{onset} + 4.34) eV. [d] Estimated from the absorption edge by E_g^{opt} (eV) = 1240.8/λ_{onset}. [e] calculated from LUMO = HOMO+band gap.

As shown in **Table 3.4**, a HOMO level of -5.32 eV for **8c** is determined, which is much lower than that of pentacene (-4.60 eV)[27] and slightly lower than that of diindenocarbazole (-5.3 eV)[3]. This value is consistent with the HOMO level calculated by using Density Functional Methods (DFT) (-5.1 eV) (**Figure 4.16**). Compounds **8a**, **8b**, **8d** and **8e** are also characterized by CV indicating similar oxidation behavior as **8c**. Taking into account an optical band gap of 2.81 eV derived from the absorption onset of the UV-vis spectrum, the LUMO value of **8c** is empirically calculated to be -2.52 eV, which may deviated from the real value of the EA (electron affinity). By following the same method, the HOMO level of **16** is calculated to be -5.16 eV, which is only 0.14 eV higher than **8c**. This finding is in agreement with previous studies of thienyl-substituted heterocyclic compounds, which revealed that the substitution of a C=C double bond with a sulfur atom has little effect on the energy of the first ionization potential.[28] The redox behavior of

compound **21** indicates at E^{ox}_{onset} of around 0.98 eV as well as a reduction wave at the potential of 0.92 V (**Figure 3.15**). Therefore a similar HOMO level as compound **8c** could be calculated for compound **21 (Table 3.4)**.

3.2.10 OFET fabrication based on DBTCz derivatives

DBTCz derivatives were fabricated into OFET devices as the semiconducting channel, transport measurements of which indicate *p*-channel FET characteristics. In this section we take DBTCz-C_6H_{13} (**8c**) as an example in describing the device processing. The calculated results of all the devices are listed in **Table 3.5**.

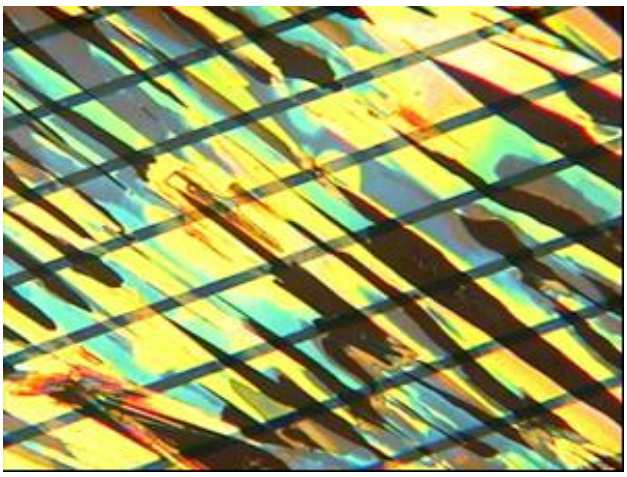

Figure 3.16. POM image between cross-polarizers of drop-cast **8c** from a 40 mg/ml 1,2-dichlorobenzene solution on an untreated SiO_2 substrate with source and drain electrodes.

Bottom-contact OFETs were fabricated by simple drop-casting of compound **8c** solution (40 mg/ml dichlorobenzene) on untreated Si/SiO_2 substrates with channel length and width of 10 μm and 5 mm, respectively. The resulting film was highly crystalline with large domains extending over several hundred micrometers, partly exhibiting optical anisotropy as shown by the polarized optical microscope (POM) images (**Figure 3.16**). The morphology of the thin film seems different from that of SEM image, which may be due to the presence of the gold electrode. After annealing the sample at 100 ^{o}C for 30 min, a hole mobility of 2 × 10^{-3} cm^2 V^{-1} s^{-1} and current

on/off ratio of 10^5 was obtained as deduced from the transistor characteristics illustrated in **Figure 3.17**. As revealed by the nonlinear increase in the drain current I_{SD} at low drain biases V_{SD} (**Figure 3.17**a), severe contact resistance is present in the devices, possibly limiting the charge carrier mobility. The problem could be solved by treatment of a thiol-based self-assembled monolayer with alkane or fluorinated alkane or aryl groups on source/drain electrodes of the devices with a bottom-contact configuration. This treatment method has been widely used and showed that the performance of OFETs such as field effect mobility and on/off ratio can be improved.[29] Thiol molecules adsorbed on source/drain electrodes cause a significant reduction of the contact resistance between the electrodes and a semiconductor depending on the energy barrier height at the interface. However, excessive treatment conversely reduces the field-effect mobility with a threshold voltage shift.[30] Remarkably, the transistor worked moderately without specific surface treatment on the dielectric (SiO_2) surface. All the other devices based on DBTCz (**8a**, **8b**, **8d**, **8e**) were fabricated following similar methods and surface modification of the dielectrics and electrode were also performed in some cases. Currently, experiments are being conducted to optimize the devices following the methods described above in order to further improve the device performance.

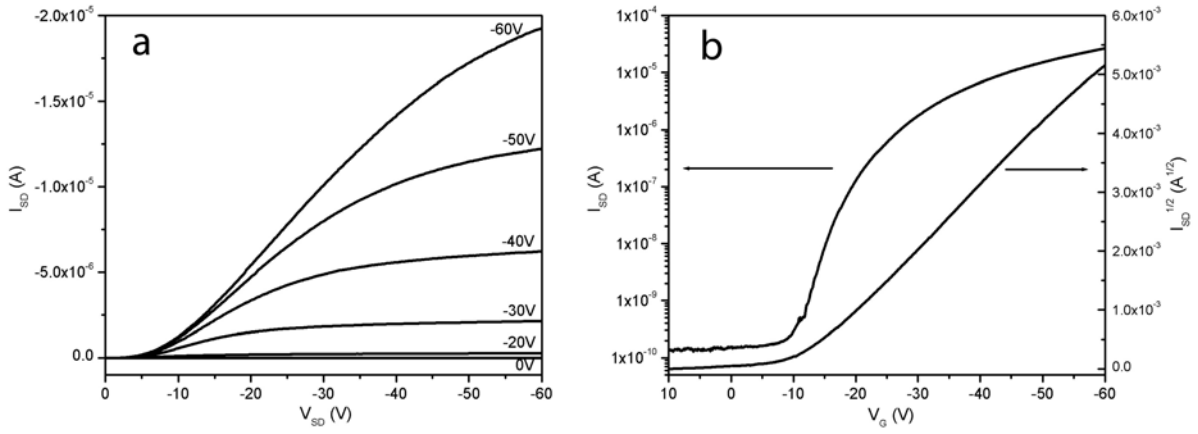

Figure 3.17. FET characteristics of **8c**-based OFET: (a) output characteristics at various gate biases V_G and (b) transfer characteristics at V_{SD} = -60 V.

Table 3.5. FET Performance of DBTCz series[a,b]

Organic layer	compound	Surface and electrode treatment reagent	μ_{FET}/cm^2 V^{-1} s^{-1}	I_{on}/I_{off}	V_{th}/V
Drop-cast film	**8a**	Perfluorodecanethiol (FDT)	1.8 (±1.0) × 10^{-4}	20	+41
	8b	4-Nitrobenzenethiol (NBT)	5.1 (±1.7) × 10^{-4}	59	+22
	8c	-	2.0 × 10^{-3}	10^5	
	8d	1-Octanethiol (OT)	4.0 (±2.8) × 10^{-4}	3 × 10^3	+17
	8e	-	-	-	-
Spin-coated film	**8a**	-	-	-	-
	8b	-	3.0 (±1.2) × 10^{-4}	6.4 × 10^4	-21.5
	8c	Phenyltriethoxysilane (PTES)	2.3 (±2.9) × 10^{-4}	652	+12.8
	8d	Phenyltriethoxysilane (PTES)	2.7 (±0.4) × 10^{-4}	8.3 × 10^3	-0.8
	8e	Phenyltriethoxysilane (PTES)	7.1 × 10^{-6}	7.0 × 10^3	7.3

[a] More than 10 devices in bottom contact configuration for each category were tested to confirm reproducibility and parameters were extracted from typical devices. [b] Best results under different conditions are selectively showed.

As seen from **Table 3.5**, the compounds of the DBTCz series showed moderate charge carrier mobilities, which are poorer than that of heteropentacenes (**1** and **2**), although the conjugation lengths of the molecules are extended to seven rings. A systematic structure-property relationship study revealed that the device performance is strongly influenced by the film morphology which is at the same time not only controlled by the molecular skeleton but to a great part governed by the alkyl substitution. In the case of DBTCz derivatives, the *N*-alkyl groups were meant to compensate the decrease in solubility due to the elongated molecular backbone. However the alkyl groups in the short molecular direction disturbed the molecular packing regime so much that these molecules formed solid structure in between herringbone and π-stacking strucutures. Meanwhile, differences between bond angles of C-S-C and C-N-C bridges were found in the single crystal structures of the molecules and supposed to be another reason for the improper packing properties that lead to the low charge carrier mobility. (**Figure 3.18**)

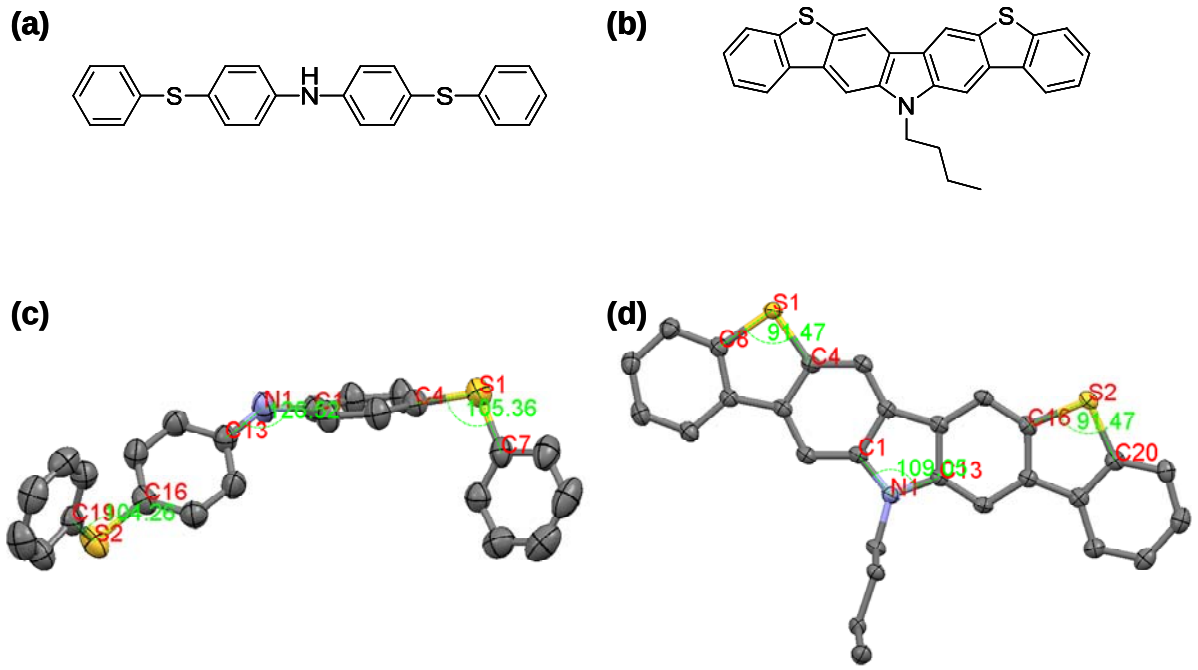

Figure 3.18. Chemical and crystal structure of bis(4-(phenylthio)phenyl)amine (a) & (c) (reproduced from Leuninger et al.[31]) and **8b** (b) & (d).

As can be seen from **Figure 3.18**, different bond-angles of the phenylene units between the amino and sulfur bridges have been found in the crystal structure of compound bis(4-(phenylthio)phenyl)amine. It can be demonstrated that the difference of the bond angles is more than 21° (**Figure 3.18c**: bond angles C7-S1-C4 = 105.4°; C1-N1-C13 = 126.5°; C16-S2-C19 = 104.2°). This large difference resulted in a poorer packing of the molecules and hence in an amorphous character of poly(phenylene sulfide-phenyleneamine).[31] Accordingly, the bond angles of compound **8b** as a representative were measured. It turned out that an angle difference of 18° is measured. (**Figure 3.18d**: bond angles C8-S1-C4 = 91.5°; C1-N1-C13 = 109.1°; C16-S2-C20 = 91.5°). The situation observed here could also lead to poor intermolecular aggregation and hence undermine the charge carrier mobility. This could be demonstrated by the fact that although the thin films of DBTCz series showed high crystallinity, their single crystal structure showed large free volumes to rearrange and encapsulate guest molecules.

3.3 Conclusion

In this chapter, the trific acid induced double electrophilic coupling reactions on carbazole were systemically studied and the key factor influencing the isomeric of the product was found to be the reaction temperature of the reaction system. Meanwhile, the reaction speed is pretty much determined by the acidity of the reaction system. Therefore, the optimized isomer-free reaction condition is at 0^{o}C in the presence of phosphorus pentoxide, under which surprisingly high regioselectivity on the 3,6 position of carbazole was achieved from precursor **11**. One test reaction at 60 ^{o}C showed the production of the **8d**-isomer 1 in 17% ratio from precursor **11d**, but no isomer 2 has ever been found. Based on this condition, new symmetrical ladder-type π-conjugated heteroacene series – DBTCz (**8**) with the inclusion of both thiophene and pyrrole ring units were successfully made from corresponding precursors respectively with overall yields of about 38% to 50%.

Precursors **15** and **20** were employed to synthesize DBTCz-diC4 and BTTCz-diC6 with solublizing alkyl chain on the long molecular axes, which is different from the molecules originated from precursor **11.** DIBBBT was obtained as by far the longest ladder-type heteroacene with well- defined structure.

Single-crystal studies demonstrated peculiar structures which are varied depending on the size/postion of the alkyl groups, encapsulation of guest molecule and isomerization. The combined thin film XRD of these new molecules showed a preferred specific orientation relative to the substrate surface. The spectroscopic and electrochemical characterizations of DBTCz, BTTCz and DIBBBT indicated their much lower HOMO energy levels and larger band gaps compared with those of pentacene, in spite of their much more extended π systems.

In the end, OFETs devices with DBTCz molecules as the semiconducting channels were fabricated but showed less glorious results compared with heteropentacenes. It is well known that the performance of the OFETs devices is determined by a combination of factors. The size of the molecules and the geometry of the crystals are two of them. The mismatch of the bond angles of the bridging

heteroatoms tends to loosen the crystal structure and decrease the charge carrier mobility. It appears from this study that the more extended π systems are not always "the longer the better" in OFETs.

3.4 References

[1] Sirringhaus, H.; Friend, R. H.; Wang, C.; Leuninger, J.; Müllen, K. *J. Mater. Chem.* **1999**, *9*, 2095-2101.

[2] (a) Bouchard, J.; Wakim, S.; Leclerc. M. *J. Org. Chem*. **2004**, *69*, 5705-5711. (b) Wakim, S.; Bouchard, J.; Blouin, N.; Michaud, A.; Leclerc, M. *Org. Lett.* **2004**, *6*, 3413-3416.

[3] Sonntag, M.; Strohriegl, P. *Tetrahedron* **2006**, *62*, 8103-8108.

[4] (a) Koguchi, R.; Kobayashi, N.; Kijima, M. *Macromolecules* **2009**, *42*, 5946-5952. (b) Boudreault, P. T.; Blouin, N.; Leclerc, M. *Advances in Polymer Science* **2008**, *212*, 99-124.

[5] Morin, J.; Leclerc, M.; Adès, D.; Siove, A. *Macromolecular Rapid Communications*. **2005**, *26*, 761-778.

[6] (a) Neugebauer, F. A.; Fischer, H. *Chem. Ber.* **1972**, *105*, 2686-2693. (b) Moskalev, N. V. *Khim. Geterotsikl. Soedin.* **1990**, *2*, 187-189. (c) Zhu, Z.; Moore, J. S. *J. Org. Chem.* **2000**, *65*, 116-123. (d) Zhu, Z.; Moore, J. S. *Macromolecules* **2000**, *33*, 801-807. (e) Joule, J. A. In *Advances in Heterocyclic Chemistry*; Katritsky, A. R., Ed.; Academic: Orlando, **1984**; Vol. 35, p 129.

[7] Dierschke, F.; Grimsdale, A. C.; Müllen, K. *Synthesis*. **2003**, 2470-2472.

[8] Mancuso, A. J.; Swern, D. *Synthesis* **1981**, 165-185.

[9] (a) Haryono, A.; Yamamoto, K.; Shouji, E.; Tsuchida, E. *Macromolecules*, **1998**, *31*, 1202-1207. (b) Leuninger, J.; Wang, C.; Soczka-Guth, T.; Enkelmann, V.; Pakula, T.; Müllen, K. *Macromolecules*, **1998,** *31*, 1720-1727.

[10] Dierschke, F.; Grimsdale, A. C.; Müllen K. *Macromol. Chem. Phys.* **2004**, *205*, 1147-1154.

[11] Zhang, M.; Yang, C.; Mishra, A. K.; Pisula, W.; Zhou, G.; Schmaltz, B.; Baumgarten, M.; Müllen, K. *Chem. Commun.*, **2007**, 1704-1706.

[12] Billingsley, K. L.; Barder, T. E.; Buchwald, S. L. *Angew. Chem. Int. Ed.* **2007**, *46*, 5359-5363.

[13] (a) Anthony, J. E. *Chem. Rev.* **2006**, *106*, 5028-5048; (b) Anthony, J. E. *Angew. Chem.* **2008**, *120*, 460-492; *Angew. Chem. Int. Ed.* **2008**, *47*, 452-483.

[14] (a) Campbell, R. B.; Robertson, J. M.; Trotter, J. *Acta Crystallogr.* **1962**, *15*, 289-290. (b) Holmes, D.; Kumaraswamy, S.; Matzger, A. J.; Vollhardt, K. P. C. *Chem. Eur. J.* **1999**, *5*, 3399-3412. (c) Siegrist, T.; Kloc, C.; Schön, J. H.; Batlogg, B.; Haddon, R. C.; Berg, S.; Thomas, G. A. *Angew. Chem., Int. Ed.* **2001**, *40*, 1732-1736. (d) Mattheus, C. C.; Dros, A. B.; Baas, J.; Meetsma, A.; de Boer, J. L.; Palstra, T. T. M. *Acta Cryst., Sect. C: Cryst. Struct. Commun.* **2001**, *C57*, 939-941.

[15] Nishio, M.; Hirota, M.; Umezawa, Y. *The CH/π Interaction: Evidence, Nature, and Consequences.* Wiley-VCH, **1998**, p 217.

[16] Knipp, D.; Street, R. A.; Volkel, A.; Ho, A. *J. Appl. Phys.* **2003**, *93*, 347-355.

[17] Laquindanum, J. G.; Katz, H. E.; Lovinger, A. J. *J. Am. Chem. Soc.* **1998**, *120*, 664-672.

[18] (a) Briseno, A. L.; Mannsfeld, S. C.; Shamberger, P. J.; Ohuchi, F. S.; Bao, Z.; Jenekhe, S. A.; Xia, Y. *Chemistry of Materials*. **2008**, *20*, 4712-4719. (b) Briseno, A. L.; Mannsfeld, S. C.; Lu, X.; Xiong, Y.; Jenekhe, S. A.; Bao, Z.; Xia, Y. *Nano letters*. **2007**, *7*, 668-675.

[19] (a) Clar, E. *Polycyclic Hydrocarbons*, Academic Press, London, **1964**.; (b) Platt, J. R. *J. Chem. Phys.*, **1949**, *17*, 484-495.

[20] Mondal, R.; Shah, B. K.; Neckers, D. C. *J. Am. Chem. Soc.*, **2006**, *128*, 9612-9613.

[21] Maliakal, A,; Raghavachari, K.; Katz, H.; Chandross, E.; Siegrist, T. *Chem. Mater.* **2004,** *16,* 4980-4986.

[22] Zhang, X.; Matzger, A. J. *J. Org. Chem.* **2003**, *68*, 9813-9815.

[23] Morris, J. V.; Mahaney, M. A.; Huber, J. R. *J. Phys. Chem.*, **1976**, *80*, 969-974.

[24] Scherf, U. *J. Mater. Chem.* **1999**, *9*, 1853-1864.

[25] Muccini, M. ; Lunedei, E. ; Taliani, C.; Beljonne, D. ; Cornil, J. ; Brédas, J. L.; *J. Chem. Phys.* **1998**, *109*, 10513-10520.

[26] Bard, A. J.; Faulkner, L. A. *Electrochemical Methods Fundamentals and Applications*; Wiley: New York, **1984**.

[27] Meng, H.; Bendikov, M.; Mitchell, G.; Helgeson, R.; Wudl, F.; Bao, Z.; Siegrist, T.; Kloc, C.; Chen, C. H. *Adv. Mater.* **2003**, *15*, 1090-1093.

[28] Coropceanu, V.; Kwon, O.; Wex, B.; Kaafarani, B. R.; Gruhn, N. E.; Durivage, J. C.; Neckers, D. C.; Bridas, J. -L.; *Chem. Eur. J.* **2006,** *12*, 2073-2080.

[29] (a) Bock, C.; Pham, D. V.; Kunze, U.; Kafer, D.; Witte, G.; Terfort, A. *Appl. Phys. Lett.* **2007**, *91*, 052110. (b) Asadi, K.; Gholamrezaie, F.; Smits, E. C. P.; Blom, P. W. M.; de Boer, B. *J. Mater. Chem.* **2007**, *17*, 1947.

[30] Kawasaki, M.; Imazeki, S.; Oh-e, M.; Ando, M. *Jpn. J. Appl. Phys.* **2008**, *47*, 6247-6250.

[31] Leuninger, J.; Wang, C.; Soczka-Guth, T.; Enkelmann, V.; Pakula, T.; Müllen, K. *Macromolecules*. **1998**, *31*, 1720-1727.

Chapter 4
Study of Structure-Property Relationship of Sulfur and (or) Nitrogen-Bridged Heptacenes

4.1 Introduction

In this chapter, the regioselective synthesis of four different types of new heteroheptacenes bisbenzo[*b*,*b*']thienodithieno[3,2-*b*:2',3'-*d*]pyrrole (BBTDP), bis-benzo[*b*,*b*']thienocyclopenta [2,1-*b*:3,4-*b*']dithiophene (BBTCPDT), thieno[2',3':4,5]-thieno[3,2-*b*]thieno[2'',3'':4',5']thieno[2',3':4,5] thieno[3,2-*f*][1]benzo-thiophene (TTTTTBT) and dibenzo[*b*,*b*']thieno[2,3-*f*:,4-*f* ']bis[1] benzothiophene (DBTBT) as well as the structure-property relationships are presented. BBTDP, BBTCPDT and TTTTTBT were synthesized via triflic acid induced intramolecular electrophilic coupling reaction, while compound DBTBT as known compound was resynthesized through a new strategy without the production of isomers. Dramatic differences in the solid structure between BBTDP and BBTCPDT were detected by single crystal XRD measurements. The temperature dependant single-crystal-single-crystal phase transitions of compound BBTCPDT were intensively studied. The new compounds were characterized by a combination of optical spectroscopic (UV/Vis and photoluminescence) and electrochemical (cyclic voltammetry) techniques. In addition, DFT calculations provided valuable insights into the molecular electronic structure.

4.1.1 New electronically active organic molecular building blocks

As mentioned in previous chapters, the incorporation of thiophene moieties into oligomeric or macromolecular systems has recently become a topic of significant interest owing to their highly intriguing photophysical properties.[1] However, the introduction of the desired electronic properties is often connected with synthetic difficulties that would significantly increase the production costs of the resulting devices. A great deal of attention has therefore been focused on efficiently tuning the optoelectronic structure of the thiophene-based materials to modify their electronic nature in such a way that it suits the targeted applications (i.e. to generate small, well defined band gaps).[2]

In this context, fused bithiophene materials are promising candidates since they provide a high degree of π-conjugation due to their rigidified, planar structure which intrinsically affords smaller HOMO- LUMO-gaps for the materials; fused arenes can generally impart quinoid character to the oligomer/polymer and thus lower the band gap relative to e.g. simple polythiophenes where twisting from planarity can easily disrupt conjugation.[3]

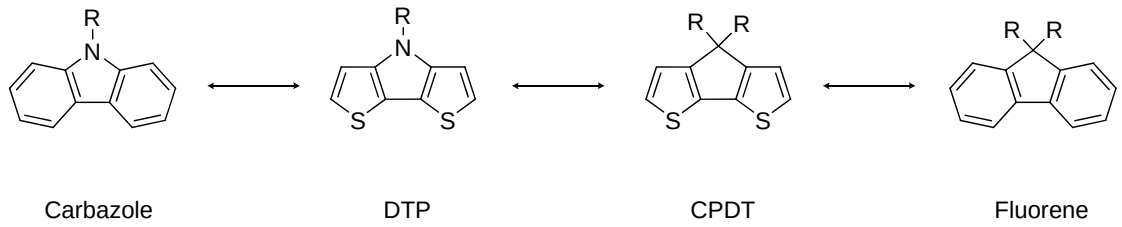

Figure 4.1. Carbazole versus dithienopyrrole versus cyclopentadithiophene versus fluorine

Dithieno[3,2-*b*:2',3'-*d*]pyrroles (**DTP**), as a structural analogue of carbazole (**Figure 4.1**), are a topic of current interest as popular building blocks for polymeric semiconducting materials owing to their favourable optoelectronic properties.[4] Although the first synthesis of the **DTP**s dates back to 1983,[5] it wasn't until 2003 that the first comprehensive study on the synthesis and optoelectronic properties including theoretical calculations was presented by Ogawa and Rasmussen.[6] Later

on, Koeckelberghs et al. described transition metal catalyzed routes to functionalized dithienopyrroles using 3,3'-dibromo-bithiophene and primary amines to build up the central pyrrole ring.[7] (**Scheme 4.1**) Structural investigations on the **DTP**s show that the fused-ring system is completely flat indicating a high degree of π-conjugation across the three ring-units.

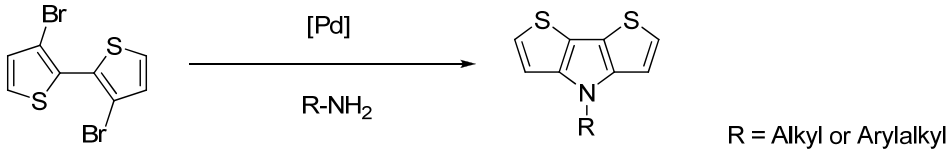

Scheme 4.1. Synthesis of soluble dithieno[3,2-*b*:2',3'-*d*]pyrroles.

Cyclopenta[2,1-*b*:3,4-*b*']dithiophene (**CPDT**), which is, on the other hand, regarded as a fused-ring analogue of 3-alkylthiophene and a structural analogue of fluorenes, has been widely investigated in constructing low-band-gap polymers.[8] Kraak et al. first reported the structural unit of **CPDT** in 1968,[9] and an improved synthetic strategy from 3-bromothiophene was reported by Brzezinski et al. in 2002.[10] Because of the planarized backbone, long conjugation lengths, narrow band gaps, and strong intermolecular π-π interactions of the **CPDT** units, **CPDT**-based polymers have recently been found for applications in infrared electrochromic displays, solar cells, and semiconductor layers in field-effect transistors.[11] It has also been reported that homopolymers based on **CPDT** can not self-assemble into ordered structures [12], due to the sp^3 hybridised *carbon* in the bridge position and an out-of-plane arrangement of the substituents.

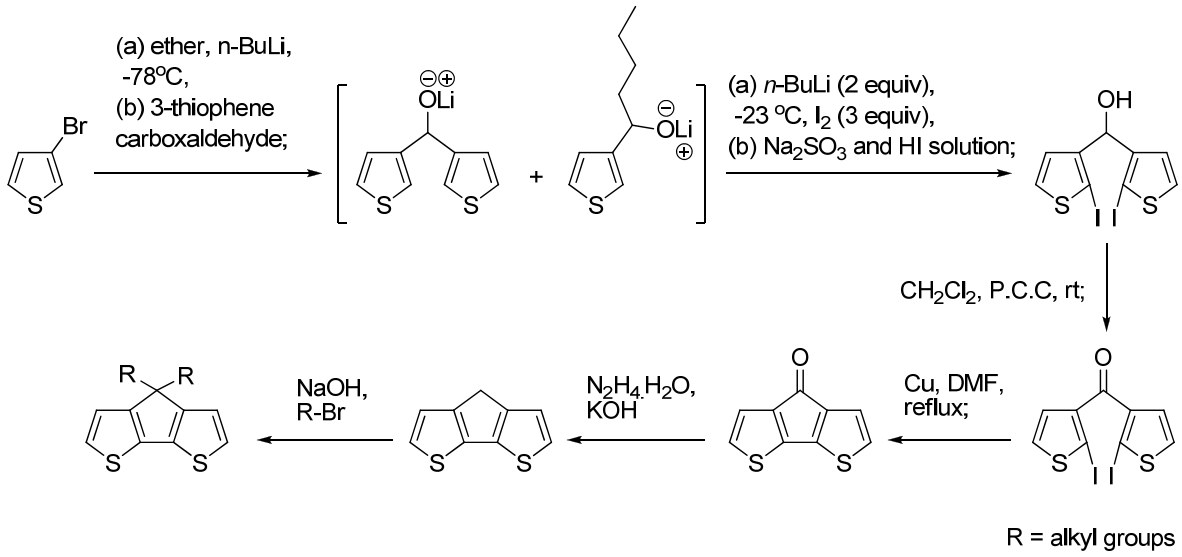

Scheme 4.2. Synthetic route to cyclopenta[2,1-*b*:3,4-*b*']dithiophene

However, much less research has been devoted to the structurally defined oligomeric counterparts of **DTP** and **CPDT**, which may contribute to the understanding of their polymeric counterparts.

4.1.2 Single crystal to single crystal phase transition

It is well known that phase transitions in molecular solids are of high importance in solid-state chemistry and in material science. Besides their importance, the mechanisms of transformations in molecular crystals are largely unknown.[13] From energy considerations it is believed that the differences between polymorphs are usually quite small[14] and that they are sometimes temperature dependent. The dependence on temperature is due to the difference between the entropy of the polymorphs and the molecules adopt different stable arrangements in different temperature range. If there are large differences between the structures of the polymorphs then usually the crystal lattice of the transformed phase is destroyed and followed by nucleation and growth of the new phase.[15],[16]

With the development of crystal engineering, temperature dependent single-crystal-to-single-crystal (SCSC) phase transformations have received considerable interest.[17] However, such SCSC phase transformations are still rare

since crystals can hardly retain single crystallinity after the solid-state rearrangement of atoms.[18],[19],[20],[21],[22] It is not clear to what extent the structures of the two polymorphs may be different and yet allowing transformation without destruction of the crystal lattice.

Most of the reported cases on SCSC phase transformations involve the dimerization or polymerization of unsaturated molecules[18] or guest exchange of porous materials.[19],[20],[20] However, only several examples have been reported on SCSC transformations by molecular conformational movements, e.g. alkyl translations, olefin rotations, and rotational tilts, which give insight to understand how organic solids can support the development of crystalline molecular machines and devices.[23] (**Figure 4.2**) Although it is still difficult to tailor this kind of transformation, we believe that the pendent alkyl substitutes on the heteroheptacenes in this study could induce conformational changes of the molecules. Molecules with such kind of small motions will not destroy single crystallinity and lattice structures and are expected to show SCSC transformations.

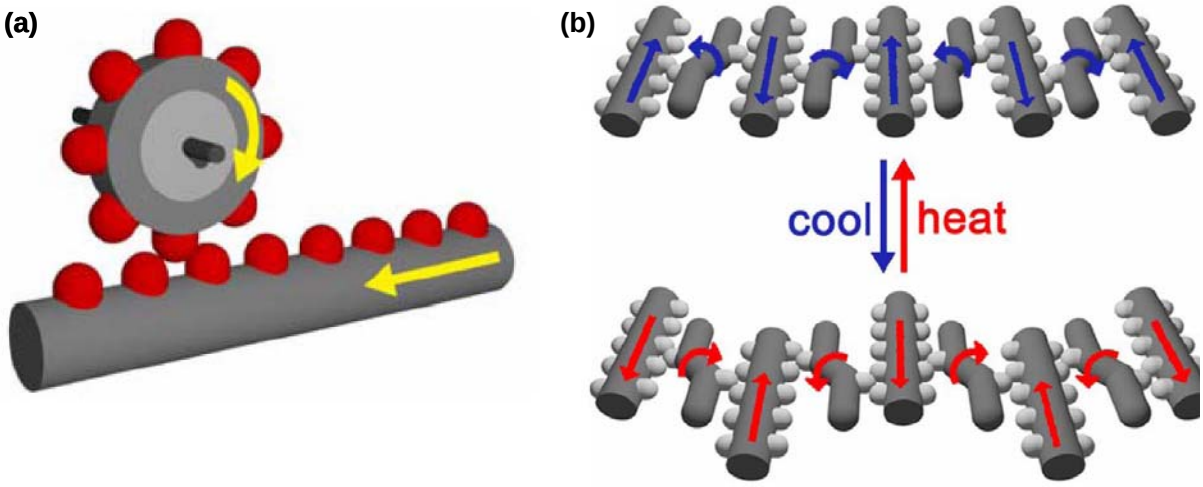

Figure 4.2. Model of potential application of SCSC transformations. (a) Illustrations of rack-and-pinion gear; (b) schematic of one thermo-controlled molecular machine. (Reproduced from Sokolvo et al.[23b])

4.1.3 Sulfur-extrusion reaction in dibenzo- or dithieno[l,2]dithiin

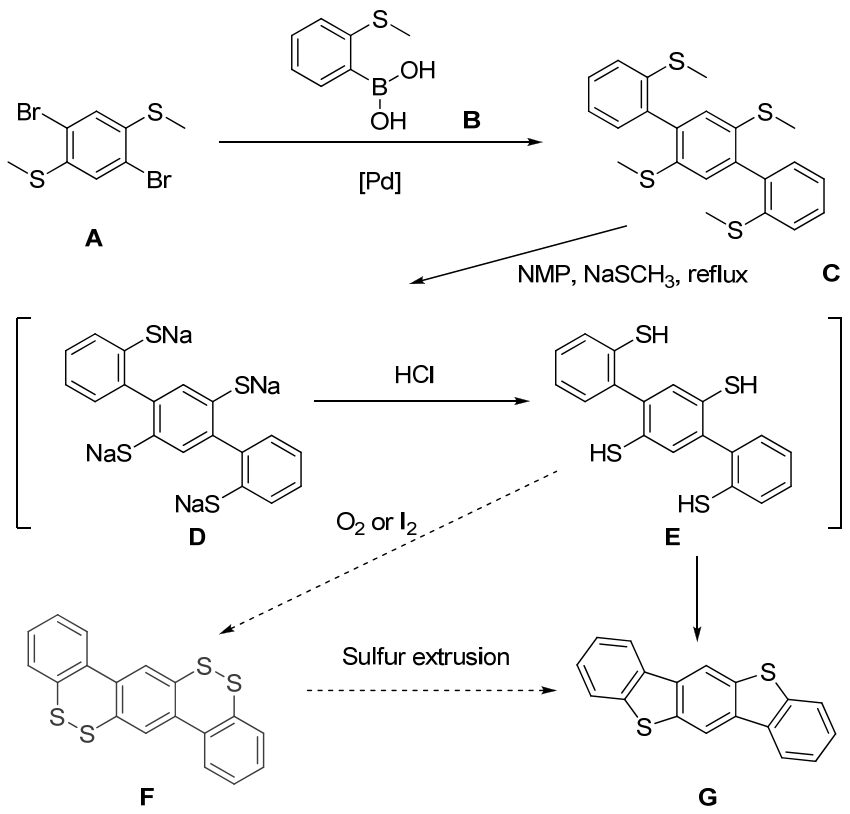

Scheme 4.3. Proposed sulfur extrusion reaction to give S bridge instead of S-S bridge

It is know that disulfide bond (S-S-bond), also called disulfide bridge, is strong covalent bond between two sulfhydryl groups. This bond is very important to the folding, structure, and function of proteins.[24] Oxidation of two adjacent thiol groups (-SH) yields a disulfide (S-S) bond. The presence of S-S then helps to maintain the tertiary structure of the protein. In an initial effort to make redox active disulfide bonds bridged molecules **F**, precursor molecule **C** was made via a two fold Suzuki coupling between **A** and **B**. (**Scheme 4.3**) Following a combined methods,[25] precursor **C** was treated with $NaSCH_3$ in boiling NMP, and then acidified by HCl to yield the intermediate tetrathiol compound **E**. I_2 in ethanol was added to the reaction mixture containing **E** to oxidize the tetrathiol, which was expected to form S-S bonds bridging on the *p*-terphenyl structure **F**. The white precipitation that was obtained almost quantitatively out of this step was characterized by FD-MS. Surprisingly the molecular weight was assigned to the double sulfur extruded

product **G**. A comparison of the ^{1}H NMR spectra between **G** and known BBBT indicated that the product is purely BBBT instead of double S-S bonds bridged **F**.

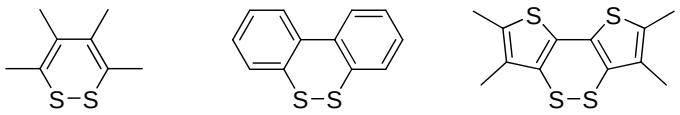

H **I** **J**

Figure 4.3. Structures of 1,2-dithiin **H**, dibenzodithiin **I** and dithienodithiin **J**.

This unexpected result motivated us to investigate the reaction of S-S bond containing aromatic systems. The 1,2-dithiin system (**H**) has attracted considerable attention.[26] (**Figure 4.3**) Studies on this type of compound have revealed that they extrude sulfur to form thiophenes at ambient temperature and in the presence of light. Although annulation significantly increases the stability of 1,2-dithiins, because dibenzo-l,2-dithiin **I** and dithieno-l,2-dithiin **J** show no tendency to extrude sulfur at room temperature,[27] **I** and **J** extrude sulfur to form thiophenes when heated in the presence of Cu or UV light.[28] (**Scheme 4.4**) The mechanism by which this transformation occurs (catalyzed or uncatalyzed) is, however, still unclear and has been the subject of considerable debate. However, based on this unexpected sulfur extrusion reaction, it is possible to construct some thiophene ring fused oligoacenes.

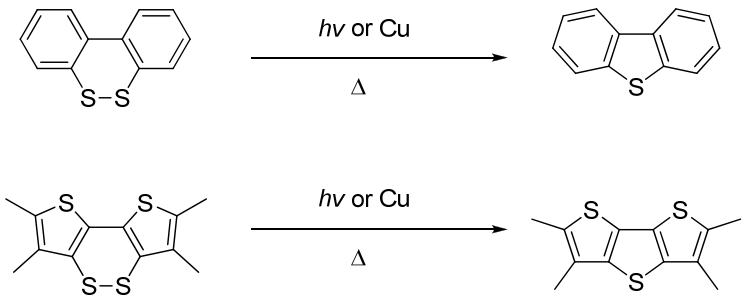

Scheme 4.4. Sulfur extrusion reaction of annulated 1,2-dithiins.

Based on the knowledge and interesting building blocks described above, we tried to further broaden the family of π-extended heteroheptacences, with the variation of electron rich thiophene and/or pyrrole ring units. (**Figure 4.4**)

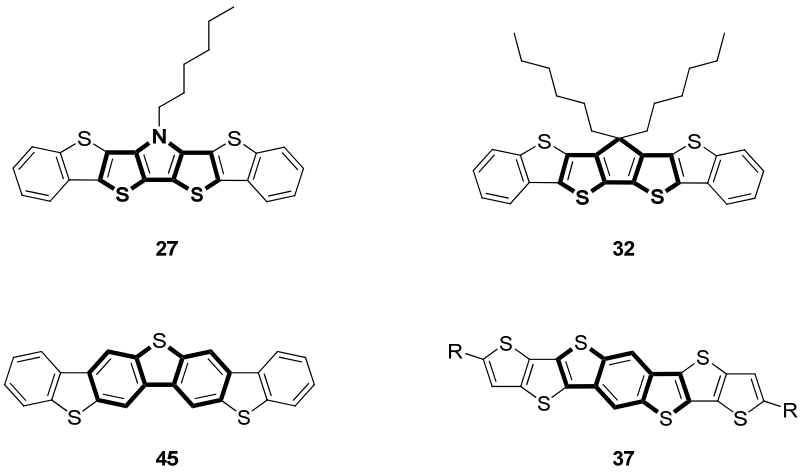

Figure 4.4. New ladder-type π-conjugated heteroheptacenes

4.2 Synthesis and characterization of sulfur and (or) nitrogen-bridged heptacenes with dithienopyrrole (DTP) and cyclopenta[2,1-*b*:3,4-*b'*]dithiophene (CPDT) as the central π system

DTP and **CPDT** are five-member-ring fused aromatic systems. The different structure characteristics from carbazole make them good candidates for the super acid induced ring-closure reaction due to absence of isomeric products.

4.2.1 Synthesis of bisbenzo[*b*,*b'*]thienodithieno[3,2-*b*:2',3'-*d*]pyrrole (27) and bisbenzo[*b*,*b'*]thienocyclopenta [2,1-*b*:3,4-*b'*]dithiophene (32)

As shown in **Scheme 4.5**, oxidative coupling of lithiated 2,3-dibromo thiophene with copper(II) chloride in diethyl ether at -78 °C gave 3,3'-dibromo-2,2'-bithiophene (**28**). According to the procedure reported by Koeckelberghs,[7] the 4-hexyl-4H-dithienopyrrole (DTP) core (**29**) was successfully synthesized via a Buchwald–Hartwig reaction of the 1-hexyl amine with **28**. In order to perform the Stille-coupling, di(trimethyltin)-substituted DTP (**30**) was prepared. This was

accomplished by reacting the dithienopyrrole **28** with 2.1 equiv of *t*-BuLi in tetrahydrofuran at room temperature. The reaction can be driven to completeness by working at sufficiently low dilution. Then trimethyltin choride was added to quench the dilithiated DTP. Since distannylated dithienopyrrole degrades during purification by column chromatography,[4a] compound **30** was used without purification in the next step. Stille coupling of **30** and 1-bromo-2-(methylsulfinyl)benzene[29] was conducted in the presence of Pd(0) catalyst with DMF as the solvent and afforded the compound **31** in good yield. Subsequent intramolecular ring-closure was performed with an excess of pure triflic acid, where the as-formed clear solution was poured into water to give a yellowish precipitate, followed by filtering, drying, and reflux in pyridine. The new heteroheptacene bisbenzo[*b*,*b*']thienodithieno[3,2-*b*:2',3'-*d*]pyrrole (BBTDP, **27**) was achieved as an off-white solid with an overall yield (referring to **31**) of ca. 85% after purification by flash column chromatography.

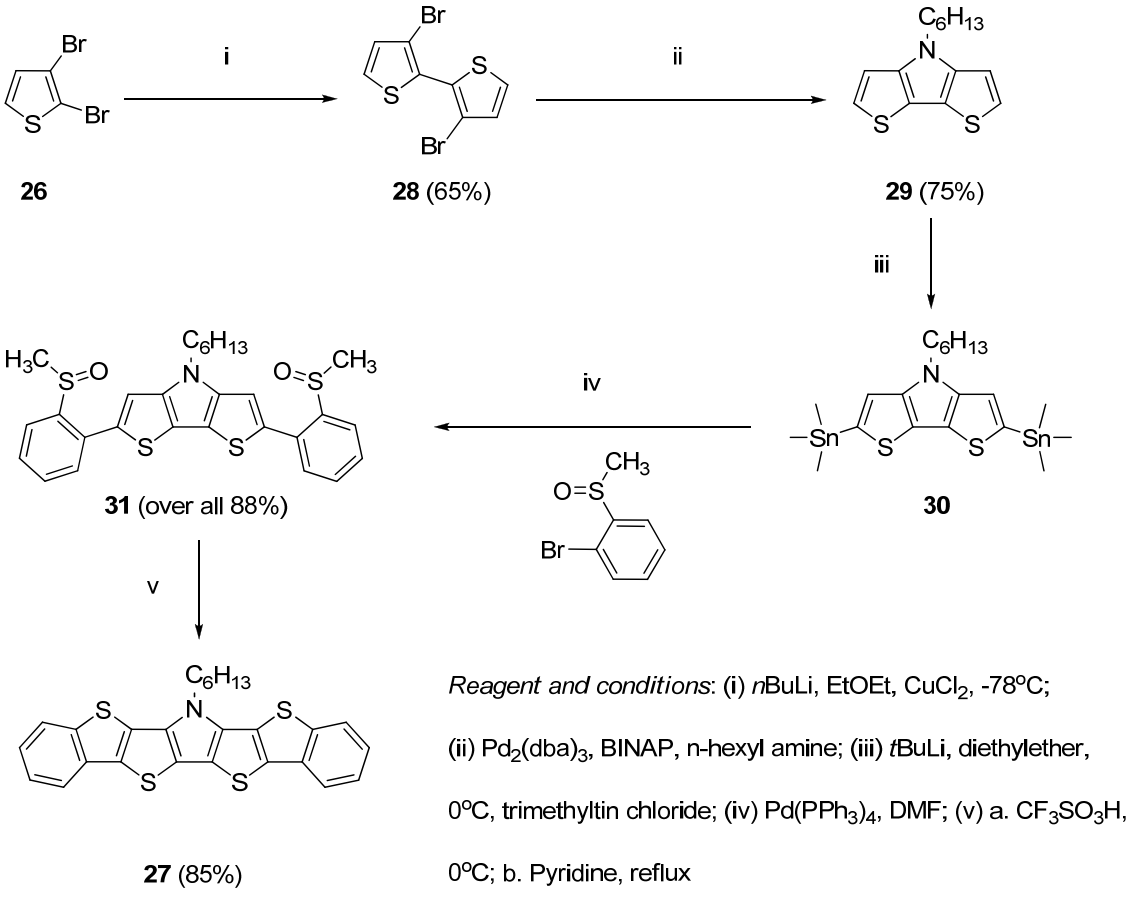

Scheme 4.5. Synthesis of bisbenzo[*b*,*b*']thienodithieno[3,2-*b*:2',3'-*d*]pyrrole (**27**)

Cyclopenta[2,1-*b*:3,4-*b*']dithiophene (**33**) was prepared by following a reported method[30] and was then dialkylated with hexyl bromide in the presence of KOH as the base and KI as the catalyst in DMSO, affording **34** in excellent yield (**Scheme 4.6**). The distannylated CPDT (**35**) was prepared by dilithiation of **34** using *t*-BuLi, followed by quenching with Me_3SnCl. The tin compound was an oil, which could not be purified by column chromatography (due to protiodestannylation).[31] However, the compound was sufficiently pure to be used in the next step. Precursor **36** was synthesized by a Stille coupling of **35** and 1-bromo-2-(methylsulfinyl)benzene[29] in an overall yield of 85%. Finally, by following the same procedure as for precursor **31**, bisbenzo[*b*,*b'*]thienocyclopenta[2,1-*b*:3,4-*b'*]dithiophene (BBTCPDT, **32**) was achieved as a light yellow powder in 88 % yield.

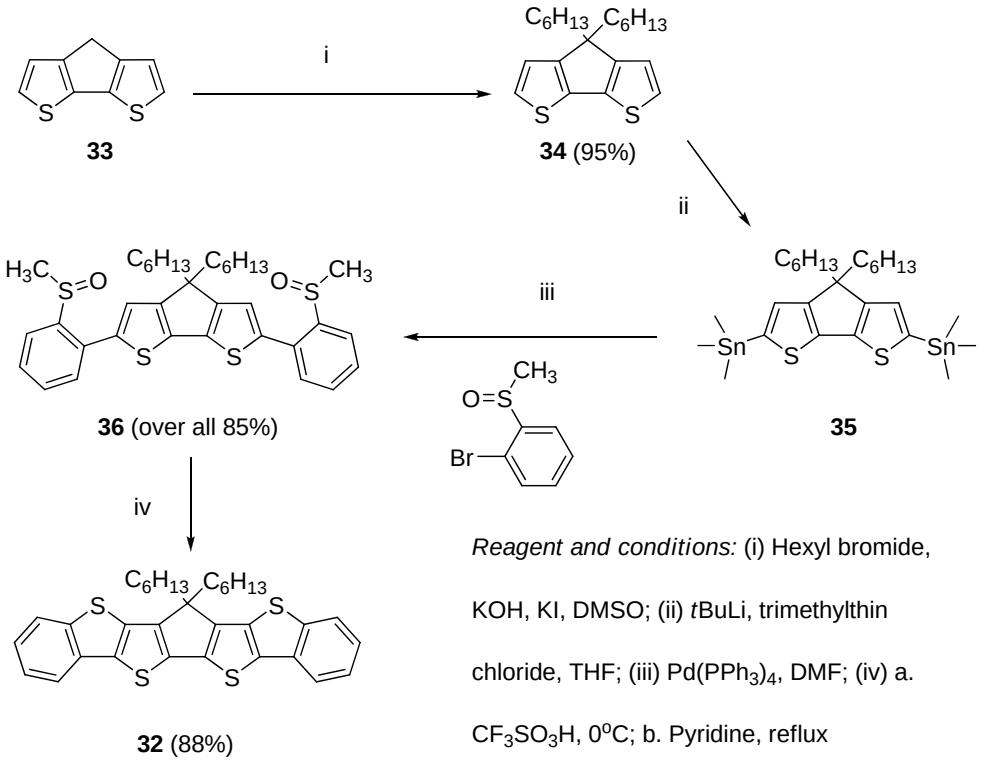

Scheme 4.6. Synthesis of bisbenzo[*b*,*b*']thienocyclopenta[2,1-*b*:3,4-*b*']dithiophene (**32**)

4.2.2 Structure proof of the heteroacenes by ^{1}H NMR spectroscopy

BBTDP and BBTCPDT were air stable solids and fully characterized by ^{1}H NMR, ^{13}C NMR spectroscopy, elemental analysis, and mass spectrometry (FD). As

depicted in **Figure 4.5**, the ^{1}H NMR spectra show the highly symmetric structures of the heteroheptacenes and there was no proton signal arising from the inner thiophene rings, but signals from the outside benzene rings could be observed, which is fully in agreement with the desired structure. From **Figure 4.5a** and **4.5b**, it was found that all the proton signals of compound **32** slightly shifted upfield by 0.12 ppm as compared with compound **27**. This trend, which may originate from the fact that the nitrogen atom in **27** is more electronegative than the carbon atom in **32**, has also been observed in proton NMR spectra of carbazole[32] and fluorene[33].

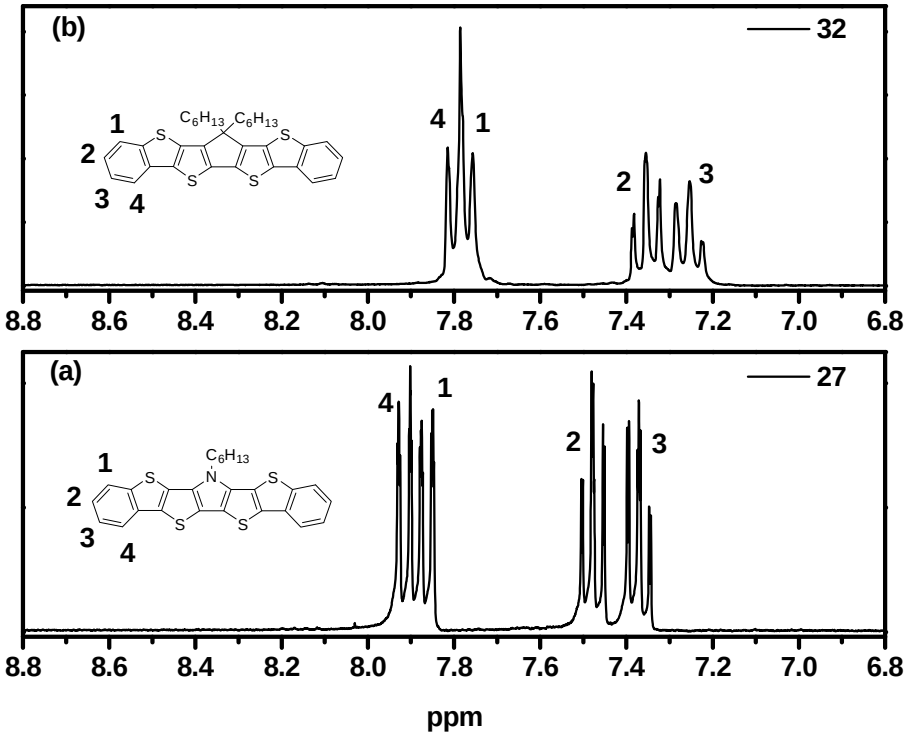

Figure 4.5. Expanded aromatic region of ^{1}H NMR spectra of compounds (a) BBTDP and (b) BBTCPDT (250 MHz, 300 K, d_2-dichloromethane).

4.2.3 Solid-state crystal structure and packing of the new heteroheptacenes and the unexpected single-crystal-to-single-crystal (SCSC) phase transition in the crystal structure of BBTCPDT

Elucidating the solid-state packing of conjugated materials in single crystals is essential to understand how the molecular assembly is influenced by substituents.[34]

Single crystals of the heteroheptacenes suitable for single crystal X-ray diffraction studies were obtained from CH_2Cl_2-hexane (for **27**) and CH_2Cl_2-MeOH (for **32**) at room temperature.

4.2.3.1 Solid-state crystal structure and packing of compound BBTDP

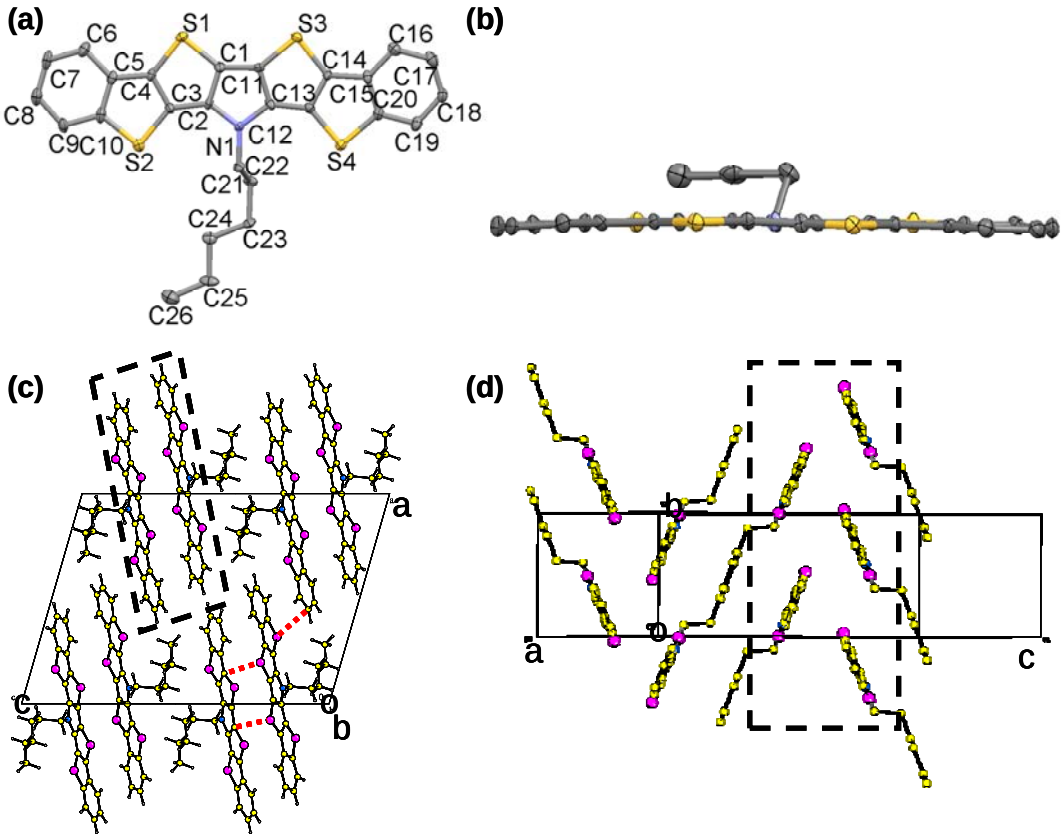

Figure 4.6. Packing diagram of **27**. (a) Thermal ellipsoid of **27**. The hydrogen atoms were omitted for clarity. Thermal ellipsoids are drawn at 50% probability. (b) Views along the short molecular axis. (c) View down the stacking axis of head-to-head column pairs. (Dashed rectangular illustrate the head-to-head pairs, Dashed lines illustrate intermolecular close-contacts within and between the columns) (d) View along the long molecular axis showing "lamella herringbone" structure formed by antiparallel column pairs. (Dashed rectangular illustrate the antiparallel lamella structure. The hydrogen atoms are omitted for clarity.

Compound **27** crystallizes in the monoclinic $P\ 2_1/c$ space group with four molecules in the unit cell. As seen in **Figure 4.6**, **27** has two more sulfur atoms in the

molecular than **8c** and similarly has one hexyl chain on the nitrogen atom. These structure variation results in a completely different crystal packing diagram. The skeleton of **27** is planar and two molecules form a pair with head-to-head structure, then the pairs further stack into a column with aromatic skeleton forming herringbone structure, where the tilt angle between two mean planes of the **BBTDP** framework is 45.6°, compared to 60° or 0° in **8c**[35] and 52° in pentacene.[36]

Two intermolecular S-C close-contacts are observed between the two molecules in the pair. (**Figure 4.6c**, marked in red dashed line). For instance, the distances between the sulfur atoms in a molecules of **27** (i.e., S1 and S3, see supporting information) and carbon atoms (i.e., C14 and C2) from the adjacent molecules are 3.44 Å and 3.34 Å, which is shorter than the sum of their van der Waals radii (3.55 Å). The same distances could be observed between the two carbon atoms of each molecule and the sulfur atoms of one additional molecule as well. In addition, these columns form antiparallel lamella with aliphatic chains lying between every two aromatic columns (**Figure 4.6d**, marked in dashed rectangular). Interestingly, intermolecular close-contacts are also found between the columns. As marked in **Figure 4.6c**, the distance between S2 of one molecule and the C8 of the molecule in another column is measured to be 3.48 Å, which suggests that a single crystal of **27** may have a two-dimensional electronic structure. A similar packing has been found in DBTCz-C6 but with only one-dimensional electronic structure (Chapter 3).

4.2.3.2 Single-crystal-to-single-crystal (SCSC) phase transition in the crystal structure of compound BBTCPDT

By changing the *N*-alkyl group in **27** to a dialkylmethylene unit in **32**, the single crystals of **32** exhibit dramatic differences from that of **27** as confirmed by SCXRD analysis. Suitable crystals were grown by addition of little methanol in a THF solution of the compound. This structure presents some interesting features that will be discussed in detail.

Single crystals of compound **32** show *three* temperature-dependent phases: A, B and I. (**Table 4.1**) The three phases are conformational polymorphs. This unusual

crystalline (thermal) transformation is to be distinguished from other single-crystal-to-single-crystal transformations in which no dimerization or polymerization of unsaturated molecules[37] or guest exchange of porous materials is involved.[38] An X-ray structure determination at room temperature afforded a structure in the monoclinic $P2_1/c$ space group with *one* crystallographically independent molecule in the asymmetric unit, which is termed phase A. When the crystal was slowly cooled to 120 K a triclinic structure was observed which had twice the unit cell volume of phase A. This structure (phase B) formed at low temperature has the centrosymmetric space group *P* -1 and compared to phase A twice the un cell volume. Thus here the asymmetric unit consists of four crystallographically independent molecules.

The difference between the two crystal lattices can be easily observed in **Figure 4.7**, where the packing diagrams of the molecules have been depicted. The conversion was evidenced by the sudden appearance of new reflections which describe the doubling of the cell volume and the loss of symmetry (glide planes and screw axes). Remarkably, the cycle could be repeated multiple times without loss of the single crystallinity. Only limited examples have been found in the literature. [23]

The single crystal structure (Phase A) determined at room temperature is shown in **Figure 4.7**a and b. The fully ladderized skeleton is planar while with the 4, 4' substituted alkyl chains lying above and below the plane of the skeleton respectively in an almost vertical geometry. In one unit cell, two adjacent molecules are packed to form a pair with head-to-head structure like compound **27**. However, due to the extended extra alkyl chain, the two molecules' backbones in the pair are separated from each other and are oriented almost perpendicular. To fill the space, one molecule from a second pair embeds in and has a small extent of cofacial overlap with one molecule in the first pair. The loose packing nature of the material could be seen from the interplanar distance (3.83 Å) of the cofacial part and no short contact was detected in the solid structure. Obviously, the perpendicularly oriented alkyl chain causes a distinct bulge, which is essential in preventing the molecule of **32** from

close packing of the aromatic rings and hence undergoing severe fluorescence quenching.[39] (vide infra)

X-ray data of compound **32** collected at 120 K (Phase B) are shown in **Figure 4.7**c and d. Unlike the phase A, the structure was solved in the triclinic *P* -1 space group with eight molecules in the unit cell. All the molecules are separated by the alkyl chains showing vertical translations of neighboring molecules with neither π-π interaction nor even confacial overlap in the packing structures.

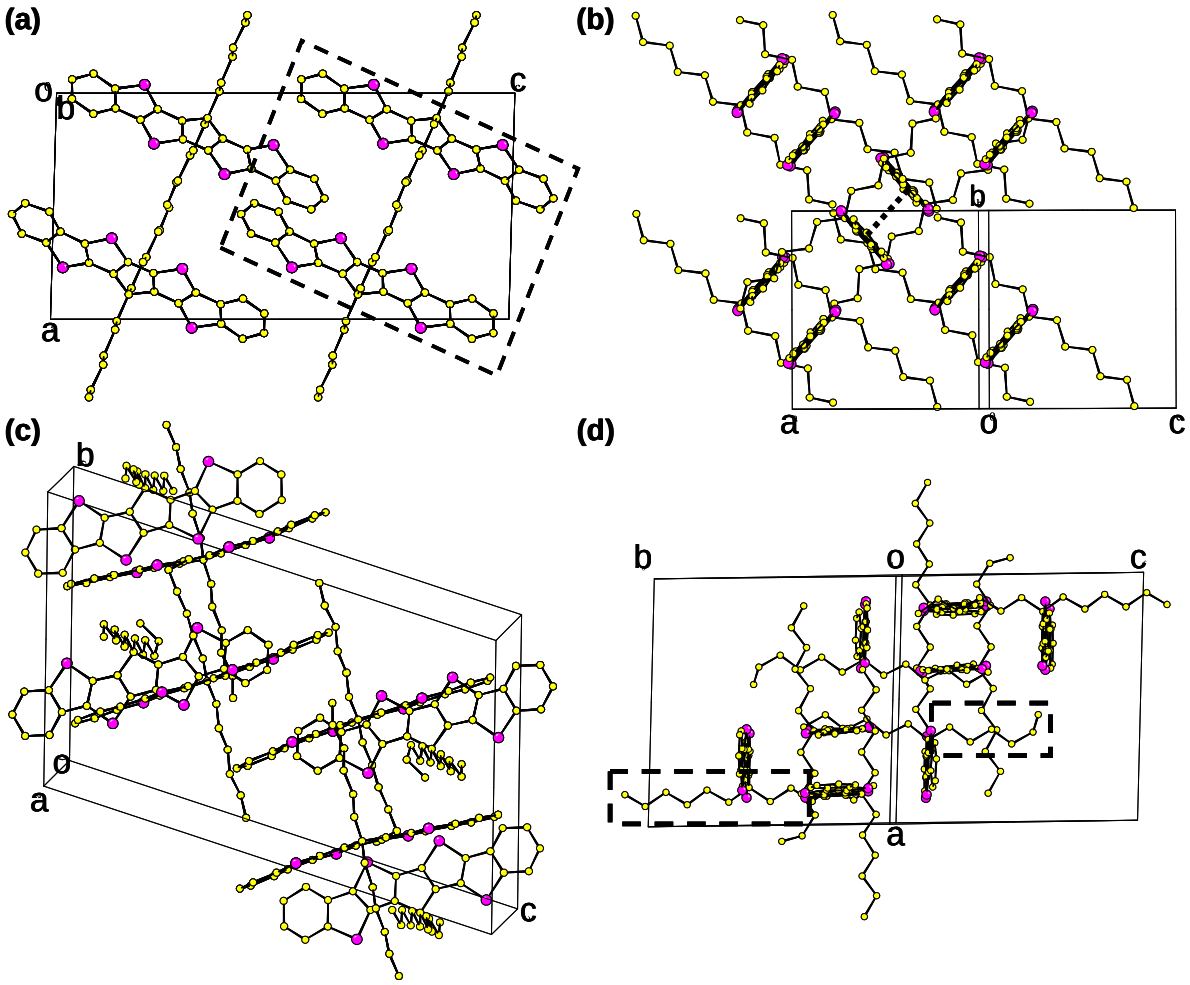

Figure 4.7. Packing diagram of **32** at room temperature (Phase A) (a) View down the *b*-axis of the unit cell (Dashed rectangular illustrate the head-to-head pairs). (b) View along the long molecular axis showing the perpendicularly oriented alkyl chain (Dashed lines illustrate cofacial distance). Packing diagram of **32** at 120 K. (Phase B) (c) Crystal packing showing vertical trasnsitions of neighboring molecules. (d) View along the long molecular axis showing the two different conformations of the alkyl

chain (Dashed rectangular illustrate two different kinds of alkyl conformation). The hydrogen atoms are omitted for clarity.

As shown in **Figure 4.7**d, in the unit cells, both hexyl groups in four of the molecules are arranged almost vertically around the plane of the backbone, with the carbon atoms in both substituents in a mean *anti* geometry, whereas the two *n*-hexyl groups in each of the other four molecules were arranged in different conformations, with the six carbon atoms of one *n*-hexyl substituent adopting a mean 'anti' geometry and the other a partial gauche conformation at the fifth methylene carbon. A torsion angle of 60.5° is measured. This arrangement may be because of the steric hindrance between two adjacent molecules in one unit cell.

4.2.3.3 Temperature dependant study of the crystal structures

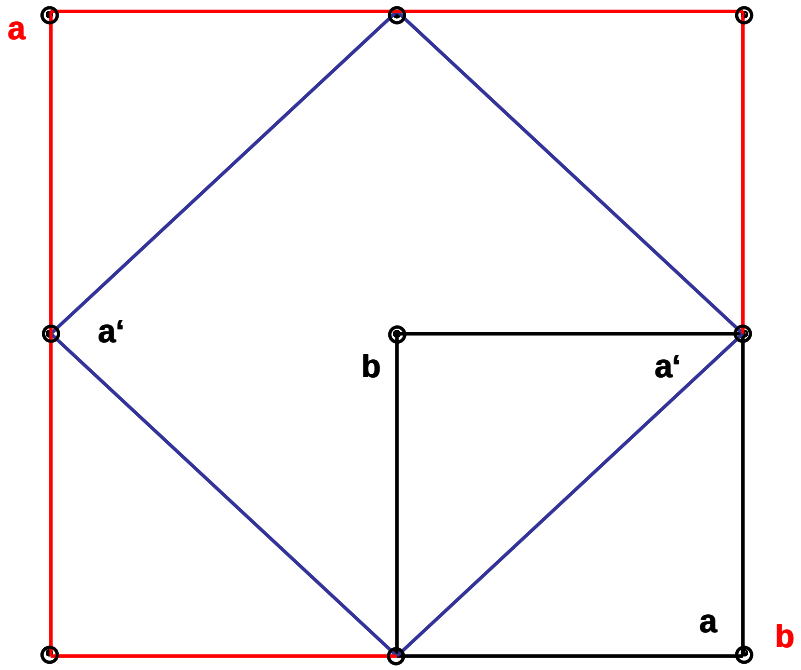

Figure 4.8. Superposition in the *ab* plane of the crystalline cell at 140 K (blue rectangular) with unit cells belonging to the structure at room temperature (black rectangular) and 160 K (red rectangular). Black circles represent common inversion centers for all structures. In the structure at room temperature there is only one independent molecule and the number of inversion centers is 2 times higher than in the structure at 160 K.

To get more information about this phase transition, it was decided to perform a variable temperature X-ray study on compound **32**'s single crystal. The temperature dependence of the unit cell parameters were investigated between 100 and 300 K.

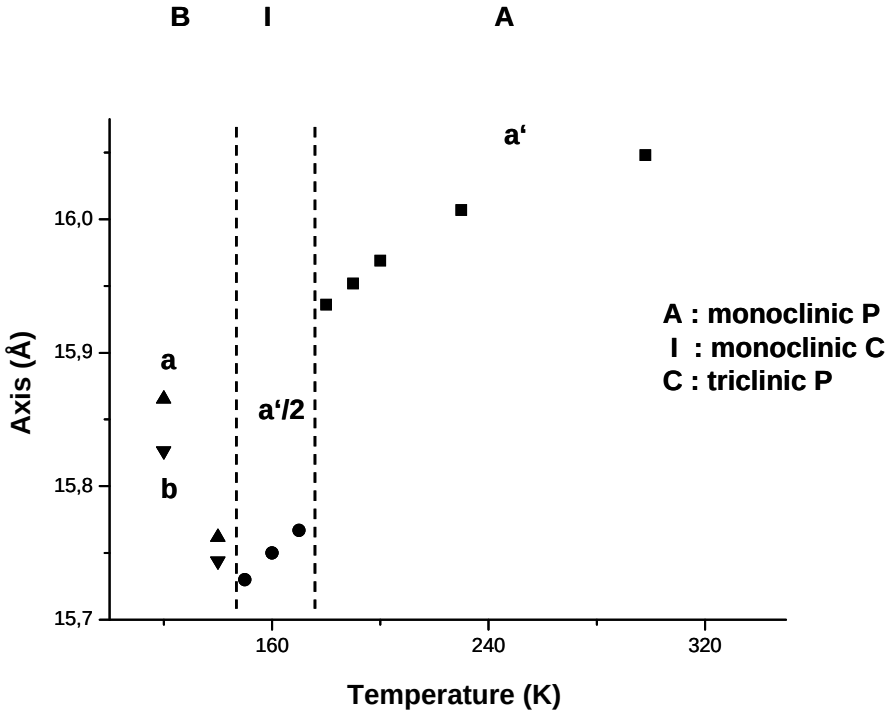

Figure 4.9. Temperature dependence of the equivalent cell parameters *a'*, *a* and *b* (left *y* axis). Error bars are negligible for *a* and *c* parameters with respect to the drawing scale. The two vertical dotted lines indicate the phase transition temperature

Surprisingly, in this study an intermediate phase (phase I) between phase A and phase B was detected. The relation between the three lattices is shown in **Fig. 4.8.** It shows the a – b plane of the three phases. The intermediate phase I is monoclinic C centered and has four times the volume of phase A. A common direction in all three lattices is the diagonal a' in phases A and I which in phase B is the lattice parameter a and c. The length of this diagonal a' and the lattice parameters a and c, respectively, are plotted in **Fig. 4.9** versus temperature. At the transition A – I (at approximately 175 K) a distinct sudden drop of a' is observed. The slope of the temperature dependence does not change at this point. At the transition I – B a distortion of the lattice is observed, i.e. the angle γ deviates from 90° which it assumes by symmetry in the monoclinic lattices. Thus two different diagonals are observed which are the a

and b lattice parameters of the triclinic low temperature form B. It should be noted that at this point the slope changes and an unusual expansion in this lattice plane with decreasing temperature is observed. To determine the crystalline structure in the intermediary phase I, an X-ray data collection was performed at 160 K. The structure was solved in the monoclinic $C2_1/c$ space group with *two* crystallographically independent molecules in the asymmetric unit (**Figure 4.10**).

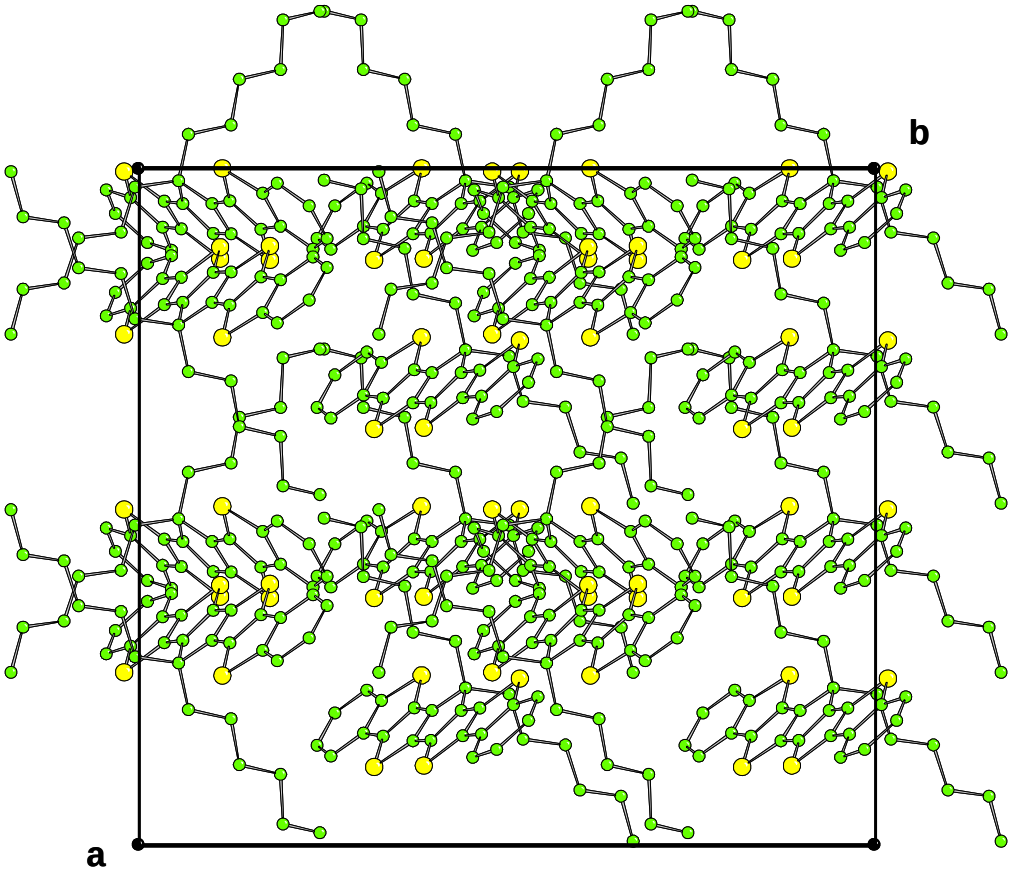

Figure 4.10. Packing diagram of **32** at 160 K (Phase I)

The origin and mechanisms of crystalline phase transitions in organic[40] and organometallic[41],[42] compounds have been extensively discussed in the literature within the last years. To our knowledge, the two structural transitions observed here in **BBTCPDT** are a unique example of a fully characterized *stepwise* symmetry lowering upon cooling with a successive decrease of the lattice symmetry so that at lower temperaures the molecules which are related in phase A by symmetry become inequivalent.

These very different solid-state structures of the three heteroheptacenes nicely illustrate how the effect of the alkyl and heteroatom substituents could efficiently be utilized to tune the organization in the solid-state of organic semiconductors. The more sulfur atoms are present, the more intermolecular short contacts exist, which can facilitate the charge carrier transport. It is known that tight packing of the chromophores in the solid state will lead to self-quenching of photoluminescence and excimer or exciplex formation.[43] To prevent this phenomenon, bulky or branched substituents are always employed to intrinsically disperse the packing arrangement of the chromophores. In this study, a branched alkyl substitution instead of a linear one can effectively loosen the solid packing, therefore prevent self-quenching and suppress the formation of aggregates/excimers. By accident, the large free volume leads also to the unexpected SCSC transformation that could be induced by external thermal stimulus. These observations attest to the degree of motion that can be experienced by a single crystal and suggests that solids that exhibit more complex motion can be pursued and developed.[44] The study of the concerted transformations may be considered a step to understanding how movements in molecular solids can support the development of correlated and collective crystalline molecular machines and devices.[45]

Table 4.1. Crystallographic Parameters of **27** and **32**

	27	**32**		
		Phase A	Phase I	Phase B
Empirical formula	$C_{26}H_{21}N_1S_4$	$C_{33}H_{34}S_4$	$C_{33}H_{34}S_4$	$C_{33}H_{34}S_4$
Formula weight	475.72 g/mol	558.9 g/mol	558.9 g/mol	558.9 g/mol
Crystal color, habit	prism	-	-	-
crystal system	monoclinic	monoclinic	monoclinic	triclinic
a, Å	15.4263(4)	11.8090(4)	22.837(1)	15.8655(4)
b, Å	6.8789(1)	10.8680(2)	21.699(1)	15.8264(4)
c, Å	21.6728(5)	23.9300(9)	23.652(1)	25.9589(6)
β, deg	106.01(0)	91.5230(12)		105.4199(14)
V, Å^3	2210.66(58)	3070.10(17)		5928.6(3)
ρ_{calc}, g/cm^3	1.42926	1.209		1.252
Space group	*P* 1 21/c 1 (14)	*P* 1 21/c 1 (14)	$C2_1/c$	*P* -1 (2)
Z value	4	4		8
Temperature, K	120	293		120
No. of reflections measured	6189	6942		30211
No. of variables	280	334		1333
Residuals: *R*; wR^2	0.0412; 0.0401	0.0485; 0.0480		0.0671; 0.0629

4.2.4 Powder X-ray diffraction (PXRD) analyses and film microstructure for compounds BBTDP and BBTCPDT

Unlike films of the other heteroheptacenes, thin films of **27** contain at least two major crystallite orientations or phases when cast from solution. Based on the single crystal diffraction data, the reflection peaks could be assigned as shown in **Figure 4.11a**. It seems that the *d*-spacing calculated is not applicable when the molecules have alkyl substitution in the short molecular direction due the presence of several primary reflection peaks. Therefore, it is not possible to draw the molecular arrangement on the substrate. (**Figure 4.11b**) This phenomenon has been observed in various substituted oligothiophenes as well,[46] including the carbazole analogue of **8c**, α,ω-dihexylquaterthiophene.[47]

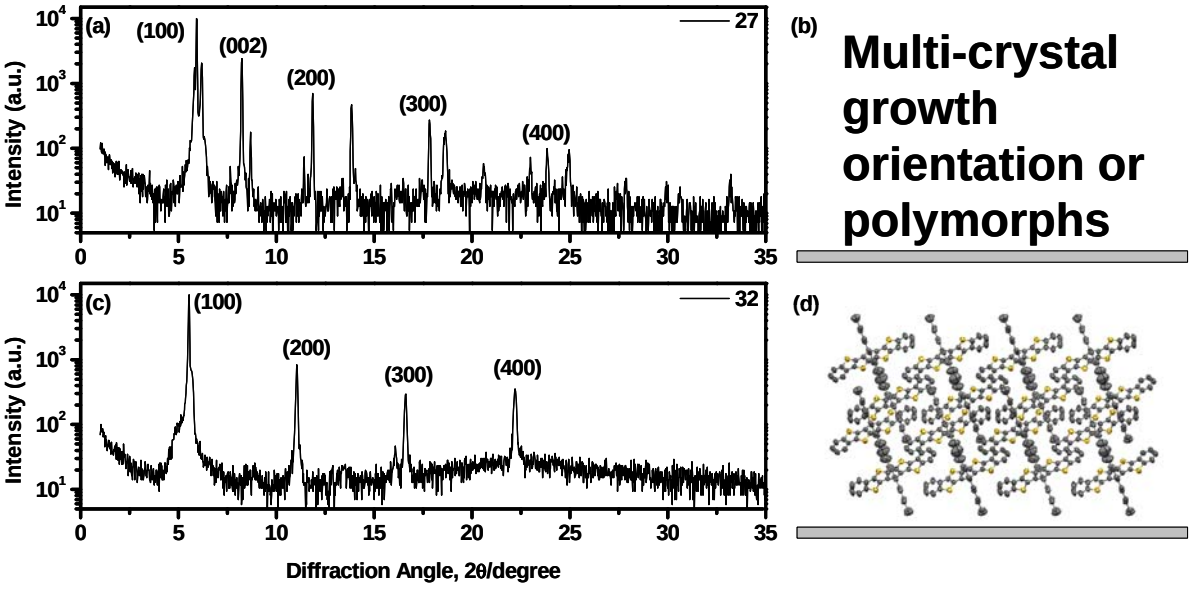

Figure 4.11. X-ray diffractogram of the drop-cast thin films (40 mg/ml 1,2-dichlorobenzene solution). (a) **27** on an untreated SiO_2 substrate. (b) unknown complicated lamellar packing on the substrate. (c) **32** on an untreated SiO_2 substrate. The reflections are assigned by the Miller's indices. (d) Supposed organization of **32** in the solution processed thin layer on the substrate.

Unexpectedly, although having two branched alkyl chains, the X-ray diffractogram of compound **32** exhibits a single set of reflections and the peaks are assigned as (*l*00) reflections based on the single crystal diffraction data. (**Figure 4.11c**) Assisted by Mercury software[48], the tile angle between the long molecular axes and the (100) plane that is parallel to the substrate surface is calculated to be 48°. (**Figure 4.11d**) The derived *d*-spacings (15.94 Å) can not be related to all the three unit cell parameters of the corresponding single crystal got at room temperature (**Table 4.1**). This indicates that compound **32** formed unique thin film crystal phases with different reciprocal cell spacing.

4.2.5 Scanning electron microscopy morphological characterization of compounds BBTDP and BBTCPDT

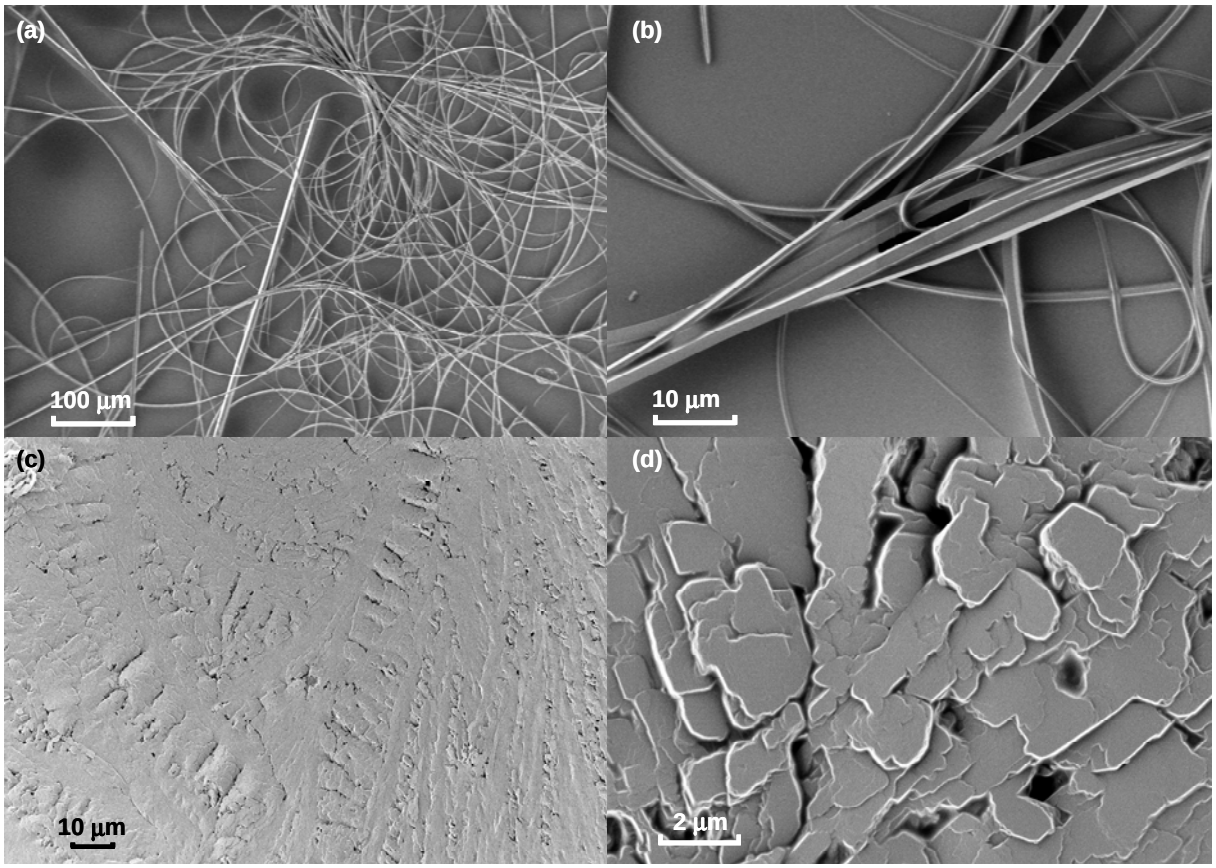

Figure 4.12. Scanning electron micrographs of dropcasted films from *o*-dichlorobenzene on untreated Si/SiO_2 substrates of (a) & (b) BBTDP (**27**), 25 °C; (c) & (d) BBTCPDT (**32**), 25 °C.

When a solution of **27** in dichlorobenzene was cast on untreated Si/SiO_2 substrates, microwires formed after the solvents evaporation. **Figure 4.12** a, b show the morphologies of microwires (**Figure 4.12** a, b) cast on substrate. The diameter of microwires changes from hundreds of nanometers to several micrometers and the length reaches several millimeters. Because the products are obtained by cast assembly, they are easily obtained in a large area. PXRD patterns indicate that the whole microwires are crystalline in nature. It has been reported that a field-effect transistor (FET) device has been fabricated based on an individual microwire of an organic molecule.[49]

In marked contrast, compound **32** formed a much more homogeneous film when cast on the Si/SiO_2 substrates as shown in **Figure 4.12** c. From **Figure 4.12** d, a completely different morphology with highly intermingled and larger squared-shaped grains is found. The branched alkyl groups decreased the anisotropic crystallinity to a large extent and helped to form thin film crystals with much larger grain boundary.

4.2.6 Photophysical properties

UV absorption and photoluminescence spectra (PL) of compounds **27** and **32** were measured in both solution and as drop-casted thin films (**Figure 4.13**) to assess the effect of heteroatom and alkyl substitution on the heteroheptacene absorption/emission maxima and the optical energy gap. **Table 4.2** collects the UV/Vis and PL data for all compounds in THF solution. The UV/Vis absorption spectra of **27** and **32** display structured absorption bands in the UV range which are attributed to the β (Platt's ^1B_b band), and *p*-band of the π-π^* transitions.[50] Compared to the **DTP** based heteroheptacene **27**, the absorption maxima of **CPDT** based **32** is red-shifted by 26 nm from 387 nm when the central *pyrrole* ring is replaced by a *1,3-cyclopentadiene* unit. This result for **27** is surprising because the introduction of electron rich heterocycles into conjugated systems has been a proven strategy for achieving low-bandgap chromophores.[51] In fact, a similar case has been observed in

the homopolymers of **DTP** and **CPDT** before.[52] In a comprehensive study of polyDTPs, Ogawa et al.[53] attributed this phenomenon to the difference in the rigidity of the two monomers and founded that changing the bridgehead from CHR to NR results in no change in the absorbance spectra.[4a]

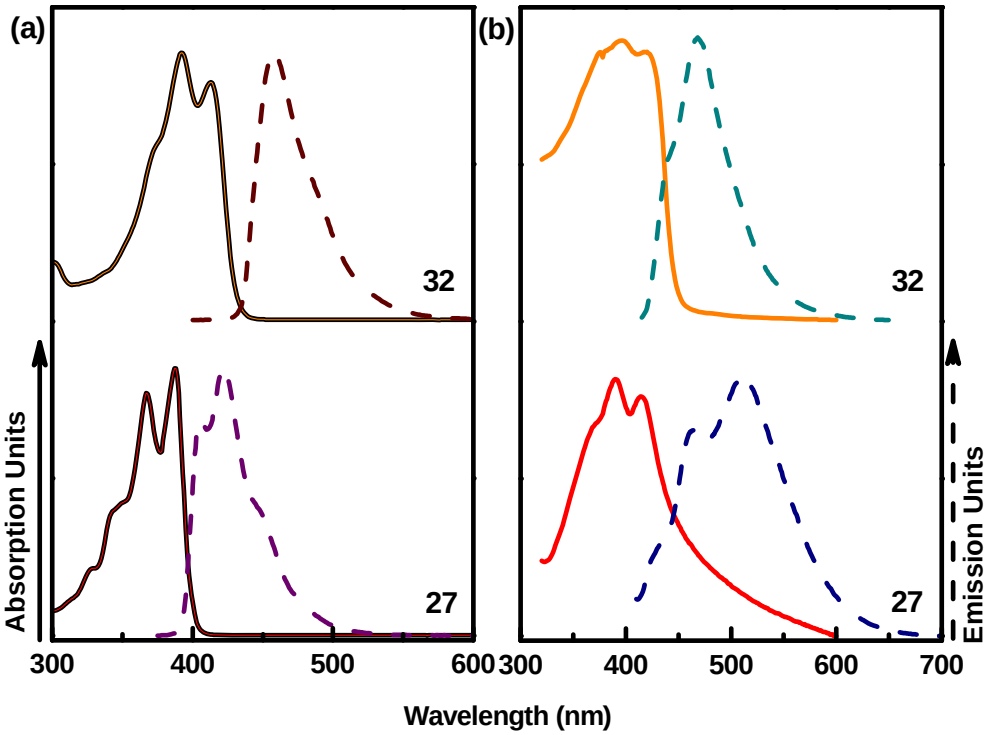

Figure 4.13. (a) Normalized UV-vis absorption, PL spectra of compounds **27** and **32** in THF (10^{-6} M). (b) Normalized UV-vis absorption, PL spectra of compounds **27** and **32** as thin film.

Table 4.2. UV-Vis absorption and PL data for **27** and **32**

compound	Solution[a]			Film	
	Absorption λ_{max} [b] /nm peak/edge	PL λ_f /nm	Quantum yield[c] (Φ_f)	Solid-state absorption λ_{max}/nm	Solid-state PL λ_f /nm
27	387	407	0.22	414	465
32	413	457	>0.95	420	468

[a] In THF 10^{-6} M. η = 1.4070. [b] λ_{max} as π-π HOMO-LUMO transition. [c] Quantum yield relative to diphenyl anthracene (10^{-7} M, cyclohexane solution), excitation at 365 nm.

Solution optical band gaps (E_g^{op}) of compounds **27** and **32**, defined by the 0-0 transition energies, were estimated based on the λ_{max} absorption edge and listed in

Table 3.6. All compounds have significantly larger band gaps than that of hydrocarbon-heptacene (1.5 eV),[54] pentacene (2.15 eV),[55] diindolocarbazole (2.59 eV)[56] and smaller than that of diindenocarbazole (3.2 eV)[57].

Photoluminescence spectra (PL) of compounds **27** and **32** were measured in THF by exciting 10^{-6} M solutions at the corresponding λ_{max} values. The shapes of the PL excitation spectra match these of the absorption spectra. Interestingly, compound **32** shows an unstructured strong emission maxima (λ_{PL} at 457 nm), which is bathochromically shifted by 50 nm compared to the emission wavelength of compound **27** and shows a Stokes shift of 44 nm. In marked contrast, compound **27** exhibits weak emissions with the maximum at 407 nm and much smaller Stokes shifts due to more rigid coplanar structure. Relative photoluminescence quantum yields (Φ_f) of these heteroheptacenes were determined using diphenyl anthracene in cyclohexane as the standard,[58] and the PL data were also collected in **Table 4.2**. In this study, the Φ_f value of compound **32** (Φ_f > 0.95) increases dramatically as compared to **27**, which indicates that non-radiative decay pathways are nearly suppressed. This is in agreement with the single crystal X-ray diffraction results that compounds **27** has both a coplanar conjugated skeleton and linear alkyl side chains that favour the molecular interactions in the excited state and weaken the PL efficiency. In contrast, compound **32** has two alkyl chains on the central tetrahedral carbon of **CPDT** core, which effectively hinder the molecular association as shown in the single crystal packing diagram.

The solid-state optical absorption/PL data for molecules **27** and **32** are collected in **Table 4.2**. In general, the film absorption spectra exhibit characteristic transitions that are bathochromically shifted compared to their solution values, which is indicative of the presence of π-π stacking in the solid state. Compound **27** showed a large red-shift by 27 nm, while in contrast compound **32** exhibited only a red-shift of 5 nm (**Figure 4.13b**), which again indicates a weaker intermolecular interaction of compound **32**. Thin film photoluminescence spectra were obtained by λ_{max} excitation, and data are compiled in **Table 4.2**. The spectral shapes and maxima strongly depend on the molecular structure and its packing characteristics, with most of the

plots exhibiting red shift relative to the emission maxima in solution. It can be seen that the intermolecular interactions dominate the optical properties in the solid state and surmount the effects of the heteroatom substitution on the photophysics of the materials.

4.2.7 Electrochemical Properties

As already indicated by the abs/PL properties of the heteroheptacenes, variation of the heteroatom substitution has a significant impact on the optical properties. These results led us to further investigate the electrochemical behavior of the heteroheptacenes **27** and **32**, in order to determine their important aspects of chemical/electronic structure, substituent effects, and other physical characteristics. Cyclic voltammetry (CV) measurements were performed under N_2 in 0.1 M CH_2Cl_2/$TBAPF_6$ solutions with scanning rate at 50 mV/s^{-1}. All of the systems exhibit one or two reversible and/or quasi-reversible one electron oxidation waves within the solvent/electrolyte window range.

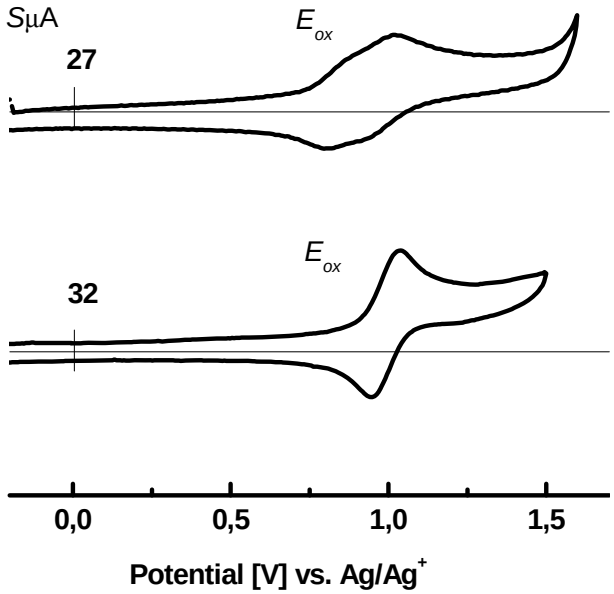

Figure 4.14. Cyclic voltammogram of **27** and **32**. Conditions: Glassy carbon as working electrode (diameter 1 mm); solution (ca.10^{-3} M) in CH_2Cl_2 with NBu_4PF_6 as supporting electrolyte (0.1 M); scan rate 50 mVs^{-1}; potentials are referred to an Ag/AgCl electrode.

Figure 4.14 shows voltammograms of compounds **27** and **32** and the electrochemical data are summarized in **Table 4.3** below. It is possible to extract the formal halfwave potentials ($E^{1/2}$), as the midpoints between peak potentials for the forward and reverse scans, when the voltammograms are (quasi)reversible. Single-electron oxidations (versus SCE) are obtained at 0.84/0.99 V for **27** and at 0.99 V for **32**. The oxidation of **27** (**Figure 4.14**) occurs in two reversible steps, the maxima of which are at E_{a1} (0.87 V) and E_{a2} (1.02 V), while **32** with a **CPDT** core shows only one quasi-reversible oxidation at E_{a1} = 1.04 V. The potential difference between the first oxidation potential E_{a1} of **27** and **32** is around 0.17 V, which clearly shows the comparatively higher ionization potential of **27**.

Table 4.3. Electrochemical data for **27** and **32** in dry CH_2Cl_2 under nitrogen

Compound	E_{ox}[a]/V anodic			cathodic		Half		HOMO[c]/eV	E_g^{opt} [d] /eV	LUMO[e]/eV
	E^{onset}	E_{a1}	E_{a2}	E_{c1}	E_{c2}	$E_1^{1/2}$	$E_2^{1/2}$			
1	0.71	0.87	1.02	0.81	0.96	0.84	0.99	-5.09	3.10	-1.99
2	0.90	1.04		0.94		0.99		-5.28	2.90	-2.38

[a] Versus. Ag/AgCl in CH_2Cl_2 with 0.1 M *n*-Bu_4NPF_6 as supporting electrolyte (scan speed = 50 mVs). [b] Absorption spectra. [c] Calculated based on HOMO = - (E_{ox}^{onset} + 4.34) eV. [d] Estimated from the absorption edge by E_g^{opt} (eV) = 1240.8/ $_{onset}$. [e] calculated from LUMO = HOMO+band gap.

The electrochemical studies on heteroheptacenes **27** and **32** indicate that they are intrinsically electron-donor molecules. According to E_{HOMO}=-(E^{ox}_{onset}+4.34) eV,[30] the HOMO levels of **27** and **32** could be estimated and listed in **Table 4.3**. These values are compared with the HOMO levels calculated by using Density Functional Methods (DFT). Taking into account their optical band gaps that derived from the absorption onset of the UV-vis spectrum, the LUMO values are also empirically calculated.

4.3 Synthesis of thieno[2',3':4,5]thieno[3,2-*b*]thieno[2'',3'':4',5'] thieno-[2',3':4,5]thieno [3,2-*f*][1]benzothiophene (TTTTTBT) and dibenzo[*b*,*b'*] thieno[2,3-*f*:,4-*f'*]bis[1] benzothiophene (DBTBT)

4.3.1 Synthesis of thieno[2',3':4,5]thieno[3,2-*b*]thieno[2'',3'':4',5']thieno[2',3':4,5]-thieno[3,2-*f*] [1]benzothiophene (TTTTTBT)

The synthesis of **DTBDT** (Chapter 2, section 2.3) and **DIBBBT** (section 3.2.3) suggested that the accessibility of heptacene based on thieno[3,2-*b*]thiophene and super acid induced ring closure methods. (**Scheme 4.7**)

3-Bromothiophene-2-carbaldehyde (**38**) was treated with ethyl 2-sulfanylacetate (DMF–K_2CO_3) at room temperature. After 72 hrs, it gave ethyl thieno[3,2-*b*]thiophene-2-carboxylate (**39**) in a yield of 81%. Then compound **39** was hydrolyzed with aqueous lithium hydroxide in THF to give the corresponding acid **40** in 90% yields. Thermal decarboxylation of thiophene and thienothiophene carboxylic acids is possible in quinoline in the presence of copper.[59] Thieno[3,2-*b*]-thiophene-2-carboxylic acid (**40**) was decarboxylated in this way, to give the parent ring system **41** in 88% yield. Use of a sand bath allowed us to control the temperature at a constant 260 ^{o}C. After removal of the bulk of quinoline with hydrochloric acid, flash chromatography of the crude product on silica gel allowed efficient removal of the final amounts of quinoline and gave the thieno[3,2-*b*]thiophene **41** in higher yields and better quality than previous work-up procedures.[59c]

Thieno[3,2-*b*]thiophene (**41**) was reacted with *n*-butyllithium and 1-bromoalkyl to give 2-alkylthieno[3,2-*b*]thiophene (**42**). The lithiated 2-alkylthieno[3,2-*b*]thiophene was reacted with trimethyltin chloride to produce (5-alkylthieno[3,2-*b*]thiophen-2-yl)trimethylstannane (**43**). Then the precursors **44** were prepared by the Stille coupling reaction with moderate yield. Subsequent intramolecular ring-closure was performed by following the same methods as for compound **22**. However due to the poor solubility and strong aggregation effects, the red products **37** are difficult to be

purified through column chromatography. Even though the alkyl chain is changed from hexyl to nonyl, the solubility is still very poor. It seems that the annulation of two more thiophene ring into the molecule skeleton could dramatically increase the intermolecular interaction and decrease the silubilty. *Due to the limitation of the ring closure method, it is not possible to add longer alkyl chains (C_n > C_{10}) on to the molecular system.* New methods are developed to build up this molecule in the future.

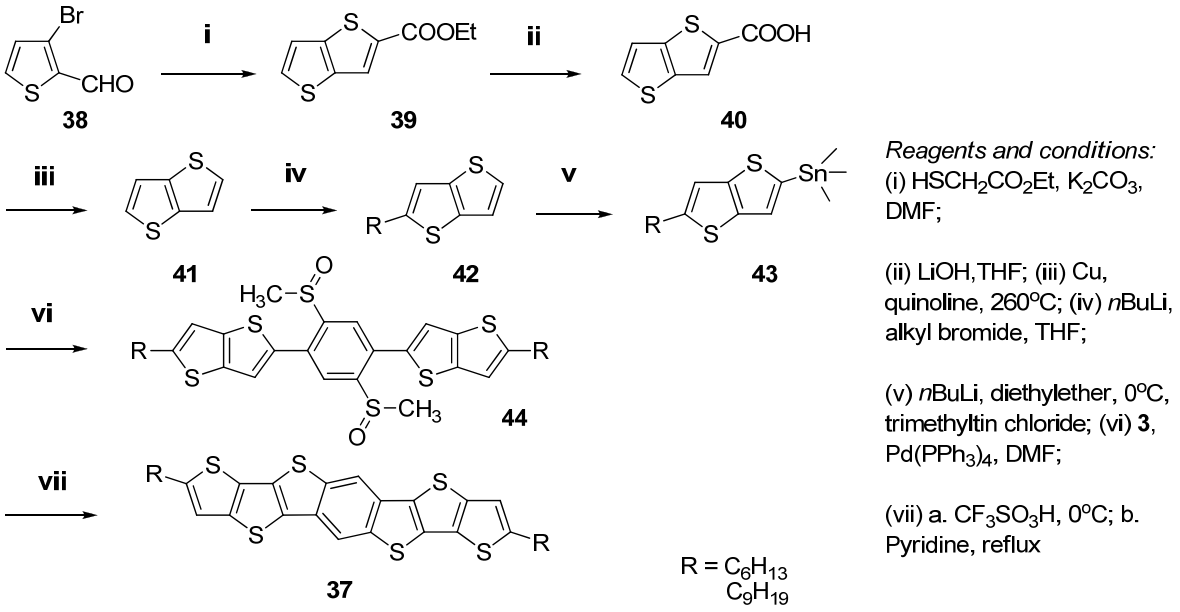

Scheme 4.7. Synthesis of TTTTTBT (**37**) through triflic acid induced ring-closure reaction

4.3.2 Synthesis and characterization of dibenzo[*b,b'*]thieno[2,3-*f*:,4-*f '*]bis[1]benzo thiophene (DBTBT) via sulfur-extrusion reaction

Compound **46** was made as an intermediate product in the synthesis of compound **3**. Asymmetric Suzuki coupling of **46** and 2-bromophenylboronic acid gave compound **47** in 55% yields. Then the monobromide compound was dissolved in dry THF and cooled to -78°C, at which temperature *n*BuLi was added dropwise. After 30 min, the lithiated species was quenched with 2-isopropoxy-4,4,5,5-tetramethyl-1,3,2-dioxaborolane to give monoboronic ester **48** in moderate yield. After the Suzuki reaction between compound **48** and monobromide **47**,

hexa-thiomethyl substituted tetraphenylene **49** was afforded as off-white solid. In the end, **49** was treated with sodium methylthiolatc in NMP at reflux conditions (186°C), and subsequently with HCl at room temperature to give **45** in 98 % yield. A proposed intermediate state is shown in **Scheme 4.8**.

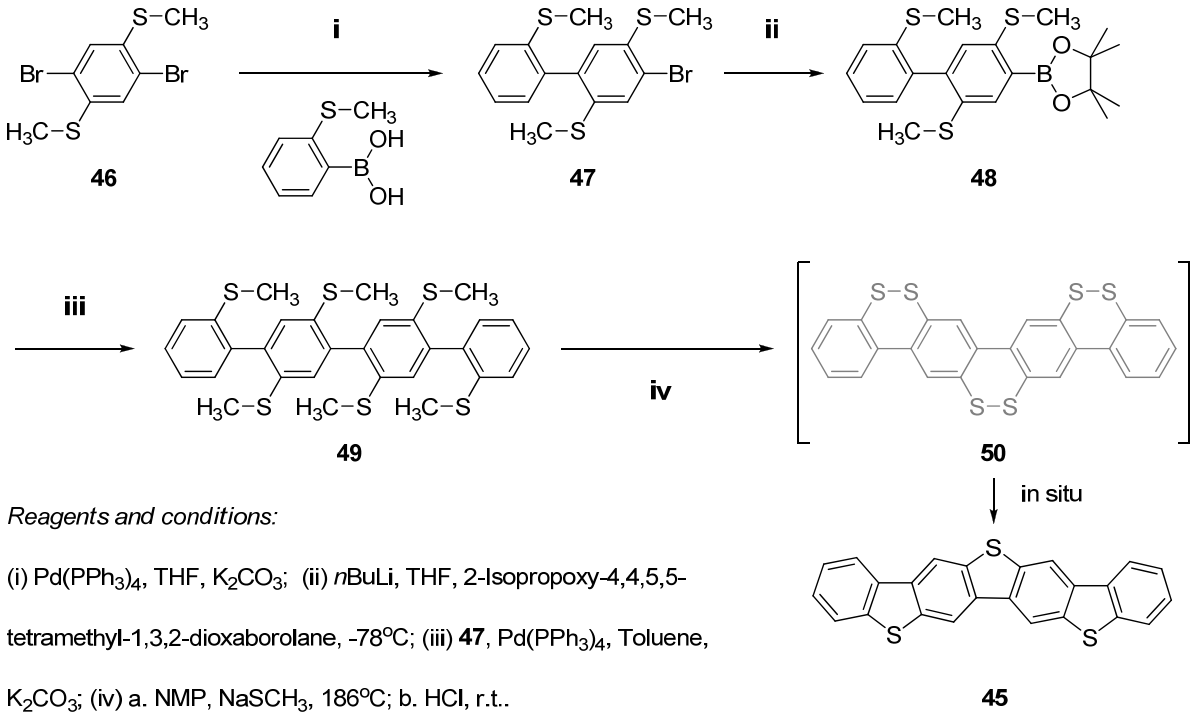

Scheme 4.8. Resynthesis of DBTBT via sulfur-extrusion reaction

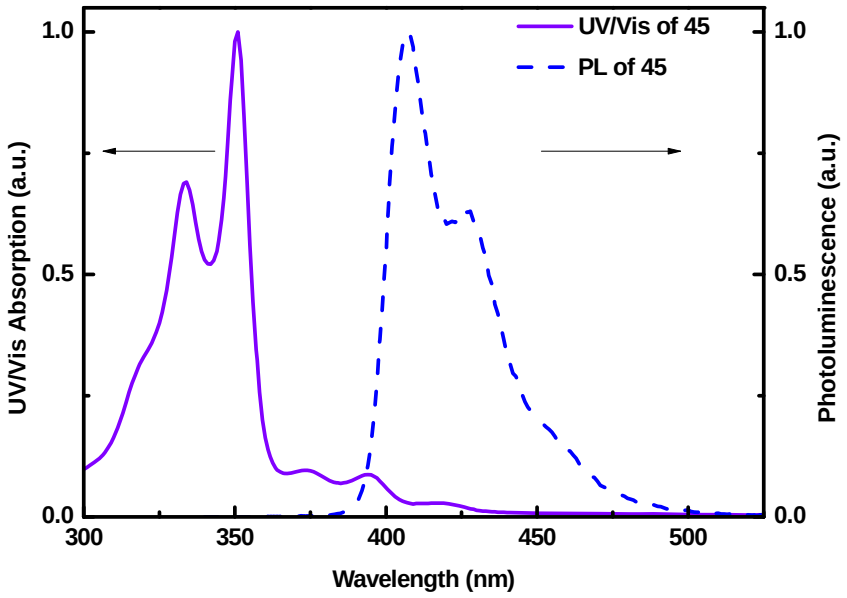

Figure 4.15. Normalized absorption spectra of solution of **45** in THF (10^{-6} M)

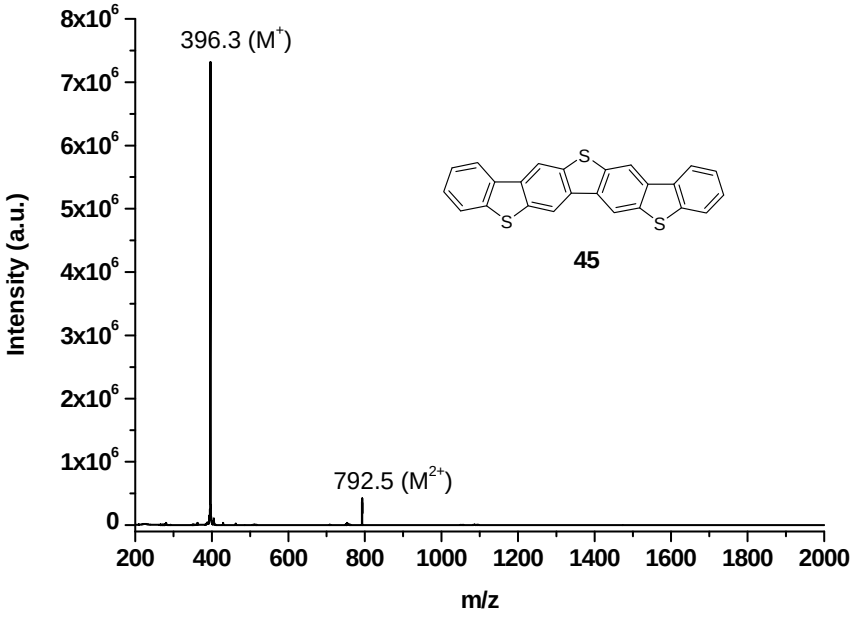

Figure 4.16. FD-Mass spectroscopy of compound **45**

The normalized optical absorption/photoluminescence spectra of solution of DBTBT are shown in **Figure 4.15**. Similar to that of DBTCz (Chapter 3, 3.2.6) and diindolocarbazole (DIoCz)[56], the absorption spectrum of DBTBT has an absorption maximum (λ_{max}) at 394 nm that belongs to *a* (Platt's ^1L_b band) *p*-band, since sulfur-based n-p* transitions have not been identified for thiophenes.[60] The structured absorption bands at 351 nm, 334 nm are attributed to the *β* (Platt's ^1B_b band), and *p*-band of the π-π* transitions. The absorption spectrum in this study is in full agreement with what was reported ten years ago by Jörg Leuninger.[61] The optical band gap of DBTBT is calculated based on the absorption onset (438 nm) to be 2.83 eV. A comparison of the band gaps of a series of heteroheptacenes is listed in **Table 4.4**. Samples of DBTCz are pale yellow solids and exhibit blue fluorescence in solution. There is a small Stokes shift ($\Delta\lambda$ = 13 nm) between the absorption maximum (λ_{max} = 394 nm) and the emission maximum (λ_{em} = 407, 425(sh) nm), which is in agreement with the rigid coplanar backbone. The molecular mass is also proven by FD-mass spectroscopy. (**Figure 4.16**) However, due to the extremely low solubility, it is difficult to measure a clear cyclic voltammetry curve out of compound **45**. Therefore the experimental redox property is still unknown.

4.4 MO calculation and electronic structure of heptacenes by varying the heteroatoms

Molecular orbital (MO) calculations for the electronic structures of the heteroheptacene such as electron affinity, ionization potential and band gaps were also performed using DFT methods. **Table 4.4** summarizes electrochemical energy level, optical, and computed energy gaps for compounds **8**, **16**, **27**, **32** and **45**. At the same time, reported heptacenes (diindolocarbazole (**DIoCz**),[56] diindenocarbazoles (**DIeCz**),[57] ladder-type tetraphenylene (**LTP**)[62]) are also included and compared in terms of energy level from both experiment and calculation. The excellent agreement between the experimental HOMO energy and the theoretical results, with differences of only ≈ 0.1-0.2 eV for almost all molecules is observed. However, the theoretical gaps predicated from vertical transitions are significantly larger than the optical band gap (E_g^{op}) (**Table 4.4**). Doubtlessly, besides other more complicated reasons, the differences in environments (e.g. solvation) lead to the disparity between computed and experimental LUMO or band gap values. From DFT calculation, the little difference between the HOMO\LUMO energy levels of **8** and **16** is in line with the CV experiments, indicating that the electronic structures of the heteroacenes is less affected by the variation of outside rings.

As visualized in **Figure 4.17**, the HOMO and LUMO are delocalized practically along the entire π-conjugated backbones with generally two different types of HOMO delocalization states and identical LUMO states. The HOMOs of **27** and **32** hold antibonding character (or intra-ring bonding) between the adjacent heterorings, whereas the LUMO represents inter-ring bonding interactions. By contrast, the HOMO energies of **8**, **16** and **45** are distinct from those of **27** and **32**, with obvious inter-ring bonding interaction and mainly localized around the central π system. On the other side, their LUMOs represent the same mode of delocalization as **27** and **32**.

Table 4.4. Comparison of electrochemical, optical, and calculated HOMO-LUMO energy gaps (E_g) and absolute HOMO and LUMO energies for the studied heteroheptacenes.

Compound	E/eV				E_g/eV	
	Experimental[a]		Theoretical		E_g^{op} [b]	E_g^{th} [c]
	HOMO	LUMO	HOMO	LUMO		
8	-5.19	-2.36	-5.11	-1.51	2.83	3.60
16	-5.20	-2.30	-5.18	-1.54	2.90	3.64
27	-5.09	-1.99	-4.98	-1.42	3.10	3.56
32	-5.28	-2.38	-5.03	-1.72	2.90	3.31
45			-5.50	-1.71	2.83	3.79
DIoCz [d]	-	-	-4.54	-1.15	2.59	3.39
DIeCz [e]	-5.30	-2.10	-5.07	-1.22	3.20	3.85
LTP [f]	-	-	-4.98	-1.43	-	3.55

[a] HOMO energy estimated from the relathioship: E_{HOMO} = -(E^{ox}_{onset}+4.34) eV. LUMO energy estimated from the empirical relationship: LUMO (eV) = HOMO (eV) + E_g^{op}. [b] From absorption onset of the UV-vis absorption data. [c] From DFT calculation. [d] Diindolocarbazole. [e] Diindolocarbazoles. [f] Ladder-type tetraphenylene.

As seen in **Figure 4.17**, it is surprising that the LUMO energy of **32** is lower by 0.3 eV than that of **27** when the carbon is replaced by a more electronegative N atom. In the work of Nguyen et. al., it is found by DFT calculation that the LUMO energy of the organic molecule is dramatically influenced by their aromacity and the LUMO level of non-aromatic cyclopentadiene is 1.7 eV lower than that of pyrrole, on the other hand, however the HOMOs are not significantly influenced by the building block aromaticity.[63] Obviously, the heteroheptacenes **27** and **32** in this study follow the same trend.

To further compare the electronic effects of heteroatoms on the frontier orbitals of heteroheptacenes, we also calculated **DIoCz**, **DIeCz** and **LTP** by using the same computational method and listed the results in **Table 4.4**. As shown in **Figure 4.17**, the HOMO of **DIoCz** resembles those of **8**, **16** and **45** in shape, wherein the orbital shows inter-ring bonding interaction and is mainly localized around the central π system. By contrast, E_{HOMO} of **DIoCz** differs markedly from E_{HOMO} of **45** (ΔE_{HOMO}= 0.96 eV). The LUMO of **DIoCz** differs only slightly from LUMO of **8**, **16** and **45** in shape, but is located at a more positive level (E_{LUMO}= -1.15 eV). It seems that more

pyrrole ring-fusion into the ladder-type heteroacenes tends to destabilize HOMO and LUMO energy levels. The calculation of **DieCz** and **LTP** indicates that their HOMOs resemble those of **27** and **32** in shape, in which the bridging (hetero)atoms are on the node of the orbitals. E_{HOMO} of **DieCz** and **LTP** lie close to E_{HOMO} of **27** and **32** (ΔE_{HOMO}< 0.09 eV). The LUMOs of **DieCz** and **LTP** reveal similar inter-ring bonding interactions to that of **27** and **32** and move slightly upwards. Among all the heteroheptacenes in this study, thiophene-ring containing heteroheptacenes **8**, **16**, **27**, **32** and **45** have average HOMO and LUMO energies of -5.07 eV and -1.55 eV that are lower than those of the other three analogues (average HOMO = -4.86 eV and LUMO = -1.27eV). At the same time, an interesting comparison of energy levels of compound **45** (containing three sulfur bridging atoms), **DIoCz** (containing three nitrogen bridging atoms) and **LTP** (containing three carbon bridging atoms) indicates that the thienyl ring-fusion inside the ladder-type heteroacenes is an effective method to stabilize both HOMO and LUMO levels.

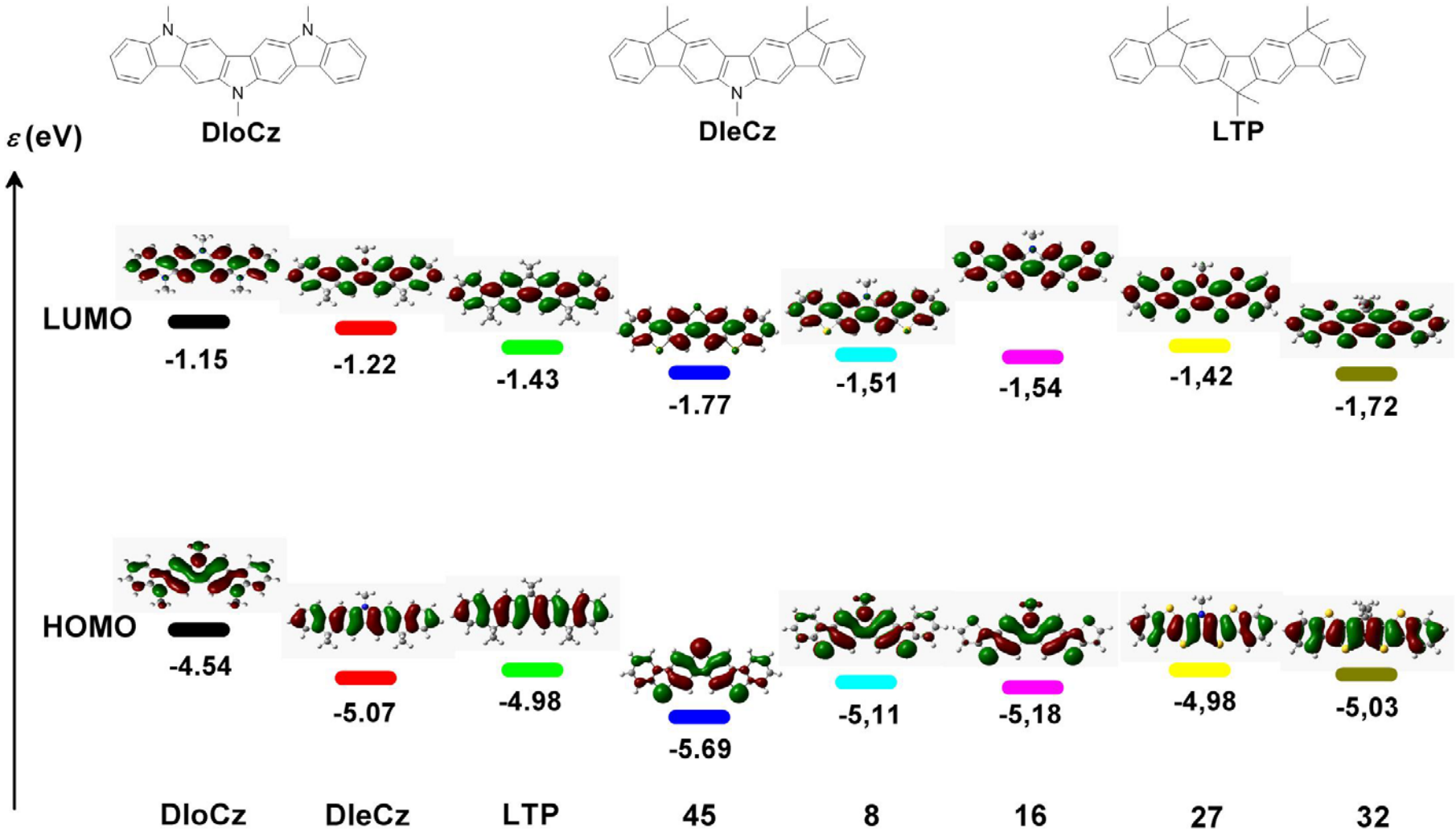

Figure 4.17. Schematic representation of the HOMOs and LUMOs of **8**, **16**, **27**, **32** and **45** as well as **DIoCz, DIeCz, PTP** for comparison (DFT//B3LYP/6-31G**)

4.5 Conclusion

In this chapter, three parts were discussed. In the first part, to further extend the scope of the triflic acid induced electrophilic substitution reaction and broaden the family of heteroheptacenes, two new ladder-type -conjugated heteroheptacenes (BBTDP **27** and BBTCPDT **32**) with dithieno[3,2-*b*:2',3'-*d*]pyrroles (**DTP**) and cyclopenta[2,1-*b*:3,4-*b*']dithiophene (**CPDT**) as the central π system. The final ring closure reaction went smoothly in the presence of phosphorus pentoxide and gave the new heteroheptacenes in good yields. The new oligoacenes with inclusion of thiophene and\or pyrrole ring units exhibit highly symmetry structures as disclosed by NMR measurements. Besides the good solubility the substituted alkyl groups also give rise to interesting solid structure to the new molecules as evidenced by XRD characterization. Moreover, single crystals of compound **32** show two temperature dependant single-crystal-to-single-crystal (SCSC) phase transitions at 175 K and 145 K, which is caused by slight movements of the neighboring molecules following a conformational change of the alkyl chains. To our best knowledge, this is the first example of SCSC transformation found in a conjugated oligomer system. The experimental results (absorption/emission spectroscopy and cyclic voltammetry) have revealed that both the pattern of ring-fusion and the substituents on the molecules have a significant impact on the optical and electrochemical properties of the heteroheptacenes.

In the second part another two thiophene ring fused heteroheptacenes (TTTTTBT **37** and DBTBT **45**) have been synthesized. **37** is the extended version of compound **2** (Chapter 2) with six thiophene rings fused symmetrically on two sides of a benzene ring. Due to limitation of the ring closure reaction, purification of the product failed. New methods that could introduce longer alkyl groups are needed. Driven by an unexpected sulfur extrusion reaction, **45** was obtained almost quantitatively from the hexa-methylsulfde precursor. According to the supposed reaction mechanism no isomer could be produced and it is possible to synthesize even longer fully

ladderized acenes.

In the end, a combined DFT calculation of a series of heteroheptacenes was performed and showed that appropriate substitution of thiophene units inside the ladder-type heteroacenes could effectively stabilize their frontier orbitals. Visualization of the MO demonstrated that compounds **8**, **16** and **45** represent unique inter-ring bonding character between the adjacent hetero-rings and less delocalized HOMO compared with that of **27** and **32**. The present study suggested that the new heteroheptacenes are promising candidates for optoelectronic applications. Further studies on the structure-properties relationship of more complicatedly substituted heteroheptacenes and the study of the new semiconductors as compounds of devices are currently underway in our laboratory.

4.6 References

[1] (a) Fichou, D. Handbook of Oligo- and Polythiophenes, **1998**, Wiley-VCH, Weinheim; (b) Kiess, H., Conjugated Conducting Polymers, Vol. 102, **1992**, Springer-Verlag, New York.

[2] Roncali, J. *Chem. Rev.* **1997**, *97*, 173-206.

[3] (a) Hong, S. Y.; Song, J. M., *J. Chem. Phys.* **1997**, *107*, 10607-10253. (b) Zhang, X.; Matzger, A. J. *J. Org. Chem.* **2003**, *68*, 9813-9815.

[4] (a) Radke, K. R.; Ogawa, K.; Rasmussen, S. C. *Org. Lett.*, **2005**, *7*, 5253–5256. (b) Ogawa, K.; Rasmussen, S. C. *Macromolecules*, **2006**, *39*, 1771–1778. (c) Liu, J.; Zhang, R.; Sauve, G.; Kowalewski, T.; McCullough, R. D. *J. Am. Chem. Soc.* **2008**, *130*, 13167–13176. (d) Zhou, E.; Nakamura, M.; Nishizawa, T.; Zhang, Y.; Wei, Q.; Tajima, K.; Yang, C.; Hashimoto, K. *Macromolecules*, **2008**, *41*, 8302–8305. (e) Zhang, W.; Li, J.; Zou, L.; Zhang, B.; Qin, J.; Lu, Z.; Poon, Y. F.; Chan-Park, M. B.; Li, C. M. *Macromolecules*, **2008**, *41*, 8953–8955.

[5] Zanirato, P.; Spagnolo, P.; Zanardi, G. *J. Chem. Soc. Perkin Trans. 1*, **1983**, 2551-2554.

[6] Ogawa, K.; Rasmussen, S. C. *J. Org. Chem.* **2003**, *68*, 2921-2928.

[7] Koeckelberghs, G.; De Cremer, L.; Vanormelingen, W.; Dehaen, W.; Verbiest, T.; Persoons, A.; Samyn, C. *Tetrahedron,* **2005**, *61*, 687-691.

[8] (a) Zhang, M.; Tsao, H. N.; Pisula, W.; Yang, C.; Mishra, A. K.; Müllen, K. *J. Am. Chem. Soc.* **2007**, *129*, 3472-3473; (b) Soci, C.; Hwang, I.-W.; Moses, D.; Zhu, Z.; Waller, D.; Gaudiana, R.; Brabec, C. J.; Heeger, A. J. *Adv. Funct. Mater.* **2007**, *17*, 632-636; (c) Zhu, Z.; Waller, D.; Gaudiana, R.; Morana, M.; Mühlbacher, D.; Scharber, M.; Brabec, C. *Macromolecules* **2007**, *40*, 1981-1986; (d) Peet, J.; Kim, J. Y.; Coates, N. E.; Ma, W. L.; Moses, D.;

Heeger, A. J.; Bazan, G. C. *Nat. Mater.* **2007**, *6*, 497-500; (e) Palacios, R. E.; Fan, F.-R. F.; Grey, J. K.; Suk, J.; Bard, A. J.; Barbara, P. F. *Nat. Mater.* **2007**, *6*, 680-685.

[9] Kraak, A.; Wieserma, A. K.; Jordens, P.; Wynberg, H. *Tetrahedron* **1968**, *24*, 3381–3398;

[10] Brzezinski, J. Z.; Reynolds, J. R. *Synthesis* **2002**, 1053-1056.

[11] (a) Lambert, T. L.; Ferraris, J. P. *J. Chem. Soc., Chem. Commun.* **1991**, 752-754. (b) Ferraris, J. P.; Lambert, T. L. *J. Chem. Soc., Chem. Commun.* **1991**, 1268-1270. (c) Coppo, P.; Lurner, M. L. *Mater. Res. Soc. Symp. Proc.* **2003**, 771 L4.9.1. (d) Coppo, P.; Cupertino, D. C.; Yeates, S. G.; Turner, M. L. *J. Mater. Chem.* **2002**, *12*, 2597-2599.

[12] (a) Asawapirom, U.; Scherf, U. *Macromol. Rapid Commun.* **2001**, *22*, 746-749; (b) Coppo, P.; Cupertino, D. C.; Yeates, S. G.; Turner, M. L. *Macromolecules* **2003**, *36*, 2705-2711; (c) Coppo, P.; Turner, M. *J. Mater. Chem.* **2005**, *15*, 1123-1133; (d) Wu, C. G.; Lu, M. I.; Chang, S. J.; Wei, C. S. *Adv. Funct. Mater.* **2007**, *17*, 1063-1070.

[13] Dunitz, J. D.; Bernstein, J. *Acc. Chem. Res.* **1995**, *28*, 193-200.

[14] Kitaigorodskii, A. I. *Adv. Struct. Res. Diffr. Methods*, **1970**, *3*, 173.

[15] Mnyukh, Yu. V. *J. Cryst. Growth*, **1977**, *38*, 284-291.

[16] Mnyukh, Yu. V. *Mol. Cryst. Liq. Cryst.* **1979**, *52*, 467-503.

[17] (a) Hu, C.; Englert, U. *Angew. Chem., Int. Ed.*, **2005**, *44*, 2281-2283. (b) Ma, J. -P.; Dong, Y. -B.; Huang, R. -Q.; Smith, M. D.; Su, C. -Y. *Inorg. Chem.*, **2005**, *44*, 6143-6145. (c) Caira, M. R.; Nassimbeni, L. R.; Su H.; Weber, E. *CrystEngComm*, **2003**, *5*, 351-354. (d) Spencer, E. C.; Howard, J. A. K.; Baruah P. K.; Sanjayan, G. J. *CrystEngComm*, **2006**, *8*, 468-472.

[18] (a) Ranford, J. D.; Vittal, J. J.; Wu, D.-Q. *Angew. Chem., Int. Ed.* **1998**, *37*, 1114-1116. (b) Ranford, J. D.; Vittal, J. J.; Wu, D.-Q.; Yang, X.-D. *Angew. Chem., Int. Ed.* **1999**, *38*, 3498-3501. (c) Iordanidis, L.; Kanatzidis, M. G. *Angew. Chem., Int. Ed.* **2000**, *39*, 1928-1930. (d) Iordanidis, L.; Kanatzidis, M. G. *J. Am. Chem. Soc.* **2000**, *122*, 8319-8320. (e) Vittal, J. J.; Yang, X.-D. *Cryst. Growth Des.* **2002**, *2*, 259-262. (f) Hu, C.-H.; Englert, U. *Angew. Chem., Int. Ed.* **2005**, *44*, 2281-2283.

[19] (a) Toh, N. L.; Nagarathinam, M.; Vittal, J. J. *Angew. Chem., Int. Ed.* **2005**, *44*, 2237-2241. (b) Ouyang, X.; Fowler, F. W.; Lauher, J. W. *J. Am. Chem. Soc.* **2003**, *125*, 12400-12401. (c) Papaefstathiou, G. S.; Zhong, Z.; Geng, L.; MacGillivray, L. R. *J. Am. Chem. Soc.* **2004**, *126*, 9158-9159.

[20] (a) Lee, E. Y.; Suh, M. P. *Angew. Chem., Int. Ed.* **2004**, *43*, 2798-2801. (b) Su, C.-Y.; Goforth, A. M.; Smith, M. D.; Pellechia, P. J.; Zur Loye, H.-C. *J. Am. Chem. Soc.* **2004**, *126*, 3576-3586. (c) Li, H.-L.; Eddaoudi, M.; O'Keefe, M.; Yaghi, O. M. *Nature* **1999**, *402*, 276-279.

[21] (a) Biradha, K.; Hongo, Y.; Fujita, M. *Angew. Chem., Int. Ed.* **2002**, *41*, 3395-3398. (b) Zeng, M.-H.; Feng, X.-L.; Chen, X.-M. *Dalton Trans.* **2004**, 2217-2223. (c) Wu, C.-D.; Lin,

W.-B. *Angew. Chem., Int. Ed.* **2005**, *44*, 1958-1961. (d) Biradha, K.; Fujita, M. *Angew. Chem., Int. Ed.* **2002**, *41*, 3392-3395. (e) Halder, G. J.; Keppert, C. J. *J. Am. Chem. Soc.* **2005**, *127*, 7891-7900. (f) Maji, T. K.; Uemura, K.; Chang, H.-C.; Matsuda, R.; Kitagawa, S. *Angew. Chem., Int. Ed.* **2004**, *43*, 3269-3272.

(g) Hanson, K.; Calin, N.; Bugaris, D.; Scancella, M.; Sevov, S. C. *J. Am. Chem. Soc.* **2004**, *126*, 10502-10503.

[22] (a) Kitagawa, S.; Kitaura, R.; Noro, S. *Angew. Chem., Int. Ed.* **2004**, *43*, 2234-2275. (b) Kitagawa, S.; Uemura, K. *Chem. Soc. Rev.* **2005**, *34*, 109-119 and references cited therein.

[23] (a) Avarvari, N.; Faulques, E.; Fourmigué, M. *Inorganic Chemistry*. **2001**, *40*, 2570-2577. (b) Sokolov, A. N.; Swenson, D. C.; MacGillivray, L. R. *Proceedings of the National Academy of Sciences of the United States of America*. **2008**, *105*, 1794-1797.

[24] Kishore, R.; Raghothama, S.; Balaram, P. *Biochemistry*, **1988**, *27*, 2462–2471.

[25] (a) Shaw, J. E. *The Journal of Organic Chemistry*. **1991**, *56*, 3728-3729. (b) Fujii, T. *Tetrahedron*. **1999**, *55*, 5027-5046.

[26] (a) Schroth, W.; Hintzsche, E.; Viola, H.; Winkler, R.; Boese, R.; Kempe, R.; Sieler, J. *Chem. Ber.* **1994**, *127*, 401-408. (b) Schroth, W.; Hintzsche, E.; Spitzner, R.; Irn- gartinger, H.; Siemund, V. *Tetrahedron Lett.* **1994**, *35*, 1973-1976. (c) Schroth, W.; Felicetti, M.; Hintzsche, E.; Spitzner, R.; Pink, M. *Tetrahedron Lett.* **1994**, *35*, 1977-1980. (d) Schroth, W.; Hintzsche, E.; Felicetti, M.; Spitzner, R.; Sieler, J.; Kempe, R. *Angew. Chem.* **1994**, *106*, 808-810; *Angew. Chem. Int. Ed. Engl.* **1994**, *33*,739-741.

[27] (a) Barber, H. J.; Smiles, S. *J. Chem. Soc.* **1928**, 1141-1149. (b) Cossu, S.; Delogu, G.; Fabbri, D. *Org. Prep. Proced. Int.* **1991**, *23*, 455-457; (c) Armarego, W. L. F. *J. Chem. Soc.* **1960**, 433-436.

[28] (a) Schroth, W. *Tetrahedron*. **1997**, *53*, 7509-7528. (b) Okamoto, T.; Kudoh, K.; Wakamiya, A.; Yamaguchi, S. *Organic letters*. **2005**, *7*, 5301-5304.

[29] Sirringhaus, H.; Friend, R. H.; Wang, C.; Leuninger, J.; Müllen, K. *J. Mater. Chem.* **1999**, *9*, 2095-2101.

[30] Philippe, M. Naïma El, H. H. Anh, B. Daniel, B. Livain, Synthesis 2000, 9, 1253-1258.

[31] Wu, C. G.; Hsieh, C. W.; Chen, D. C.; Chang, S. J.; Chen, K. Y. *Syn. Met*, **2005**, *155*, 618-622.

[32] Bonesi, S. M.; Ponce, M. A.; Erra-Balsells, R. *Journal of Heterocyclic Chemistry* **2004**, *41*, 161-171.

[33] Rathore, R.; Abdelwahed, S. H.; Guzei, I. A. *J. Am. Chem. Soc.* **2003**, *125*, 8712–8713

[34] (a) Anthony, J. E. *Angew. Chem.* **2008**, *120*, 460-492; *Angew. Chem. Int. Ed.* **2008**, *47*, 452-483; (b) Miao, Q.; Chi, X.; Xiao, S.; Zeis, R.; Lefenfeld, M.; Siegrist, T.; Steigerwald, M. L.; Nuckolls, C. *J. Am. Chem. Soc.* **2006**, *128*, 1340-1345; (c) Anthony, J. E.; Eaton, D. L.; Parkin, S. R. *Org. Lett.* **2002**, *4*, 15-18; (d) Walzer, K.; Maennig, B.; Pfeiffer, M.; Leo, K. *Chem. Rev.* **2007**, *107*, 1233 -1271; (e) Doi, I.;

Miyazaki, E.; Takimiya, K.; Kunugi, Y. *Chem. Mater.* **2007**, *19*, 5230-5237; (f) Izawa, T.; Miyazaki, E.; Takimiya, K. *Chem. Mater.* **2009**, *21*, 903–912.

[35] See Figure 3.5 in 3.2.3

[36] (a) Campbell, R. B.; Robertson, J. M.; Trotter, J. *Acta Crystallogr.* **1962**, *15*, 289–290; (b) Holmes, D.; Kumaraswamy, S.; Matzger, A. J.; Vollhardt, K. P. C. *Chem. Eur. J.* **1999**, *5*, 3399–3412; (c) Siegrist, T.; Kloc, C.; Schön, J. H.; Batlogg, B.; Haddon, R. C.; Berg, S.; Thomas, G. A. *Angew. Chem. Int. Ed.* **2001**, *40*, 1732–1736; (d) Mattheus, C. C.; Dros, A. B.; Baas, J.; Meetsma, A.; de Boer, J. L.; Palstra, T. T. M. *Acta Cryst., Sect. C: Cryst. Struct. Commun.* **2001**, *C57*, 939–941.

[37] (a) Toh, N. L.; Nagarathinam, M.; Vittal, J. J. *Angew. Chem., Int. Ed.* **2005**, *44*, 2237-2241. (b) Ouyang, X.; Fowler, F. W.; Lauher, J. W. *J. Am. Chem. Soc.* **2003**, *125*, 12400-12401. (c) Papaefstathiou, G. S.; Zhong, Z.; Geng, L.; MacGillivray, L. R. *J. Am. Chem. Soc.* **2004**, *126*, 9158-9159.

[38] (a) Lee, E. Y.; Suh, M. P. *Angew. Chem., Int. Ed.* **2004**, *43*, 2798-2801. (b) Su, C.-Y.; Goforth, A. M.; Smith, M. D.; Pellechia, P. J.; zur Loye, H.-C. *J. Am. Chem. Soc.* **2004**, *126*, 3576-3586. (c) Li, H.-L.; Eddaoudi, M.; O'Keefe, M.; Yaghi, O. M. *Nature* **1999**, *402*, 276-279. (d) Biradha, K.; Hongo, Y.; Fujita, M. *Angew. Chem., Int. Ed.* **2002**, *41*, 3395-3398. (e) Zeng, M.-H.; Feng, X.-L.; Chen, X.-M. *Dalton Trans.* **2004**, 2217-2223. (f) Wu, C.-D.; Lin, W.-B. *Angew. Chem., Int. Ed.* **2005**, *44*, 1958-1961. (g) Biradha, K.; Fujita, M. *Angew. Chem., Int. Ed.* **2002**, *41*, 3392-3395. (h) Halder, G. J.; Keppert, C. J. *J. Am. Chem. Soc.* **2005**, *127*, 7891-7900. (i) Maji, T. K.; Uemura, K.; Chang, H.-C.; Matsuda, R.; Kitagawa, S. *Angew. Chem., Int. Ed.* **2004**, *43*, 3269-3272. (l) Hanson, K.; Calin, N.; Bugaris, D.; Scancella, M.; Sevov, S. C. *J. Am. Chem. Soc.* **2004**, *126*, 10502-10503. (m) Kitagawa, S.; Kitaura, R.; Noro, S. *Angew. Chem., Int. Ed.* **2004**, *43*, 2234-2275. (n) Kitagawa, S.; Uemura, K. *Chem. Soc. Rev.* **2005**, *34*, 109-119 and references cited therein.

[39] (a) Chou, C. H.; Shu, C. F. *Macromolecules* **2002**, *35*, 9673–9677; (b) Lyu, Y. Y.; Kwak, J.; Kwon, O.; Lee, S. H.; Kim, D.; Lee, C.; Char, K. *Adv. Mater.* **2008**, *20*, 2720–2729; (c) Chien, C. H.; Shin, P.; Wu, F.; Shu, C. F., Chi, Y. *J.Poly.Sci: Part A: Polymer Chemistry*, **2007**, *45*, 2073–2084. (d) Jiao, S. B.; Liao, Y.; Xu, X. J.; Wang, L. P.; Yu, G.; Wang, L.; Su, Z.; Ye, S.; Liu, Y. Q. *Adv. Funct. Mater.* **2008**, *18*, 2335–2347.

[40] (a) Dunitz, J. D.; Bernstein, J. *Acc. Chem. Res.* **1995**, *28*, 193-200. (b) Dunitz, J. D. Acta Crystallogr. 1995, B51, 619-631.

[41] Braga, D.; Grepioni, F. *Chem. Soc. Rev.* **2000**, *29*, 229-238.

[42] Braga, D. *Chem. Rev.* **1992**, *92*, 633-665 and references cited herein.

[43] Fan, X.; Sun, J. L.; Wang, F. Z.; Chu, Z. Z.; Wang, P.; Dong, Y. Q.; Hu, R. R.; Tang, B. Z.; Zou, D. C. *Chem.Commun.***2008**, 2989-2991, and references therein.

[44] (a) Kobatake, S.; Takami, S.; Muto, H.;

Ishikawa, T.; Irie, M. *Nature* **2007**, *446*, 778-781. (b) Irie, M.; Kobatake, S.; Horichi, M.; Science, **2001**, *291*, 1769–1772.

[45] Garcia-Garibay M. A. *Angew. Chem. Int. Ed.* **2007**, *46*, 8945–8947.

[46] Fichou, D. *J. Mater. Chem.* **2000**, *10*, 571-588.

[47] Garnier, F.; Hajlaoui, R.; El Kassmi, A.; Horowitz, G.; Laigre, L.; Porzio, W.; Armanini, M.; Provasoli, F. *Chem. Mater.* **1998**, *10*, 3334-3339.

[48] (a) Bruno, I. J.; Cole, J. C.; Edgington, P. R.; Kessler, M. K.; Macrae, C. F.; McCabe, P.; Pearson, J.; Taylor, R. *Acta Crystallogr.* **2002**, *B58*, 389-397. (b) Taylor, R.; Macrae, C. F. *Acta Crystallogr.* **2001**, *B57*, 815-827. (c) *Mercury 1.3*; The Cambridge Crystallographic Data Centre: Cambridge, U.K., 2001.

[49] Zhou, Y.; Liu, W.; Ma, Y.; Wang, H.; Qi, L.; Cao, Y.; Wang, J.; Pei, J. *J. Am. Chem. Soc.* **2007**, *129*, 12386-12387.

[50] (a) Clar, E. *Polycyclic Hydrocarbons*, Academic Press Inc., London, **1964**. (b) Platt, J. R. *J. Chem. Phys.*, **1949**, *17*, 484-495.

[51] Roncali, J. *Chem. Rev.* **1997**, *97*, 173-206.

[52] (a) Coppo, P.; Cupertino, D. C.; Yeates, S. G.; Turner, M. L. *Macromolecules*, **2003**, *36*, 2705-2711; (b) Koeckelberghs, G.; De Cremer, L.; Vanormelingen, W.; Verbiest, T.; Persoons, A.; Samyn, C. *Macromolecules*, **2005**, *38*, 4545-4547.

[53] Ogawa, K.; Stafford, J.; Rothestein, S.; Tallman, D.; Rasmussen, S. S*yn. Met.* **2005**, *152*, 137-140.

[54] Mondal, R.; Shah, B. K.; Neckers, D. C. *J. Am. Chem. Soc.*, **2006**, *128*, 9612-9613.

[55] Maliakal, A.; Raghavachari, K.; Katz, H.; Chandross, E.; Siegrist, T. *Chem. Mater.* **2004,** *16*, 4980-4986.

[56] Wakim, S.; Bouchard, J.; Blouin, N.; Michaud, A. ; Leclerc, M. *Org. Lett.* **2004**, *6*, 3413-3416

[57] Sonntag, M.; Strohriegl, P. *Tetrahedron* **2006**, *62*, 8103-8108.

[58] Morris, J. V.; Mahaney, M. A.; Huber, J. R. *J. Phys. Chem.*, **1976**, *80*, 969-974.

[59] (a) Kobayashi, K. *Phosphorus, Sulfur and Silicon* **1989**, *43*, 187-208. (b) Rutherford, D. R.; Stille, J. K.; Elliott, C. M.; Reichert, V. R. *Macromolecules*, **1992**, *25*, 2294-2306. (c) Bugge, A. *Acta Chem. Scand.*, **1968**, *22*, 63. (d) Bugge, A. *Acta Chem. Scand.*, **1969**, *23*, 2704.

[60] Katritzky, A. R.; Pozharskii, A. F. Handbook of Heterocyclic Chemistry, 2nd ed.; Pergamon: New York, **2000**; pp 68-71.

[61] Leuninger, J. PhD Thesis, Johannes Gutenberg-Universita Mainz (**1999**).

[62] Zheng, Q.; Gupta, S. K.; He, G. S.; Tan, L. S.; Prasad, P. N. *Adv. Funct. Mater.* **2008**, *18*, 2770-2779.

[63] Delaere, D.; Nguyen, M. T.; Vanquickenborne, L. G. *Phys. Chem. Chem. Phys.* **2002**, *4*, 1522–1530.

Chapter 5
Summary and Outlook

This study followed "the oligomer approach". The main focus of this work was the synthesis, characterization and application of conjugated semiconducting heteroacenes for organic electronics.

In the first part, we showed the modulation of the electronic properties of sulfur substituted heteropentacenes which has been achieved by variation of the position and number of sulfur atoms. These heteropentacenes are derived from a corresponding hydrocarbon counterpart, one double bond of which is replaced by a sulfur atom. (**Figure 5.1**) Besides the inserted sulfur atoms, these new molecules also inherit the "*kinked*" structures from their parent as shown in Figure 5.1. To further develop the family of sulfur containing pentacenes, two molecules (benzo[1,2-*b*:4,5-*b*'] bis[*b*]benzodithiophene **1** and dithieno-[2,3-*d*:2',3'-*d*']- benzo-[1,2-*b*:4,5-*b*']dithiophene **2**) were facilely synthesized and characterized by a combination of different methods. **Figure 5.1** shows the origin of these two molecules (rectangular in IV) and a comparison of all the similar molecules in view of their geometrically "kinked" structures.

From the photophysical and electrochemical experiments, it turned out that the two new molecules exhibit outstanding environmental stability as expected from by their wide band gap and low-lying HOMO orbital. This could be ascribed to their "kinked" structure and the decrease of double bonds due to the sulfur insertion. A reasonable stability is the first criterion for useful semiconducting materials. Then these compounds were applied in OFETs devices as *p*-channel materials. The preliminary tests gave charge carrier mobilities of 0.1 $cm^2 V^{-1} s^{-1}$ for **1** and 1.6 $cm^2 V^{-1} s^{-1}$ for **2**. We tried in the end to explain the efficient charge transport by comparing the calculated frontier orbitals with that of pentacene and pentathienoacene.

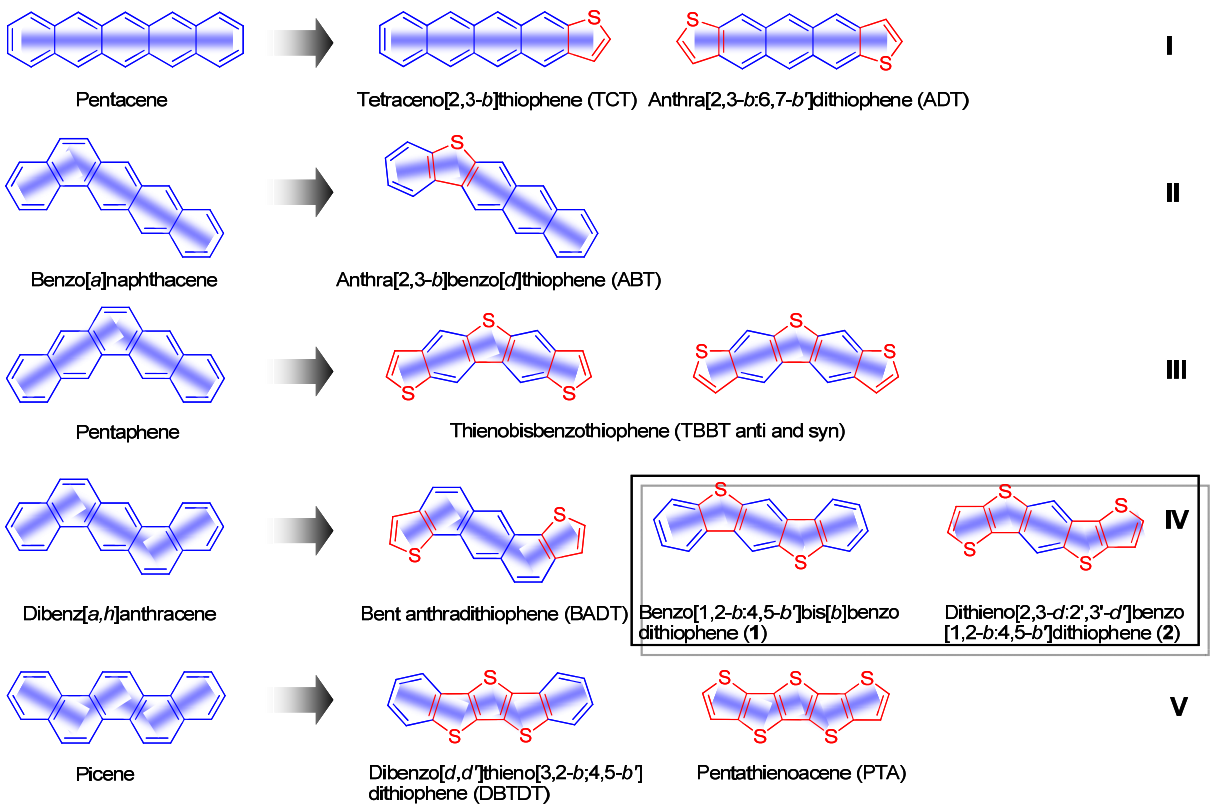

Figure 5.1. Schematic of derivation of sulfur containing heteropentacenes and the "kinked" structure outlined by the blue bar.

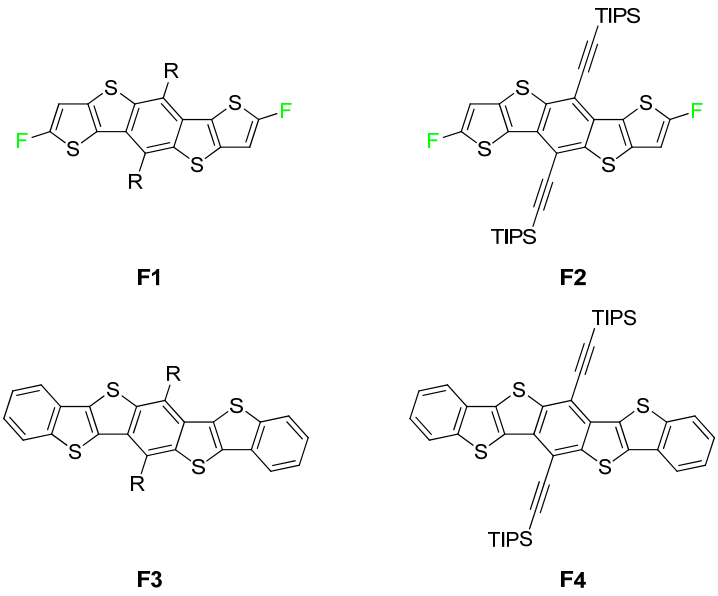

Figure 5.2. Structures of new *p*-channel heteroacenes for the future

Although the preliminary device study has represented excellent results, it gave very high threshold voltages, which means that there are contact problems with the dielectric materials or trapping sites within the channels. To solve this problem, one has to make sure that firstly the semiconducting material has extremely high purity. Oligoheteroacenes as small molecules could be purified by means of both column chromatography and vacuum sublimation. Secondly, attention should also be put in to the surface treatment of the dielectric layer with proper reagents that fit to the semiconducting materials. From an electronic structure point of view, the two molecules **1** and **2** could be further modified by introducing electron withdrawing groups onto the molecular backbones (**F1** and **F2**). Bulky groups can also be introduced to influence the thin morphology (**F3** and **F4**). Several possible structures are drawn and shown in **Figure 5.2**. These structures are designed based on the works of Ong et al. and Anthony et al and are expected to have the same stability as their parent molecules but with much varied electronic structure and improved contact with the dielectric materials.

Heteroheptacenes are seldom studied due to the lack of efficient synthetic methods. At the same time, the only example of sulfur containing heteroheptacene was totally insoluble in spite of the high charge carrier mobility reported ten years ago. Triggered by the question of "the longer the better?", a series of new heteroheptacenes were synthesized and intensively studied in view of their solid structure, self-assenbly on the surface, opto-electro properties and frontier orbital characteristics. The deductions of heteroheptacenes from hydrocarbon heptacenes are shown in **Figure 5.3**.

In achieving the symmetrical ladderized product **8**, triflic acid induced electrophilic substitution reaction was employed. The reaction condition was systematically studied and the optimized condition precluded the generation of regio-isomers. Then the pure compounds of **8** were tested as the active channels in OFET devices. However, in spite of the more extended conjugation length the devices based on the heptacenes showed much worse charge carrier mobilities than the heteropentacenes. Does it tell us that it is not really "the longer the better"? Of

course, we have to be aware that many factors could determine the final performances of the devices and the chemical structure is just one of them. In this case, we found that the solid structure of **8** is quite unique not only because of the sulfur/nitrogen bridged backbone, but also due to the *N*-alkyl groups in the direction of the short molecular axis. This resulted in a "lamellar herringbone" structure, in which the large roll displacements give rise to structures with essentially no π-overlap between adjacent molecules in a stack. This could be a reason to the low device performance.

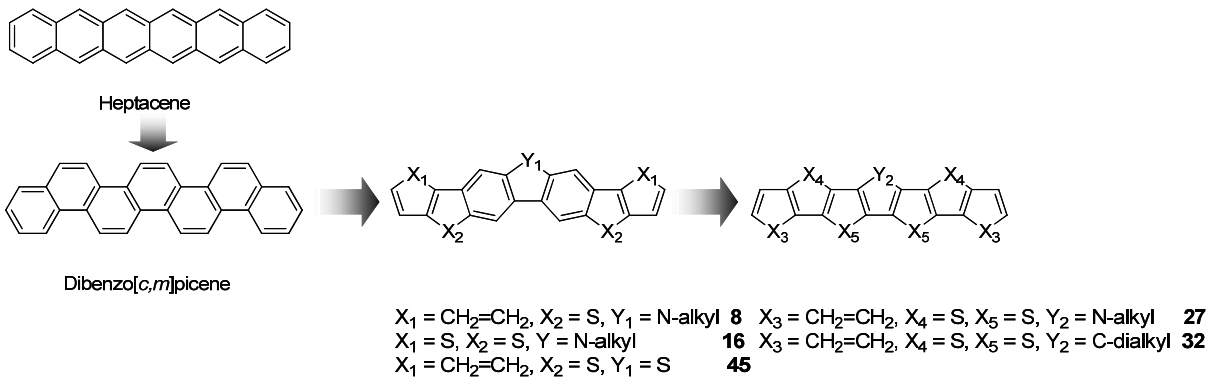

Figure 5.3. Structural evolution of heptacenes

In this regard, it seems that it is also meaningful to study the influence of heteroatoms and alkyl substitution on the solid and electronic structures. Therefore, heteroheptacenes **16**, **27**, **32** and **45** were synthesized. Instead of using the same synthetic method like the other three molecules, compound **45**, which was known as DBTBT before, was resynthesized via new sulfur extrusion method and obtained as isomer free compound in high yield. In the X-ray crystallography study of compound **32**, we found two temperature dependent single-crystal-to-single-crystal phase transitions induced by the slight movements of the branched alkyl groups. This phenomenon is quite rare in the solid structure of conjugated molecules and if precisely controlled, could be used to make molecular machines. Varied in the number and type of heteroatomic bridge, these oligoacenes exhibited dramatically different opto-electronic properties. As we have expected, they all showed much improved environmental stability comparing to hydrocarbon heptacenes. Moreover,

a combined DFT calculation of the molecular orbitals of these heptacenes indicated that the introduction of nitrogen bridges will destabilize the π orbitals, while, the sulfur bridges stabilize both HOMO and LUMO energies. This is important if one wants to synthesize highly π extended oligoacenes while keeping a reasonable stability.

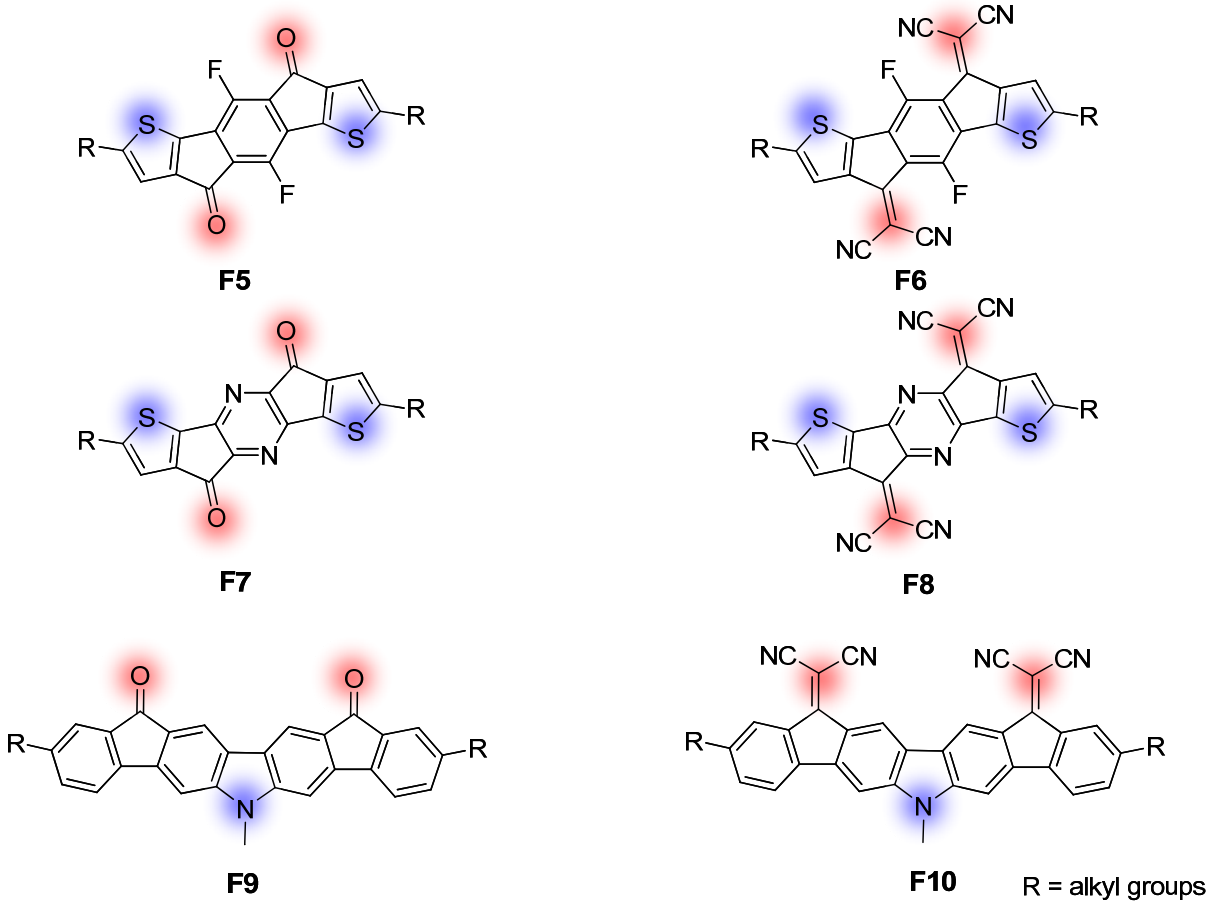

Figure 5.4. Structures of new *n*-channel heteroacenes for the future

Thiophene and pyrrole containing oligoacenes as *p*-type semiconducting materials were synthesized and fully characterized. Some of them have been applied as active materials in organic field-effect transistors and showed outstanding performances. On the other hand, as we have discussed in chapter 1, *n*-type materials are also very important in the construction of electronic circuits. In the next step, new heteroheptacenes with the inclusion of electron rich thiophene and pyrrole as well as electron-withdrawing bridging groups (eg. fluoro, pyrazine, carbonyl and dicyanomethylene groups) will be prepared. (**Figure 5.4**) At the same time, due to the

presence of electron rich Sulfur and Nitrogen atoms, we expect that they have intramolecular charge transfer inside the molecules. Meanwhile, electron withdrawing groups may enhance the intermolecular interaction thus increase the electronic coupling between each two adjacent molecules.

Chapter 6

Experimental Section

6.1 General procedures

6.1.1 Chemicals and solvents

All used chemicals and solvents were obtained from the companies ABCR, Acros, Aldrich, Fluka, Lancaster, Merck and Strem. Unless otherwise mentioned, they were used as obtained.

6.1.2 Chromatography

Preparative column chromatography was performed on silica gel from Merck with a grain size of 0.063 – 0.200 mm (silica gel) or 0.04-0.063 mm (flash silica gel, Geduran Si 60). For analytical thin layer chromatography (TLC), silica gel coated substrates "60 F254" from Merck were used. Compounds were detected by fluorescence quenching at 254 nm, self-fluorescence at 366 nm or staining in an iodine vapour chamber. For eluents, analytically pure solvents (p.a. or technical grade) were distilled prior to the use. The compositions of the eluents are given together with the retension value R_f.

6.1.3 Inert atmosphere

Oxygen or moisture sensitive reactions were carried out in an argon atmosphere (Linde). If not mentioned specifically, reactions were degassed by bubbling a stream of argon though the reaction mixture.

6.1.4 Apparatus for analysis

^{1}H-NMR and ^{13}C-NMR spectroscopy

Bruker DPX 250

Brucker AMX 300

Brucker DRX 500

With the solvent proton or carbon signal as an internal standard.

Mass spectroscopy

FD: VG ZAB 2 SE-FPD (Range: 110-3300)

MALDI – TOF: Brucker Reflex II; Matrix: 1, 8, 9-Anthracentriol

Solvents: THF, DCM

Melting points

Büchi B-545 and not corrected.

Single crystal XRD

Nonius KCCD diffractometer with graphite monochromated MoK radiation. The structures were solved by direct methods (SHELXS-97). Refinement was done with anisotropic temperature factors for C and Cl, the hydrogen atoms were refined with fixed isotropic temperature factors in the riding mode. Some of the solvent molecules are disordered. These were refined with fixed isotropic temperature factors and occupancy factors which were fixed according to the geometry of disorder.

Crystals were mounted on glass fibers and the data collected at 173(1) K on a diffractometer with graphite monochromated Mo KR radiation. Data were collected in a series of φ and ω scans in 0.50° oscillations with 10-30 s exposures, and collected and integrated using the SAINT software package. Data were corrected for absorption effects using the multiscan technique (SADABS) and corrected for Lorentz and polarization effects. The structures were solved using direct methods and refined using the SHELXTL crystallographic software package. For each structure, all non-hydrogen atoms were refined anisotropically and all hydrogen atoms were included in calculated positions but were not refined.

Powder XRD

X-ray diffraction (XRD) measurements were recorded on a Siemens D-500 powder diffractometer (Cu-Ka: 1.541 Å) with scan rate of 0.1°/20 s.

UV-vis spectroscopy

Perkin Elmer Lambda 9

Perkin Elmer Lambda 15

UV-vis absorption spectra were recorded at room temperature on a Perkin-Elmer Lambda 9 spectrophotometer. PL spectra were recorded on a SPEX-Fluorolog II (212) spectrometer. Solutions were prepared with an absorbance between 0 and 0.1 at the wavelength region of experimental interest.

PL spectroscopy

J&M TIDAS spectrofluorometer

Photoluminescence quantum yields were determined by comparison with 10^{-7} M diphenyl anthracene in cyclo hexane as reference and corrected for the refractive index of different solvents.

Cyclic voltammetry (CV)

Cyclic voltammetry experiments were performed in 0.1M tetrabutyl ammonium hexafluorophosphate (TBAPF6) solutions in dry, oxygen-free CH_2Cl_2. On a conventional three-electrode cell using glassy-carbon working electrodes of 2 mm diameter, a platinum wire counter electrode, and a Ag/AgCl reference electrode on a computer-controlled PGSTAT12 at room temperature, which was checked against the Fc/Fc^+ couple after each measurement. Measurements were carried out on a computer-controlled PGSTAT12 at room temperature.

Thermogravimetry (TGA)

Mettler 500 Thermogravimetry Analyzer

Differential scanning calorimetry (DSC)

Mettler DSC 30

Elemental analysis (performed at University of Mainz)

C, H ,N, S : Heraeus Vario EL

Computational methods: Density functional theory (DFT) calculations were carried with the Gaussian 03 program package.[1] Becke's three-parameter exchange functional combined with the LYP correlation functional (B3LYP) was used.[2] Optimized molecular geometries were determined on isolated entities. The 6-31G** basis was chosen for all molecules.

6.1.5 OFET devices

OFETs in this study have been fabricated with various device geometries. The most commonly configurations used device geometries is *bottom gate* with *bottom contact* and *bottom gate* with *top contact* using thermally grown Si/SiO_2 oxide as gate dielectric and gold as the source/drain electrode.

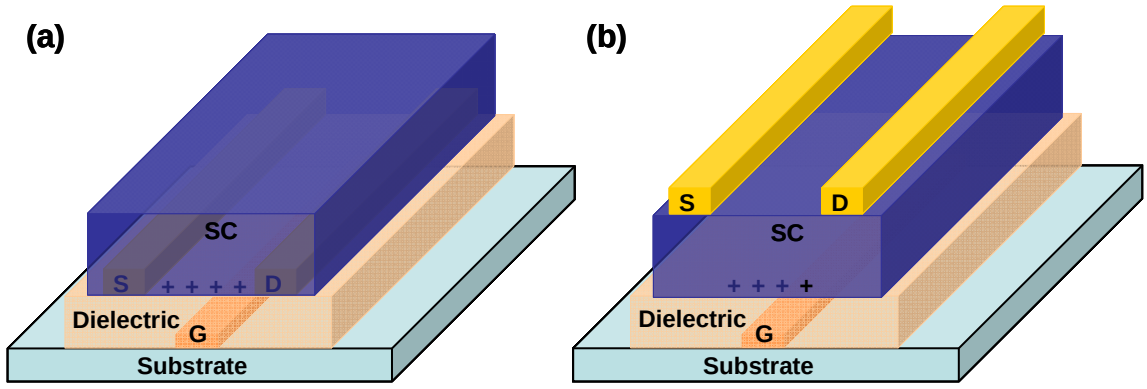

Figure 6.1. Schematic of (a) the *bottom-gate* organic field-effect transistors (OFETs) with *bottom contact* (coplanar) structures. (b) The *bottom-gate* organic field-effect transistors (OFETs) with *top contact* (staggered) structures.

The physical difference between the two is the order of fabrication steps. That is, the source/drain contacts are either deposited before or after the semiconductor layer is deposited to create a bottom contact or top contact device, respectively. Two of these OFET architectures are shown schematically in **Figure 6.1**.

For all devices, to avoid charge carrier trapping by the polar silanol groups on the silicon dioxide surface it was treated with phenyltriethoxysilane (PTES) via vapour phase deposition. The bottom contact gold electrodes were treated with 1-octanethiol to reduce contact resistance. Heavily doped silicon wafers with a

thermally grown silicon dioxide layer 150nm thick are used as substrates.

For the solution-processing of the semiconductor, common organic solvents, such as toluene, chloroform, THF, chlorobenzene, or dichlorobenzene (DCB), were used. A schematic of the dip-coating procedure is illustrated in **Figure 6.2**. The semiconductor toluene solution was filled up to 11 mm in a cylindrical glass container with a diameter of 12 mm and a height of 39 mm. The dip-coated film was grown by completely immersing the transistor substrates (10×10 cm in size) in this solution and by slowly taking the sample out at a rate of 0.5 μm s^{-1} using an electrically controlled engine. The dip-coating direction is highlighted by the red arrow in Figure 6.2. The dry film was appeared by eye above the solution level and a meniscus of about 1 mm. The whole experiment was performed at ambient conditions at room temperature (about 23 ^{o}C). Both the substrate and the solution were not temperature influenced, that is, both were left at room temperature.

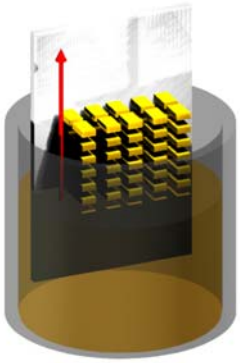

Figure 6.2. Schematic presentation of dip-coating.

All electrical measurements are performed in a glovebox under nitrogen atmosphere. The device characteristics are measured with a Keithley 4200-SCS.

6.2. Synthetic procedures

1,4-Dibromo-2,5-bis(methylsulfinyl)benzene (3)

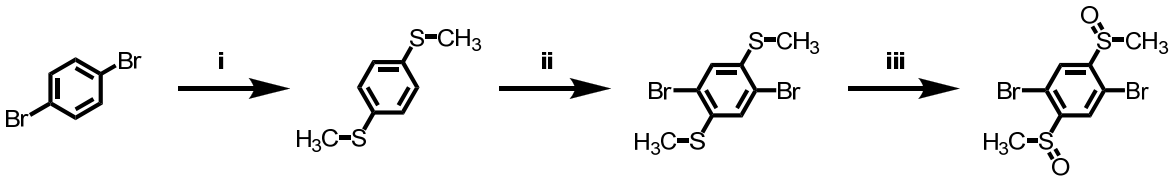

1, 4-dibromobenzene (10 g, 42.4 mmol) was dissolved in dry THF (200 ml) and cooled to −78 °C. *n*-butyllithium solution (1.6 M in hexane, 55.6 ml, 89 mmol) was added dropwise at this temperature. After the addition was complete the mixture was stirred for an additional hour, while a precipitate formed. Dimethyl disulfide (8.39 g, 89 mmol) was added dropwise. The cooling bath was removed and the solution was stirred at room temperature overnight. Water was added and the mixture was extracted with dichloromethane. The solvent was evapour ated under reduced pressure and absorbed onto silicon gel. After silica chromatography with hexane as the eluent, **12** was got as fine colourless plates. (5.1 g, 70% yield) mp: 41–43 °C.

^{1}H-NMR (250 MHz, CD_2Cl_2): δ = 2.44 (s, 6H, Me), 7.18 (s, 4H, Ar-H) ppm.

^{13}C-NMR (62.5 MHz, CD_2Cl_2): δ = 16.2, 127.5, 135.1 ppm.

Anal. Calcd. for $C_8H_{10}S_2$: C, 56.42; H, 5.92. Found: C, 56.41; H, 5.92.

A catalytic amount of iodine (0.23 g) was added to a solution of 1,4-bis(methylthio)benzene (5.1 g, 30 mmol) in CH_2Cl_2 (90 mL) maintained at 0 °C. With constant stirring in the dark, bromine (24.0 g, 150 mmol) was added to the solution which was then kept stirring at room temperature for 3 d. After the reaction, the residual bromine was reduced by Na_2SO_3. Extraction of the product with CH_2Cl_2 followed by dehydration with anhydrous Na_2SO_4 and rotary evapour ation afforded 2,5-dibromo-1,4-bis(methylthio)benzene. After recrystallization from ethanol 9.2 g of product was got in 88% yield as yellow crystals. mp: 155–160 °C.

^{1}H NMR (250 MHz, CD_2Cl_2): δ = 2.45 (s, 6H, Me), 7.27 (s, 2H, Ar-H) ppm.

^{13}C NMR (62.5MHz, CD_2Cl_2): δ = 16.3, 121.7, 129.7, 137.6 ppm.

FD-MS: m/z = 328.09 (M^+, 100%).

Anal. Calcd. for $C_8H_8Br_2S_2$: C, 29.29; H, 2.46. Found: C, 29.28; H, 2.45.

A mixture of glacial acetic acid/CH_3Cl = 1:1 (300 ml) and 2,5-dibromo-1,4-bis(methylthio)benzene (6.4 g, 19.5 mmol) was heated to 55°C until the solid was completely dissolved. Afterwards a mixture of glacial acetic acid (130 ml) and hydrogen peroxide (35%, 3.85 g, 39.58 mmol) was added very slowly and the solution was stirred for 5 h. The glacial acetic acid was removed under vacuum and the residue was dissolved in CH_2Cl_2 and washed several times with water. The organic phase was finally washed with aqueous $NaHCO_3$-solution, dried over MgSO4 and the solvent removed under vacuum. The resulting solid was recrystallized from DMF and gave **3** as a colorless crystal in 60% yield. mp: 182–185 °C.

^{1}H NMR (250 MHz, CD_2Cl_2): δ = 2.76 (s, 6H, Me), 7.99 (s, 2H, Ar-H) ppm.

^{13}C NMR (62.5 MHz, 300 K, CD_2Cl_2): δ = 42.2, 119.2, 130.5, 151.1 ppm.

FD-MS: m/z: 360.09 (M^+, 100%).

Anal. Calcd. for $C_8H_8Br_2O_2S_2$: C, 26.68; H, 2.24. Found: C 26.67; H 2.24.

2-(4-Butylphenyl)-4,4,5,5-tetramethyl-1,3,2-dioxaborolane (4b)

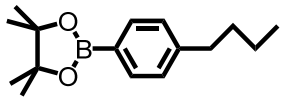

1-Bromo-4-butyl-benzene (1.0 g, 4.7 mmol) was dissolved in absolute THF under argon. The solution was cooled to -78 °C before 3.1 ml (5.0 mmol) n-BuLi (1.6 M solution in hexane) were added dropwise. The reaction mixture was stirred for 10 min, before 1.0 ml (5.0 mmol) of 2-isopropoxy-4,4,5,5-tetramethyl-1,3,2-dioxaborolane was added. The reaction mixture was allowed to warm to room temperature and stirred for another 12 h before it was poured into ice water. The solution was extracted with diethyl ether, the organic phase washed with brine and dried with Na_2SO_4 before the solvent was removed. Purification by column chromatography on silica gel with hexane/THF (15:1) as an eluent yielded 1.0 g (85%)

of **4b** as a colourless oil.

^{1}H NMR (250 MHz, CD_2Cl_2): δ = 0.86 (t, 3H, Me, *J* = 7.0 Hz), 1.18–1.26 (m, 4H, 2 × CH_2), 1.33 (s, 12H, 4 × Me), 2.62 (t, 2H, CH_2, *J* = 7.6 Hz), 7.20 (d, 2H, *J* = 7.6 Hz), 7.73 (d, 2H, *J* = 7.6 Hz) ppm.

FD-MS: m/z = 260 (M^+, 100%).

1,4-Bisphenyl-2,5-bis(methylsulfinyl)benzene (5a), 4-bis(4-butylphenyl)-2,5-bis-(methyl-sulfinyl)benzene (5b)

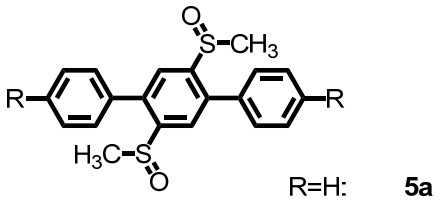

R=H: **5a**
R=C_4H_9: **5b**

1,4-dibromo-2,5-bis(methylsulfinyl)benzene (0.253 g, 0.70 mmol) and 0.316 g (1.55 mmol) of the borolane compound **4a** were dissolved in 25 ml of toluene. A 2 M K_2CO_3 solution (6 ml) and 0.1 g of trimethylbenzylammonium chloride were added. The reaction mixture was degassed by three freeze/thaw cycles before 16 mg (1.46×10^{-5} mol) of $Pd(PPh_3)_4$ was added under argon. The mixture was stirred for 24 h at 90 °C. The reaction mixture was extracted three times with CH_2Cl_2 and dried with $MgSO_4$. Compound **5a** (162 mg, 65 %, related to **3**) was obtained as white crystals from silica chromotography with hexane/THF (10:1 to 1:1) as an eluent and recrystalization from DMSO.

^{1}H NMR (250 MHz, CD_2Cl_2): δ = 2.28 (s, 6H, 2 × (SO)Me), 7.17 (t, 2H, *J* = 8.1 Hz), 7.27 (m, 8H), 7.91 (s, 2H) ppm.

^{13}C NMR (62.5 MHz, CD_2Cl_2): δ = 14.09, 22.73, 33.91, 35.69, 41.94, 125.87, 127.35, 127.6, 134.59, 139.92, 144.28, 147.90 ppm.

FD-MS: m/z = 354.49 (M+, 100.0 %).

Anal. Calcd. for $C_{20}H_{18}O_2S_2$: C, 67.76; H, 5.12. Found: C, 67.52; H, 5.33.

Similar procedure for **5a** and starting with 0.34 mmol of 1,4-dibromo-2,5-bis(methylsulfinyl)benzene, the product **5b** (128 mg, 85 %, related to

2) was obtained as a white solid.

^{1}H NMR (250 MHz, CD_2Cl_2): δ = 0.88 (t, 6H, 2 × Me, *J* = 7.3 Hz), 1.32 (m, 4H, 2 × CH_2), 1.58 (m, 4H, 2 × CH_2), 2.28 (s, 6H, 2 × (SO)Me), 2.6 (t, 4H, 2 × CH_2, *J* = 7.3 Hz), 7.22 (d, 4H, *J* = 8.1 Hz), 7.30 (d, 4H, *J* = 8.1 Hz), 7.91 (s, 2H) ppm.

^{13}C NMR (62.5 MHz, CD_2Cl_2): δ = 14.09, 22.73, 33.91, 35.69, 41.94, 125.87, 129.35, 129.36, 134.59, 139.92, 144.28, 147.70 ppm.

FD-MS: m/z = 466.20 (M+, 100.0 %).

Anal. Calcd. for $C_{28}H_{34}O_2S_2$: C, 72.06; H, 7.34. Found: C, 71.83; H, 7.52

Benzo[1,2-*b*:4,5-*b'*]bis[*b*]benzothiophene (1a and 1b)

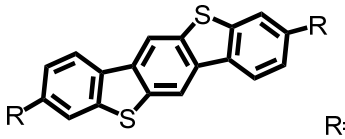

R=H: **1a**
R=C_4H_9: **1b**

A 10 ml round bottomed flask was filled with 1,4-bisphenyl-2,5-bis-(methylsulfinyl)benzene (**5a**) (100 mg, 0.282 mmol), Phosphorus pentoxide (14 mg, 0.1 mmol) and trifluoromethanesulfonic acid (4 ml). The mixture was stirred for 72 h at room temperature to give a dark brown solution, which was then poured into ice–water (100 ml). The yellow precipitate was collected by suction filtration and dried under vacuum. The structure of this compound, which was insoluble in apolar organic solvents, was assumed to be the sulfonium salt. Demethylation of the solid was achieved by refluxing in pyridine (30 ml) for 12 h. When the suspension was cooled to room temperature, a large volume of H_2O was added to precipitate the product. Colorless crystals were got after recrystallization from $C_2H_2Cl_4$. (61 mg, 75 %). mp: 323 °C.

^{1}H NMR (500 MHz, $C_2D_2Cl_4$, 413 K): δ = 7.47 (td, 2H), 7.48 (td, 2H), 7.85 (dd, 2H, *J* = 6.1, 3.1 Hz), 8.19 (dd, 2H, *J* = 6.1, 3.1 Hz), 8.56 (s, 2H) ppm.

^{13}C NMR (500 MHz, $C_2D_2Cl_4$, 413 K): δ = 115.13, 121.45, 122.75, 124.41, 126.98, 134.80, 135.25, 136.68, 140.26 ppm.

FD-MS: m/z = 290.40 (M+, 100 %).

Anal. Calcd. for $C_{18}H_{10}S_2$: C, 74.45; H, 3.47. Found: 74.18; H, 3.70.

By following the similar method compound BBBT-C4 (**1b**) was thus obtained as colorless plates by silica chromotography with hexane/CH_2Cl_2 (10:1) as an eluent (82 mg, 98 %). mp: 299.6 °C.

^{1}H NMR (250 MHz, CD_2Cl_2): δ = 0.88 (t, 6H, 2 × Me, *J* = 7.3 Hz), 1.34 (m, 4H, 2CH_2), 1.63 (m, 4H, CH_2), 2.71 (t, 4H, 2 × CH_2, *J* = 7.3 Hz), 7.24 (d, 2H, *J* = 8.1 Hz), 7.60 (s, 2H), 8.03 (d, 2H, *J* = 8.1 Hz), 8.47 (s, 2H) ppm.

^{13}C NMR (62.5MHz, CD_2Cl_2): δ = 14.10, 22.75, 30.07, 34.18, 36.16, 115.37, 121.64, 122.65, 125.92, 132.95, 135.20, 136.63, 140.49, 143.11 ppm.

FD-MS: m/z = 402.61 (M+, 100 %).

Anal. Calcd. for $C_{26}H_{26}S_2$: C, 77.56; H, 6.51. Found: 77.23; H, 6.73

5-Methyl-2-trimethylstannylthiophene (6a), 5-hexyl-2-trimethylstannylthiophene (6b), 5-nonanyl-2-trimethylstannylthiophene (6c), 5-(2-ethylhexyl)-2-trimethylstannylthiophene (6d)

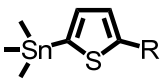

R = CH_3 6a
R = C_6H_{13} 6b
R = C_9H_{19} 6c
R = $C_{6,2}H_{17}$ 6d

To a cooled (-70 °C) mixture of thiophene (17.6 g, 0.21 mol) in anhydrous THF (100 mL) was added dropwize a solution of *n*-BuLi (137.5 ml, 1,6 M, 0.22 mol) in hexane. After stirring for 1 hour at 0 °C, the mixture was cooled to –40 °C followed by addition of 1-hexylbromide (0.22 mol). The mixture was slowly heated to r.t. Water (250 mL) was added and the mixture was extracted with diethylether (3 x 150 mL). The combined organic fractions were dried over $MgSO_4$ and concentrated in vacuo. The 2-hexyl thiophene was purified by means of vacuum distillation and obtained as a colourless oil (26.5 g, 75 %).

2-Hexylthiophene (23.0 g, 0.137 mol) was dissolved in 250 ml THF and *n*-BuLi (94 ml, 1.6 M in hexanes, 0.150 mol) was added dropwise at 0 °C. The mixture was stirred at 0 °C for 1 h and then cooled down to –78 °C. A solution of trimethyltin chloride (32.8 g, 0.164 mol) in 100 ml THF was added dropwise. The mixture was allowed to warm slowly to room temperature and stirred for 2 h. After quenching

with ice water and aqueous work-up, the product was distilled at 108 °C under high vacuum. **6b** was obtained as a colorless liquid (40.8 g, 90 % yield). **6a**, **6c** and **6d** were prepared according to the same methods in yields of 85% to 92%.

5,5'-(2,5-Bis(methylsulfinyl)-1,4-phenylene)bis(2-methylthiophene) (7a), 5,5'-(2,5-bis(methylsulfinyl)-1,4-phenylene)bis(2-hexylthiophene) (7b), 5,5'-(2,5-bis(methylsulfinyl)-1,4-phenylene)bis(2-nonanylthiophene) (7c), 5,5'-(2,5-bis(methylsulfinyl)-1,4-phenylene)bis(2-hexylthiophene) (7d)

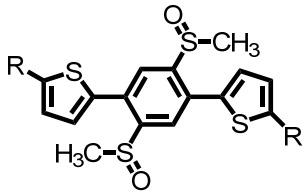

$R = CH_3$ 7a
$R = C_6H_{13}$ 7b
$R = C_9H_{19}$ 7c
$R = C_{6,2}H_{17}$ 7d

1,4-dibromo-2,5-bis(methylsulfinyl)benzene **3** (0.900 g, 2.5 mmol) was added to a solution of 6b (1,82 g, 5.5 mmol) in anhydrous DMF (30 mL), and the resulting mixture was purged with Ar for 30 min. $Pd(PPh_3)_4$ (87 mg, 0.075 mmol) was then added, and the reaction mixture was heated to 80 °C overnight. Excess DMF was removed under high vacuum, and the residue was dissolved in ethyl acetate and treated with 10% aqueous KF. The mixture was filtered through a pad of Celite. The filtrate was dried over Mg_2SO_4, filtered, and the solvent removed in vacuo. The crude product was purified by flash chromatography (silica gel, eluent: hexane/THF = 3:1) to afford 1.16 g (87%) of 7b as white powder. mp: 205-207°C.

^{1}H NMR (300 MHz, CD_2Cl_2): δ = 1.05 (t, 6H), 1.50 (m, 12H), 1.86 (m, 4H), 2.99 (t, 4H), 6.92 (d, 2H, *J* = 7.5 Hz), 7.06 (d, 2H, *J* = 7.5 Hz), 7.87 (s, 2H) ppm.

^{13}C NMR (62.5MHz, CD_2Cl_2): δ = 14.21, 22.96, 29.10, 30.46, 31.90, 31.99, 125.51, 126.02, 128.54, 132.62, 135.30, 147.74, 149.68 ppm

FD-MS: m/z: 534.86 (M+, 100.0%).

Anal. Calcd. $C_{28}H_{38}O_2S_4$: C, 62.88; H, 7.16, Found: C, 62.86; H, 7.17. By following the same method **7a**, **7c** and **7d** were also synthesized.

Compound **7a** (600 mg, 85%, related to **3**) was obtained as white powder after purification by column chromotography (SiO_2) with THF: hexane (3:1) as an eluent. mp: 210-213°C.

^{1}H NMR (250 MHz, CD_2Cl_2): δ = 2.46 (s, 6H), 2.50 (s, 6H), 6.73 (d, 2H, *J* = 7.5 Hz), 6.99 (d, 2H, *J* = 7.5 Hz), 7.98 (s, 2H) ppm.

^{13}C NMR (62.5MHz, CD_2Cl_2): δ = 15.47, 42.14, 126.08, 126.66, 128.75, 132.55, 135.65, 143.41, 147.75 ppm.

FD-MS: m/z: 394.59 (M^+, 100.0%).

Anal. Calcd. $C_{18}H_{18}O_2S_4$: C, 54.79; H, 4.60, Found: C, 54.78; H, 4.66.

Compound **7c** (900 mg, 87%, related to **3**) was obtained as white powder after purification by column chromotography (SiO_2) with THF: hexane (2:1) as an eluent. mp: 207-210°C.

^{1}H NMR (250 MHz, CD_2Cl_2): δ = 0.80 (t, 6H), 1.23 (m, 24H), 1.63 (m, 4H), 2.46 (s, 6H), 2.78 (t, 4H), 6.75 (d, 2H, *J* = 7.5 Hz), 7.03 (d, 2H, *J* = 7.5 Hz), 7.99 (s, 2H) ppm.

^{13}C NMR (62.5MHz, CD_2Cl_2): δ = 14.26, 23.07, 29.44, 29.68, 29.71, 29.89, 30.46, 32.04, 32.27, 42.19, 125.50, 126.02, 128.54, 132.62, 135.29, 147.72, 149.69 ppm.

FD-MS: m/z: 619.02 (M^+, 100.0%).

Anal. Calcd. $C_{34}H_{50}O_2S_4$: C, 65.97; H, 8.14. Found: C, 65.98; H, 8.13.

Compound **7d** (850 mg, 90%, related to **3**) was obtained as white powder after purification by column chromotography (SiO_2) with THF: hexane (2:1) as an eluent. mp:195-200°C.

^{1}H NMR (250 MHz, CD_2Cl_2): δ = 0.82 (t, 6H), 1.29 (m, 22H), 1.55 (m, 2H), 2.45 (s, 6H), 2.72 (d, 4H, *J* = 7.5 Hz), 6.74 (d, 2H, *J* = 7.5 Hz), 7.04 (d, 2H, *J* = 7.5 Hz), 7.99 (s, 2H) ppm.

^{13}C NMR (62.5MHz, CD_2Cl_2): δ = 11.01, 14.26, 23.37, 25.95, 29.20, 30.46, 32.72, 34.42, 41.93, 125.99, 126.58, 128.47, 132.61, 135.54, 147.71, 148.28 ppm.

FD-MS: m/z: 590.24 (M^+, 100.0%).

Anal. Calcd. for $C_{32}H_{46}O_2S_4$: C, 65.04; H, 7.85. Found: C, 65.01; H, 7.88.

Dithieno[2,3-*d*:2',3'-*d'*]benzo [1,2-*b*:4,5-*b'*]dithiophene (2a, 2b, 2c and 2d)

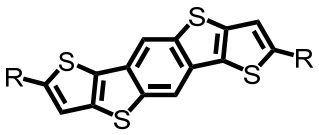

R = CH_3 2a
R = C_6H_{13} 2b
R = C_9H_{19} 2c
R = $C_{6,2}H_{17}$ 2d

A 10 ml round bottomed flask was filled with 5,5'-(2,5-bis(methylsulfinyl)-1,4-phenylene)bis(2-hexylthiophene) (**7b**) (200 mg, 0.53 mmol), Phosphorus pentoxide (28 mg, 0.2 mmol) and trifluoromethanesulfonic acid (6 ml). The mixture was stirred for 72 h at room temperature to give a dark brown solution, which was then poured into ice–water (100 ml). The yellow precipitate was collected by suction filtration and dried under vacuum. The structure of this compound, which was insoluble in apolar organic solvents, was assumed to be the sulfonium salt. Demethylation of the solid was achieved by refluxing it in pyridine (40 ml) for 12 h. When the suspension was cooled to room temperature, a large volume of CH2Cl2 was added to extract the product. Dithieno[2,3-d:2',3'-d']benzo [1,2-*b*:4,5-*b'*]dithiophene (2b) was thus obtained as off-white flakes by Hexane as an eluent (155 mg, 93 %). mp: 150-155°C.

^{1}H NMR (250 MHz, CD_2Cl_2): δ = 0.80 (t, 6H), 1.27 (m, 12H), 1.69 (m, 4H), 2.88 (t, 4H), 6.96 (s, 2H), 8.11 (s, 2H) ppm.

^{13}C NMR (62.5MHz, CD_2Cl_2): δ = 14.22, 20.97, 29.11, 30.07, 41.98, 31.63, 31.99, 115.30, 117.84, 130.46, 131.73, 137.90, 139.94, 150.50 ppm.

FD-MS: m/z: 470.78 (M+, 100.0%).

Anal. Calcd. $C_{26}H_{30}S_4$: C, 66.33; H, 6.42, Found: C, 66.35; H, 6.41.

By following the same method **1a**, **1c** and **1d** were also synthesized.

Compound **1a** (125 mg, 93%, related to **2a**) was obtained as white powder after purification by column chromotography (SiO_2) with DCM: hexane (1:10) as an eluent. mp: > 300°C.

^{1}H NMR (250 MHz, CD_2Cl_2): δ = 2.63 (s, 6H), 7.00 (s, 2H), 8.16 (s, 2H) ppm.

^{13}C NMR (62.5MHz, CD_2Cl_2): δ = 30.07, 115.32, 118.93, 130.39, 131.77, 138.04,

139.91, 144.26 ppm.

FD-MS: m/z: 330.51 (M^+, 100.0%).

Anal. Calcd for $C_{16}H_{10}S_4$: C, 58.14; H, 3.05. Found: C, 58.16; H, 3.07.

Compound **1c** (120 mg, 95%, related to **2c**) was obtained as white flakes after purification by column chromotography (SiO_2) with hexane as an eluent. mp: 145-150°C.

^{1}H NMR (250 MHz, CD_2Cl_2): δ = 0.90 (t, 6H), 1.30 (m, 24H), 1.79 (m, 4H), 2.99 (t, 4H), 7.08 (s, 2H), 8.23 (s, 2H) ppm.

^{13}C NMR (62.5MHz, CD_2Cl_2): δ = 14.58, 23.39, 29.76, 30.01, 30.07, 30.22, 30.40, 30.73, 32.36, 115.63, 118.16, 130.79, 138.22, 140.27, 150.84 ppm.

FD-MS: m/z: 558.97 (M^+, 100.0%).

Anal. Calcd for $C_{32}H_{46}S_4$:C, 68.76; H, 8.29. Found: C, 68.77; H, 8.25.

Compound **1d** (100 mg, 95%, related to **2d**) was obtained as white powder after purification by column chromotography (SiO_2) with hexane as an eluent. mp: 128-135°C.

^{1}H NMR (250 MHz, CD_2Cl_2): δ = 0.82 (t, 6H), 1.26 (m, 22H), 1.61 (m, 2H), 2.82 (d, 4H, *J* = 7.5 Hz), 6.95 (s, 2H), 8.11 (s, 2H) ppm.

^{13}C NMR (62.5MHz, CD_2Cl_2): δ = 9.51, 12.81, 21.93, 24.45, 27.78, 31.28, 34.17, 40.52, 113.85, 117.37, 128.98, 130.53, 136.38, 138.49, 147.71 ppm.

FD-MS: m/z = 530.91 (M^+, 100.0%).

Anal. Calcd. for $C_{30}H_{42}S_4$:C, 67.87; H, 7.97. Found: C, 67.85; H, 7.96.

1-Bromo-2-(methylsulfinyl)benzene

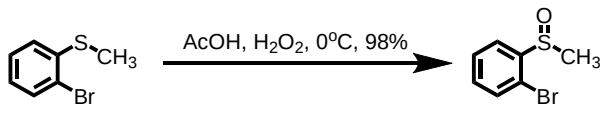

2-Bromothioanisole (3.3 g, 16.25 mmol) was dissolved in glacial acetic acid and cooled with an ice-bath till the solvent was about to freeze. Hydrogen peroxide (35%, 1.81 g) was added slowly. The cooling bath was removed and the mixture was stirred at room temperature for 12 h. Acetic acid was removed by vacuum evapour ation

and water (50 ml) was added to the residue. The precipitated oil was taken up with dichloromethane, the solution washed with saturated $NaHCO_3$ solution and dried over $MgSO_4$. Evapour ation of the solvent yielded 3.5 g (98%) of 1-bromo-2-(methylsulfinyl)benzene as a viscous colorless oil.

^{1}H-NMR (250 MHz, CD_2Cl_2): δ = (m, 1H), 7.59 (m, 2H), 7.38 (m, 1H), 2.82 (s,3H) ppm.

^{13}C-NMR (62.5 MHz, CD_2Cl_2): δ = 145.3, 132.6, 132.0, 128.4, 125.4, 117.8, 41.7 ppm.

FD-MS: m/z = 218.9 (M^+, 100%).

2, 7-Bis[2-(methylsulfinyl)phenyl]-*N*-methyl-carbazole (11a); 2, 7-bis[2-(methyl-sulfinyl)phenyl]-*N*-butyl-carbazole (11b); 2, 7-bis[2-(methylsulfinyl)-phenyl]-*N*-hexyl-carbazole (11c); 2, 7-bis[2-(methylsulfinyl)phenyl]-*N*-octyl- carbazole (11d)

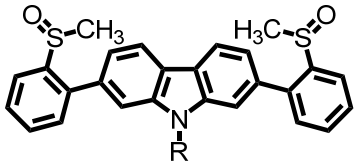

a: R = CH_3; R' = H
b: R = C_4H_9; R' = H
c: R = C_6H_{13}; R' = H
d: R = C_8H_{17}; R' = H

A mixture of **10c** (1.5 g, 2.98 mmol), 2-bromo(methylsulfinyl)benzene (1.44 g, 6.56 mmol) was dissolved in 25 ml of toluene. Then a 2 M K_2CO_3 solution (8 ml) was added. The reaction mixture was degassed by three freeze/ pump thaw cycles before 80 mg (6.92×10^{-5} mol) of $Pd(PPh_3)_4$ was added under argon. The mixture was stirred for 24 h at 90 ^{o}C. The mixture was then allowed to cool to room temperature and the reaction mixture was extracted three times with CH_2Cl_2 and dried with $MgSO_4$. The product was purified by silica chromatography with THF: hexane (2:1) as the eluent, affording the pure product as colorless powder (1.1 g, 70 % yield). mp: 95-98 °C.

^{1}H NMR (250 MHz, CD_2Cl_2): δ = 0.75 (t, 2H), 1.19 (m, 8H,), 1.80 (m, 2H), 2.22 (s, 6H). 4.27 (t, 2H), 7.18 (dd, 2H), 7.40 (d, 2H, J = 7.5 Hz), 7.42 (s, 2H), 7.50 (m, 4H), 8.04 (dd, 2H, J = 7.5 Hz), 8.12 (d, 2H, J = 7.5 Hz) ppm.

^{13}C NMR (62.5MHz, CD_2Cl_2): δ = 14.1, 21.0, 25.0, 27.5, 29.4, 32.0, 41.9, 110.1, 120.8, 121.2, 122.6, 123.7, 128.9, 130.9, 131.0, 136.3, 140.6, 141.4, 145.2 ppm.

FD-MS: m/z = 527.20 (M^+, 100.0%).

Anal. Calcd. for $C_{32}H_{33}NO_2S_2$: C, 72.83; H, 6.30. Found: C, 72.82; H, 6.33.

Compound **11a** (1.28 g, 70 % yield, related to **10a**) was obtained as white powder after purification by column chromatography (SiO_2) with THF: hexane (2:1) as an eluent. mp: 120-122 °C.

^{1}H NMR (250 MHz, CD_2Cl_2): δ = 2.23 (s, 6H), 3.81 (s, 3H), 7.21 (dd, 2H, *J* = 7.5 Hz), 7.40 (d, 2H, *J* = 7.5 Hz), 7.43 (s, 2H), 7.53 (m, 4H), 8.04 (dd, 2H, *J* = 7.5 Hz), 8.12 (d, 2H, *J* = 7.5 Hz) ppm.

^{13}C NMR (62.5 MHz, CD_2Cl_2): δ = 29.7, 42.1, 110.3, 121.3, 121.5, 124.0, 129.3, 131.3, 131.4, 136.7, 136.8, 141.0, 142.4, 145.5 ppm.

FD-MS: m/z = 457.12 (M^+, 100.0 %).

Anal. Calcd. for $C_{27}H_{23}NO_2S_2$: C, 70.87; H, 5.07. Found: C, 70.85; H, 5.10.

Compound **11b** (1.16 g, 75%, related to **10b**) was obtained as white powder after purification by column chromatography (SiO_2) with THF: hexane (2:1) as an eluent. mp: 100-102 °C.

^{1}H NMR (250 MHz, CD_2Cl_2): δ = 0.85 (s, 3H), 1.33 (m, 2H), 1.79 (m, 2H), 2.23 (s, 6H), 4.27 (t, 2H), 7.18 (dd, 2H), 7.40 (d, 2H, *J* = 7.5 Hz), 7.42 (s, 2H), 7.50 (m, 4H), 8.04 (dd, 2H, *J* = 7.5 Hz), 8.12 (d, 2H, *J* = 7.5 Hz) ppm.

^{13}C NMR (62.5MHz, CD_2Cl_2): δ = 14.1, 20.9, 25.0, 31.5, 42.0, 110.1, 120.8, 121.2, 122.6, 123.7, 128.9, 130.9, 131.0, 136.3, 140.6, 141.4, 145.1 ppm.

FD-MS: m/z = 499.16 (M^+, 100.0%).

Anal. Calcd. for $C_{30}H_{29}NO_2S_2$: C, 72.11; H, 5.85. Found: C, 72.13; H, 5.82.

Compound **11d** (1.21 g, 72%, related to **11d**) was obtained as off-white powder after purification by column chromatography (SiO_2) with THF: hexane (2:1) as an eluent. mp: 70-72 °C.

^{1}H NMR (250 MHz, CD_2Cl_2): δ = 0.74 (t, 2H), 1.12 (m, 8H,), 1.80 (m, 2H), 2.22 (s, 6H). 4.26 (t, 2H), 7.18 (dd, 2H), 7.40 (d, 2H, *J* = 7.5 Hz), 7.42 (s, 2H), 7.50 (m, 4H), 8.04 (dd, 2H, *J* = 7.5 Hz), 8.12 (d, 2H, *J* = 7.5 Hz) ppm.

^{13}C NMR (62.5MHz, CD_2Cl_2): δ = 14.2, 21.0, 25.0, 27.8, 29.5, 29.6, 29.8, 32.2, 42.0, 110.1, 120.8, 121.2, 122.6, 123.7, 128.9, 130.9, 131.0, 136.3, 140.6, 141.4, 145.2 ppm.

FD-MS: m/z = 527.20 (M^+, 100.0%).

Anal. Calcd. for $C_{32}H_{33}NO_2S_2$: C, 72.83; H, 6.30. Found: C, 72.81; H, 6.32.

Dibenzo[*b*,*b*']thieno[2,3-*f*:5,4-*f*']-*N*-methyl carbazole (8a); dibenzo[*b*,*b*']thieno-[2,3-*f*:5,4-*f*']-*N*-butylcarbazole (8b); dibenzo[*b*,*b*']thieno[2,3-*f*:5,4-*f*']-*N*-hexyl carbazole (8c); dibenzo[*b*,*b*']thieno[2,3-*f*:5,4-*f*']-*N*-octyl carbazole (8d)

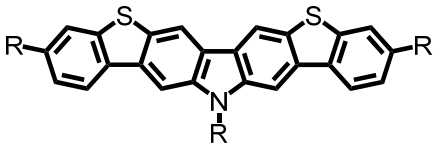

a: R = CH_3; R' = H
b: R = C_4H_9; R' = H
c: R = C_6H_{13}; R' = H
d: R = C_8H_{17}; R' = H

A 10 ml round bottomed flask was filled with, 7-bis[2-(methylsulfinyl)-phenyl]-*N*-hexyl-carbazole (**11c**) (200 mg, 0.38 mmol), phosphorus pentoxide (28 mg, 0.2 mmol) and trifluoromethanesulfonic acid (6 ml). The mixture was stirred for 72 h at room temperature to give a dark brown solution, which was then poured into ice–water (100 ml). The yellow precipitate was collected by suction filtration and dried under vacuum. The structure of this compound, which was insoluble in apolar organic solvents, was assumed to be the sulfonium salt. Demethylation of the solid was achieved by refluxing in pyridine (30 ml) for 12 h. When the suspension was cooled to room temperature, a large volume of CH_2Cl_2 was added to extract the product. **8c** was thus obtained as yellow powder after silica chromatography with CH_2Cl_2/Hexane=1/9 as an eluent (165 mg, 94 % yield). mp: 215-217 °C.

^{1}H NMR (250 MHz, CD_2Cl_2): δ = 0.80 (t, 3H), 1.31 (m, 6H), 1.94 (m, 2H), 4.43 (t, 2H), 7.41 (m, 2H), 7.81 (d, 2H, *J* = 7.5 Hz), 8.06 (s, 2H), 8.22 (d, 2H, *J* = 7.5 Hz), 8.49 (s, 2H) ppm.

^{13}C NMR (62.5MHz, CD_2Cl_2): δ = 14.2, 23.0, 27.4, 28.9, 32.1, 101.0, 121.9, 123.3, 123.5, 124.6, 127.1, 130.7, 135.0, 136.1, 140.6, 140.9 ppm.

FD-MS: m/z = 463.14 (M^+, 100%).

Anal. Calcd. for $C_{30}H_{25}NS_2$: C, 77.71; H, 5.43. Found: 77.75; H, 5.36.

Compound **8a** (120 mg, 70 % yield, related to **11a**) was obtained as yellow powder from silica chromatography using CH_2Cl_2 / Hexane mixture from 1/9 to 1/1

as an eluent. mp: > 350 °C.

^{1}H NMR (250 MHz, CD_2Cl_2): δ = 4.00 (s, 3H), 7.43 (m, 4H), 7.82 (d, 2H, *J* = 7.3 Hz), 8.12 (s, 2H), 8.26 (d, 2H, *J* = 8.1 Hz), 8.52 (s, 2H) ppm.

FD-MS: m/z = 393.06 (M^+, 100%).

Anal. Calcd. for $C_{25}H_{15}NS_2$: C, 76.30; H, 3.84 Found: C, 76.34; H, 3.83

Compound **8b** (150 mg, 85%, related to **11b**) was obtained as yellow powder from silica chromatography using CH_2Cl_2/Hexane=1/9 as the eluent. mp: 270-272 °C.

^{1}H NMR (250 MHz, CD_2Cl_2): δ = 0.92 (t, 3H), 1.42 (m, 2H, *J* = 7.5 Hz), 1.96 (m, 2H, *J* = 7.5 Hz), 4.46 (t, 2H), 7.43 (m, 2H), 7.81 (d, 2H, *J* = 7.5 Hz), 8.09 (s, 2H), 8.24 (d, 2H, *J* = 7.5 Hz), 8.50 (s, 2H) ppm.

^{13}C NMR (62.5MHz, CD_2Cl_2): δ = 14.1, 21.1, 31.2, 43.7, 101.0, 114.3, 121.9, 123.3, 123.5, 124.6, 127.1, 130.7, 135.0, 136.1, 140.6, 140.9 ppm.

FD-MS: m/z = 435.11 (M^+, 100%).

Anal. Calcd. for $C_{28}H_{21}NS_2$: C, 77.20; H, 4.86. Found: C, 76.13; H, 4.90.

Compound **18d** (162 g, 92%, related to **11d**) was obtained as yellow powder from silica chromatography using CH_2Cl_2/Hexane=1/9 as the eluent. mp: 210-212 °C.

^{1}H NMR (250 MHz, CD_2Cl_2): δ = 0.73 (t, 3H), 1.35 (m, 10H), 1.93 (m, 2H), 4.39 (t, 2H), 7.41 (m, 4H), 7.80 (d, 2H, *J* = 7.5 Hz), 8.03 (s, 2H), 8.21 (d, 2H, *J* = 7.5 Hz), 8.46 (s, 2H) ppm.

^{13}C NMR (62.5MHz, CD_2Cl_2): δ = 14.2, 23.0, 27.7, 28.9, 29.6, 29.8, 32.2, 43.8, 100.9, 114.3, 121.8, 123.3, 123.5, 124.5, 127.1, 130.7, 135.0, 136.1, 140.6, 140.9 ppm.

FD-MS: m/z = 491.17 (M^+, 100%).

Anal. Calcd. for $C_{32}H_{29}NS_2$: C, 78.16; H, 5.94. Found: C, 78.18; H, 5.92.

2,7-Bis(4-n-butyphenyl)-*N*-methyl-carbazole (12)

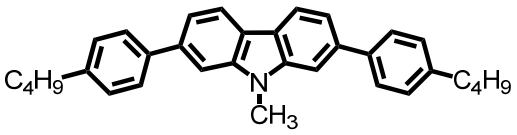

2,7-Dibromo-*N*-methyl-carbazole **9a** (1.5g, 4.42 mmol) and 2.53 g (9.73 mmol) of **4b** were dissolved in 25 ml of toluene. A 2 M K_2CO_3 solution (6 ml) and 0.1 g of trimethylbenzylammonium chloride were added. The reaction mixture was degassed by three freeze/thaw cycles before 100 mg (8.6×10^{-6} mol) of $Pd(PPh_3)_4$ was added under argon. The mixture was stirred for 24 h at 90 °C. The reaction mixture was extracted three times with CH_2Cl_2 and dried with $MgSO_4$. The product was purified by silica chromotography with hexane as an eluent. Compound **12** (1.67 g, 85%, related to **9a**) was obtained as a white solid. mp: 192-193 °C.

^{1}H NMR (250 MHz, CD_2Cl_2): δ = 1.03 (t, 6H), 1.44 (m, 4H), 1.74 (m, 4H), 2.74 (s, 6H), 3.96 (s, 3H), 7.36 (d, 4H, *J* = 8.1 Hz), 7.53 (dd, 2H, *J* = 8.1 Hz), 7.67 (s, 2H), 7.72 (dd, *J* = 8.1 Hz), 8.16 (d, 2H, *J* = 8.1 Hz) ppm.

^{13}C NMR (62.5MHz, CD_2Cl_2): δ = 14.2, 22.8, 29.5, 34.2, 35.7, 107.2, 118.9, 120.8, 121.9, 127.6, 129.3, 139.4, 139.7, 142.5, 142.6 ppm.

FD-MS: m/z = 445.64 (M^+, 100.0%).

Anal. Calcd. for $C_{33}H_{35}N$: C, 88.94; H, 7.92. Found: 88.93; H, 7.91.

3,6-Dibromo-2,7-bis(4-n-butyphenyl)-*N*-methyl-carbazole (13)

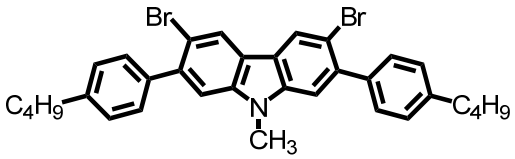

A 100 mL flask was charged with 1 g (2.24 mmol) of **12** and a 1:1 mixture of CH_3Cl and acetic acid and cooled in an ice-water bath. Then, 818.7 mg (4.6 mmol) of *N*-bromosuccinimide (NBS) was added in several portions, and the mixture was stirred overnight at room temperature in the dark. The mixture was quenched with 15 mL of distilled water and extracted three times with CH_2Cl_2. The combined organic fractions were dried over magnesium sulfate and the solvent was removed under reduce pressure. The crude material was purified by silica chromatography with hexane as an eluent to offer 1.16 g of the product as a white solid (86 % yield). mp: 203-205 °C.

^{1}H NMR (250 MHz, CD_2Cl_2): δ = 0.89 (t, 6H), 1.29 (m, 4H), 1.61 (m, 4H), 2.61 (t, 4H), 3.69 (s, 3H), 7.20 (d, 4H, *J* = 8.1 Hz), 7.29 (s, 2H), 7.33 (d, 2H, *J* = 8.1 Hz), 8.23 (s, 2H) ppm.

^{13}C NMR (62.5MHz, CD_2Cl_2): δ = 14.2, 22.9, 29.7, 34.1, 35.8, 111.8, 113.1, 122.4, 124.8, 128.3, 130.0, 139.7, 140.7, 141.3, 142.9 ppm.

FD-MS: m/z = 603.43 (M+, 100.0%).

Anal. Calcd. for $C_{33}H_{33}Br_2N$: C, 65.68; H, 5.51. Found: 65.67; H, 5.52.

3,6-Dimethylsulfide-2,7-bis(4-n-butyphenyl)-*N*-methyl-carbazole (14)

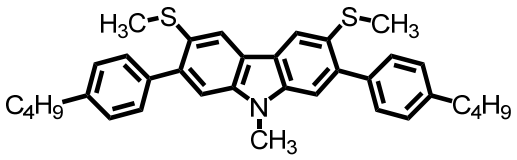

3,6-Dibromo-2,7-bis(4-n-butyphenyl)-*N*-methyl-carbazole (**13**) (600 mg, 0.994 mmol) was dissolved in dry THF (40 ml) and cooled to −78 °C. n-Butyllithium (1.6 M in hexane, 1.37 ml, 2.19 mmol) was added dropwise at this temperature. After the addition was complete the mixture was stirred for an additional hour. Dimethyl disulfide (206 mg, 2.19 mmol) was added dropwise. The cooling bath was removed and the solution was stirred at room temperature overnight. The crude material was purified by silica chromotography with hexane/CH_2Cl_2 = 10:1 as the eluent, **14** was gotten as light yellow solid. (374 mg, 70% yield) mp: 208–213 °C.

^{1}H-NMR (250 MHz, CD_2Cl_2): δ = 0.89 (t, 6H), 1.33 (t, 4H), 1.58 (t, 4H), 2.35 (s, 6H), 2.62 (t, 4H), 3.71 (s, 3H), 7.19 (d, 4H, *J* = 8.1 Hz), 7.22 (s, 2H), 7.35 (d, 2H, *J* = 8.1 Hz), 8.00 (s, 2H) ppm.

^{13}C-NMR (62.5 MHz, CD_2Cl_2): δ = 14.1, 18.2, 22.9, 29.6, 34.1, 35.8, 111.0, 120.1, 122.1, 127.2, 128.3, 129.9, 139.3, 140.4, 140.9, 142.6 ppm.

FD-MS: m/z = 537,82 (M+, 100.0%).

Anal. Calcd. for $C_{35}H_{39}NS_2$: C, 78.16; H, 7.31. Found: C, 78.158; H, 7.32.

3,6-Dimethylsulfoxide-2,7-bis(4-n-butyphenyl)-*N*-methyl-carbazole (15)

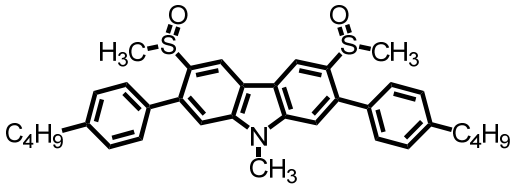

3,6-Dimethylsulfide-2,7-bis(4-n-butyphenyl)-*N*-methyl-carbazole (**14**) (300 mg, 0.558 mmol) was dissolved in a 1:1 mixture of glacial acetic acid and chloroform and cooled with an ice-bath till the solvent was about to freeze. Hydrogen peroxide (35%, 109 mg, 1.13 mmol) was added slowly. The cooling bath was removed and the mixture was stirred at room temperature for 12 h. Acetic acid was removed by vacuum evapour ation and CH_2Cl_2 was added to the residue. The organic fraction was washed with saturated $NaHCO_3$ solution and dried over $MgSO_4$. The product was purified by silica chromatography with THF: hexane (3:1) as the eluent, affording the pure product as a diastereomeric mixture of white solid (228 mg, 72 % yield). mp: 230-235 °C.

^{1}H NMR (250 MHz, CD_2Cl_2; signals of diastereomer A are marked with ′, those of diastereomer B with ′′): δ = 0.88 (t, 6H), 1.30 (m, 4H), 1.58 (m, 4H), 2.32 (s′, 3H), 2.34 (s′′, 3H), 2.61 (t, 4H), 3.81 (s, 3H), 7.22 (d, 4H, *J* = 8.1 Hz), 7.31 (s, 2H), 7.33 (d, 4H, *J* = 8.1 Hz), 8.83 (s′, 1H), 8.84 (s′′, 1H) ppm.

^{13}C NMR (62.5 MHz, CD_2Cl_2): δ = 14.15, 22.81, 30.08, 34.01, 35.72, 42.89(′), 42.98(′′), 111.10(′), 111.14(′′), 117.23(′), 117.28(′′), 122.51(′), 122.56(′′), 129.05(′), 129.08(′′), 129.87(′), 129.89(′′), 136.13(′), 136.16(′′), 136.41, 138.49(′), 138.58(′′), 143.27(′), 143.30(′′), 143.66(′), 143.67(′′) ppm.

FD-MS: m/z = 569.82 (M^+, 100.0 %).

Anal. Calcd. for $C_{35}H_{39}NO_2S_2$: C, 73.77; H, 6.90. Found: C, 76.78; H, 6.91.

6,6′-Dibutyl dibenzo[*b*,*b*′]thieno[2,3-*f*:5,4-*f*′]-*N*-methyl carbazole (8e)

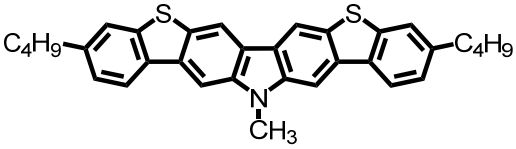

Following the same method as **8c**, 6, 6′-dibutyl dibenzo[*b,b'*]thieno[2,3-*f*:5,4-*f'*]-*N*-methyl carbazole was gotten as yellow powder after silica chromatography with CH_2Cl_2/Hexane=1/9 as an eluent (90 mg, 96 % yield). mp: 256-263 °C.

^{1}H NMR (250 MHz, CD_2Cl_2): δ = 0.95 (t, 6H), 1.42 (m, 4H), 1.69 (m, 4H), 2.77 (t, 4H), 3.98 (s, 3H), 7.30 (dd, 2H, *J* = 8.1 Hz), 7.66 (s, 2H), 8.04 (s, 2H), 8.14 (d, 2H), 8.49 (s, 2H) ppm.

^{13}C NMR (62.5MHz, CD_2Cl_2): δ = 14.1, 22.8, 39.9, 34.2, 36.2, 100.4, 114.2, 121.5, 122.7, 123.1, 125.6, 130.6, 133.9, 135.0, 140.8, 141.5, 142.6 ppm.

FD-MS: m/z = 505,74 (M^+, 100%).

Anal. Calcd. for $C_{33}H_{31}NS_2$: C, 78.37; H, 6.18. Found: C, 78.36; H, 6.17.

2,7-Bis(5-hexylthiophen-2-yl)-9-methyl-9*H*-carbazole (18)

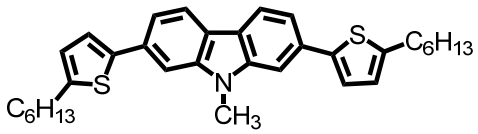

A similar procedure was followed as described for the synthesis of **31**, starting from **9a** and 2.2 equivalent of **17**. The crude product was purified by flash chromatography (silica gel, eluent: hexane/CH_2Cl_2 = 7:1) to afford 0.5 g (80%) of **18**.

^{1}H NMR (250 MHz, CD_2Cl_2): δ = 7.93 (d, *J* = 8.13 Hz, 2H), 7.49 (s, 2H), 7.38 (dd, *J* = 8.13, 1.50 Hz, 2H), 7.18 (d, *J* = 3.56 Hz, 2H), 6.73 (d, *J* = 3.55 Hz, 2H), 3.81 (s, 3H), 2.77 (t, *J* = 7.59, 7.59 Hz, 4H), 1.63 (dd, *J* = 14.74, 7.05 Hz, 4H), 1.39-1.19 (m, 12H), 0.83 (t, *J* = 8.71, 6H) ppm.

^{13}C NMR (62.5MHz, CD_2Cl_2): δ = 145.04, 141.90, 141.40, 131.83, 124.46, 121.95, 121.01, 119.68, 116.59, 104.49, 31.03, 30.93, 29.57, 28.44, 28.13, 21.93, 13.18 ppm.

FD-MS: m/z = 513,80 (M^+, 100%).

Anal. Calcd. for $C_{33}H_{39}NS2$: C, 77.14; H, 7.65. Found: 77.22; H, 7.59.

3,6-Dibromo-2,7-bis(5-hexylthiophen-2-yl)-9-methyl-9*H*-carbazole (19)

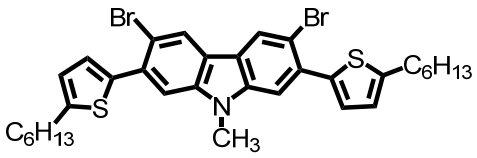

A 100 mL flask was charged with 0.3 g (0.58 mmol) of **18** and a 1:1 mixture of CH_3Cl and acetic acid and cooled in an ice-water bath. Then, 210 mg (1.18 mmol) of *N*-bromosuccinimide (NBS) was added in several portions, and the mixture was stirred overnight at room temperature in the dark. The mixture was quenched with 15 mL of distilled water and extracted three times with CH_2Cl_2. The combined organic fractions were dried over magnesium sulfate and the solvent was removed under reduce pressure. The crude material was purified by silica chromatography with hexane/CH_2Cl_2 = 9:1 as an eluent to offer 294 mg of the product as a white solid (75 % yield).

^{1}H NMR (250 MHz, CD_2Cl_2): δ = 8.13 (s, 2H), 7.36 (s, 2H), 7.07 (d, *J* = 3.54 Hz, 2H), 6.73 (d, *J* = 3.55 Hz, 2H), 3.65 (s, 3H), 2.78 (t, *J* = 7.60, 7.60 Hz, 4H), 1.72-1.57 (m, 4H), 1.38-1.18 (m, 12H), 0.83 (dd, *J* = 8.75, 5.13 Hz, 6H) ppm.

^{13}C NMR (62.5MHz, CD_2Cl_2): δ = 147.62, 141.21, 140.27, 133.61, 128.21, 125.33, 124.42, 122.45, 113.22, 112.11, 32.14, 32.00, 30.52, 29.71, 29.29, 23.01, 14.26 ppm.

FD-MS: m/z = 669,07 (M^+, 100%).

Anal. Calcd. for $C_{33}H_{37}Br_2NS_2$: C, 59.02; H, 5.55. Found: 59.08; H, 5.48.

2,7-Bis(5-hexylthiophen-2-yl)-9-methyl-3,6-bis(methylthio)-9*H*-carbazole (20)

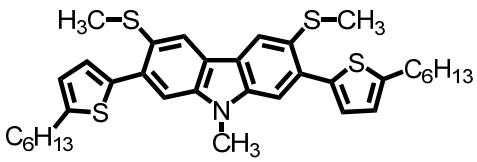

3,6-dibromo-2,7-bis(5-hexylthiophen-2-yl)-9-methyl-9*H*-carbazole (**19**) (250 mg, 0.37 mmol) was dissolved in dry THF (40 ml) and cooled to −78 °C. *n*-Butyllithium (1.6 M in hexane, 0.5 ml, 0.78 mmol) was added dropwise at this temperature. After the addition was complete the mixture was stirred for an additional hour. Dimethyl

disulfide (73.6 mg, 0.8 mmol) was added dropwise. The cooling bath was removed and the solution was stirred at room temperature overnight. The crude material was purified by silica chromatography with hexane/CH_2Cl_2 = 5:1 as the eluent, **20** was gotten as light yellow solid. (113 mg, 50% yield)

^{1}H NMR (250 MHz, CD_2Cl_2): δ = 8.09 (s, 2H), 7.47 (s, 2H), 7.19 (d, *J* = 3.49 Hz, 2H), 6.86 (d, *J* = 3.51 Hz, 2H), 3.83 (s, 3H), 2.91 (t, *J* = 7.65, 7.65 Hz, 4H), 2.52 (s, 6H), 1.84-1.72 (m, 4H), 1.51-1.32 (m, 12H), 0.96 (t, *J* = 8.75, 5.13 Hz, 6H) ppm.

^{13}C NMR (62.5MHz, CD_2Cl_2): δ = 146.91, 140.06, 139.61, 133.11, 127.39, 127.28, 123.95, 121.88, 12032, 111.06, 31.75, 31.59, 30.12, 29.24, 28.88, 22.60, 17.98, 13.83 ppm.

FD-MS: m/z = 605,23 (M^+, 100%).

Anal. Calcd. for $C_{35}H_{43}NS_4$: C, 69.37; H, 7.15. Found: 69.35; H, 7.10.

2,7-Bis(5-hexylthiophen-2-yl)-9-methyl-3,6-bis(methylsulfinyl)-9H-carbazole (21)

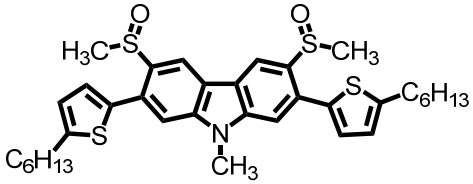

2,7-bis(5-hexylthiophen-2-yl)-9-methyl-3,6-bis(methylthio)-9*H*-carbazole (**20**) (100 mg, 0.17 mmol) was dissolved in a 1:1 mixture of glacial acetic acid and chloroform and cooled with an ice-bath till the solvent was about to freeze. Hydrogen peroxide (35%, 35 mg, 0.36 mmol) was added slowly. The cooling bath was removed and the mixture was stirred at room temperature for 12 h. Acetic acid was removed by vacuum evapour ation and CH_2Cl_2 was added to the residue. The organic fraction was washed with saturated $NaHCO_3$ solution and dried over $MgSO_4$. The product was purified by silica chromatography with THF: hexane (1:1) as the eluent, affording the pure product as a white solid (101 mg, 95 % yield).

^{1}H NMR (250 MHz, CD_2Cl_2): δ = 8.93 (d, *J* = 3.97 Hz, 2H), 7.55 (d, *J* = 1.76 Hz, 2H), 7.13 (dd, *J* = 3.51, 1.71 Hz, 2H), 6.88 (d, *J* = 3.51 Hz, 2H), 3.95 (d, *J* = 0.84 Hz, 3H), 2.92 (t, *J* = 7.59, 7.59 Hz, 4H), 2.58 (d, *J* = 4.99 Hz, 6H), 1.85-1.71 (m, 4H), 1.48-1.33 (m, 12H), 0.96 (t, *J* = 8.77, 5.17 Hz, 6H) ppm.

^{13}C NMR (62.5 MHz, CD_2Cl_2): δ = 148.68, 143.20, 137.13, 136.88, 130.93, 128.19, 125.24, 122.72, 117.56, 111.43, 43.25, 32.12, 31.99, 30.51, 30.17, 29.20, 23.03, 14.29 ppm.

FD-MS: m/z = 637,22 (M^+, 100.0 %).

Anal. Calcd. for $C_{35}H_{43}NO_2S_4$: C, 65.89; H, 6.79. Found: C, 65.85; H, 6.88.

Bisthieno[3,2-*b*]thieno[2,3-*f*:5,4-*f'*]-carbazoles (BTTCz) (16)

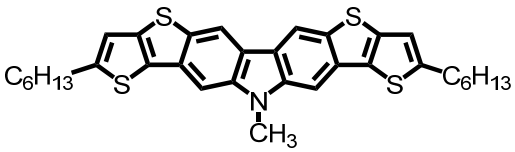

The same procedure was followed as described for the synthesis of **8c**, starting from **21**. The product **16** was isolated as light yellow oil after silica chromatography with CH_2Cl_2/Hexane=1/9 as an eluent and solidified to yellow crystals when cooled down (55 mg, 80 % yield).

^{1}H NMR (250 MHz, CD_2Cl_2): δ = 8.55 (s, 2H), 7.74 (s, 2H), 7.10 (s, 2H), 3.98 (s, 3H), 3.02 (t, *J* = 7.55, 7.55 Hz, 4H), 1.89-1.77 (m, 4H), 1.53-1.43 (m, 4H), 1.39 (ddd, *J* = 7.39, 4.59, 2.45 Hz, 8H), 0.95 (t, *J* = 9.34, 4.82 Hz, 6H) ppm.

^{13}C NMR (62.5MHz, CD_2Cl_2): δ = 150.10, 141.65, 138.34, 133.65, 132.48, 132.12, 121.33, 118.02, 115.13, 99.18, 32.04, 31.68, 30.08, 29.86, 29.15, 23.00, 14.25 ppm.

FD-MS: m/z = 573,90 (M^+, 100%).

Anal. Calcd. for $C_{33}H_{35}NS_4$: C, 69.06; H, 6.15; Found: 69.12; H, 6.23.

2-Chloro-7-hexyl-*N*-ethyl-carbazole (24)

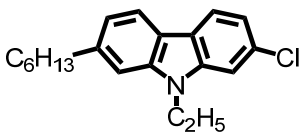

2-Chloro-7-bromo-9-ethyl-carbazole (**23**) (1.5 g, 4.86 mmol) was dissolved in dry THF (40 ml) and cooled to −78 °C. n-Butyllithium solution (1.6 M in hexane, 3.34 ml, 5.35 mmol) was added dropwise at this temperature. After the addition was complete the mixture was stirred for an additional hour. Hexyl iodide (0.71 g, 5.35 mmol) was added dropwise. The cooling bath was removed and the solution was

stirred at room temperature overnight. The crude material was purified by silica chromatography with hexane as the eluent, **24** was gotten as off-white solid. (1.06 g, 70% yield) mp: 156–163 °C.

^{1}H-NMR (300 MHz, CD_2Cl_2): δ = 0.81(t, 3H), 1.24 (m, 6H), 1.31 (t, 3H), 1.62 (m, 2H), 1.98 (2.71), 4.20 (m, 2H), 6.68 (dd, 1H, *J* = 8.1 Hz), 7.02 (dd, 1H, *J* = 8.1 Hz), 7.14 (s, 1H), 7.29 (dd, 1H, *J* = 8.1 Hz), 7.83 (dd, 2H, *J* = 8.1 Hz) ppm.

^{13}C-NMR (75.5 MHz, CD_2Cl_2): δ = 13.9, 14.3, 23.1, 29.5, 32.1, 32.5, 37.1, 38.0, 108.7, 108.9, 119.3, 120.3, 120.6, 120.7, 121.2, 122.0, 131.0, 141.0, 141.1, 142.1 ppm.

FD-MS: m/z = 313,86 (M^+, 100%).

Anal. Calcd. for $C_{20}H_{24}ClN$: C, 76.53; H, 7.71. Found: C, 78.52; H, 7.72.

2-hexyl-*N*-ethyl-7-(4,4,5,5-tetramethyl-1,3,2-dioxaborolan-2-yl)-carbazole (25)

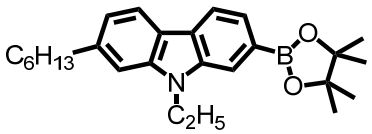

An oven-dried Schlenk tube was charged with Pd_2dba_3 (27.6 mg, 0.03 mmol), 2-dicyclohexylphosphino-2′,4′,6′-triisopropylbiphenyl (57.6 mg, 0.12 mmol), bis(pinacolato)diboron (2.28 g, 9 mmol), **24** (942 mg, 3 mmol) and KOAc (883.2 mg, 9 mmol). The Schlenk tube was capped with a rubber septum and then evacuated and backfilled with argon (this sequence was carried out three times). 1,4-Dioxane (10 mL) was added via a syringe, through a septum. The reaction mixture was heated to 110 °C and reacted overnight. At this point the reaction mixture was allowed to cool to room temperature. The reaction solution was then filtered through a thin pad of celite (eluting with ethyl acetate) and the eluent was concentrated under reduced pressure. The crude material so obtained was purified via flash chromatography on silica gel with Hexane/EtOAc=10:1 as the eluent to give **25** as light yellow oil.

^{1}H NMR (250 MHz, CD_2Cl_2): δ = 0.84 (t, 3H), 1.34 (m, 12H), 1.37 (m, 6H), 1.63 (t, 3H), 1.68 (t, 2H), 2.77 (t, 2H), 4.34 (m, 2H), 7.02 (dd, 1H, *J* = 8.1 Hz), 7.20 (s, 1H), 7.56 (d, 1H, *J* = 8.1 Hz), 7.82 (s, 1H), 7.94 (d, 1H, *J* = 8.1 Hz), 8.00 (d, 1H, *J* = 8.1 Hz) ppm.

^{13}C NMR (62.5 MHz, CD_2Cl_2): δ = 12.3, 12.4, 21.1, 23.3, 27.7, 28.3, 30.3, 30.6, 35.3, 35.9, 82.2, 106.7, 113.3, 117.7, 118.3, 118.9, 119.0, 123.3, 123.9, 138.1, 139.4, 140.5 ppm.

FD-MS: m/z = 405,38 (M^+, 100.0 %).

7,7'-(2,5-Bis(methylsulfinyl)-1,4-phenylene)bis(2-hexyl-*N*-ethyl-carbazole) (26)

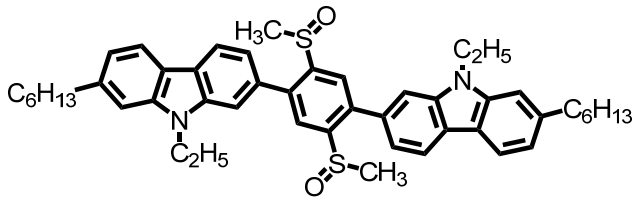

Compound **25** (486 mg, 1.2 mmol) and 1,4-dibromo-2,5-bis(methylsulfinyl)-benzene (**3**) (100 mg, 0.28 mmol) were dissolved in 10 ml of toluene. A 2 M K_2CO_3 solution (3 ml) was added. The reaction mixture was degassed by three freeze/ pump thaw cycles before 15 mg (1.3×10^{-5} mol) of $Pd(PPh_3)_4$ was added under argon. The mixture was stirred for 24 h at 90 °C. The mixture was then allowed to cool to room temperature and extracted three times with CH_2Cl_2 and dried with $MgSO_4$. The product was purified by silica chromatography with THF: hexane (3:1) as the eluent, affording the pure product as colorless powder (152 mg, 72 % yield). mp: 198-201 °C.

^{1}H NMR (250 MHz, CD_2Cl_2): δ = 0.83 (t, 6H), 1.29 (m, 18H), 1.59 (m, 4H), 2.27 (s, 6H), 2.76 (t, 4H), 4.33 (m, 4H), 7.05 (d, 2H, *J* = 7.5 Hz), 7.22 (s, 2H), 7.26 (d, 2H, *J* = 7.5 Hz), 7.48 (s, 2H), 7.96 (s, 2H), 8.09 (d, 2H, *J* = 7.5 Hz), 8.12 (s, 2H) ppm.

^{13}C NMR (62.5 MHz, CD_2Cl_2): δ = 14.3, 23.1, 29.5, 32.2, 32.5, 37.1, 38.0, 41.8, 108.8, 109.5, 120.1, 120.6, 120.7, 120.9, 123.7, 126.1, 134.1, 140.5, 140.8, 141.5, 142.5, 147.9 ppm.

FD-MS: m/z = 757,20 (M^+, 100.0 %).

Anal. Calcd. for $C_{48}H_{56}N_2O_2S_2$: C, 76.15; H, 7.46. Found: C, 76.25; H, 7.40.

Diindolo[3,2-*b*:2',3'-*h*]benzo[1,2-*b*:4,5-*b*']bis[1]benzothiophene (22)

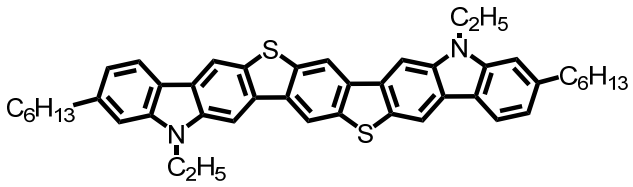

A 10 ml round bottomed flask was filled with 7,7'-(2,5-bis(methylsulfinyl)-1,4-phenylene)bis(2-hexyl-*N*-ethyl-carbazole) (**26**) (120 mg, 0.16 mmol), phosphorus pentoxide (1.2 mg, 0.008 mmol) and trifluoromethanesulfonic acid (3 ml). The mixture was stirred for 72 h at room temperature to give a dark brown solution, which was then poured into ice–water (100 ml). The yellow precipitate was collected by suction filtration and dried under vacuum. After refluxing the yellow powder in pyridine (30 ml) for 12 h, the suspension was cooled to room temperature and a large volume of CH_2Cl_2 was added to extract the product. Diindolo[3,2-*b*:2',3'-*h*]benzo-[1,2-*b*:4,5-*b*']bis[1] benzothiophene (**22**) was thus obtained as yellow powder by silica chromotography with hexane as the eluent (104 mg, 95 %).

^{1}H NMR (250 MHz, CD_2Cl_2): δ = 0.83 (t, 6H), 1.29 (m, 18H), 1.59 (m, 4H), 2.76 (t, 4H), 4.33 (m, 4H), 7.03 (d, 2H, *J* = 7.5 Hz), 7.17 (s, 2H), 7.97 (d, 2H, *J* = 7.5 Hz), 8.07 (s, 2H), 8.40 (s, 2H), 8.61 (s, 2H) ppm.

FD-MS: m/z = 693.02 (M^+, 100%).

3,3'-Dibromo-2,2'-bithiophene (28)

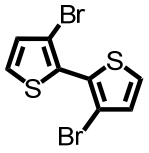

2,3-dibromothiophene (21 mmol, 5.00 g) was dissolved in diethyl ether (250 mL) and *n*BuLi (22 mmol, 14 mL) was added at -78 °C. The reaction mixture was stirred for 30 min at this temperature. Then $CuCl_2$ (30 mmol, 4 g) was added and the reaction mixture was stired at -78 °C for 3 hours further before it was allowed to warm to room temperature and was further stirred at this temperature for 10 h. The brown precipitate was filtered off and HCl (2 N, 300 mL) was added at 0°C. The

product was extracted with CH_2Cl_2 and diethyl ether, and the red organic phase was washed with HCl (2 N) and H_2O and dried with $MgSO_4$. After evapour ating all volatile materials the crude product was obtained as dark oil. The pure product could be obtained after a flash column with hexane as the eluent. Needle-shaped crystals of **28** could be obtained by crystallization from hexane (2.2 g, 65% yield).

^{1}H NMR (250 MHz, CD_2Cl_2): δ = 7.39-7.34 (m, 2H), 7.03-6.99 (m, 2H) ppm.

^{13}C NMR (62.5 MHz, CD_2Cl_2): δ = 131.165, 129.293, 128.233, 113.031 ppm.

FD-MS: m/z = 324.06 (M^+, 100%).

Anal. Calcd. for $C_8H_4Br_2S_2$: C, 29.65; H, 1.24. Found: C, 29.60; H, 1.26.

4-Hexyl-4H-dithieno[3,2-*b*:2',3'-*d*]pyrrole (29)

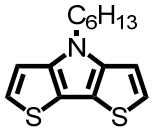

Into a mixture of **28** (0.60 g, 1.85 mmol), sodium t-butoxide (0.43 g, 4.44 mmol), tris(dibenzyliden eacetone)dipalladium (Pd_2dba_3, 0.042 g, 0.046 mmol) and 2,20-bis(diphenylphosphino)-1,10-binaphthyl (BINAP, 0.115 g, 0.185 mmol) were added the solution of n-hexyl amine (0.21 g, 2.04 mmol) in toluene (4 mL). The resultant mixture was stirred at 110 ^{o}C for 24 h under an argon atmosphere. After the mixture was cooled to room temperature, water (30 mL) was added, and the aqueous layer was extracted with diethyl ether (3 × 50 mL). The combined organic layers were washed with brine (2 × 100 mL) and dried over $MgSO_4$. After the solvent had been removed, the residue was purified by column chromatography on silica gel with hexane as eluent to afford **29** as a white solid in a yield of 75 % (0.36 g).

^{1}H NMR (250 MHz, CD_2Cl_2): δ = 7.03 (dd, *J* = 5.28 , 2.61 Hz, 2H), 6.93 (dd, *J* = 5.28, 2.55 Hz, 2H), 4.09 (t, *J* = 7.06, 7.06 Hz, 2H), 1.84-1.65 (m, 2H), 1.28-1.06 (m, 6H), 0.77 (t, *J* = 8.87, 8.87 Hz, 3H) ppm.

^{13}C NMR (62.5 MHz, CD_2Cl_2): δ = 145.434, 123.074, 114.792, 111.525, 47.817, 31.837, 30.705, 27.037, 22.936, 14.179 ppm.

FD-MS: m/z = 263.42 (M^+, 100%).

Anal. Calcd. for $C_{14}H_{17}NS_2$: C, 63.83; H, 6.50. Found: C, 63.89; H, 6.45.

4-Hexyl-2,6-bis(trimethylstannyl)-4H-dithieno[3,2-*b*:2',3'-*d*]pyrrole (30)

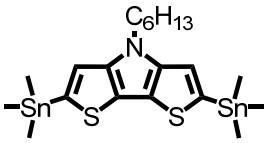

At 0 °C and under an argon atmosphere, *t*-BuLi (2.47 mL, 4.20 mmol, 1.7 M in pentane) was cannulated to a solution of **29** (0.527 g, 2.00 mmol) in dry diethyl ether (100 mL). After the reaction was stirred for 1 h at room temperature, a solution of Me_3SnCl 1M in Hexane (4.3 mL) was added dropwise via syringe. After stirring for another 2 h, the mixture was transferred into a separatory funnel and was successively washed with an ammonium chloride solution. The organic layer was dried over $MgSO_4$, and the solvent was removed via rotary evapour ation leaving dark green, viscous oil, which was used without further purification. (1.05 g)

^{1}H NMR (CD_2Cl_2): δ = 6.98 (s, 2H), 4.09 (m, *J* = 7.06 Hz, 2H), 1.84-1.65 (m, 2H), 1.28-1.06 (m, 6H), 0.77 (t, *J* = 8.87, 8.87 Hz, 3H) ppm.

FD-MS: m/z = 589.03 (M^+, 100.0%).

4-Hexyl-2,6-bis(2-(methylsulfinyl)phenyl)-4H-dithieno[3,2-b:2',3'-d]pyrrole (31)

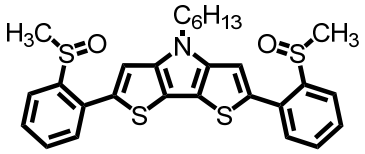

2-bromo(methylsulfinyl)benzene (736 mg, 3.36 mmol) was was added to a solution of 30 (0.9 g, 1.53 mmol) in anhydrous DMF (25 mL), and the resulting mixture was purged with Ar for 30 min. Pd(PPh3)4 (87 mg, 0.075 mmol) was then added, and the reaction mixture was heated to 80 °C overnight. Excess DMF was removed under high vacuum, and the residue was dissolved in ethyl acetate and treated with 10% aqueous KF. The mixture was filtered through a pad of Celite. The filtrate was dried over Mg2SO4, filtered, and the solvent removed in vacuo. The crude product was purified by flash chromatography (silica gel, eluent: hexane/THF

= 3:1) to afford 0.95 g (88%, related to 29) of 31 as off-white solid.

^{1}H NMR (250 MHz, CD_2Cl_2): δ = 7.03 (s, 2H), 7.40 (ddd, *J* = 14.20, 9.58, 4.15 Hz, 6H), 7.88 (d, *J* = 7.53 Hz, 2H), 4.06 (t, *J* = 6.88, 6.88 Hz, 2H), 2.30 (s, 6H), 1.77-1.61 (m, 2H), 1.18-0.99 (m, 6H), 0.66 (t, *J* = 6.68, 6.68 Hz, 3H) ppm.

^{13}C NMR (62.5MHz, CD_2Cl_2): δ = 145.553, 145.009, 136.753, 133.024, 131.181, 131.045, 129.456, 124.098, 115.986, 112.256, 47.98, 42.34, 31.82, 30.69, 27.11, 22.94, 14.14 ppm.

FD-MS: m/z = 539.80 (M+, 100.0%).

Anal. Calcd for $C_{28}H_{29}NO_2S_4$: C, 62.30; H, 5.42, Found: C, 62.35; H, 5.39.

Bisbenzo[*b*,*b*']thienodithieno[3,2-*b*:2',3'-*d*]pyrrole (BBTDP) (27)

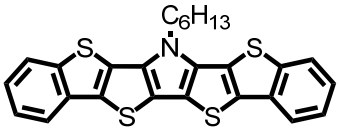

A 10 ml round bottomed flask was filled with 4-hexyl-2,6-bis(2-(methyl-sulfinyl)phenyl)-4H-dithieno [3,2-*b*:2',3'-*d*]pyrrole (**31**) (200 mg, 0.37 mmol), phosphorus pentoxide (28 mg, 0.2 mmol) and trifluoromethanesulfonic acid (6 ml). The mixture was stirred for 72 h at room temperature to give a dark blue solution, which was then poured into ice–water (100 ml). The yellow precipitate was collected by suction filtration and dried under vacuum. The structure of this compound, which was insoluble in apolar organic solvents, was assumed to be the sulfonium salt. Demethylation of the solid was achieved by refluxing in pyridine (30 ml) for 12 h. When the suspension was cooled to room temperature, a large volume of CH_2Cl_2 was added to extract the product. Bisbenzo[*b*,*b*']thienodithieno[3,2-*b*:2',3'-*d*]pyrrole (BBTDP) (**27**) was thus obtained as light yellow powder after silica chromatography with CH_2Cl_2/Hexane=1/9 as an eluent (145 mg, 85 % yield).

^{1}H NMR (300 MHz, CD_2Cl_2): δ = 7.91 (d, *J* = 7.83 Hz, 2H), 7.86 (d, *J* = 7.87 Hz, 2H), 7.52-7.44 (m, 2H), 7.41-7.33 (m, 2H), 4.48 (t, *J* = 7.13, 7.13 Hz, 2H), 2.13-2.00 (m, 2H), 1.32 (td, *J* = 13.44, 5.09, 5.09 Hz, 6H), 0.93-0.84 (m, 3H) ppm.

^{13}C NMR (62.5MHz, CD_2Cl_2): δ = 141.14, 136.53, 134.09, 133.65, 125.53, 124.41, 122.32, 120.42, 118.34, 32.36, 31.81, 30.07, 26.95, 22.84, 14.09 ppm.

FD-MS: m/z = 475,71 (M^+, 100%).

Anal. Calcd. for $C_{26}H_{21}NS_4$: C, 65.64; H, 4.45. Found: 64.70; H, 4.45.

4,4-Dihexyl-cyclopenta[2,1-*b*:3,4-*b'*]dithiophene (34)

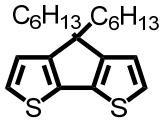

At 0 °C and under argon atmosphere, grinded KOH (0.2 g, 3.56 mmol) was added in portions to a solution of **1** (0.2 g, 1.12 mmol), 1-bromo hexane (463 mg, 2.8 mmol), and KI (5 mg, 30 mol) in DMSO (25 mL). After overnight stirring at room temperature, the solution was cooled in an ice bath and water (25 mL) was added. The crude compound was extracted with hexanes and extensively washed with water and a saturated NH_4Cl solution. After being dried over anhydrous MgSO4, the solvent was removed in vacuo. The crude compound was purified by column chromatography (silica gel; eluent: hexanes) and isolated as a clear oil. Yield: 360 mg (95%)

^{1}H NMR (250 MHz, CD_2Cl_2): δ = 7.22 (d, *J* = 4.87 Hz, 2H), 7.00 (d, *J* = 4.88 Hz, 2H), 1.92-1.82 (m, 4H), 1.23-1.09 (m, 12H), 0.96 (ddd, *J* = 6.77, 4.76, 1.55 Hz, 4H), 0.85 (t, *J* = 6.74, 6.74 Hz, 6H) ppm.

^{13}C NMR (62.5 MHz, CD_2Cl_2): δ = 157.19, 135.24, 123.34, 120.65, 52.23, 36.64, 30.54, 28.57, 23.39, 21.49, 12.69 ppm.

4,4-Dihexyl-2,6-bis(trimethylstannyl)cyclopenta[2,1-*b*:3,4-*b'*]dithio- phene (35)

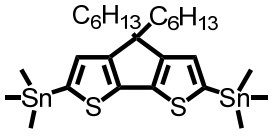

The same procedure was followed as described for the synthesis of **30**, starting from **34**. The product was isolated as yellow, viscous oil and was used without

further purification. (715 mg).

^{1}H NMR (250 MHz, CD_2Cl_2): δ = 6.90 (s, 2H), 1.92-1.82 (m, 4H), 1.23-1.09 (m, 12H), 0.96 (ddd, *J* = 6.77, 4.76, 1.55 Hz, 4H), 0.85 (t, *J* = 6.74, 6.74 Hz, 6H) ppm.

FD-MS: m/z = 672.20 (M^+, 100%).

4,4-Dihexyl-2,6-bis(2-(methylsulfinyl)phenyl)cyclopenta[2,1-*b*:3,4-*b*']dithiophene (36)

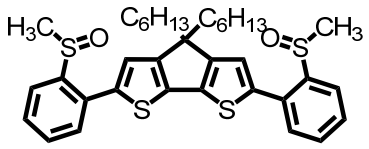

The same procedure was followed as described for the synthesis of **31**, starting from **35**. The crude product was purified by flash chromatography (silica gel, eluent: hexane/THF = 3:1) to afford 0.56 g (88% related to **34**) of **36**.

^{1}H NMR (250 MHz, CD_2Cl_2): δ = 8.06 (dd, *J* = 6.84, 1.20 Hz, 2H), 7.63-7.47 (m, 6H), 7.11 (s, 2H), 3.92-3.83 (m, 4H), 2.49 (s, 6H), 1.18 (td, *J* = 10.06, 9.33, 9.33 Hz, 12H), 1.04-0.89 (m, 4H), 0.81 (td, *J* = 13.44, 6.74, 6.74 Hz, 6H) ppm.

^{13}C NMR (62.5MHz, CD_2Cl_2): δ = 145.424, 139.72, 133.0, 131.54, 131.31, 129.81, 124.6, 123.27, 68.36, 38.57, 30.41, 29.94, 25.44, 23.36, 14.60 ppm.

FD-MS: m/z = 622,97 (M^+, 100%).

Anal. Calcd. for $C_{35}H_{42}O_2S_4$: C, 67.48; H, 6.80. Found: 67.40; H, 6.75.

Bisbenzo[*b*,*b*']thienocyclopenta[2,1-*b*:3,4-*b*']dithiophene (BBTCPDT) (32)

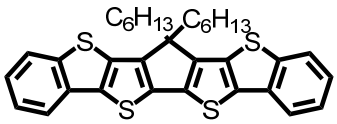

The same procedure was followed as described for the synthesis of **1**, starting from **13**. The product was isolated as light yellow oil after silica chromatography with CH_2Cl_2/Hexane=1/9 as an eluent and solidified to yellow crystals when cooled down (165 mg, 85 % yield).

^{1}H NMR (250 MHz, CD_2Cl_2): δ = 7.79 (t, *J* = 7.23, 7.23 Hz, 4H), 7.39-7.31 (m, 2H), 7.30-7.21 (m, 2H), 2.14-2.01 (m, 4H), 1.10-0.91 (m, 12H), 0.89-0.74 (m, 4H), 0.63 (t, *J* = 6.73, 6.73 Hz, 6H) ppm.

^{13}C NMR (62.5MHz, CD_2Cl_2): δ = 148.84, 142.13, 139.97, 135.72, 133.69, 132.72, 125.37, 124.47, 124.31, 120.5037.04, 31.82, 29.83, 24.86, 22.86, 14.06 ppm.

FD-MS: m/z = 558,15 (M^+, 100%).

Anal. Calcd. for $C_{33}H_{34}S_4$: C, 70.92; H, 6.13; Found: C, 70.98; H, 5.30.

Ethyl thieno[3,2-*b*]thiophene-2-carboxylate (39)

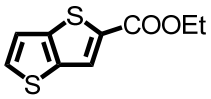

3-Bromothiophene-2-carbaldehyde **38** (25.71 g, 134.0 mmol) was added to a stirred mixture of ethyl 2-sulfanylacetate (14.8 ml, 16.22 g, 135.0 mmol), potassium carbonate (25.0 g) and *N*,*N*dimethylformamide (250 ml) at ambient temperature and the resulting mixture was stirred for a further 72 h. Then it was poured into water (500 ml) and extracted with dichloromethane. The combined extracts were dried ($MgSO_4$), filtered and distillation of the solvents under reduced pressure gave the *ester* **39** (23.0 g, 81%), bp: (Kugelrohr distillation) 120–125 °C at 0.1 mmHg.

^{1}H NMR (250 MHz, CD_2Cl_2): δ = 1.37 (3 H, t, *J* = 7.0 Hz, Me), 4.34 (2 H, q, *J* = 7.0 Hz, CH_2), 7.24 (1 H, d, *J* = 5.0 Hz), 7.55 (1 H, d, *J* = 5.0 Hz) and 7.97 (1 H, s) ppm.

FD-MS: m/z =212.29 (M^+, 100%).

Anal. Calcd. for $C_9HS_2O_2$: C, 50.9; H, 3.8; Found: C, 51.1; H, 5.30.

Thieno[3,2-*b*]thiophene-2-carboxylic acid (40)

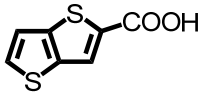

A stirred mixture of the ester **39** (15.0 g, 71.0 mmol), aqueous lithium hydroxide (1.0 mol /ml, 150 ml) and tetrahydrofuran (150 ml) was heated under reflux for 3 h (until TLC analysis indicated absence of starting material) when the solvent was

distilled off under reduced presssure and conc. Hydrochloric acid (300 ml) was added to the residue. The precipitate was filtered off, washed with water and dried in a vacuum desiccator, to give the acid **40** (11.76 g, 90%), mp 221–222 °C.

^{1}H NMR (250 MHz, DMSO): δ = 7.50 (1 H, d, *J* = 6,5 Hz), 7.91 (1 H, d, *J* = 5,6 Hz) and 8.09 (1 H, s) ppm.

FD-MS: m/z = 202 (M^+, 100%).

Thieno[3,2-*b*]thiophene (41)

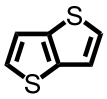

A stirred solution of the acid **40** (10.0 g, 54.3 mmol), copper powder (2.0 g) and quinoline (80 ml) was heated at 260 °C in a sand bath. When no further bubbles of carbon dioxide gas could be seen escaping from the mixture (~ 30 min) the reaction mixture was cooled to ambient temperature. TLC analysis confirmed the absence of starting material. Ether (100 ml) was added to the mixture and most of the quinoline was removed by repeated washing of the resulting solution with hydrochloric acid (1.0 M), after which the residue was chromatographed on silica. Light petroleum eluted compound **5** (6.70 g, 88%), mp 55–56 °C.

^{1}H NMR (250 MHz, CD_2Cl_2): δ = 7.25 (2 H, d, *J* = 5.0 Hz) and 7.37 (2 H, d, *J* = 5.0 Hz) ppm.

FD-MS: m/z = 140 (M^+, 100%).

Anal. Calcd. for $C_6H_4S_2$: C, 50.9; H, 2.8; Found: C, 51.39; H, 2.88.

2-Alkylthieno[3,2-*b*]thiophene (42a,b)

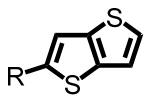

n-Butyllithium (23.1 g, 0.083 mol) was added dropwise to a solution of thieno[3,2-*b*]thiophene (13 g, 0.093 mol) in THF (200 mL) at -78 °C. One hour after addition, 1-bromohexane (15.3 g, 0.093 mol) was added to the solution. The reaction

mixture was then warmed to room temperature, stirred for another 5 h, and poured into water. The mixture was extracted with ether and dried over magnesium sulfate, and the solvent was evapour ated. The product was purified by vacuum distillation. **42a**. Yield: 10.3 g (55%), bp: 120-124 °C/1 mmHg.

^{1}H NMR (250 MHz, CD_2Cl_2): δ = 7.31 (d, 1H, *J* = 4.46 Hz), 7.23 (d, 1H, *J* = 4.46 Hz), 6.99 (s, 1H), 2.94 (t, 2H, *J* = 5.4, 5.4 Hz), 1.72-1.81 (m, 2H), 1.36-1.49 (m, 6H), 0.95 (t, 3H, *J* = 5.24, 5.24 Hz) ppm.

FD-MS: m/z = 224.39 (M^+, 100%).

42b. Yield: 12.5 g (65%), bp: 128-133 °C/1 mmHg.

FD-MS: m/z = 266.47 (M^+, 100%).

5-Alkylthieno[3,2-*b*]thiophen-2-yl)trimethylstannane (43a,b)

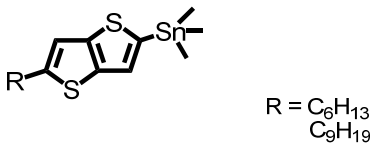

n-Butyllithium (6.94 mmol) was slowly added dropwise to a solution of 2-alkylthieno[3,2-*b*]thiophene (5.94 mmol) in anhydrous THF at −78 °C under Ar. The mixture was stirred at this temperature for 30 min and then for 1.5 h at room temperature followed, after cooling to -78 °C, by the addition of tributylstannyl chloride (7.52 mmol). After stirring for 4 h at room temperature, the reaction was terminated by adding a saturated NH_4Cl aqueous solution. The mixture was extracted with CH_2Cl_2 and dried over $MgSO_4$. After the removal of solvent, the crude tributyl(5-octylthieno[3,2-*b*]thiophen-2-yl)stannane (5.2 mmol) was collected and used without further purification.

5,5'-(2,5-Bis(methylsulfinyl)-1,4-phenylene)bis(2-hexylthieno[3,2-*b*]thiophene) (44a,b)

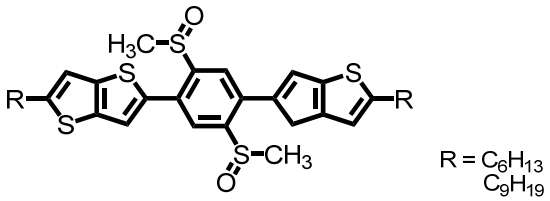

The crude 5-alkylthieno[3,2-b]thiophen-2-yl)trimethylstannane (5.2 mmol) was mixed with 1,4-dibromo-2,5-bis(methylsulfinyl)benzene (**3**) (1.72 mmol) in 150 mL DMF. The catalyst $Pd(PPh_3)_4$ (0.08 mmol) was added to the solution and the mixture was heated at 85 °C under Ar overnight. After the removal of DMF, the resulting solid was purified by column chromatography on silica gel using THF/Hexane = 1:1 as eluent to afford an deep red solid. Yield: 74%.

^{1}H NMR (250 MHz, CD_2Cl_2): δ = 8.73 (s, 2H, *J* = 5.66 Hz), 8.67 (d, 2H, *J* = 5.46 Hz), 7.84 (s, 2H), 7.52 (d, 2H, *J* = 5.64 Hz), 6.99 (s, 2H), 2.90 (t, 4H), 1.76−1.72 (m, 4H), 1.41−1.28 (m, 20H), 0.89 (t, 6H, *J* = 4.66, 4.56 Hz).

FD-MS: m/z = 647.03 (M^+, 100%) for **44a** and m/z = 731.19 (M^+, 100%) for **44b**.

Thieno[2',3':4,5]thieno[3,2-*b*]thieno[2'',3'':4',5']thieno[2',3':4,5]thieno[3,2-*f*][1]benzo thiophene (TTTTTBT) (37a,b)

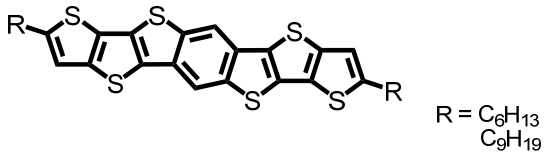

The same procedure was followed as described for the synthesis of **1**, starting from **44a,b**. The products were isolated as red solid but still a mixture after silica chromatography with CH_2Cl_2 as an eluent and several attempts to further purification were failed due to the low solubility.

FD-MS: m/z = 582.95 (M^+, 100%) for **37a** and m/z = 667.11 (M^+, 100%) for **37b**.

(4-bromobiphenyl-2,2',5-triyl)tris(methylsulfane) (47)

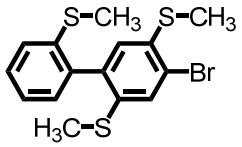

To a stirred solution of **46** (1.2 mmole) and about 2 mole % of $Pd[(PPh_3)]_4$ in 15 mL of THF was added with 5 mL of 2M K_2CO_3 under N_2 and 1 eqv. of 2-(methylthio)phenylboronic acid, respectively. After being heated to 85 °C for overnight, the reaction mixture was added with 50 mL of 2M NaCl and then

extracted twice with CH_2Cl_2 (50 mL). The combined organic layers were dried over anhydrous $MgSO_4$ and evapour ated to dryness. The crude product was purified by silica-gel column chromatography using petroleum ether and CH_2Cl_2 as eluent. Yield: 420 mg (95%).

^{1}H NMR (250 MHz, CD_2Cl_2): δ = 7.69 (d, 1H, *J* = 4.34 Hz), 7.45 (d, 1H, *J* = 4.74 Hz), 7.27-7.31 (m, 3H), 7.19 (s, 1H), 1.72-1.81 (m, 2H), 2.53 (s, 9H) ppm.

^{13}C NMR (62.5MHz, CD_2Cl_2): δ = 137.7, 137.4, 136.0, 131.4, 128.6, 125.2, 124.8, 124.4, 117.7 ppm.

FD-MS: m/z = 371.38 (M^+, 100%).

4,4,5,5-Tetramethyl-2-(2,2',5-tris(methylthio)biphenyl-4-yl)-1,3,2-dioxaborolane (48)

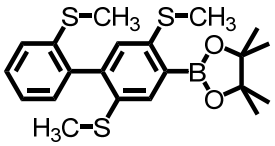

(4-bromobiphenyl-2,2',5-triyl)tris(methylsulfane) (220 mg, 0.6 mmol) was dissolved in absolute THF under argon. The solution was cooled to -78 °C before 0.4 ml (0.8 mmol) *n*-BuLi (1.6 M solution in hexane) were added dropwise. The reaction mixture was stirred for 30 min, before 0.2 ml (1.0 mmol) of 2-isopropoxy-4,4,5,5-tetramethyl-1,3,2-dioxaborolane was added. The reaction mixture was allowed to warm to room temperature and stirred for another 12 h before it was poured into ice water. The solution was extracted with diethyl ether, the organic phase washed with brine and dried with Na_2SO_4 before the solvent was removed. Purification by column chromatography on silica gel with hexane/THF (15:1) as an eluent yielded 213 mg (85%) of **48** as a light yellow oil.

^{1}H NMR (250 MHz, CD_2Cl_2): δ = 7.69 (d, 1H, *J* = 5.74 Hz), 7.45 (d, 1H, *J* = 5.64 Hz), 7.27-7.31 (m, 3H), 7.19 (s, 1H), 1.72-1.81 (m, 2H), 2.53 (m, 9H), 1.24 (s, 12H) ppm.

^{13}C NMR (62.5MHz, CD_2Cl_2): δ = 137.4, 135.7, 134.5, 133.8, 131.4, 128.6, 125.4, 124.38, 88.1, 24.7, 15.1 ppm.

FD-MS: m/z = 418.44 (M^+, 100%).

1,1′:4′,1′:4′′,1′′′-Quaterphenyl, 2,2',2'',2''',5',5''-hexamethylthio-(9CI) (49)

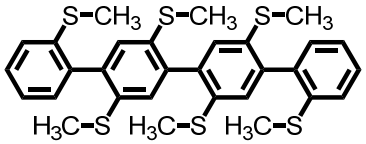

To a stirred solution of **48** (0.51 mmole) and about 2 mole % of $Pd[(PPh_3)]_4$ in 15 mL of toluene was added with 5 mL of 2M K_2CO_3 under N_2 and 1 eqv. of (4-bromobiphenyl-2,2',5-triyl)tris(methylsulfane), respectively. After being heated to 85 ^oC for overnight, the reaction mixture was added with 50 mL of 2M NaCl and then extracted twice with CH_2Cl_2 (50 mL). The combined organic layers were dried over anhydrous $MgSO_4$ and evapour ated to dryness. The crude product was purified by silica-gel column chromatography using petroleum ether and CH_2Cl_2 as eluent. Yield: 238 mg (95%).

^{1}H NMR (250 MHz, CD_2Cl_2): δ = 7.64 (d, 2H, *J* = 5.6 Hz), 7.45-7.31 (m, 10H), 2.53 (m, 18H) ppm.

^{13}C NMR (62.5MHz, CD_2Cl_2): δ = 137.4, 134.3, 131.4, 128.6, 125.8, 126.2, 125.6, 124.7 ppm.

FD-MS: m/z = 582.95 (M^+, 100%).

Dibenzo[*b*,*b*']thieno[2,3-*f*:5,4-*f*']bis[1]benzothiophene (45)

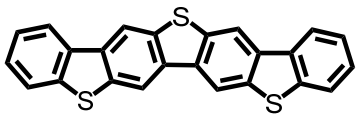

To a solution of compound **49** (100 mg, 0.17 mmol) in 40 mL of *N*-methyl-2-pyrrolidone (NMP) was added a large excess of sodium methylthiolate (1.41 g, 20 mmol) with stirring under reflux conditions. After 20 h, the solution was quenched with a 10 ml of 10% HCI solution at room temperature and 100 ml of water. The yellowish precipitation was filtered out and collected. Yield: 65 mg (96%).

FD-MS: m/z = 396.55 (M^+, 100%).

6.3. Reference

[1] Gaussian 03, Revision B.04, M. J. Frisch, G. W. Trucks, H. B. Schlegel, G. E. Scuseria, M. A. Robb, J. R. Cheeseman, J. A. Montgomery, Jr., T. Vreven, K. N. Kudin, J. C. Burant, J. M. Millam, S. S. Iyengar, J. Tomasi, V. Barone, B. Mennucci, M. Cossi, G. Scalmani, N. Rega, G. A. Petersson, H. Nakatsuji, M. Hada, M. Ehara, K. Toyota, R. Fukuda, J. Hasegawa, M. Ishida, T. Nakajima, Y. Honda, O. Kitao, H. Nakai, M. Klene, X. Li, J. E. Knox, H. P. Hratchian, J. B. Cross, V. Bakken, C. Adamo, J. Jaramillo, R. Gomperts, R. E. Stratmann, O. Yazyev, A. J. Austin, R. Cammi, C. Pomelli, J. W. Ochterski, P. Y. Ayala, K. Morokuma, G. A. Voth, P. Salvador, J. J. Dannenberg, V. G. Zakrzewski, S. Dapprich, A. D. Daniels, M. C. Strain, O. Farkas, D. K. Malick, A. D. Rabuck, K. Raghavachari, J. B. Foresman, J. V. Ortiz, Q. Cui, A. G. Baboul, S. Clifford, J. Cioslowski, B. B. Stefanov, G. Liu, A. Liashenko, P. Piskorz, I. Komaromi, R. L. Martin, D. J. Fox, T. Keith, M. A. Al-Laham, C. Y. Peng, A. Nanayakkara, M. Challacombe, P. M. W. Gill, B. Johnson, W. Chen, M. W. Wong, C. Gonzalez, J. A. Pople, Gaussian, Inc., Wallingford, CT, **2004**.

[2] A. D. Becke, *J. Chem. Phys.* **1993**, *98*, 1372-1377.

Appendix
Single Crystal Structures

A1. benzo[1,2-*b*:4,5-*b'*]bis[*b*]benzothiophene (1a)

Atomic parameters

Atom	x / a	y / b	z / c	U [Å^2]
S1	0.74849(3)	0.16147(5)	0.50447(3)	
C1	1.03768(13)	0.2994(2)	0.56927(11)	
C2	0.89643(13)	0.3411(2)	0.50862(10)	
C3	0.85710(13)	0.5397(2)	0.43954(10)	
C4	0.70376(13)	0.5426(2)	0.38399(10)	
C5	0.63187(13)	0.3482(2)	0.4123(1)	
C6	0.48278(14)	0.3194(2)	0.37036(12)	
C7	0.40657(14)	0.4858(2)	0.29751(11)	
C8	0.47680(14)	0.6774(2)	0.26579(11)	
C9	0.62499(14)	0.7068(2)	0.30894(11)	
H11	1.0603	0.1641	0.6157	0.05
H61	0.437	0.1865	0.3927	0.05
H71	0.304	0.4709	0.2686	0.05
H81	0.4227	0.7886	0.2136	0.05
H91	0.6723	0.8393	0.2881	0.05

Anisotropic displacement parameters, in Å^2

Atom	U_{11}	U_{22}	U_{33}	U_{12}	U_{13}	U_{23}
S1	0.01382(16)	0.01401(16)	0.01906(16)	-0.00288(11)	0.00297(10)	0.00220(11)
C1	0.0144(5)	0.0126(5)	0.0137(5)	0.0000(4)	0.0035(4)	0.0020(4)
C2	0.0128(5)	0.0130(5)	0.0125(5)	-0.0025(4)	0.0037(4)	-0.0006(4)
C3	0.0132(5)	0.0121(5)	0.0110(5)	-0.0001(4)	0.0024(4)	-0.0010(4)
C4	0.0128(5)	0.0145(5)	0.0116(5)	-0.0004(4)	0.0028(4)	-0.0017(4)
C5	0.0133(5)	0.0159(6)	0.0126(5)	-0.0002(5)	0.0031(4)	-0.0011(4)
C6	0.0143(6)	0.0220(6)	0.0171(5)	-0.0041(5)	0.0040(4)	-0.0032(5)
C7	0.0117(5)	0.0262(7)	0.0164(5)	-0.0002(5)	0.0015(4)	-0.0034(5)
C8	0.0157(6)	0.0211(6)	0.0161(5)	0.0036(5)	0.0018(4)	0.0004(5)
C9	0.0156(6)	0.0175(6)	0.0139(5)	0.0004(5)	0.0027(4)	-0.0004(4)

Selected geometric informations

Atoms 1,2	d 1,2 [Å]	Atoms 1,2	d 1,2 [Å]	Atoms 1,2	d 1,2 [Å]
S1-2	1.7520(12)	C5-6	1.4002(17)	C2-3	1.4213(17)
S1-5	1.7469(13)	C6-7	1.3882(19)	C3-4	1.4540(17)
C1-3i	1.3987(17)	C6-61	0.96	C4-5	1.4110(17)
C1-2	1.3894(17)	C7-8	1.403(2)	C4-9	1.4010(17)
C1-11	0.96	C7-71	0.96	C8-81	0.96
		C8-9	1.3944(18)	C9-91	0.96

Atoms 1,2,3	Angle 1,2,3 [°]	Atoms 1,2,3	Angle 1,2,3 [°]	Atoms 1,2,3	Angle 1,2,3 [°]
C2-1-5	91.68(6)	C4-5-6	121.48(12)	C2-3-1i	119.96(11)
C3i-1-2	117.84(11)	S1-5-6	126.06(11)	C2-3-4	111.71(11)
C3i-1-11	122.159	C5-6-7	118.28(13)	C1i-3-4	128.33(11)
C2-1-11	120.001	C5-6-61	119.292	C3-4-5	112.08(11)
S1-2-1	125.71(10)	C7-6-61	122.425	C3-4-9	128.71(12)
S1-2-3	112.07(9)	C6-7-8	121.07(12)	C5-4-9	119.21(11)
C1-2-3	122.20(11)	C6-7-71	119.797	C4-5-1	112.46(9)
C4-9-91	120.335	C8-7-71	119.134	C7-8-81	119.849
C8-9-91	120.181	C7-8-9	120.45(12)	C9-8-81	119.703
				C4-9-8	119.48(12)

(i) 2-x, 1-y, 1-z.

A2. benzo[1,2-*b*:4,5-*b'*]bis[*b*]benzothiophene-C4 (1b)

Atomic parameters

Atom	x/a	y/b	z/c	U [Å^2]
S1	0.54339(12)	0.79951(6)	0.54116(4)	
C2	0.8054(4)	0.6322(2)	0.52620(18)	
C3	0.8139(4)	0.5577(2)	0.42632(17)	
C4	0.6048(5)	0.6379(2)	0.36286(16)	
C5	0.4427(5)	0.7712(2)	0.41492(17)	
C6	0.1793(5)	0.8300(2)	0.26602(17)	
C7	0.2310(5)	0.8661(2)	0.36853(18)	
C8	0.3407(5)	0.6965(2)	0.21357(17)	
C9	0.5494(5)	0.6013(2)	0.26060(18)	
C10	0.9865(5)	0.5779(2)	0.59969(18)	
C11	-0.0305(5)	0.9382(2)	0.21188(18)	
C12	0.1201(5)	1.0626(2)	0.1610(2)	
C13	-0.0911(5)	1.1816(3)	0.1124(2)	

C14	0.0628(7)	1.3025(3)	0.0607(2)	
H71	0.1218	0.9548	0.4061	0.0275
H81	0.3081	0.6714	0.1435	0.0237
H91	0.6579	0.5121	0.2236	0.0294
H101	0.9782	0.6317	0.6653	0.0276
H111	-0.1978	0.981	0.2661	0.0294
H112	-0.0996	0.8892	0.1573	0.0294
H121	0.1982	1.1077	0.2151	0.0334
H122	0.2815	1.0196	0.1046	0.0334
H131	-0.2534	1.2243	0.1686	0.0357
H132	-0.1681	1.1369	0.0578	0.0357
H141	-0.0774	1.3739	0.0315	0.0485
H142	0.1395	1.3485	0.1148	0.0485
H143	0.2247	1.261	0.004	0.0485

Anisotropic displacement parameters, in Å²

Atom	U_{11}	U_{22}	U_{33}	U_{12}	U_{13}	U_{23}
S1	0.0175(2)	0.0207(3)	0.0186(3)	-0.00277(18)	-0.00274(18)	0.00017(18)
C2	0.0120(8)	0.0151(8)	0.0223(10)	-0.0053(7)	0.0005(7)	0.0007(7)
C3	0.0149(9)	0.0163(9)	0.0203(10)	-0.0069(7)	-0.0025(7)	0.0036(7)
C4	0.0175(9)	0.0189(9)	0.0161(9)	-0.0069(7)	-0.0033(7)	0.0012(7)
C5	0.0159(9)	0.0195(9)	0.0202(10)	-0.0084(7)	-0.0026(7)	0.0034(8)
C6	0.0170(9)	0.0153(9)	0.0206(10)	-0.0066(7)	-0.0032(7)	0.0048(7)
C7	0.0144(9)	0.0199(9)	0.0212(10)	-0.0052(7)	-0.0001(7)	0.0017(8)
C8	0.0218(10)	0.0233(10)	0.0145(9)	-0.0075(8)	-0.0049(7)	0.0022(8)
C9	0.0212(10)	0.0200(9)	0.0204(10)	-0.0060(8)	0.0002(8)	0.0008(8)
C10	0.0188(9)	0.0174(9)	0.0225(10)	-0.0059(8)	-0.0004(8)	0.0035(8)
C11	0.0209(10)	0.0206(10)	0.0217(10)	-0.0048(8)	-0.0059(8)	0.0026(8)
C12	0.022(1)	0.021(1)	0.0253(10)	-0.0043(8)	-0.0028(8)	0.0043(8)
C13	0.0255(11)	0.0263(11)	0.0276(12)	-0.0055(9)	-0.0101(9)	0.0054(9)
C14	0.0408(14)	0.0276(12)	0.0343(14)	-0.0095(11)	-0.0099(11)	0.0116(10)

Selected geometric informations

Atoms 1,2	d 1,2 [Å]	Atoms 1,2	d 1,2 [Å]	Atoms 1,2	d 1,2 [Å]
S1-2	1.756(2)	C9-91	0.95	C6-8	1.407(3)
S1-5	1.754(2)	C10-101	0.95	C6-11	1.499(3)
C2-3	1.416(3)	C11-12	1.527(3)	C7-71	0.95
C2-10	1.378(3)	C11-111	0.95	C8-9	1.384(3)
C3-10i	1.404(3)	C11-112	0.95	C8-81	0.95
C3-4	1.449(3)	C12-13	1.522(3)	C6-8	1.407(3)
C4-5	1.404(3)	C12-121	0.95	C13-132	0.95

C4-9	1.400(3)	C12-122	0.95	C14-141	0.95
C5-7	1.387(3)	C13-14	1.512(3)	C14-142	0.95
C6-7	1.395(3)	C13-131	0.95	C14-143	0.95

Atoms 1,2,3	**Angle 1,2,3 [°]**	**Atoms 1,2,3**	**Angle 1,2,3 [°]**	**Atoms 1,2,3**	**Angle 1,2,3 [°]**
C2-1-5	91.89(10)	C3i-10-101	121.285	C6-7-71	120.17
S1-2-3	111.38(16)	C2-10-101	120.756	C5-7-71	120.47
S1-2-10	125.71(17)	C6-11-12	111.95(18)	C6-8-9	121.8(2)
C3-2-10	122.90(19)	C6-11-111	107.789	C6-8-81	119.261
C2-3-10i	119.15(19)	C12-11-111	107.974	C9-8-81	118.946
C2-3-4	112.40(18)	C6-11-112	110.204	C4-9-8	119.7(2)
C10i-3-4	128.46(19)	C12-11-112	109.393	C4-9-91	119.665
C3-4-5	112.36(18)	H111-11-112	109.467	C8-9-91	120.626
C3-4-9	129.36(19)	C11-12-13	113.90(19)	C3i-10-2	118.0(2)
C5-4-9	118.28(19)	C11-12-121	108.879	C12-13-132	108.594
S1-5-4	111.97(15)	C13-12-121	108.467	C14-13-132	107.99
S1-5-7	125.86(17)	C11-12-122	107.537	H131-13-132	109.467
C4-5-7	122.2(2)	C13-12-122	108.533	C13-14-141	110.152
C7-6-8	118.70(19)	H121-12-122	109.467	C13-14-142	108.676
C7-6-11	119.37(19)	C12-13-14	113.2(2)	H141-14-142	109.476
C8-6-11	121.82(19)	C12-13-131	108.656	C13-14-143	109.568
C6-7-5	119.4(2)	C14-13-131	108.879	H141-14-143	109.476
				H142-14-143	109.476

(i) 2-x, 1-y, 1-z.

A3. dithieno[2,3-*d*;2′,3′-*d*′]benzo-[1,2-*b*;4,5-*b*′]dithiophene-C6 (2b)

Atomic parameters

Atom	**x / a**	**y / b**	**z / c**	**U [Å²]**
S1	0.93208(6)	0.28128(5)	0.13923(2)	
S2	1.35428(7)	0.86354(5)	0.11683(2)	
C3	1.4509(3)	0.6699(2)	0.04991(7)	
C4	1.1415(3)	0.6699(2)	0.14661(8)	
C5	1.3159(2)	0.4607(2)	0.04963(7)	
C6	0.4246(3)	-0.0361(2)	0.37020(8)	
C7	1.6335(3)	0.7108(2)	0.00170(7)	
C8	1.1415(2)	0.4685(2)	0.10642(7)	
C9	0.6634(2)	0.2263(2)	0.29571(7)	
C10	0.4354(2)	0.1741(2)	0.33905(8)	
C11	0.8453(2)	0.4767(2)	0.20676(8)	
C12	0.9736(3)	0.6754(2)	0.20399(8)	

C13	0.6414(3)	0.4207(3)	0.25636(9)	
C14	0.1988(3)	-0.0804(2)	0.41527(9)	
C15	0.1760(3)	-0.2976(3)	0.44133(10)	
H15A	0.03233	-0.31635	0.46962	0.0483
H15B	0.3288	-0.30615	0.4737	0.0483
H15C	0.15342	-0.40764	0.39727	0.0483
H14A	0.21752	0.02535	0.46049	0.038
H14B	0.04214	-0.07613	0.38406	0.038
H6A	0.40848	-0.15136	0.3281	0.033
H6B	0.57817	-0.03471	0.40374	0.033
H10A	0.28508	0.17041	0.30382	0.0334
H10B	0.44418	0.2888	0.38097	0.0334
H9A	0.81717	0.25578	0.33113	0.0306
H9B	0.6736	0.10803	0.25685	0.0306
H13A	0.48173	0.39919	0.22388	0.0371
H13B	0.64995	0.54429	0.29475	0.0371
H12	0.96449	0.80917	0.23502	0.0332
H7	1.71916	0.85382	0.00345	0.03

Anisotropic displacement parameters, in Å²

Atom	U_{11}	U_{22}	U_{33}	U_{12}	U_{13}	U_{23}
S1	0.0302(2)	0.0254(2)	0.0244(2)	0.00046(13)	0.00293(13)	0.00404(14)
S2	0.0422(2)	0.0211(2)	0.0245(2)	0.00113(15)	0.00621(14)	0.00178(14)
C3	0.0355(6)	0.0210(6)	0.0179(6)	0.0007(5)	-0.0010(5)	0.0032(5)
C4	0.0339(6)	0.0226(7)	0.0200(6)	0.0036(5)	-0.0001(5)	0.0050(5)
C5	0.0307(6)	0.0225(6)	0.0153(5)	0.0000(5)	-0.0022(4)	0.0040(4)
C6	0.0283(6)	0.0280(7)	0.0282(7)	0.0083(5)	0.0067(5)	0.0029(5)
C7	0.0349(6)	0.0220(7)	0.0185(6)	0.0001(5)	-0.0009(5)	0.0027(5)
C8	0.0293(6)	0.0242(7)	0.0185(6)	0.0014(5)	-0.0013(4)	0.0044(5)
C9	0.0244(5)	0.0283(7)	0.0244(6)	0.0065(5)	0.0035(4)	0.0037(5)
C10	0.0272(6)	0.0293(7)	0.0291(7)	0.0086(5)	0.0072(5)	0.0053(5)
C11	0.0286(6)	0.0295(7)	0.0233(6)	0.0065(5)	0.0001(5)	0.0060(5)
C12	0.0339(6)	0.0274(7)	0.0241(6)	0.0078(5)	0.0025(5)	0.0050(5)
C13	0.0283(6)	0.0345(8)	0.0341(7)	0.0100(5)	0.0064(5)	0.0106(6)
C14	0.0350(7)	0.0305(8)	0.0344(7)	0.0075(5)	0.0127(5)	0.0060(6)
C15	0.0483(9)	0.0321(8)	0.0488(10)	0.0041(6)	0.0150(7)	0.0078(7)

Selected geometric informations

Atoms 1,2	d 1,2 [Å]	Atoms 1,2	d 1,2 [Å]	Atoms 1,2	d 1,2 [Å]
S1-8	1.726(2)	C9-9B	0.960(2)	C4-12	2.066(2)
S1-11	1.749(3)	C9-13A	2.053(2)	C5-7i	2.073(2)
S2-3	1.758(2)	C9-13B	2.048(2)	C6-14A	2.056(2)

S2-4	1.738(3)	C10-6A	2.048(3)	C6-14B	2.065(2)
C3-5	1.430(3)	C10-6B	2.051(3)	C6-6A	0.960(2)
C3-7	1.381(3)	C10-10A	0.960(2)	C6-6B	0.960(2)
C4-8	1.381(4)	C10-10B	0.960(2)	C6-10A	2.051(2)
C4-12	1.420(3)	C10-9A	2.056(2)	C6-10B	2.048(3)
C5-7i	1.397(3)	C10-9B	2.063(2)	C7-7	0.960(2)
C5-8	1.437(3)	C11-13A	1.999(2)	C9-10A	2.024(2)
C6-10	1.520(4)	C11-13B	1.989(2)	C9-10B	2.029(2)
C6-14	1.526(3)	C11-12	2.109(3)	C9-9A	0.960(2)
C9-10	1.526(3)	C12-12	0.960(3)	C14-15B	2.046(3)
C9-13	1.521(4)	C13-9A	2.038(3)	C14-15C	2.050(3)
C11-12	1.368(4)	C13-9B	2.033(3)	C14-14A	0.960(3)
C11-13	1.502(3)	C13-13A	0.960(3)	C14-14B	0.960(3)
C14-15	1.518(4)	C13-13B	0.960(3)	C14-6A	2.031(2)
C3-7	2.039(2)	C14-15A	2.051(3)	C14-6B	2.039(2)
C15-15C	0.960(3)	C15-14B	2.020(3)	C15-15A	0.960(3)
C15-14A	2.025(3)			C15-15B	0.960(3)

Atoms 1,2,3	**Angle 1,2,3 [°]**	**Atoms 1,2,3**	**Angle 1,2,3 [°]**	**Atoms 1,2,3**	**Angle 1,2,3 [°]**
C8-1-11	91.67(12)	S1-11-13B	147.7(2)	C6-10-9B	97.24(14)
C3-2-4	91.03(11)	S1-11-12	132.53(14)	C9-10-6A	100.5(2)
S2-3-5	112.4(2)	C12-11-13A	127.8(2)	C9-10-6B	98.98(15)
S2-3-7	125.0(2)	C12-11-13B	100.3(2)	C9-10-10A	106.8(2)
C5-3-7	122.6(2)	C12-11-12	20.72(11)	C9-10-10B	107.2(2)
S2-4-8	112.3(2)	C13-11-13A	27.42(11)	C9-10-9A	26.12(9)
S2-4-12	133.5(2)	C13-11-13B	27.68(12)	C9-10-9B	25.91(10)
C8-4-12	114.2(2)	C13-11-12	106.6(2)	H6A-10-6B	44.97(6)
C3-5-7i	119.5(2)	H13A-11-13B	46.29(5)	H6A-10-10A	94.4(2)
C3-5-8	109.7(2)	H13A-11-12	110.94(11)	H6A-10-10B	135.5(2)
C7i-5-8	130.8(2)	H13B-11-12	79.57(9)	H6A-10-9A	100.28(10)
C10-6-14	113.1(2)	C4-12-12	119.2(3)	H6A-10-9B	77.67(8)
C3-7-5i	117.9(2)	C11-12-12	129.0(3)	H6B-10-10A	135.7(2)
S1-8-4	110.6(2)	C9-13-9A	26.55(9)	H6B-10-10B	96.0(2)
S1-8-5	134.9(2)	C9-13-9B	26.7(1)	H6B-10-9A	80.77(9)
C4-8-5	114.5(2)	C9-13-13A	109.7(2)	H6B-10-9B	91.28(9)
C10-9-13	111.4(2)	C9-13-13B	109.2(2)	H10A-10-10B	109.5(2)
C6-10-9	114.4(2)	C11-13-9A	102.6(2)	H10A-10-9A	132.4(2)
S1-11-12	111.8(2)	C11-13-9B	99.1(2)	H10A-10-9B	96.5(2)
S1-11-13	120.8(2)	C11-13-13A	106.5(2)	H10B-10-9A	90.7(2)
C12-11-13	127.3(2)	C11-13-13B	105.7(2)	H10B-10-9B	132.9(2)
C4-12-11	111.8(2)	H9A-13-9B	45.30(6)	H9A-10-9B	44.75(5)
C9-13-11	116.1(2)	H9A-13-13A	136.1(2)	S1-11-13A	110.38(12)
C6-14-15	113.2(2)	H9A-13-13B	93.1(2)	C9-10A-10	46.2(2)

S2-3-7	100.91(11)	H9B-13-13A	97.5(2)	C6-10B-9	77.78(9)
C5-3-7	146.7(2)	H9B-13-13B	135.7(2)	C6-10B-10	44.5(2)
C7-3-7	24.05(11)	H13A-13-13B	109.5(2)	C9-10B-10	45.9(2)
S2-4-12	109.59(12)	C6-14-15A	139.4(2)	C9-9A-10	44.4(2)
C8-4-12	138.1(2)	C6-14-15B	98.5(2)	C9-9A-13	45.1(2)
C12-4-12	23.92(11)	C6-14-15C	98.8(2)	C10-9A-13	75.86(10)
C3-5-7i	142.6(2)	C6-14-14A	109.4(2)	C9-9B-10	44.0(2)
C7i-5-7i	23.11(11)	C6-14-14B	110.2(2)	C9-9B-13	45.4(2)
C8-5-7i	107.7(2)	C6-14-6A	26.82(10)	C10-9B-13	75.82(10)
C10-6-14A	100.25(14)	C6-14-6B	26.59(10)	C9-13A-11	78.49(9)
C10-6-14B	97.32(14)	C15-14-15A	26.16(12)	C9-13A-13	44.2(2)
C10-6-6A	109.3(2)	C15-14-15B	26.31(13)	C11-13A-13	46.1(2)
C10-6-6B	109.5(2)	C15-14-15C	26.18(12)	C9-13B-11	78.84(10)
C10-6-10A	26.17(10)	C15-14-14A	107.4(2)	C9-13B-13	44.5(2)
C10-6-10B	26.26(10)	C15-14-14B	107.0(2)	C11-13B-13	46.6(2)
C14-6-14A	26.13(11)	C15-14-6A	96.6(2)	C4-12-11	67.12(10)
C14-6-14B	25.87(11)	C15-14-6B	99.5(2)	C4-12-12	36.8(2)
C14-6-6A	107.4(2)	H15A-14-15B	45.00(6)	C11-12-12	30.3(2)
C14-6-6B	108.0(2)	H15A-14-15C	44.95(6)	C3-7-5i	70.71(9)
C14-6-10A	99.2(2)	H15A-14-14A	92.8(2)	C3-7-7	35.9(2)
C14-6-10B	97.8(2)	H15A-14-14B	92.6(2)	C5i-7-7	34.8(2)
H14A-6-14B	44.73(5)	H15A-14-6A	120.69(13)	H10A-9-13B	90.98(9)
H14A-6-6A	133.4(2)	H15A-14-6B	123.00(14)	H10B-9-9A	92.3(2)
H14A-6-6B	92.8(2)	H15B-14-15C	45.01(6)	H10B-9-9B	136.7(2)
H14A-6-10A	97.31(10)	H15B-14-14A	93.7(2)	H10B-9-13A	93.80(9)
H14A-6-10B	78.43(8)	H15B-14-14B	133.3(2)	H10B-9-13B	79.17(8)
H14B-6-6A	95.2(2)	H15B-14-6A	92.12(10)	H9A-9-9B	109.5(2)
H14B-6-6B	133.9(2)	H15B-14-6B	78.08(9)	H9A-9-13A	134.4(2)
H14B-6-10A	77.40(8)	H15C-14-14A	133.6(2)	H9A-9-13B	92.5(2)
H14B-6-10B	91.93(9)	H15C-14-14B	93.5(2)	H9B-9-13A	96.2(2)
H6A-6-6B	109.5(2)	H15C-14-6A	76.07(9)	H9B-9-13B	134.0(2)
H6A-6-10A	94.2(2)	H15C-14-6B	95.96(11)	H13A-9-13B	44.94(5)
H6A-6-10B	135.5(2)	H14A-14-14B	109.5(2)	C6-10-6A	26.26(10)
H6B-6-10A	135.7(2)	H14A-14-6A	136.1(2)	C6-10-6B	26.17(10)
H6B-6-10B	96.2(2)	H14A-14-6B	93.8(2)	C6-10-10A	109.5(2)
H10A-6-10B	44.97(5)	H14B-14-6A	97.3(2)	C6-10-10B	109.3(2)
C3-7-7	120.1(2)	H14B-14-6B	136.7(2)	C6-10-9A	102.92(15)
C5i-7-7	122.1(2)	H6A-14-6B	45.31(5)	C14-15B-15	44.5(2)
C10-9-10A	27.01(10)	C14-15-15A	109.6(3)	C14-15C-15	44.2(2)
C10-9-10B	26.86(10)	C14-15-15B	109.2(3)	C6-14A-14	44.4(2)
C10-9-9A	109.5(2)	C14-15-15C	109.6(3)	C6-14A-15	77.06(11)
C10-9-9B	110.1(2)	C14-15-14A	26.90(11)	C14-14A-15	45.7(2)
C10-9-13A	95.21(14)	C14-15-14B	27.03(12)	C6-14B-14	43.9(2)
C10-9-13B	98.9(2)	H15A-15-15B	109.5(3)	C6-14B-15	76.96(11)

C13-9-10A	93.17(14)	H15A-15-15C	109.5(3)	C14-14B-15	45.9(2)
C13-9-10B	99.29(14)	H15A-15-14A	94.5(2)	C6-6A-10	44.5(2)
C13-9-9A	108.4(2)	H15A-15-14B	94.5(2)	C6-6A-14	45.8(2)
C13-9-9B	107.9(2)	H15B-15-15C	109.5(3)	C10-6A-14	77.07(10)
C13-9-13A	26.12(10)	H15B-15-14A	95.0(2)	C6-6B-10	44.3(2)
C13-9-13B	26.27(11)	H15B-15-14B	136.2(3)	C6-6B-14	45.4(2)
H10A-9-10B	45.51(5)	H15C-15-14A	136.5(3)	C10-6B-14	76.82(10)
H10A-9-9A	136.0(2)	H15C-15-14B	95.3(2)	C6-10A-9	77.83(10)
H10A-9-9B	99.0(2)	H14A-15-14B	45.61(7)	C6-10A-10	44.3(2)
H10A-9-13A	71.70(7)	C14-15A-15	44.2(2)		

(i) 3-x, -y, -z.

A4. dithieno[2,3-*d*;2′,3′-*d*′]benzo-[1,2-*b*;4,5-*b*′]dithiophene (2c)

Atomic parameters

Atom	x / a	y / b	z / c	U [Å^2]
S1	1.26009(7)	-0.81229(5)	0.09369(2)	
S2	0.82679(6)	-0.21311(5)	0.11247(1)	
C1	1.6292(3)	-0.7131(2)	0.00048(6)	
C2	1.4093(3)	-0.6485(2)	0.03991(6)	
C3	1.2789(3)	-0.4371(2)	0.04018(6)	
C4	1.0602(3)	-0.4175(2)	0.08597(6)	
C5	1.0270(3)	-0.6017(2)	0.11808(6)	
C6	0.8130(3)	-0.5810(2)	0.16404(7)	
C7	0.6851(3)	-0.3792(2)	0.16658(6)	
C8	0.4410(3)	-0.2995(2)	0.20564(7)	
C9	0.4419(3)	-0.1043(2)	0.24224(7)	
C10	0.1741(3)	-0.0277(2)	0.27426(7)	
C11	0.1491(3)	0.1790(2)	0.30695(7)	
C12	-0.1227(3)	0.2514(2)	0.33745(7)	
C13	-0.1537(3)	0.4610(2)	0.36863(8)	
C14	-0.4294(3)	0.5388(2)	0.39580(7)	
C15	-0.4547(3)	0.7402(3)	0.43106(8)	
C16	-0.7299(3)	0.8199(3)	0.45805(8)	
H11	1.7136	-0.8549	0.0011	0.0253
H61	0.765	-0.6938	0.1898	0.0295
H81	0.4063	-0.4084	0.2348	0.0294
H82	0.3058	-0.2676	0.1785	0.0294
H91	0.5622	-0.1374	0.2731	0.0267
H92	0.4912	0.0031	0.2144	0.0267
H101	0.1336	-0.1318	0.3045	0.0271
H102	0.0533	-0.0094	0.2434	0.0271

H111	0.2671	0.1611	0.3385	0.0303
H112	0.191	0.2835	0.277	0.0303
H121	-0.1621	0.1484	0.3682	0.0283
H122	-0.2409	0.2647	0.306	0.0283
H131	-0.0427	0.4456	0.4016	0.0321
H132	-0.1049	0.5623	0.3384	0.0321
H141	-0.4829	0.4334	0.4238	0.0296
H142	-0.5388	0.5641	0.3624	0.0296
H151	-0.3455	0.7144	0.4645	0.0372
H152	-0.4	0.8451	0.403	0.0372
H161	-0.734	0.945	0.4794	0.0424
H162	-0.7863	0.7168	0.4865	0.0424
H163	-0.8407	0.8475	0.425	0.0424

Anisotropic displacement parameters, in Å²

Atom	**U_{11}**	**U_{22}**	**U_{33}**	**U_{12}**	**U_{13}**	**U_{23}**
S1	0.03078(19)	0.01632(17)	0.02232(18)	0.00196(13)	0.00550(13)	0.00027(12)
S2	0.02181(17)	0.01814(16)	0.01872(16)	0.00193(12)	0.00044(12)	-0.00102(12)
C1	0.0255(6)	0.0173(6)	0.0157(6)	0.0014(5)	-0.0023(5)	-0.0015(4)
C2	0.0254(6)	0.0170(6)	0.0142(6)	0.0015(5)	-0.0016(5)	-0.0001(4)
C3	0.0223(6)	0.0173(6)	0.0134(5)	0.0019(5)	-0.0032(4)	-0.0017(4)
C4	0.0223(6)	0.0192(6)	0.0129(5)	0.0004(5)	-0.0022(4)	-0.0029(4)
C5	0.0243(6)	0.0200(6)	0.0170(6)	-0.0010(5)	0.0000(5)	-0.0021(5)
C6	0.0249(6)	0.0204(6)	0.0199(6)	-0.0024(5)	0.0019(5)	-0.0021(5)
C7	0.0209(6)	0.0196(6)	0.0185(6)	-0.0015(5)	-0.0003(5)	-0.0030(5)
C8	0.0203(6)	0.0228(6)	0.0238(7)	-0.0035(5)	0.0024(5)	-0.0049(5)
C9	0.0176(6)	0.0206(6)	0.0210(6)	-0.0026(5)	0.0013(5)	-0.0025(5)
C10	0.0189(6)	0.0205(6)	0.0240(6)	-0.0028(5)	0.0032(5)	-0.0036(5)
C11	0.0205(6)	0.0206(6)	0.0270(7)	-0.0044(5)	0.0042(5)	-0.0042(5)
C12	0.0202(6)	0.0196(6)	0.0250(7)	-0.0037(5)	0.0033(5)	-0.0033(5)
C13	0.0216(6)	0.0222(7)	0.0314(7)	-0.0046(5)	0.0052(5)	-0.0064(5)
C14	0.0208(6)	0.0214(6)	0.0243(7)	-0.0023(5)	0.0018(5)	-0.0041(5)
C15	0.0255(7)	0.0268(7)	0.0345(8)	-0.0028(6)	0.0042(6)	-0.0108(6)
C16	0.0267(7)	0.0345(8)	0.0343(8)	0.0024(6)	0.0017(6)	-0.0114(7)

Selected geometric informations

Atoms 1,2	**d 1,2 [Å]**	**Atoms 1,2**	**d 1,2 [Å]**	**Atoms 1,2**	**d 1,2 [Å]**
S1-2	1.7549(14)	C10-101	0.95	C8-82	0.95
S1-5	1.7395(14)	C10-102	0.95	C9-10	1.5269(18)
S2-4	1.7268(14)	C11-12	1.5269(19)	C9-91	0.95
S2-7	1.7498(14)	C11-111	0.95	C9-92	0.95
C1-3i	1.3945(19)	C11-112	0.95	C10-11	1.5275(19)

C1-2	1.3885(18)	C12-13	1.526(2)	C15-152	0.95
C1-11	0.95	C12-121	0.95	C16-161	0.95
C2-3	1.4238(18)	C12-122	0.95	C16-162	0.95
C3-4	1.4387(18)	C13-14	1.5268(19)	C16-163	0.95
C4-5	1.3780(19)	C13-131	0.95	C8-9	1.5275(19)
C5-6	1.4233(19)	C13-132	0.95	C8-81	0.95
C6-7	1.3657(19)	C14-15	1.526(2)	C15-16	1.526(2)
C6-61	0.95	C14-141	0.95	C15-151	0.95
C7-8	1.4987(19)	C14-142	0.95		

Atoms 1,2,3	**Angle 1,2,3 [°]**	**Atoms 1,2,3**	**Angle 1,2,3 [°]**	**Atoms 1,2,3**	**Angle 1,2,3 [°]**
C2-1-5	90.90(6)	C11-10-102	108.1	C10-9-91	109.1
C4-2-7	91.71(6)	H101-10-102	109.5	C8-9-92	109.3
C3i-1-2	117.76(12)	C10-11-12	112.61(11)	C10-9-92	109.3
C3i-1-11	121.2	C10-11-111	108.6	H91-9-92	109.5
C2-1-11	121	C12-11-111	108.6	C9-10-11	114.37(11)
S1-2-1	125.03(10)	C10-11-112	108.8	C9-10-101	108.3
S1-2-3	112.6(1)	C12-11-112	108.8	C11-10-101	108.4
C1-2-3	122.36(12)	H111-11-112	109.5	C9-10-102	108.1
C2-3-1i	119.88(12)	C11-12-13	113.40(12)	H151-15-152	109.5
C2-3-4	109.73(12)	C11-12-121	108.6	C15-16-161	109.6
C1i-3-4	130.39(12)	C13-12-121	108.6	C15-16-162	109.4
C3-4-2	135.01(11)	C11-12-122	108.4	H161-16-162	109.5
C3-4-5	114.41(12)	C13-12-122	108.4	C15-16-163	109.4
S2-4-5	110.57(10)	H121-12-122	109.5	H161-16-163	109.5
S1-5-4	112.35(10)	C12-13-14	113.22(12)	H162-16-163	109.5
S1-5-6	133.44(11)	C12-13-131	108.4	C7-8-82	107.7
C4-5-6	114.21(13)	C14-13-131	108.4	C9-8-82	107.6
C5-6-7	111.76(13)	C12-13-132	108.6	H81-8-82	109.5
C5-6-61	124.1	C14-13-132	108.6	C8-9-10	110.52(11)
C7-6-61	124.2	H131-13-132	109.5	C8-9-91	109.1
S2-7-6	111.75(10)	C13-14-15	112.86(12)	C14-15-16	113.25(13)
S2-7-8	120.86(10)	C13-14-141	108.7	C14-15-151	108.4
C6-7-8	127.24(13)	C15-14-141	108.6	C16-15-151	108.6
C7-8-9	116.20(12)	C13-14-142	108.6	C14-15-152	108.4
C7-8-81	107.9	C15-14-142	108.6	C16-15-152	108.6
C9-8-81	107.9	H141-14-142	109.5		

(i) 3-x, -1-y, -z.

A5. dibenzo[*b,b'*]thieno[2,3-*f*:5,4-*f'*]-*N*-butylcarbazoles (8b)

Atomic parameters

Atom	x / a	y / b	z / c	U [Å²]
S1	0.64859(3)	-0.00502(3)	0.86815(3)	
S2	0.07172(3)	0.00119(3)	0.69773(3)	
S31	0.64586(3)	0.08327(3)	1.08559(2)	
S32	0.06896(3)	0.10747(3)	0.88625(3)	
C1	0.43971(11)	-0.10328(10)	0.65479(10)	
C2	0.41087(11)	-0.05694(10)	0.71266(10)	
C3	0.47206(11)	-0.0233(1)	0.77953(10)	
C4	0.56048(11)	-0.03829(11)	0.78763(10)	
C5	0.58932(11)	-0.08273(10)	0.7294(1)	
C6	0.52780(12)	-0.11530(11)	0.66111(10)	
C7	0.68450(11)	-0.08823(11)	0.75134(10)	
C8	0.72479(12)	-0.04983(11)	0.82521(11)	
C9	0.81636(13)	-0.04678(13)	0.85729(12)	
C10	0.86756(13)	-0.08288(13)	0.81364(13)	
C11	0.82840(13)	-0.12128(13)	0.74023(13)	
C12	0.73793(12)	-0.12398(12)	0.70882(11)	
C13	0.29121(11)	-0.10479(11)	0.61273(10)	
C14	0.31548(11)	-0.05744(10)	0.68514(10)	
C15	0.25091(12)	-0.02262(11)	0.71523(10)	
C16	0.16387(11)	-0.03756(11)	0.67274(10)	
C17	0.13970(11)	-0.08561(10)	0.60101(10)	
C18	0.20422(12)	-0.11946(11)	0.57013(10)	
C19	0.04471(12)	-0.09054(11)	0.56721(10)	
C20	0.00006(12)	-0.04652(11)	0.61325(10)	
C21	-0.09146(12)	-0.04172(12)	0.59039(12)	
C22	-0.13800(13)	-0.08234(13)	0.52088(13)	
C23	-0.09475(13)	-0.12631(12)	0.47399(12)	
C24	-0.00405(13)	-0.13032(11)	0.49667(11)	
C25	0.36845(12)	-0.18124(11)	0.5259(1)	
C26	0.35913(11)	-0.12906(11)	0.45086(10)	
C27	0.36657(11)	-0.18448(11)	0.38203(10)	
C28	0.34849(13)	-0.13666(14)	0.30338(11)	
C31	0.45214(10)	0.19706(10)	0.86995(9)	
C32	0.41683(10)	0.15308(10)	0.92488(10)	
C33	0.47282(11)	0.11771(10)	0.99389(10)	
C34	0.56279(11)	0.12651(10)	1.00577(9)	
C35	0.5981(1)	0.17011(10)	0.95111(9)	
C36	0.54202(11)	0.20617(10)	0.88205(10)	
C37	0.69331(11)	0.16562(10)	0.97414(10)	
C38	0.72776(11)	0.11787(11)	1.04414(10)	
C39	0.81712(11)	0.09798(11)	1.07206(11)	
C40	0.87238(12)	0.12753(12)	1.02932(11)	

C41	0.83971(12)	0.17724(12)	0.96071(11)	
C42	0.75093(11)	0.19590(11)	0.93286(10)	
C43	0.30497(10)	0.20327(10)	0.81868(10)	
C44	0.32175(10)	0.15637(10)	0.89146(10)	
C45	0.25199(11)	0.12439(11)	0.91636(10)	
C46	0.16728(11)	0.14138(10)	0.86828(10)	
C47	0.15087(11)	0.19049(10)	0.79745(10)	
C48	0.21999(10)	0.22098(10)	0.77138(10)	
C49	0.05733(11)	0.20166(10)	0.75913(10)	
C50	0.00567(11)	0.15926(11)	0.80014(11)	
C51	-0.08593(12)	0.15894(12)	0.77095(12)	
C52	-0.12493(12)	0.20329(13)	0.70139(12)	
C53	-0.07449(12)	0.24739(12)	0.66087(12)	
C54	0.01639(11)	0.24628(11)	0.68904(11)	
C55	0.39715(11)	0.27421(10)	0.73988(10)	
C56	0.42813(10)	0.21979(11)	0.68130(9)	
C57	0.35767(12)	0.16271(12)	0.62837(11)	
C58	0.39436(13)	0.10971(13)	0.57226(12)	
N1	0.3669(1)	-0.13173(9)	0.59549(8)	
N31	0.38412(9)	0.22643(9)	0.80662(8)	
H31	0.4542	0.0089	0.818	0.0313
H61	0.546	-0.1447	0.6212	0.0329
H91	0.8426	-0.0203	0.9074	0.0442
H101	0.9298	-0.0819	0.8342	0.0486
H111	0.8644	-0.1455	0.711	0.0465
H121	0.7118	-0.1503	0.6586	0.0399
H151	0.2657	0.0098	0.7631	0.0325
H181	0.1891	-0.1512	0.5219	0.033
H211	-0.121	-0.0113	0.6218	0.0436
H221	-0.2004	-0.0807	0.5047	0.0471
H231	-0.1278	-0.1535	0.4262	0.0441
H241	0.0253	-0.1599	0.4646	0.0378
H251	0.4227	-0.2109	0.5379	0.0321
H252	0.3213	-0.2206	0.5152	0.0321
H261	0.4043	-0.0876	0.4615	0.0327
H262	0.3034	-0.102	0.4361	0.0327
H271	0.4244	-0.207	0.3951	0.0328
H272	0.3254	-0.2294	0.3756	0.0328
H281	0.3539	-0.174	0.2625	0.043
H282	0.3896	-0.0918	0.3091	0.043
H283	0.2906	-0.1142	0.2896	0.043
H331	0.4505	0.0887	1.0314	0.0295
H361	0.5646	0.2359	0.845	0.0286
H391	0.8393	0.0653	1.1193	0.0365

H401	0.9332	0.114	1.0468	0.0387
H411	0.8787	0.1982	0.933	0.0387
H421	0.7288	0.2292	0.8861	0.034
H451	0.2621	0.0923	0.9642	0.0316
H481	0.2096	0.2525	0.7232	0.0302
H511	-0.1205	0.1289	0.7981	0.0397
H521	-0.1872	0.2042	0.6809	0.0417
H531	-0.1028	0.2781	0.6137	0.0398
H541	0.0509	0.2754	0.6612	0.0347
H551	0.4399	0.3168	0.7605	0.0314
H552	0.343	0.2999	0.7118	0.0314
H561	0.4747	0.185	0.7114	0.0309
H562	0.4493	0.2559	0.6475	0.0309
H571	0.336	0.1261	0.6614	0.0383
H572	0.311	0.1968	0.5973	0.0383
H581	0.3492	0.0748	0.54	0.0443
H582	0.4409	0.0753	0.6031	0.0443
H583	0.4159	0.146	0.5389	0.0443

Anisotropic displacement parameters, in Å²

Atom	U_{11}	U_{22}	U_{33}	U_{12}	U_{13}	U_{23}
S1	0.0298(2)	0.0295(2)	0.0267(2)	-0.00416(17)	0.01072(16)	-0.00571(17)
S2	0.0302(2)	0.02490(19)	0.0286(2)	0.00383(16)	0.01221(16)	0.00003(17)
S31	0.02515(19)	0.0299(2)	0.02318(19)	0.00075(16)	0.00522(15)	0.00470(16)
S32	0.02420(19)	0.0269(2)	0.0319(2)	-0.00108(15)	0.01332(16)	0.00014(17)
C1	0.0299(8)	0.0210(7)	0.0212(7)	0.0026(6)	0.0093(6)	0.0004(6)
C2	0.0283(8)	0.0193(7)	0.0231(7)	0.0018(6)	0.0104(6)	0.0021(6)
C3	0.0306(8)	0.0208(7)	0.0247(7)	0.0006(6)	0.0128(6)	-0.0011(6)
C4	0.0299(8)	0.0211(7)	0.0226(7)	-0.0011(6)	0.0100(6)	-0.0001(6)
C5	0.0304(8)	0.0196(7)	0.0256(7)	-0.0006(6)	0.0126(6)	-0.0002(6)
C6	0.0317(8)	0.0218(7)	0.0245(7)	0.0019(6)	0.0127(6)	-0.0006(6)
C7	0.0286(8)	0.0221(8)	0.0277(8)	0.0003(6)	0.0103(6)	0.0008(6)
C8	0.0293(9)	0.0251(8)	0.0313(9)	-0.0021(7)	0.0127(7)	0.0000(7)
C9	0.0321(9)	0.0320(9)	0.0359(10)	-0.0036(7)	0.0086(8)	-0.0014(8)
C10	0.0267(9)	0.0356(10)	0.0457(11)	-0.0007(7)	0.0101(8)	-0.0002(9)
C11	0.0332(10)	0.0337(10)	0.0434(11)	0.0046(8)	0.0177(8)	0.0013(8)
C12	0.0336(9)	0.0271(9)	0.0341(9)	0.0010(7)	0.0145(7)	-0.0025(7)
C13	0.0278(8)	0.0216(7)	0.0218(7)	0.0024(6)	0.0090(6)	0.0009(6)
C14	0.0297(8)	0.0195(7)	0.0227(7)	0.0013(6)	0.0105(6)	0.0018(6)
C15	0.0322(8)	0.0209(7)	0.0214(7)	0.0021(6)	0.0107(6)	0.0012(6)
C16	0.0290(8)	0.0213(8)	0.0271(8)	0.0034(6)	0.0120(6)	0.0033(6)
C17	0.0292(8)	0.0200(7)	0.0236(7)	0.0006(6)	0.0090(6)	0.0029(6)
C18	0.0312(8)	0.0219(8)	0.0227(7)	0.0012(6)	0.0087(6)	-0.0008(6)

C19	0.0298(8)	0.0217(8)	0.0263(8)	0.0003(6)	0.0096(6)	0.0049(6)
C20	0.0305(8)	0.0228(8)	0.0283(8)	0.0009(6)	0.0095(7)	0.0043(7)
C21	0.0303(9)	0.0300(9)	0.041(1)	0.0040(7)	0.0141(8)	0.0072(8)
C22	0.0283(9)	0.0343(10)	0.0440(11)	-0.0008(7)	0.0073(8)	0.0082(8)
C23	0.0321(9)	0.0304(9)	0.0346(9)	-0.0051(7)	0.0044(7)	0.0066(8)
C24	0.0333(9)	0.0256(8)	0.0278(8)	-0.0013(7)	0.0082(7)	0.0028(7)
C25	0.0311(8)	0.0222(7)	0.0226(7)	0.0024(6)	0.0109(6)	-0.0020(6)
C26	0.0272(8)	0.0238(8)	0.0245(7)	0.0000(6)	0.0103(6)	0.0006(6)
C27	0.0223(7)	0.0297(8)	0.0224(7)	0.0005(6)	0.0079(6)	-0.0012(6)
C28	0.0314(9)	0.0433(11)	0.0248(8)	-0.0023(8)	0.0098(7)	0.0025(8)
C31	0.0212(7)	0.0197(7)	0.0221(7)	0.0012(6)	0.0071(6)	0.0003(6)
C32	0.0218(7)	0.0210(7)	0.0229(7)	-0.0001(6)	0.0084(6)	-0.0021(6)
C33	0.0260(8)	0.0223(7)	0.0223(7)	-0.0015(6)	0.0105(6)	0.0002(6)
C34	0.0237(7)	0.0222(7)	0.0202(7)	0.0012(6)	0.0046(6)	-0.0010(6)
C35	0.0226(7)	0.0190(7)	0.0216(7)	-0.0003(6)	0.0062(6)	-0.0018(6)
C36	0.0228(7)	0.0214(7)	0.0229(7)	-0.0018(6)	0.0085(6)	0.0001(6)
C37	0.0233(7)	0.0210(7)	0.0227(7)	-0.0023(6)	0.0066(6)	-0.0028(6)
C38	0.0238(7)	0.0227(8)	0.0238(7)	-0.0013(6)	0.0058(6)	-0.0024(6)
C39	0.0259(8)	0.0262(8)	0.0264(8)	0.0011(6)	0.0022(6)	-0.0025(6)
C40	0.0227(8)	0.0327(9)	0.0304(8)	0.0003(7)	0.0037(6)	-0.0073(7)
C41	0.0242(8)	0.0343(9)	0.0293(8)	-0.0061(7)	0.0085(7)	-0.0048(7)
C42	0.0231(8)	0.0274(8)	0.0250(8)	-0.0038(6)	0.0064(6)	-0.0009(6)
C43	0.0223(7)	0.0190(7)	0.0246(7)	-0.0001(6)	0.0098(6)	-0.0013(6)
C44	0.0217(7)	0.0212(7)	0.0238(7)	0.0017(6)	0.0080(6)	-0.0003(6)
C45	0.0251(8)	0.0232(8)	0.0247(7)	-0.0005(6)	0.0101(6)	0.0000(6)
C46	0.0226(7)	0.0223(7)	0.0291(8)	-0.0010(6)	0.0124(6)	-0.0033(6)
C47	0.0223(7)	0.0201(7)	0.0281(8)	0.0008(6)	0.0101(6)	-0.0024(6)
C48	0.0232(7)	0.0210(7)	0.0243(7)	0.0008(6)	0.0082(6)	-0.0002(6)
C49	0.0211(7)	0.0207(7)	0.0298(8)	0.0011(6)	0.0093(6)	-0.0043(6)
C50	0.0237(8)	0.0233(8)	0.0320(8)	0.0000(6)	0.0111(6)	-0.0041(7)
C51	0.0237(8)	0.0310(9)	0.0402(10)	-0.0022(7)	0.0131(7)	-0.0029(8)
C52	0.0207(8)	0.035(1)	0.0429(10)	-0.0001(7)	0.0086(7)	-0.0024(8)
C53	0.0241(8)	0.0286(9)	0.0358(9)	0.0033(7)	0.0061(7)	0.0000(7)
C54	0.0254(8)	0.0224(8)	0.0314(8)	0.0017(6)	0.0100(7)	-0.0026(6)
C55	0.0225(7)	0.0228(7)	0.0243(7)	0.0009(6)	0.0077(6)	0.0038(6)
C56	0.0219(7)	0.0255(8)	0.0223(7)	0.0024(6)	0.0083(6)	0.0044(6)
C57	0.0266(8)	0.0266(8)	0.0316(9)	-0.0006(7)	0.0093(7)	-0.0009(7)
C58	0.0329(9)	0.0338(9)	0.0324(9)	-0.0007(8)	0.0090(7)	-0.0062(8)
N1	0.0275(7)	0.0255(7)	0.0224(6)	0.0022(5)	0.0085(5)	-0.0031(5)
N31	0.0202(6)	0.0221(6)	0.0238(6)	0.0007(5)	0.0078(5)	0.0024(5)

Selected geometric informations

Atoms 1,2	d 1,2 [Å]	Atoms 1,2	d 1,2 [Å]	Atoms 1,2	d 1,2 [Å]

S1-4	1.7532(18)	C27-272	0.95	C21-22	1.383(3)
S1-8	1.7486(18)	C28-281	0.95	C21-211	0.95
S2-16	1.7552(17)	C28-282	0.95	C22-23	1.398(3)
S2-20	1.7520(18)	C28-283	0.95	C22-221	0.95
S31-34	1.7571(16)	C31-32	1.425(2)	C23-24	1.381(3)
S31-38	1.7504(17)	C31-36	1.389(2)	C23-231	0.95
S32-46	1.7640(16)	C31-31	1.384(2)	C24-241	0.95
S32-50	1.7516(19)	C32-33	1.391(2)	C25-26	1.519(2)
C1-2	1.427(2)	C32-44	1.454(2)	C25-1	1.452(2)
C1-6	1.385(2)	C33-34	1.391(2)	C25-251	0.95
C1-1	1.385(2)	C33-331	0.95	C25-252	0.95
C2-3	1.391(2)	C34-35	1.418(2)	C26-27	1.520(2)
C2-14	1.451(2)	C35-36	1.397(2)	C26-261	0.95
C3-4	1.391(2)	C35-37	1.450(2)	C26-262	0.95
C3-31	0.95	C36-361	0.95	C27-28	1.521(2)
C4-5	1.417(2)	C37-38	1.406(2)	C27-271	0.95
C5-6	1.403(2)	C37-42	1.404(2)	C53-54	1.384(2)
C5-7	1.451(2)	C38-39	1.397(2)	C53-531	0.95
C6-61	0.95	C39-40	1.388(3)	C54-541	0.95
C7-8	1.402(2)	C39-391	0.95	C55-56	1.524(2)
C7-12	1.399(2)	C40-41	1.401(3)	C55-31	1.454(2)
C8-9	1.401(3)	C40-401	0.95	C55-551	0.95
C9-10	1.389(3)	C41-42	1.384(2)	C55-552	0.95
C9-91	0.95	C41-411	0.95	C56-57	1.525(2)
C10-11	1.392(3)	C42-421	0.95	C56-561	0.95
C10-101	0.95	C43-44	1.428(2)	C56-562	0.95
C11-12	1.383(3)	C43-48	1.392(2)	C57-58	1.528(3)
C11-111	0.95	C43-31	1.384(2)	C57-571	0.95
C12-121	0.95	C44-45	1.398(2)	C57-572	0.95
C13-14	1.424(2)	C45-46	1.391(2)	C58-581	0.95
C13-18	1.386(2)	C45-451	0.95	C58-582	0.95
C13-1	1.389(2)	C46-47	1.419(2)	C58-583	0.95
C14-15	1.395(2)	C47-48	1.392(2)	C19-20	1.402(2)
C15-16	1.387(2)	C47-49	1.453(2)	C19-24	1.400(3)
C15-151	0.95	C48-481	0.95	C20-21	1.394(3)
C16-17	1.420(2)	C49-50	1.406(2)	C51-511	0.95
C17-18	1.396(2)	C49-54	1.399(2)	C52-53	1.400(3)
C17-19	1.455(2)	C50-51	1.396(2)	C52-521	0.95
C18-181	0.95	C51-52	1.384(3)		

Atoms 1,2,3	**Angle 1,2,3 [°]**	**Atoms 1,2,3**	**Angle 1,2,3 [°]**	**Atoms 1,2,3**	**Angle 1,2,3 [°]**
C4-1-8	91.47(8)	C32-31-31	109.46(13)	C23-24-241	120.3
C16-2-20	91.47(8)	C36-31-31	128.12(15)	C26-25-1	114.04(14)

C34-31-38	91.59(8)	C31-32-33	120.11(14)	C26-25-251	108.3
C46-32-50	91.30(8)	C31-32-44	106.16(14)	N1-25-251	108.4
C2-1-6	122.59(15)	C33-32-44	133.73(15)	C26-25-252	108.2
C2-1-1	109.03(14)	C32-33-34	117.42(14)	N1-25-252	108.3
C6-1-1	128.38(15)	C32-33-331	121.3	H251-25-252	109.5
C1-2-3	120.08(15)	C34-33-331	121.3	C25-26-27	110.96(14)
C1-2-14	106.36(14)	S31-34-33	125.64(13)	C25-26-261	109.1
C3-2-14	133.55(15)	S31-34-35	111.75(12)	C27-26-261	109.1
C2-3-4	117.37(15)	C33-34-35	122.57(15)	C25-26-262	109.2
C2-3-31	121.3	C34-35-36	120.12(15)	C27-26-262	109
C4-3-31	121.3	C34-35-37	111.96(14)	H261-26-262	109.5
S1-4-3	125.36(13)	C36-35-37	127.78(15)	C26-27-28	112.90(15)
S1-4-5	112.04(13)	C35-36-31	117.36(14)	C26-27-271	108.5
C3-4-5	122.60(16)	C35-36-361	121.2	C28-27-271	108.7
C4-5-6	120.10(16)	C31-36-361	121.4	C26-27-272	108.4
C4-5-7	111.68(15)	C35-37-38	112.30(14)	C28-27-272	108.8
C6-5-7	128.22(15)	C35-37-42	128.63(15)	H271-27-272	109.5
C5-6-1	117.17(15)	C38-37-42	118.83(15)	C27-28-281	109.6
C5-6-61	121.2	S31-38-37	112.25(12)	C27-28-282	109.5
C1-6-61	121.6	S31-38-39	125.99(14)	H281-28-282	109.5
C5-7-8	112.34(15)	C37-38-39	121.66(16)	C27-28-283	109.3
C5-7-12	129.09(16)	C38-39-40	118.29(16)	H281-28-283	109.5
C8-7-12	118.56(16)	C38-39-391	120.7	H282-28-283	109.5
S1-8-7	112.47(13)	C40-39-391	121.1	C32-31-36	122.42(15)
S1-8-9	125.66(15)	C39-40-41	120.90(16)	N31-55-552	108.6
C7-8-9	121.84(16)	C39-40-401	119.6	H551-55-552	109.5
C8-9-10	118.19(18)	C41-40-401	119.5	C55-56-57	114.74(14)
C8-9-91	120.8	C40-41-42	120.49(17)	C55-56-561	108
C10-9-91	121	C40-41-411	119.8	C57-56-561	108
C9-10-11	120.56(18)	C42-41-411	119.7	C55-56-562	108.5
C9-10-101	119.8	C37-42-41	119.80(16)	C57-56-562	108.1
C11-10-101	119.7	C37-42-421	119.8	H561-56-562	109.5
C10-11-12	120.97(18)	C41-42-421	120.4	C56-57-58	111.37(14)
C10-11-111	119.5	C44-43-48	122.10(15)	C56-57-571	108.9
C12-11-111	119.5	C44-43-31	109.24(14)	C58-57-571	109.1
C7-12-11	119.87(18)	C48-43-31	128.66(15)	C56-57-572	108.9
C7-12-121	119.8	C32-44-43	106.26(14)	C58-57-572	109
C11-12-121	120.4	C32-44-45	133.44(15)	H571-57-572	109.5
C14-13-18	122.42(15)	C43-44-45	120.30(15)	C57-58-581	109.6
C14-13-1	108.98(14)	C44-45-46	117.28(15)	C57-58-582	109.3
C18-13-1	128.59(15)	C44-45-451	121.3	H581-58-582	109.5
C2-14-13	106.56(14)	C46-45-451	121.4	C57-58-583	109.5
C2-14-15	133.24(16)	S32-46-45	125.87(13)	H581-58-583	109.5
C13-14-15	120.20(16)	S32-46-47	111.91(12)	H582-58-583	109.5

C14-15-16	117.36(16)	C45-46-47	122.22(15)	C25-1-13	124.94(14)
C14-15-151	121.5	C46-47-48	120.78(15)	C25-1-1	126.01(14)
C16-15-151	121.1	C46-47-49	111.89(14)	C13-1-1	109.05(13)
S2-16-15	125.58(13)	C48-47-49	127.32(16)	C55-31-43	127.36(13)
S2-16-17	112.00(13)	C43-48-47	117.26(15)	C55-31-31	123.76(13)
C15-16-17	122.41(15)	C43-48-481	121.4	C43-31-31	108.87(13)
C16-17-18	120.33(16)	C47-48-481	121.3	C21-22-23	121.12(18)
C16-17-19	111.73(15)	C47-49-50	112.18(15)	C21-22-221	119.7
C18-17-19	127.92(16)	C47-49-54	128.20(15)	C23-22-221	119.2
C17-18-13	117.27(15)	C50-49-54	119.61(15)	C22-23-24	120.29(18)
C17-18-181	121.4	S32-50-49	112.69(13)	C22-23-231	119.9
C13-18-181	121.4	S32-50-51	126.18(14)	C24-23-231	119.8
C17-19-20	112.25(15)	C49-50-51	121.10(17)	C19-24-23	119.80(18)
C17-19-24	128.72(16)	C50-51-52	118.22(17)	C19-24-241	119.9
C20-19-24	119.00(17)	C50-51-511	120.8	C54-53-531	119.8
S2-20-19	112.55(13)	C52-51-511	121	C49-54-53	119.34(16)
S2-20-21	125.97(15)	C51-52-53	121.34(17)	C49-54-541	120
C19-20-21	121.47(17)	C51-52-521	119.4	C53-54-541	120.6
C20-21-22	118.31(18)	C53-52-521	119.3	C56-55-31	113.14(13)
C20-21-211	120.8	C52-53-54	120.36(18)	C56-55-551	108.7
C22-21-211	120.9	C52-53-531	119.8	N31-55-551	108.5
				C56-55-552	108.4

A6. dibenzo[*b,b'*]thieno[2,3-*f*:5,4-*f'*]-*N*-hexylcarbazoles (8c) (crystallized with $CDCl_3$)

Atomic parameters

Atom	x / a	y / b	z / c	U [Å²]
S1	0.27799(5)	0.33905(5)	0.29644(2)	
S2	-0.58960(5)	0.61394(5)	0.30239(2)	
N82	-0.24439(19)	0.35196(13)	0.46083(8)	
C57	-0.4802(2)	0.53772(16)	0.34787(9)	
C66	-0.0061(2)	0.40072(15)	0.32956(9)	
C67	0.2731(2)	0.24063(14)	0.40183(9)	
C64	0.1303(2)	0.28973(14)	0.39904(9)	
C65	0.1179(2)	0.34673(16)	0.34331(9)	
C59	-0.3377(2)	0.41255(15)	0.42899(9)	
C54	-0.7030(2)	0.54588(16)	0.40681(10)	
C63	0.0115(2)	0.28893(15)	0.44113(9)	
C49	-0.7367(2)	0.60546(18)	0.35593(10)	
C61	-0.1226(2)	0.39786(15)	0.37183(9)	
C70	0.5593(2)	0.16671(18)	0.39286(12)	
C58	-0.4808(2)	0.44221(17)	0.44423(10)	

C71	0.4698(3)	0.14370(18)	0.44483(10)	
C60	-0.2668(2)	0.44466(15)	0.37336(9)	
C56	-0.33403(19)	0.50711(14)	0.33163(8)	
C53	-0.8089(2)	0.53001(15)	0.45287(10)	
C75	-0.1147(3)	0.41714(16)	0.58513(9)	
C72	0.3264(2)	0.18030(17)	0.44833(10)	
C68	0.3630(2)	0.26295(15)	0.35011(9)	
C73	-0.2799(2)	0.30549(16)	0.51972(9)	
C50	-0.8775(2)	0.64976(16)	0.34977(9)	
C51	-0.9793(2)	0.63450(15)	0.39706(10)	
C55	-0.5510(2)	0.50647(15)	0.40240(9)	
C74	-0.2690(2)	0.37341(16)	0.57610(9)	
C62	-0.1142(2)	0.34278(14)	0.42681(8)	
C52	-0.9467(2)	0.57342(18)	0.44717(10)	
C78	0.0522(3)	0.6110(3)	0.69591(12)	
C69	0.5073(2)	0.22636(17)	0.34526(11)	
C76	-0.1053(2)	0.48586(18)	0.63990(11)	
C77	0.0355(3)	0.54525(19)	0.63864(12)	
Cl48	0.42593(7)	0.44547(6)	0.67727(3)	
Cl80	0.21612(9)	0.29825(7)	0.71093(3)	
Cl81	0.31624(8)	0.31414(7)	0.58408(3)	
C79	0.3661(2)	0.3295(2)	0.66224(11)	
H661	-0.0114	0.4374	0.2923	0.0159
H631	0.0181	0.2518	0.4782	0.0116
H701	0.6582	0.1431	0.3907	0.0374
H581	-0.5296	0.4178	0.4802	0.0201
H711	0.5072	0.102	0.4762	0.0254
H561	-0.2885	0.5269	0.2938	0.0105
H531	-0.7887	0.4884	0.487	0.0281
H751	-0.0444	0.367	0.5911	0.0247
H752	-0.0906	0.4518	0.5483	0.0247
H721	0.264	0.1637	0.4824	0.023
H731	-0.3783	0.2812	0.5168	0.0212
H732	-0.2124	0.2537	0.5252	0.0212
H501	-0.8987	0.6904	0.3153	0.031
H511	-1.0731	0.6655	0.3946	0.0237
H741	-0.2917	0.3373	0.6125	0.0207
H742	-0.3395	0.4237	0.5714	0.0207
H521	-1.0208	0.5626	0.4779	0.0194
H781	0.1413	0.6473	0.6924	0.0418
H782	0.0553	0.5735	0.7329	0.0418
H783	-0.0304	0.6534	0.6976	0.0418
H691	0.5688	0.2403	0.3104	0.0183
H761	-0.1063	0.4491	0.6772	0.0288

H762	-0.1897	0.5268	0.639	0.0288
H771	0.1194	0.5039	0.6374	0.0426
H772	0.0337	0.5838	0.6021	0.0426
H791	0.4459	0.2869	0.6711	0.031

Anisotropic displacement parameters, in Å²

Atom	U_{11}	U_{22}	U_{33}	U_{12}	U_{13}	U_{23}
S1	0.0191(2)	0.0273(3)	0.0157(2)	0.0017(2)	0.00151(17)	0.0003(2)
S2	0.0203(2)	0.0231(3)	0.0161(2)	0.0031(2)	-0.00217(18)	0.0048(2)
N82	0.0230(8)	0.0238(10)	0.0145(8)	-0.0024(8)	0.0029(6)	0.0036(7)
C57	0.0183(9)	0.0220(11)	0.0155(9)	0.0003(9)	-0.0009(7)	0.0054(7)
C66	0.0222(9)	0.0173(10)	0.0124(8)	-0.0034(8)	0.0022(8)	-0.0084(7)
C67	0.0238(9)	0.0115(9)	0.0131(8)	0.0000(8)	0.0015(7)	-0.0049(7)
C64	0.0191(9)	0.0096(9)	0.0207(10)	-0.0038(7)	0.0043(7)	0.0046(7)
C65	0.0185(8)	0.0225(11)	0.0145(8)	-0.0080(8)	0.0026(7)	0.0060(8)
C59	0.0176(9)	0.0193(10)	0.0121(8)	-0.0004(8)	-0.0049(7)	-0.0031(7)
C54	0.0128(8)	0.0207(11)	0.0277(11)	-0.0025(8)	-0.0038(8)	0.0000(8)
C63	0.0205(9)	0.0127(10)	0.0204(10)	-0.0025(8)	-0.0040(8)	0.0072(7)
C49	0.0161(8)	0.0325(12)	0.0228(9)	-0.0007(9)	0.0003(8)	-0.0032(9)
C61	0.0118(8)	0.0197(10)	0.0138(8)	-0.0035(7)	0.0021(6)	-0.0050(7)
C70	0.0175(9)	0.0309(14)	0.0366(13)	0.0106(9)	0.0040(9)	-0.0045(10)
C58	0.0201(9)	0.0195(10)	0.0211(9)	-0.0040(9)	-0.0071(8)	-0.0005(8)
C71	0.0337(11)	0.0290(13)	0.0198(10)	0.0065(10)	-0.0015(9)	0.0063(9)
C60	0.0262(9)	0.0139(10)	0.0177(9)	-0.0081(9)	0.0007(8)	0.0013(8)
C56	0.0121(7)	0.0118(9)	0.0144(8)	-0.0027(7)	0.0003(7)	0.0031(7)
C53	0.0180(9)	0.0142(10)	0.0261(10)	0.0011(8)	-0.0040(8)	-0.0074(8)
C75	0.0356(11)	0.0276(12)	0.0077(8)	0.0023(10)	0.0017(8)	-0.0017(8)
C72	0.0221(9)	0.0335(13)	0.0181(9)	-0.0035(9)	-0.0049(8)	0.0030(9)
C68	0.0234(9)	0.0194(10)	0.0123(8)	0.0004(8)	0.0050(7)	-0.0003(7)
C73	0.0189(8)	0.022(1)	0.0143(9)	0.0049(8)	0.0032(7)	-0.0016(8)
C50	0.0193(8)	0.0255(11)	0.0107(8)	0.0052(8)	-0.0050(7)	-0.0038(8)
C51	0.0214(8)	0.0133(11)	0.0336(11)	-0.0077(8)	-0.0048(8)	-0.0080(8)
C55	0.0204(9)	0.0109(9)	0.0222(9)	-0.0075(7)	0.0004(8)	-0.0052(8)
C74	0.0274(10)	0.0225(11)	0.0110(8)	-0.0070(9)	0.0071(8)	0.0041(8)
C62	0.0152(7)	0.0152(9)	0.0085(7)	-0.0019(8)	-0.0008(6)	0.0047(7)
C52	0.0195(10)	0.0368(13)	0.0163(9)	-0.0018(9)	-0.0078(8)	0.0027(9)
C78	0.0481(14)	0.0453(16)	0.0300(12)	-0.0087(15)	0.0046(11)	0.0015(12)
C69	0.0206(10)	0.0320(13)	0.0222(10)	-0.0055(9)	0.0001(8)	0.0002(9)
C76	0.0245(10)	0.0334(13)	0.0219(11)	0.0056(9)	-0.0042(9)	-0.0028(9)
C77	0.0414(13)	0.0334(14)	0.0276(12)	-0.0111(11)	0.0039(10)	-0.0122(10)
Cl48	0.0354(3)	0.0391(4)	0.0441(4)	-0.0146(3)	0.0095(3)	-0.0099(3)
Cl80	0.0572(4)	0.0759(6)	0.0342(4)	-0.0325(4)	0.0093(3)	0.0115(4)
Cl81	0.0481(4)	0.0775(6)	0.0276(3)	-0.0318(4)	0.0124(3)	-0.0143(3)

C79	0.0248(10)	0.0459(16)	0.0314(12)	0.0023(11)	0.0015(9)	0.0224(12)

Selected geometric informations

Atoms 1,2	d 1,2 [Å]	Atoms 1,2	d 1,2 [Å]	Atoms 1,2	d 1,2 [Å]
S1-65	1.759(2)	C60-56	1.386(3)	C61-62	1.408(3)
S1-68	1.741(2)	C56-561	0.95	C70-71	1.412(3)
S2-57	1.745(2)	C53-52	1.385(3)	C70-69	1.396(3)
S2-49	1.756(2)	C53-531	0.95	C70-701	0.95
N82-59	1.372(3)	C75-74	1.528(3)	C58-55	1.415(3)
N82-73	1.454(3)	C75-76	1.517(3)	C58-581	0.95
N82-62	1.386(2)	C75-751	0.95	C71-72	1.389(3)
C57-56	1.426(3)	C75-752	0.95	C71-711	0.95
C57-55	1.401(3)	C72-721	0.95	C76-761	0.95
C66-65	1.377(3)	C68-69	1.399(3)	C76-762	0.95
C66-61	1.386(3)	C73-74	1.537(3)	C77-771	0.95
C66-661	0.95	C73-731	0.95	C77-772	0.95
C67-64	1.457(3)	C73-732	0.95	Cl48-79	1.732(3)
C67-72	1.389(3)	C50-51	1.382(3)	Cl80-79	1.760(2)
C67-68	1.407(3)	C50-501	0.95	Cl81-79	1.747(3)
C64-65	1.438(3)	C51-52	1.401(3)	C79-791	0.95
C64-63	1.398(3)	C51-511	0.95	C63-631	0.95
C59-58	1.391(3)	C74-741	0.95	C49-50	1.415(3)
C59-60	1.424(3)	C74-742	0.95	C61-60	1.452(3)
C54-49	1.403(3)	C52-521	0.95	C78-783	0.95
C54-53	1.390(3)	C78-77	1.539(4)	C69-691	0.95
C54-55	1.477(3)	C78-781	0.95	C76-77	1.513(3)
C63-62	1.391(3)	C78-782	0.95		

Atoms 1,2,3	Angle 1,2,3 [°]	Atoms 1,2,3	Angle 1,2,3 [°]	Atoms 1,2,3	Angle 1,2,3 [°]
C65-1-68	91.12(9)	C71-72-721	120.087	C59-58-55	116.87(19)
C57-2-49	91.11(10)	C67-72-721	119.656	C59-58-581	120.792
C59-82-73	124.81(17)	C67-68-1	113.70(15)	C55-58-581	122.282
C59-82-62	108.21(16)	C67-68-69	120.8(2)	C70-71-72	119.3(2)
C73-82-62	126.97(16)	S1-68-69	125.48(16)	C70-71-711	119.611
S2-57-56	124.46(15)	N82-73-74	113.26(18)	C72-71-711	121.054
S2-57-55	113.47(15)	N82-73-731	107.841	C61-60-59	106.17(17)
C56-57-55	122.06(18)	C74-73-731	109.26	C61-60-56	131.06(18)
C65-66-61	117.21(19)	N82-73-732	107.741	C59-60-56	122.75(19)
C65-66-661	120.97	C74-73-732	109.212	C57-56-60	115.64(17)
C61-66-661	121.81	H731-73-732	109.467	C57-56-561	121.348
C64-67-72	128.15(18)	C49-50-51	117.22(19)	C60-56-561	122.973
C64-67-68	111.81(18)	C49-50-501	120.743	C54-53-52	118.8(2)

C72-67-68	120.01(19)	C51-50-501	121.983	C54-53-531	120.81
C67-64-65	111.17(17)	C50-51-52	121.1(2)	C52-53-531	120.33
C67-64-63	130.08(18)	C50-51-511	118.599	C74-75-76	113.57(18)
C65-64-63	118.75(18)	C52-51-511	120.254	C74-75-751	109.225
C64-65-1	112.16(15)	C54-55-58	127.43(19)	C76-75-751	108.754
C64-65-66	122.79(18)	C54-55-57	111.07(18)	C74-75-752	107.722
S1-65-66	125.05(15)	C58-55-57	121.45(19)	C76-75-752	108.041
N82-59-58	129.21(19)	C73-74-75	113.73(16)	H751-75-752	109.466
N82-59-60	109.56(18)	C73-74-741	107.78	C71-72-67	120.3(2)
C58-59-60	121.23(19)	C75-74-741	107.612	C75-76-761	108.151
C49-54-53	119.85(18)	C73-74-742	109.1	C77-76-761	108.502
C49-54-55	111.71(18)	C75-74-742	109.078	C75-76-762	108.518
C53-54-55	128.43(19)	H741-74-742	109.467	C77-76-762	109.978
C64-63-62	118.34(18)	C61-62-63	121.45(17)	H761-76-762	109.467
C64-63-631	119.8	C61-62-82	110.15(16)	C78-77-76	113.1(2)
C62-63-631	121.858	C63-62-82	128.39(17)	C78-77-771	107.717
S2-49-54	112.63(15)	C51-52-53	121.3(2)	C76-77-771	109.572
S2-49-50	125.77(17)	C51-52-521	118.824	C78-77-772	108.876
C54-49-50	121.56(18)	C53-52-521	119.863	C76-77-772	108.028
C66-61-60	132.66(19)	C77-78-781	109.596	H771-77-772	109.467
C66-61-62	121.45(18)	C77-78-782	109.984	Cl80-79-I81	109.96(14)
C60-61-62	105.88(16)	H781-78-782	109.476	Cl80-79-I48	110.99(16)
C71-70-69	121.3(2)	C77-78-783	108.817	Cl81-79-I48	111.84(13)
C71-70-701	119.619	H781-78-783	109.477	Cl80-79-791	107.826
C69-70-701	119.004	H782-78-783	109.476	Cl81-79-791	108.077
C70-69-691	120.064	C68-69-70	118.3(2)	Cl48-79-791	108.001
C75-76-77	112.18(19)	C68-69-691	121.672		

A7. dibenzo[*b,b'*]thieno[2,3-*f*:5,4-*f'*]-*N*-hexylcarbazoles (8c)

Atomic parameters

Atom	x / a	y / b	z / c	U [Å²]
S1	-0.26748(7)	0.32763(2)	0.58103(2)	
S2	-0.37687(8)	-0.11089(2)	0.40880(2)	
S31	0.12184(7)	0.47339(3)	-0.11171(2)	
S32	0.26773(7)	0.39858(3)	0.26261(2)	
N1	0.2487(2)	0.12302(7)	0.41780(7)	
N31	0.7613(2)	0.33645(8)	0.03855(7)	
C1	0.1445(3)	0.17742(10)	0.45752(8)	
C2	-0.0463(3)	0.15125(9)	0.47815(8)	
C3	-0.1804(3)	0.19504(9)	0.51765(7)	
C4	-0.1166(3)	0.26427(9)	0.53481(7)	
C5	0.0767(2)	0.29115(9)	0.51459(7)	

C6	0.2116(3)	0.24705(9)	0.47577(8)
C7	0.0985(3)	0.36495(8)	0.53816(7)
C8	-0.0758(3)	0.39181(9)	0.57476(8)
C9	-0.0877(3)	0.46144(9)	0.60132(8)
C10	0.0751(3)	0.50622(10)	0.59121(8)
C11	0.2516(3)	0.48147(9)	0.55504(8)
C12	0.2638(3)	0.41136(9)	0.52918(7)
C13	0.1153(3)	0.06322(9)	0.41204(8)
C14	-0.0650(3)	0.07861(9)	0.44918(8)
C15	-0.2270(3)	0.02609(10)	0.45052(8)
C16	-0.1954(3)	-0.03906(9)	0.41443(8)
C17	-0.0174(3)	-0.05472(9)	0.37740(8)
C18	0.1435(3)	-0.00280(9)	0.37534(8)
C19	-0.0285(3)	-0.12688(9)	0.34354(9)
C20	-0.2128(3)	-0.16305(10)	0.35630(9)
C21	-0.2552(3)	-0.23374(11)	0.32897(11)
C22	-0.1076(4)	-0.26662(11)	0.28856(12)
C23	0.0772(4)	-0.23167(11)	0.27460(12)
C24	0.1165(3)	-0.16189(10)	0.30156(10)
C31	0.6248(3)	0.36705(9)	-0.00256(8)
C32	0.4392(3)	0.39744(10)	0.02780(8)
C33	0.2778(3)	0.43188(10)	-0.00262(8)
C34	0.3068(3)	0.43449(9)	-0.06374(7)
C35	0.4909(3)	0.40492(9)	-0.09401(8)
C36	0.6558(3)	0.37049(9)	-0.06323(8)
C37	0.4795(3)	0.41403(9)	-0.15805(7)
C38	0.2881(3)	0.45011(9)	-0.17379(8)
C39	0.2437(3)	0.46448(10)	-0.23285(8)
C40	0.3951(3)	0.44285(10)	-0.27658(8)
C41	0.5881(3)	0.40723(10)	-0.26126(8)
C42	0.6279(3)	0.39323(9)	-0.20314(8)
C43	0.6620(3)	0.34661(9)	0.09495(8)
C44	0.4644(3)	0.38507(10)	0.09061(8)
C45	0.3336(3)	0.40245(10)	0.14033(8)
C46	0.4078(3)	0.38150(9)	0.19476(8)
C47	0.6070(3)	0.34463(9)	0.20054(8)
C48	0.7370(3)	0.3267(1)	0.14981(8)
C49	0.6471(3)	0.33159(9)	0.26326(8)
C50	0.4783(3)	0.35660(9)	0.30105(8)
C51	0.4805(3)	0.35000(9)	0.36278(8)
C52	0.6649(3)	0.31786(11)	0.38697(9)
C53	0.8332(3)	0.29227(10)	0.35032(9)
C54	0.8265(3)	0.29761(10)	0.28841(8)
C25	0.3999(3)	0.13054(9)	0.37281(8)

C26	0.2680(4)	0.13953(13)	0.31132(10)	
C27	0.4212(5)	0.13940(15)	0.25989(11)	
C28	0.2940(9)	0.1540(2)	0.20023(14)	
C29	0.4706(7)	0.1471(2)	0.14619(15)	
C30	0.3354(13)	0.1717(3)	0.0977(4)	
C55	0.9322(3)	0.28907(11)	0.01959(10)	
C56	0.8364(4)	0.21490(13)	-0.01162(13)	
C57	0.6662(8)	0.2007(2)	-0.07590(16)	
C58	0.5704(10)	0.1247(3)	-0.1226(3)	
C59	0.4174(11)	0.1408(3)	-0.1754(2)	
C60	0.3734(13)	0.0597(4)	-0.2117(3)	
H31	-0.3114	0.1781	0.5315	0.0478
H61	0.3423	0.2638	0.4617	0.0455
H91	-0.2075	0.478	0.6257	0.049
H101	0.0696	0.5541	0.6094	0.0487
H111	0.3636	0.5123	0.5481	0.0512
H121	0.3832	0.3943	0.5048	0.0454
H151	-0.3507	0.0356	0.4751	0.0529
H181	0.2664	-0.0125	0.3505	0.0475
H211	-0.3811	-0.258	0.3382	0.0772
H221	-0.132	-0.3146	0.2699	0.0757
H231	0.1758	-0.2558	0.2462	0.0783
H241	0.242	-0.1378	0.292	0.0657
H331	0.1535	0.4529	0.0175	0.0506
H361	0.784	0.3516	-0.0828	0.0496
H391	0.1109	0.4879	-0.2426	0.0518
H401	0.3704	0.4529	-0.3168	0.0532
H411	0.6911	0.3921	-0.2916	0.0511
H421	0.758	0.3688	-0.1931	0.047
H451	0.2001	0.4279	0.1374	0.0528
H481	0.8709	0.3014	0.1528	0.0546
H511	0.3613	0.367	0.3873	0.0512
H521	0.675	0.3135	0.4293	0.0567
H531	0.9568	0.2705	0.3681	0.0581
H541	0.9419	0.2787	0.2632	0.0523
H251	0.5027	0.1696	0.3914	0.0491
H252	0.4857	0.0908	0.3629	0.0491
H261	0.1927	0.1814	0.3205	0.0775
H262	0.156	0.1024	0.2947	0.0775
H271	0.5424	0.1735	0.2783	0.0948
H272	0.4844	0.0959	0.2476	0.0948
H281	0.2452	0.1995	0.2108	0.1476
H282	0.1634	0.1229	0.1837	0.1476
H291	0.6109	0.1737	0.1638	0.1467

H292	0.5031	0.1005	0.1301	0.1467
H301	0.4231	0.1693	0.0637	0.2901
H302	0.3026	0.218	0.1156	0.2901
H303	0.1949	0.1448	0.0819	0.2901
H551	1.012	0.3032	-0.0103	0.0634
H552	1.0375	0.2895	0.0565	0.0634
H561	0.9593	0.1854	-0.0201	0.0888
H562	0.7522	0.2017	0.0179	0.0888
H571	0.7405	0.2229	-0.1018	0.1171
H572	0.5291	0.2228	-0.0657	0.1171
H581	0.7029	0.0993	-0.1308	0.1956
H582	0.475	0.1026	-0.1012	0.1956
H591	0.5081	0.1621	-0.1985	0.1454
H592	0.2798	0.1643	-0.1693	0.1454
H601	0.2878	0.051	-0.2532	0.301
H602	0.517	0.0389	-0.2146	0.301
H603	0.2887	0.0411	-0.1854	0.301

Anisotropic displacement parameters, in Å²

Atom	**U_{11}**	**U_{22}**	**U_{33}**	**U_{12}**	**U_{13}**	**U_{23}**
S1	0.0380(2)	0.0447(3)	0.0335(2)	0.00582(17)	0.01250(16)	0.01189(19)
S2	0.0433(2)	0.0418(3)	0.0516(3)	-0.00100(18)	0.00968(18)	0.0173(2)
S31	0.0408(2)	0.0660(3)	0.0275(2)	0.0142(2)	0.00908(16)	0.0199(2)
S32	0.0409(2)	0.0572(3)	0.0282(2)	0.01199(19)	0.01006(15)	0.0187(2)
N1	0.0335(6)	0.0351(8)	0.0347(7)	0.0016(5)	0.0069(5)	0.0121(6)
N31	0.0452(8)	0.0525(10)	0.0322(8)	0.0151(7)	0.0096(6)	0.0215(7)
C1	0.0387(8)	0.0498(11)	0.0290(9)	0.0067(7)	0.0039(6)	0.0214(8)
C2	0.0374(8)	0.0385(10)	0.0326(9)	0.0003(7)	0.0038(6)	0.0185(7)
C3	0.0384(8)	0.0447(10)	0.0214(8)	0.0047(7)	0.0065(6)	0.0118(7)
C4	0.0388(8)	0.0352(9)	0.0238(8)	0.0063(6)	0.0069(6)	0.0075(6)
C5	0.0297(7)	0.0464(10)	0.0246(8)	0.0032(6)	0.0063(5)	0.0155(7)
C6	0.0396(8)	0.0368(10)	0.0290(8)	0.0046(7)	0.0045(6)	0.0175(7)
C7	0.0347(7)	0.0373(9)	0.0245(8)	0.0055(6)	0.0064(5)	0.0112(7)
C8	0.0390(8)	0.045(1)	0.0248(8)	0.0042(7)	0.0006(6)	0.0187(7)
C9	0.0307(7)	0.044(1)	0.0338(9)	0.0088(6)	0.0046(6)	0.0109(7)
C10	0.0444(8)	0.0359(9)	0.0341(9)	0.0104(7)	-0.0012(6)	0.0115(7)
C11	0.0409(8)	0.0415(10)	0.0305(9)	-0.0006(7)	0.0002(6)	0.0126(7)
C12	0.0345(7)	0.0469(10)	0.0245(8)	0.0084(7)	0.0039(6)	0.0144(7)
C13	0.0367(8)	0.0447(11)	0.0353(9)	0.0059(7)	0.0043(6)	0.0239(8)
C14	0.0334(7)	0.0412(10)	0.0372(9)	0.0025(6)	0.0069(6)	0.0201(7)
C15	0.0357(8)	0.0491(11)	0.0388(9)	0.0092(7)	0.0071(6)	0.0268(8)
C16	0.0370(8)	0.038(1)	0.041(1)	0.0058(7)	0.0009(6)	0.0224(8)
C17	0.0330(7)	0.0448(10)	0.0333(9)	0.0036(7)	0.0013(6)	0.0178(7)

C18	0.0354(8)	0.0466(11)	0.0396(10)	0.0070(7)	0.0076(6)	0.0180(8)
C19	0.0430(9)	0.0371(10)	0.0393(10)	0.0075(7)	0.0027(7)	0.0165(7)
C20	0.0381(8)	0.0418(11)	0.0500(11)	0.0018(7)	0.0041(7)	0.0221(9)
C21	0.0493(10)	0.0431(12)	0.0693(14)	0.0018(8)	0.0080(9)	0.0226(10)
C22	0.0592(12)	0.0402(12)	0.0736(16)	0.0028(9)	0.0017(10)	0.0142(10)
C23	0.0570(12)	0.0450(13)	0.0730(15)	0.0064(9)	0.0124(10)	0.0039(11)
C24	0.0451(9)	0.0454(12)	0.0573(12)	0.0006(8)	0.0065(8)	0.0103(9)
C31	0.0384(8)	0.0456(10)	0.0261(8)	0.0093(7)	0.0068(6)	0.0140(7)
C32	0.0418(8)	0.0508(11)	0.0260(8)	0.0035(7)	0.0067(6)	0.0158(8)
C33	0.0388(8)	0.0590(12)	0.0269(8)	0.0155(7)	0.0079(6)	0.0176(8)
C34	0.0334(7)	0.0476(10)	0.0249(8)	0.0043(6)	0.0041(6)	0.0122(7)
C35	0.0366(8)	0.0362(9)	0.0300(8)	0.0012(6)	0.0067(6)	0.0090(7)
C36	0.0389(8)	0.0441(10)	0.0369(9)	0.0079(7)	0.0129(6)	0.0169(8)
C37	0.0416(8)	0.040(1)	0.0207(8)	0.0013(7)	0.0050(6)	0.0132(7)
C38	0.0446(9)	0.0403(10)	0.0331(9)	0.0018(7)	0.0060(7)	0.0115(7)
C39	0.0434(9)	0.0556(12)	0.0254(8)	0.0000(8)	0.0032(6)	0.0175(8)
C40	0.0488(9)	0.0519(11)	0.0244(8)	-0.0052(8)	0.0033(6)	0.0144(8)
C41	0.0481(9)	0.0531(11)	0.0217(8)	0.0016(8)	0.0072(6)	0.0050(7)
C42	0.0383(8)	0.0442(10)	0.0301(9)	0.0050(7)	0.0097(6)	0.0058(7)
C43	0.0410(8)	0.0447(10)	0.0260(8)	0.0049(7)	0.0082(6)	0.0158(7)
C44	0.0380(8)	0.0474(10)	0.0289(9)	0.0050(7)	0.0032(6)	0.0149(7)
C45	0.0385(8)	0.0550(11)	0.0250(8)	0.0062(7)	0.0064(6)	0.0145(8)
C46	0.0354(8)	0.0422(10)	0.0267(8)	0.0043(6)	0.0070(6)	0.0071(7)
C47	0.0389(8)	0.039(1)	0.0285(8)	0.0035(7)	0.0076(6)	0.0120(7)
C48	0.0359(8)	0.0536(11)	0.0346(9)	0.0114(7)	0.0107(6)	0.0199(8)
C49	0.0354(8)	0.0434(10)	0.0335(9)	0.0042(7)	0.0085(6)	0.0218(7)
C50	0.0356(7)	0.0465(10)	0.0281(8)	-0.0002(7)	0.0038(6)	0.0218(7)
C51	0.0441(8)	0.0438(10)	0.0320(9)	0.0019(7)	0.0055(6)	0.0188(8)
C52	0.0337(8)	0.0628(12)	0.0403(10)	-0.0031(7)	0.0055(6)	0.0296(9)
C53	0.0417(9)	0.0492(11)	0.0405(10)	0.0063(7)	0.0032(7)	0.0279(9)
C54	0.0343(8)	0.0466(11)	0.0372(9)	0.0070(7)	0.0066(6)	0.0192(8)
C25	0.0407(8)	0.0395(10)	0.0348(9)	0.0051(7)	0.0156(6)	0.0114(7)
C26	0.0854(15)	0.0728(16)	0.0418(12)	0.0311(12)	0.0172(10)	0.0222(11)
C27	0.113(2)	0.0734(17)	0.0443(13)	-0.0263(15)	0.0115(13)	0.0155(12)
C28	0.237(5)	0.111(3)	0.0451(16)	0.066(3)	0.036(2)	0.0320(17)
C29	0.148(3)	0.124(3)	0.063(2)	-0.001(2)	-0.012(2)	0.038(2)
C30	0.219(7)	0.164(6)	0.295(9)	-0.016(5)	-0.059(7)	0.046(6)
C55	0.0486(10)	0.0674(14)	0.0419(11)	0.0141(9)	0.0165(8)	0.0235(10)
C56	0.0727(15)	0.0693(17)	0.0712(16)	0.0213(12)	0.0049(12)	0.0140(13)
C57	0.163(4)	0.138(4)	0.074(2)	-0.007(3)	-0.006(2)	0.038(2)
C58	0.169(5)	0.158(5)	0.165(5)	0.042(4)	0.009(4)	0.030(4)
C59	0.210(6)	0.200(6)	0.088(3)	-0.015(5)	-0.025(3)	0.052(4)
C60	0.237(7)	0.217(8)	0.208(7)	0.057(6)	-0.015(6)	0.042(6)

Selected geometric informations

Atoms 1,2	d 1,2 [Å]	Atoms 1,2	d 1,2 [Å]	Atoms 1,2	d 1,2 [Å]
S1-4	1.7454(16)	C37-42	1.388(2)	C21-22	1.373(3)
S1-8	1.7455(18)	C38-39	1.394(2)	C21-211	0.95
S2-16	1.7532(18)	C39-40	1.382(2)	C22-23	1.391(3)
S2-20	1.7462(19)	C39-391	0.95	C22-221	0.95
S31-34	1.7552(17)	C40-41	1.405(3)	C23-24	1.384(3)
S31-38	1.7443(17)	C40-401	0.95	C23-231	0.95
S32-46	1.7487(16)	C41-42	1.370(3)	C24-241	0.95
S32-50	1.7630(17)	C41-411	0.95	C31-32	1.414(2)
N1-1	1.416(2)	C42-421	0.95	C31-36	1.385(2)
N1-13	1.397(2)	C43-44	1.415(2)	C32-33	1.391(2)
N1-25	1.441(2)	C43-48	1.389(2)	C32-44	1.453(2)
N31-31	1.402(2)	C44-45	1.386(2)	C33-34	1.386(2)
N31-43	1.401(2)	C45-46	1.391(2)	C33-331	0.95
N31-55	1.426(2)	C45-451	0.95	C34-35	1.400(2)
C1-2	1.402(2)	C46-47	1.408(2)	C35-36	1.408(2)
C1-6	1.395(3)	C47-48	1.401(2)	C35-37	1.457(2)
C2-3	1.397(2)	C47-49	1.458(2)	C36-361	0.95
C2-14	1.437(2)	C48-481	0.95	C37-38	1.406(2)
C3-4	1.384(3)	C49-50	1.389(2)	C55-56	1.539(3)
C3-31	0.95	C49-54	1.401(2)	C55-551	0.95
C4-5	1.416(2)	C50-51	1.393(2)	C55-552	0.95
C5-6	1.396(2)	C51-52	1.391(2)	C56-57	1.572(4)
C5-7	1.446(2)	C51-511	0.95	C56-561	0.95
C6-61	0.95	C52-53	1.375(2)	C56-562	0.95
C7-8	1.409(2)	C52-521	0.95	C57-58	1.649(6)
C7-12	1.404(2)	C53-54	1.386(2)	C57-571	0.95
C8-9	1.385(2)	C53-531	0.95	C57-572	0.95
C9-10	1.381(3)	C54-541	0.95	C58-59	1.480(6)
C9-91	0.95	C25-26	1.521(3)	C58-581	0.95
C10-11	1.403(2)	C25-251	0.95	C58-582	0.95
C10-101	0.95	C25-252	0.95	C59-60	1.626(7)
C11-12	1.392(2)	C26-27	1.528(3)	C59-591	0.95
C11-111	0.95	C26-261	0.95	C59-592	0.95
C12-121	0.95	C26-262	0.95	C60-601	0.95
C13-14	1.405(2)	C27-28	1.521(4)	C60-602	0.95
C13-18	1.393(2)	C27-271	0.95	C60-603	0.95
C14-15	1.420(2)	C27-272	0.95	C19-20	1.391(2)
C15-16	1.379(3)	C28-29	1.651(5)	C19-24	1.397(3)
C15-151	0.95	C28-281	0.95	C20-21	1.403(3)
C16-17	1.393(2)	C28-282	0.95	C30-301	0.95
C17-18	1.412(2)	C29-30	1.444(7)	C30-302	0.95

C17-19	1.451(3)	C29-291	0.95	C30-303	0.95
C18-181	0.95	C29-292	0.95		

Atoms 1,2,3	**Angle 1,2,3 [°]**	**Atoms 1,2,3**	**Angle 1,2,3 [°]**	**Atoms 1,2,3**	**Angle 1,2,3 [°]**
C4-1-8	91.36(8)	C40-41-411	119.917	C35-36-31	116.77(14)
C16-2-20	90.90(8)	C42-41-411	119.492	C35-36-361	121.443
C34-31-38	91.37(8)	C37-42-41	120.86(16)	C31-36-361	121.764
C46-32-50	90.65(8)	C37-42-421	118.823	C35-37-38	112.45(14)
C1-1-13	106.91(13)	C41-42-421	120.313	C35-37-42	129.58(15)
C1-1-25	125.06(15)	N31-43-44	109.33(14)	C38-37-42	117.97(15)
C13-1-25	123.90(14)	N31-43-48	129.12(15)	C37-38-31	112.15(13)
C31-31-43	107.94(13)	C44-43-48	121.51(14)	C37-38-39	122.05(15)
C31-31-55	124.66(14)	C32-44-43	106.64(14)	S31-38-39	125.80(14)
C43-31-55	125.59(15)	C32-44-45	132.21(15)	C38-39-40	118.34(17)
N1-1-2	109.40(15)	C43-44-45	121.13(16)	C38-39-391	120.287
N1-1-6	128.18(15)	C44-45-46	117.03(16)	C40-39-391	121.364
C2-1-6	122.42(16)	C44-45-451	121.341	C39-40-41	120.19(16)
C1-2-3	120.50(16)	C46-45-451	121.624	C39-40-401	119.89
C1-2-14	106.85(14)	S32-46-45	124.03(13)	C41-40-401	119.909
C3-2-14	132.61(15)	S32-46-47	113.34(13)	C40-41-42	120.59(15)
C2-3-4	117.14(15)	C45-46-47	122.63(15)	C59-58-581	120.64
C2-3-31	121.451	C46-47-48	119.97(15)	C57-58-582	109.921
C4-3-31	121.405	C46-47-49	110.69(14)	C59-58-582	106.565
S1-4-3	124.30(12)	C48-47-49	129.33(15)	H581-58-582	109.465
S1-4-5	112.88(13)	C47-48-43	117.70(15)	C58-59-60	90.5(5)
C3-4-5	122.79(14)	C47-48-481	121.016	C58-59-591	108.833
C4-5-6	119.80(16)	C43-48-481	121.285	C60-59-591	109.425
C4-5-7	110.85(13)	C47-49-50	112.92(14)	C58-59-592	123.041
C6-5-7	129.34(15)	C47-49-54	128.85(14)	C60-59-592	113.893
C5-6-1	117.33(15)	C50-49-54	118.22(15)	H591-59-592	109.466
C5-6-61	121.367	S32-50-49	112.38(12)	C59-60-601	113.259
C1-6-61	121.289	S32-50-51	124.53(13)	C59-60-602	109.699
C5-7-8	112.90(14)	C49-50-51	123.08(15)	H601-60-602	109.475
C5-7-12	129.35(14)	C50-51-52	117.17(15)	C59-60-603	105.345
C8-7-12	117.75(15)	C50-51-511	121.246	H601-60-603	109.476
C7-8-1	112.01(13)	C52-51-511	121.581	H602-60-603	109.475
C7-8-9	122.16(16)	C51-52-53	120.80(16)	C19-24-23	119.68(19)
S1-8-9	125.83(13)	C51-52-521	119.749	C19-24-241	119.845
C8-9-10	119.10(15)	C53-52-521	119.455	C23-24-241	120.472
C8-9-91	120.229	C52-53-54	121.60(16)	N31-31-32	109.28(14)
C10-9-91	120.666	C52-53-531	118.817	N31-31-36	128.73(14)
C9-10-11	120.47(16)	C54-53-531	119.581	C32-31-36	121.98(15)
C9-10-101	119.999	C49-54-53	119.08(15)	C31-32-33	121.02(15)

C11-10-101	119.523	C49-54-541	120.181	C31-32-44	106.79(14)
C10-11-12	120.03(16)	C53-54-541	120.74	C33-32-44	132.19(15)
C10-11-111	120.454	N1-25-26	112.29(15)	C32-33-34	117.04(15)
C12-11-111	119.516	N1-25-251	109.475	C32-33-331	121.692
C7-12-11	120.48(14)	C26-25-251	108.137	C34-33-331	121.268
C7-12-121	119.15	N1-25-252	108.538	S31-34-33	124.99(12)
C11-12-121	120.367	C26-25-252	108.901	S31-34-35	112.67(12)
N1-13-14	109.58(15)	H251-25-252	109.468	C33-34-35	122.34(15)
N1-13-18	128.00(15)	C25-26-27	113.3(2)	C34-35-36	120.85(15)
C14-13-18	122.41(16)	C25-26-261	109.179	C34-35-37	111.36(14)
C2-14-13	107.21(14)	C27-26-261	109.067	C36-35-37	127.78(14)
C2-14-15	132.49(15)	C25-26-262	108.057	C56-55-551	107.646
C13-14-15	120.25(16)	C27-26-262	107.661	N31-55-552	107.994
C14-15-16	116.61(15)	H261-26-262	109.468	C56-55-552	108.204
C14-15-151	121.398	C26-27-28	113.6(3)	H551-55-552	109.468
C16-15-151	121.989	C26-27-271	107.216	C55-56-57	117.5(2)
S2-16-15	123.93(13)	C28-27-271	109.337	C55-56-561	110.244
S2-16-17	112.57(13)	C26-27-272	109.118	C57-56-561	106.325
C15-16-17	123.49(16)	C28-27-272	108.042	C55-56-562	107.125
C16-17-18	120.35(16)	H271-27-272	109.469	C57-56-562	105.922
C16-17-19	111.71(15)	C27-28-29	109.4(3)	H561-56-562	109.466
C18-17-19	127.93(15)	C27-28-281	109.1	C56-57-58	126.0(4)
C17-18-13	116.87(15)	C29-28-281	108.49	C56-57-571	104.702
C17-18-181	121.594	C27-28-282	110.077	C58-57-571	105.938
C13-18-181	121.529	C29-28-282	110.253	C56-57-572	106.634
C17-19-20	112.29(15)	H281-28-282	109.467	C58-57-572	103.555
C17-19-24	128.80(17)	C28-29-30	102.0(5)	H571-57-572	109.465
C20-19-24	118.91(17)	C28-29-291	111.107	C57-58-59	103.6(4)
S2-20-19	112.54(14)	C30-29-291	113.036	C57-58-581	106.269
S2-20-21	125.53(15)	C28-29-292	109.896	C22-23-24	120.2(2)
C19-20-21	121.93(17)	C30-29-292	111.112	C22-23-231	119.861
C20-21-22	117.57(19)	H291-29-292	109.467	C24-23-231	119.984
C20-21-211	121.261	C29-30-301	108.524	H302-30-303	109.477
C22-21-211	121.169	C29-30-302	108.986	N31-55-56	114.44(17)
C21-22-23	121.7(2)	H301-30-302	109.474	N31-55-551	109.022
C21-22-221	119.024	C29-30-303	110.881		
C23-22-221	119.23	H301-30-303	109.476		

A8. dibenzo[*b,b'*]thieno[2,3-*f*:5,4-*f'*]-*N*-octylcarbazoles (8d) (isomer 1)

Atomic parameters

Atom	x / a	y / b	z / c	U [Å²]
S1	0.72257(7)	-0.00127(7)	0.79889(4)	

S2	0.28513(7)	0.22380(7)	0.37917(4)	
C1	0.7077(3)	0.0859(2)	0.72524(13)	
C2	0.6137(3)	0.0894(2)	0.66630(13)	
C3	0.6211(2)	0.1675(2)	0.61227(14)	
C4	0.7188(3)	0.2401(2)	0.61708(14)	
C5	0.8108(2)	0.2345(2)	0.67375(15)	
C6	0.8070(3)	0.1578(2)	0.72700(14)	
C7	0.9008(3)	0.1364(2)	0.78852(14)	
C8	1.0183(3)	0.1853(2)	0.80435(15)	
C9	1.0957(3)	0.1498(3)	0.86285(16)	
C10	1.0601(3)	0.0691(3)	0.90620(16)	
C11	0.9440(3)	0.0194(2)	0.89167(14)	
C12	0.8665(3)	0.0553(3)	0.83151(14)	
C13	0.4495(3)	0.0633(2)	0.58306(13)	
C14	0.5135(2)	0.1504(2)	0.55874(14)	
C15	0.4715(2)	0.2024(2)	0.49560(14)	
C16	0.3617(3)	0.1663(2)	0.45805(13)	
C17	0.2986(2)	0.0782(2)	0.48059(13)	
C18	0.3410(3)	0.0260(2)	0.54415(14)	
C19	0.1855(2)	0.0568(2)	0.43194(13)	
C20	0.1662(2)	0.1284(2)	0.37523(13)	
C21	0.0637(3)	0.1230(3)	0.32285(15)	
C22	-0.0204(3)	0.0414(3)	0.32796(15)	
C23	-0.0018(3)	-0.0316(3)	0.38313(15)	
C24	0.0999(3)	-0.0256(2)	0.43515(14)	
C25	0.4701(3)	-0.0619(2)	0.68924(13)	
C26	0.3918(3)	-0.0349(2)	0.75310(14)	
C27	0.3584(3)	-0.1355(2)	0.79177(14)	
C28	0.2785(3)	-0.1268(3)	0.85579(15)	
C29	0.2461(3)	-0.2319(3)	0.88509(15)	
C30	0.1602(3)	-0.2322(3)	0.94653(15)	
C31	0.1280(3)	-0.3428(3)	0.97040(16)	
C32	0.0411(3)	-0.3444(3)	1.03326(16)	
N1	0.5089(2)	0.02779(18)	0.64846(11)	
H41	0.7215	0.2928	0.581	0.047
H51	0.878	0.283	0.6769	0.0464
H81	1.0419	0.2422	0.7756	0.0583
H91	1.1759	0.181	0.8731	0.0645
H101	1.1154	0.047	0.9465	0.0617
H111	0.9181	-0.036	0.921	0.0557
H151	0.515	0.2608	0.4789	0.0425
H181	0.2977	-0.0327	0.5606	0.0429
H211	0.052	0.1732	0.285	0.0506
H221	-0.0911	0.0353	0.2931	0.0573

H231	-0.0599	-0.087	0.3854	0.0599
H241	0.1114	-0.0756	0.4731	0.0451
H251	0.5432	-0.0977	0.7088	0.044
H252	0.4214	-0.1062	0.6565	0.044
H261	0.4389	0.009	0.7868	0.0481
H262	0.3171	-0.0002	0.7347	0.0481
H271	0.4351	-0.1685	0.8085	0.0471
H272	0.3135	-0.178	0.7561	0.0471
H281	0.3245	-0.0892	0.8938	0.0539
H282	0.2031	-0.0907	0.8409	0.0539
H291	0.3222	-0.2659	0.9018	0.058
H292	0.2049	-0.2701	0.8458	0.058
H301	0.2017	-0.197	0.9872	0.0597
H302	0.0845	-0.1969	0.931	0.0597
H311	0.2041	-0.3777	0.9859	0.0612
H312	0.0873	-0.3778	0.9294	0.0612
H321	0.0237	-0.414	1.0459	0.076
H322	0.0814	-0.3098	1.0745	0.076
H323	-0.0354	-0.3099	1.018	0.076

Anisotropic displacement parameters, in Å²

Atom	U_{11}	U_{22}	U_{33}	U_{12}	U_{13}	U_{23}
S1	0.0331(4)	0.0347(5)	0.0397(4)	-0.0003(4)	0.0042(3)	0.0073(3)
S2	0.0265(4)	0.0330(5)	0.0422(4)	0.0000(3)	0.0030(3)	0.0061(3)
C1	0.0285(17)	0.0235(18)	0.0369(14)	0.0048(13)	0.0092(11)	0.0031(12)
C2	0.0254(16)	0.0255(17)	0.0394(15)	0.0039(13)	0.0101(12)	-0.0015(12)
C3	0.0199(15)	0.0281(18)	0.0375(14)	0.0036(12)	0.0090(11)	-0.0023(12)
C4	0.0259(18)	0.034(2)	0.0341(15)	0.0038(14)	0.0038(11)	0.0036(12)
C5	0.0184(16)	0.036(2)	0.0486(16)	0.0015(12)	0.0073(11)	-0.0012(13)
C6	0.0260(16)	0.035(2)	0.0383(15)	0.0022(14)	0.0079(11)	-0.0037(13)
C7	0.0302(18)	0.0261(17)	0.0395(15)	0.0008(13)	0.0032(12)	0.0001(13)
C8	0.0366(19)	0.041(2)	0.0470(17)	-0.0044(15)	0.0039(13)	-0.0024(14)
C9	0.0344(19)	0.056(3)	0.0497(19)	0.0002(16)	-0.0019(14)	-0.0015(16)
C10	0.037(2)	0.059(3)	0.0462(18)	0.0025(17)	-0.0049(14)	-0.0006(17)
C11	0.042(2)	0.045(2)	0.0399(16)	0.0110(16)	0.0034(13)	0.0034(14)
C12	0.0262(18)	0.044(2)	0.0412(15)	0.0005(15)	0.0047(12)	-0.0028(15)
C13	0.0278(17)	0.0228(19)	0.0365(14)	-0.0023(13)	0.0114(11)	-0.0030(12)
C14	0.0161(15)	0.033(2)	0.0399(15)	0.0038(12)	0.0089(11)	-0.0054(13)
C15	0.0214(17)	0.0282(19)	0.0415(15)	-0.0017(12)	0.0124(12)	0.0014(12)
C16	0.0254(16)	0.031(2)	0.0343(14)	0.0069(13)	0.0069(11)	0.0032(12)
C17	0.0247(17)	0.031(2)	0.0380(15)	-0.0014(13)	0.0119(12)	-0.0073(12)
C18	0.0196(16)	0.031(2)	0.0422(15)	0.0021(12)	0.0102(10)	0.0000(13)
C19	0.0246(17)	0.0339(19)	0.0365(14)	0.0032(13)	0.0078(11)	-0.0027(13)

C20	0.0240(17)	0.0297(18)	0.0406(15)	0.0001(13)	0.0072(11)	-0.0039(13)
C21	0.0240(17)	0.037(2)	0.0447(16)	0.0039(14)	0.0041(12)	0.0022(14)
C22	0.0249(17)	0.050(2)	0.0445(16)	0.0050(15)	0.0005(12)	-0.0068(15)
C23	0.0243(18)	0.060(3)	0.0526(18)	-0.0078(15)	0.0102(13)	-0.0078(16)
C24	0.0276(18)	0.027(2)	0.0433(15)	0.0006(13)	0.0109(12)	-0.0057(12)
C25	0.0296(16)	0.0229(18)	0.0431(16)	-0.0012(13)	0.0059(12)	0.0004(13)
C26	0.0282(16)	0.035(2)	0.0396(14)	0.0012(13)	0.0079(11)	-0.0013(12)
C27	0.0259(17)	0.0352(18)	0.0432(15)	-0.0015(14)	0.0069(12)	0.0011(14)
C28	0.0344(18)	0.049(2)	0.0423(16)	-0.0012(16)	0.0059(13)	-0.0030(15)
C29	0.0373(19)	0.041(2)	0.0487(17)	-0.0088(15)	0.0059(13)	0.0071(14)
C30	0.0325(19)	0.053(2)	0.0477(17)	0.0006(16)	0.0091(13)	0.0009(15)
C31	0.0359(19)	0.049(2)	0.0494(18)	0.0030(16)	0.0087(14)	0.0071(16)
C32	0.051(2)	0.067(3)	0.055(2)	-0.0001(19)	0.0162(16)	0.0076(19)
N1	0.0269(14)	0.0252(16)	0.0394(12)	0.0017(10)	0.0065(9)	-0.001(1)

Selected geometric informations

Atoms 1,2	**d 1,2 [Å]**	**Atoms 1,2**	**d 1,2 [Å]**	**Atoms 1,2**	**d 1,2 [Å]**
S1-1	1.755(3)	C19-20	1.393(4)	C11-111	0.95
S1-12	1.759(3)	C19-24	1.405(4)	C13-14	1.407(4)
S2-16	1.763(3)	C20-21	1.395(4)	C13-18	1.393(4)
S2-20	1.765(3)	C21-22	1.392(4)	C13-1	1.386(3)
C1-2	1.411(4)	C21-211	0.95	C14-15	1.380(4)
C1-6	1.407(4)	C22-23	1.384(4)	C15-16	1.388(4)
C2-3	1.420(3)	C22-221	0.95	C15-151	0.95
C2-1	1.388(3)	C23-24	1.385(4)	C16-17	1.401(4)
C3-4	1.398(4)	C23-231	0.95	C17-18	1.389(3)
C3-14	1.463(4)	C24-241	0.95	C17-19	1.465(4)
C4-5	1.369(4)	C25-26	1.538(4)	C18-181	0.95
C4-41	0.95	C25-1	1.457(3)	C29-291	0.95
C5-6	1.394(4)	C25-251	0.95	C29-292	0.95
C5-51	0.95	C25-252	0.95	C30-31	1.540(4)
C6-7	1.469(4)	C26-27	1.535(4)	C30-301	0.95
C7-8	1.412(4)	C26-261	0.95	C30-302	0.95
C7-12	1.378(4)	C26-262	0.95	C31-32	1.542(4)
C8-9	1.375(4)	C27-28	1.515(4)	C31-311	0.95
C8-81	0.95	C27-271	0.95	C31-312	0.95
C9-10	1.383(4)	C27-272	0.95	C32-321	0.95
C9-91	0.95	C28-29	1.509(4)	C32-322	0.95
C10-11	1.400(4)	C28-281	0.95	C32-323	0.95
C10-101	0.95	C28-282	0.95		
C11-12	1.400(4)	C29-30	1.514(4)		

Atoms 1,2,3	**Angle**	**Atoms 1,2,3**	**Angle 1,2,3**	**Atoms 1,2,3**	**Angle**

	1,2,3 [°]		**[°]**		**1,2,3 [°]**
C1-1-12	90.85(14)	C20-21-211	121	S1-12-11	124.8(3)
C16-2-20	91.22(13)	C22-21-211	121.3	S1-12-7	112.8(2)
S1-1-2	128.5(2)	C21-22-23	120.7(3)	C11-12-7	122.3(3)
S1-1-6	112.7(2)	C21-22-221	119.8	C14-13-18	121.2(2)
C2-1-6	118.8(2)	C23-22-221	119.6	C14-13-1	109.9(2)
C1-2-3	118.6(3)	C22-23-24	121.4(3)	C18-13-1	128.9(3)
C1-2-1	131.9(2)	C22-23-231	119.4	C3-14-13	106.4(2)
C3-2-1	109.5(2)	C24-23-231	119.2	C3-14-15	132.1(3)
C2-3-4	121.1(2)	C19-24-23	119.2(3)	C13-14-15	121.5(2)
C2-3-14	105.9(2)	C19-24-241	120	C14-15-16	117.0(2)
C4-3-14	133.0(3)	C23-24-241	120.8	C14-15-151	121.6
C3-4-5	119.6(3)	C26-25-1	114.2(2)	C16-15-151	121.4
C3-4-41	120.1	C26-25-251	107.8	S2-16-15	125.4(2)
C5-4-41	120.3	N1-25-251	108.5	S2-16-17	112.5(2)
C4-5-6	120.6(3)	C26-25-252	108.4	C15-16-17	122.1(2)
C4-5-51	119.9	N1-25-252	108.4	C16-17-18	120.7(2)
C6-5-51	119.5	H251-25-252	109.5	C16-17-19	111.4(2)
C1-6-5	121.2(3)	C25-26-27	108.9(2)	C18-17-19	127.8(2)
C1-6-7	110.9(3)	C25-26-261	109.8	C13-18-17	117.4(2)
C5-6-7	127.8(3)	C27-26-261	109.4	C13-18-181	121.2
C6-7-8	127.5(3)	C25-26-262	109.3	C17-18-181	121.4
C6-7-12	112.7(3)	C27-26-262	109.9	C17-19-20	113.1(2)
C8-7-12	119.7(3)	H261-26-262	109.5	C17-19-24	128.4(3)
C7-8-9	118.4(3)	C26-27-28	117.7(3)	C20-19-24	118.5(2)
C7-8-81	120.3	C26-27-271	107.5	S2-20-19	111.8(2)
C9-8-81	121.3	C28-27-271	108	S2-20-21	125.6(2)
C8-9-10	121.5(3)	C26-27-272	107	C19-20-21	122.6(3)
C8-9-91	119	C28-27-272	107	C20-21-22	117.6(3)
C10-9-91	119.5	H271-27-272	109.5	C31-32-321	109.8
C9-10-11	121.2(3)	C27-28-29	111.8(3)	C31-32-322	109.2
C9-10-101	119.4	C27-28-281	108.5	H321-32-322	109.5
C11-10-101	119.4	C29-28-281	108.4	C31-32-323	109.3
C10-11-12	116.9(3)	C27-28-282	109.4	H321-32-323	109.5
C10-11-111	122.1	C29-28-282	109.2	H322-32-323	109.5
C12-11-111	121	H281-28-282	109.5	C25-1-2	126.3(2)
C29-30-301	108.2	C28-29-30	116.1(3)	C25-1-13	125.3(2)
C31-30-301	108.6	C28-29-291	108.3	C2-1-13	108.3(2)
C29-30-302	109.3	C30-29-291	108.3	C31-30-302	108.9
C30-31-312	108.2	C28-29-292	107.5	H301-30-302	109.5
C32-31-312	108.8	C30-29-292	107.1	C30-31-32	112.9(3)
H311-31-312	109.5	H291-29-292	109.5	C30-31-311	108.5
		C29-30-31	112.3(3)	C32-31-311	108.9

A8. dibenzo[*b*,*b'*]thieno[2,3-*f*:5,4-*f'*]-*N*-methylcarbazoles-diC4 (8e)

Atomic parameters

Atom	x / a	y / b	z / c	U [Å²]
S1	0.44047(8)	0.88709(12)	0.10929(5)	
S2	0.77855(6)	0.73106(11)	-0.20149(4)	
C1	0.4246(2)	0.5872(4)	-0.06977(17)	
C2	0.5017(2)	0.6883(4)	-0.05711(17)	
C3	0.5111(3)	0.7849(4)	-0.00233(17)	
C4	0.4428(3)	0.7771(4)	0.03779(17)	
C5	0.3655(3)	0.6768(4)	0.02454(17)	
C6	0.3566(3)	0.5795(4)	-0.02952(17)	
C7	0.3035(3)	0.6947(4)	0.07281(19)	
C8	0.3363(3)	0.8031(5)	0.1215(2)	
C9	0.2890(4)	0.8351(5)	0.1747(3)	
C10	0.2092(4)	0.7591(5)	0.1796(3)	
C11	0.1736(4)	0.6538(6)	0.1297(3)	
C12	0.2202(3)	0.6204(5)	0.0768(2)	
C13	0.1643(4)	0.7849(7)	0.2417(3)	
C14	0.0833(4)	0.8869(8)	0.2298(3)	
C15	0.0374(5)	0.8981(10)	0.2936(3)	
C16	0.0931(4)	0.9570(8)	0.3568(4)	
C17	0.5565(2)	0.6641(4)	-0.10907(17)	
C18	0.5101(2)	0.5493(4)	-0.15143(16)	
C19	0.5432(2)	0.4980(4)	-0.20717(16)	
C20	0.6269(2)	0.5613(4)	-0.21945(16)	
C21	0.6742(2)	0.6724(4)	-0.17692(17)	
C22	0.6398(2)	0.7259(4)	-0.12164(17)	
C23	0.6758(2)	0.5288(4)	-0.27473(17)	
C24	0.7582(2)	0.6136(4)	-0.27118(17)	
C25	0.8143(3)	0.6044(5)	-0.32022(17)	
C26	0.7881(3)	0.5104(5)	-0.37417(18)	
C27	0.7060(3)	0.4262(5)	-0.37784(18)	
C28	0.6499(3)	0.4334(4)	-0.32870(17)	
C29	0.8463(3)	0.4996(6)	-0.4291(2)	
C30	0.8043(4)	0.5735(8)	-0.4905(3)	
C31	0.8653(6)	0.5838(13)	-0.5432(4)	
C32	0.9361(6)	0.7125(12)	-0.5331(5)	
C33	0.3652(3)	0.3880(5)	-0.15412(18)	
N1	0.4305(2)	0.5053(3)	-0.12721(14)	
H31	0.5622	0.853	0.0072	0.0349
H61	0.3058	0.5105	-0.0386	0.0363
H91	0.3134	0.9076	0.2073	0.0621
H111	0.1165	0.6044	0.1331	0.0677

H121	0.1951	0.5495	0.0438	0.0535
H131	0.2084	0.8308	0.2748	0.0802
H132	0.1451	0.6889	0.2571	0.0802
H141	0.1024	0.9861	0.2179	0.087
H142	0.0407	0.8454	0.1947	0.087
H151	-0.0149	0.9636	0.2841	0.1012
H152	0.0176	0.7975	0.3028	0.1012
H161	0.0569	0.9573	0.3915	0.0979
H162	0.1131	1.0587	0.3496	0.0979
H163	0.1456	0.8925	0.3684	0.0979
H191	0.511	0.4234	-0.2357	0.0335
H221	0.672	0.801	-0.0934	0.0356
H251	0.8699	0.6627	-0.3169	0.0408
H271	0.6881	0.3622	-0.415	0.0431
H281	0.5947	0.3743	-0.3319	0.0379
H291	0.9043	0.5474	-0.4148	0.0535
H292	0.8558	0.3942	-0.4383	0.0535
H301	0.79	0.6764	-0.4802	0.0821
H302	0.7488	0.52	-0.5066	0.0821
H311	0.8279	0.5975	-0.5848	0.1255
H312	0.8983	0.4897	-0.5431	0.1255
H321	0.9745	0.7152	-0.5664	0.1399
H322	0.903	0.8065	-0.5332	0.1399
H323	0.9734	0.6986	-0.4915	0.1399
H331	0.3833	0.3483	-0.1933	0.0404
H332	0.3051	0.4316	-0.1639	0.0404
H333	0.3645	0.3073	-0.1231	0.0404

Anisotropic displacement parameters, in Å²

Atom	**U_{11}**	**U_{22}**	**U_{33}**	**U_{12}**	**U_{13}**	**U_{23}**
S1	0.0504(6)	0.0320(5)	0.0264(4)	0.0031(4)	0.0150(4)	-0.0034(4)
S2	0.0279(4)	0.0372(5)	0.0271(4)	-0.0039(4)	0.0090(3)	-0.0020(4)
C1	0.0299(17)	0.0246(17)	0.0241(15)	-0.0002(13)	0.0076(13)	0.0005(13)
C2	0.0271(16)	0.0278(17)	0.0211(15)	-0.0017(13)	0.0066(13)	0.0011(13)
C3	0.0315(18)	0.0291(17)	0.0214(15)	-0.0016(14)	0.0062(13)	-0.0019(13)
C4	0.0351(18)	0.0284(17)	0.0213(15)	0.0031(15)	0.0075(13)	0.0010(14)
C5	0.0320(18)	0.0289(17)	0.0270(17)	0.0037(14)	0.0113(14)	0.0071(14)
C6	0.0301(17)	0.0266(18)	0.0270(16)	-0.0008(14)	0.0083(13)	0.0021(13)
C7	0.042(2)	0.0294(19)	0.0333(19)	0.0104(16)	0.0195(16)	0.0089(15)
C8	0.052(2)	0.029(2)	0.0312(19)	0.0095(17)	0.0188(18)	0.0042(15)
C9	0.085(4)	0.033(2)	0.051(3)	0.012(2)	0.044(3)	0.004(2)
C10	0.085(4)	0.034(2)	0.072(3)	0.010(2)	0.059(3)	0.001(2)
C11	0.060(3)	0.039(2)	0.081(4)	0.005(2)	0.048(3)	0.008(2)

C12	0.046(2)	0.034(2)	0.052(2)	0.0073(18)	0.028(2)	0.0101(19)
C13	0.075(4)	0.058(3)	0.064(3)	0.004(3)	0.038(3)	0.010(3)
C14	0.051(3)	0.076(4)	0.071(4)	0.003(3)	0.024(3)	-0.001(3)
C15	0.078(4)	0.113(6)	0.082(4)	-0.002(4)	0.058(4)	-0.034(4)
C16	0.059(3)	0.069(4)	0.106(5)	-0.002(3)	0.043(3)	-0.020(4)
C17	0.0258(17)	0.0265(16)	0.0218(15)	-0.0006(14)	0.0060(12)	-0.0016(13)
C18	0.0255(16)	0.0255(16)	0.0231(15)	0.0002(13)	0.0066(12)	0.0006(13)
C19	0.0274(16)	0.0284(17)	0.0213(15)	-0.0007(14)	0.0025(13)	-0.0013(13)
C20	0.0265(16)	0.0253(16)	0.0229(16)	0.0037(13)	0.0045(13)	0.0012(13)
C21	0.0258(16)	0.0292(16)	0.0238(16)	-0.0012(14)	0.0089(13)	0.0003(13)
C22	0.0261(16)	0.0289(17)	0.0239(15)	-0.0017(14)	0.0041(12)	-0.0003(14)
C23	0.0288(17)	0.0284(17)	0.0222(15)	0.0033(14)	0.0063(13)	0.0022(13)
C24	0.0322(18)	0.0314(17)	0.0221(15)	0.0032(15)	0.0068(13)	0.0011(14)
C25	0.0295(17)	0.041(2)	0.0260(16)	-0.0001(16)	0.0099(14)	0.0035(16)
C26	0.041(2)	0.040(2)	0.0245(17)	0.0078(17)	0.0137(15)	0.0047(16)
C27	0.046(2)	0.035(2)	0.0232(17)	0.0080(17)	0.0098(15)	-0.0020(15)
C28	0.0342(19)	0.0311(18)	0.0247(16)	0.0041(15)	0.0081(14)	0.0014(14)
C29	0.048(2)	0.059(3)	0.030(2)	0.005(2)	0.0191(18)	0.003(2)
C30	0.065(3)	0.097(5)	0.047(3)	0.015(3)	0.019(3)	0.018(3)
C31	0.098(5)	0.18(1)	0.066(4)	0.066(6)	0.050(4)	0.062(5)
C32	0.076(5)	0.155(9)	0.147(9)	0.050(6)	0.048(6)	0.045(7)
C33	0.0303(17)	0.0310(18)	0.0308(17)	-0.0060(16)	0.0065(14)	-0.0034(16)
N1	0.0294(14)	0.0262(14)	0.0253(14)	-0.0038(12)	0.0084(11)	-0.0042(12)

Selected geometric informations

Atoms 1,2	**d 1,2 [Å]**	**Atoms 1,2**	**d 1,2 [Å]**	**Atoms 1,2**	**d 1,2 [Å]**
S1-4	1.759(4)	C17-18	1.427(5)	C13-131	0.95
S1-8	1.740(4)	C17-22	1.389(5)	C13-132	0.95
S2-21	1.752(3)	C18-19	1.385(5)	C14-15	1.566(7)
S2-24	1.749(4)	C18-1	1.387(4)	C14-141	0.95
C1-2	1.420(5)	C19-20	1.398(5)	C14-142	0.95
C1-6	1.388(5)	C19-191	0.95	C15-16	1.515(10)
C1-1	1.394(4)	C20-21	1.412(5)	C15-151	0.95
C2-3	1.396(5)	C20-23	1.460(5)	C15-152	0.95
C2-17	1.446(5)	C21-22	1.392(5)	C16-161	0.95
C3-4	1.389(5)	C22-221	0.95	C16-162	0.95
C3-31	0.95	C23-24	1.404(5)	C16-163	0.95
C4-5	1.420(5)	C23-28	1.392(5)	C31-32	1.516(14)
C5-6	1.388(5)	C24-25	1.395(5)	C31-311	0.95
C5-7	1.451(5)	C25-26	1.385(6)	C31-312	0.95
C6-61	0.95	C25-251	0.95	C32-321	0.95
C7-8	1.405(6)	C26-27	1.396(6)	C32-322	0.95
C7-12	1.391(6)	C26-29	1.517(5)	C32-323	0.95

C8-9	1.409(5)	C27-28	1.396(5)	C33-1	1.447(5)
C9-10	1.357(8)	C27-271	0.95	C33-331	0.95
C9-91	0.95	C28-281	0.95	C33-332	0.95
C10-11	1.414(8)	C29-30	1.466(7)	C33-333	0.95
C10-13	1.540(6)	C29-291	0.95	C12-121	0.95
C11-12	1.398(6)	C29-292	0.95	C13-14	1.469(8)
C11-111	0.95	C30-31	1.507(8)	C30-301	0.95
				C30-302	0.95

Atoms 1,2,3	**Angle 1,2,3 [°]**	**Atoms 1,2,3**	**Angle 1,2,3 [°]**	**Atoms 1,2,3**	**Angle 1,2,3 [°]**
C4-1-8	91.17(19)	C17-18-1	108.7(3)	C14-15-152	107
C21-2-24	91.14(17)	C19-18-1	128.7(3)	C16-15-152	106.3
C2-1-6	122.6(3)	C18-19-20	116.6(3)	H151-15-152	109.5
C2-1-1	108.8(3)	C18-19-191	121.9	C15-16-161	111
C6-1-1	128.5(3)	C20-19-191	121.5	C15-16-162	108.5
C1-2-3	119.9(3)	C19-20-21	121.1(3)	H161-16-162	109.5
C1-2-17	106.7(3)	C19-20-23	127.5(3)	C15-16-163	108.8
C3-2-17	133.4(3)	C21-20-23	111.3(3)	H161-16-163	109.5
C2-3-4	117.3(3)	C20-21-2	112.7(2)	H162-16-163	109.5
C2-3-31	121.4	C20-21-22	122.1(3)	C2-17-18	106.7(3)
C4-3-31	121.4	S2-21-22	125.2(3)	C2-17-22	132.9(3)
S1-4-3	125.2(3)	C21-22-17	117.3(3)	C18-17-22	120.3(3)
S1-4-5	112.3(3)	C21-22-221	121.6	C17-18-19	122.6(3)
C3-4-5	122.5(3)	C17-22-221	121.2	C31-32-323	108.4
C4-5-6	120.3(3)	C20-23-24	112.0(3)	H321-32-323	109.5
C4-5-7	111.3(3)	C20-23-28	129.1(3)	H322-32-323	109.5
C6-5-7	128.4(4)	C24-23-28	118.8(3)	N1-33-331	109.2
C1-6-5	117.4(3)	S2-24-23	112.8(2)	N1-33-332	109.5
C1-6-61	121.4	S2-24-25	125.5(3)	H331-33-332	109.5
C5-6-61	121.2	C23-24-25	121.7(3)	N1-33-333	109.7
C5-7-8	112.2(4)	C24-25-26	119.5(3)	H331-33-333	109.5
C5-7-12	129.4(4)	C24-25-251	120.4	H332-33-333	109.5
C8-7-12	118.4(4)	C26-25-251	120.2	C33-1-1	124.3(3)
C7-8-1	113.0(3)	C25-26-27	118.9(3)	C33-1-18	126.6(3)
C7-8-9	122.2(4)	C25-26-29	121.0(4)	C1-1-18	109.0(3)
S1-8-9	124.9(4)	C27-26-29	120.0(4)	C13-14-15	109.4(5)
C8-9-10	119.3(5)	C26-27-28	122.0(4)	C13-14-141	109.3
C8-9-91	120.4	C26-27-271	118.7	C15-14-141	109.8
C10-9-91	120.3	C28-27-271	119.2	C13-14-142	108.5
C9-10-11	119.1(4)	C27-28-23	119.1(4)	C15-14-142	110.3
C9-10-13	118.0(5)	C27-28-281	120.7	H141-14-142	109.5
C11-10-13	122.8(5)	C23-28-281	120.2	C14-15-16	120.0(5)
C10-11-12	122.1(5)	C26-29-30	114.0(4)	C14-15-151	107.3

C10-11-111	118	C26-29-291	108.4	C16-15-151	106.6
C12-11-111	119.9	C30-29-291	108.2	C30-31-32	114.2(8)
C11-12-7	118.9(5)	C26-29-292	108.9	C30-31-311	109.5
C11-12-121	120.8	C30-29-292	107.9	C32-31-311	108.6
C7-12-121	120.3	H291-29-292	109.5	C30-31-312	107.5
C10-13-14	112.5(5)	C29-30-31	115.5(5)	C32-31-312	107.5
C10-13-131	109.1	C29-30-301	107.4	H311-31-312	109.5
C14-13-131	107.9	C31-30-301	106.1	C31-32-321	112.6
C10-13-132	109.4	C29-30-302	108	C31-32-322	107.4
C14-13-132	108.4	C31-30-302	110.1	H321-32-322	109.5
H131-13-132	109.5	H301-30-302	109.5		

A9. bisbenzo[*b*,*b'*]thienodithieno[3,2-*b*:2',3'-*d*]pyrrole (27)

Atomic parameters

Atom	x / a	y / b	z / c	U [Å^2]
S1	-0.19653(6)	0.46131(15)	0.23803(4)	
S2	-0.31729(6)	0.99155(16)	0.26746(5)	
S3	0.07760(6)	0.46558(15)	0.32351(5)	
S4	0.16414(6)	0.98996(16)	0.42257(5)	
C1	-0.1118(3)	0.6063(6)	0.28589(19)	
C2	-0.1440(2)	0.7865(6)	0.29929(18)	
C3	-0.2370(2)	0.8103(6)	0.27063(19)	
C4	-0.2753(2)	0.6442(6)	0.23713(18)	
C5	-0.3696(3)	0.6603(6)	0.20710(18)	
C6	-0.4303(3)	0.5238(7)	0.16866(18)	
C7	-0.5196(3)	0.5793(7)	0.1431(2)	
C8	-0.5503(3)	0.7587(7)	0.1562(2)	
C9	-0.4925(3)	0.8978(7)	0.1954(2)	
C10	-0.4020(3)	0.8450(7)	0.2202(2)	
C11	-0.0180(3)	0.6114(6)	0.31397(19)	
C12	0.0020(3)	0.7913(6)	0.34438(18)	
C13	0.0951(3)	0.8114(6)	0.37738(18)	
C14	0.1438(2)	0.6474(6)	0.37001(17)	
C15	0.2391(2)	0.6594(6)	0.40034(18)	
C16	0.3085(3)	0.5261(7)	0.4025(2)	
C17	0.3963(3)	0.5753(7)	0.4357(2)	
C18	0.4152(3)	0.7525(7)	0.4665(2)	
C19	0.3478(3)	0.8890(7)	0.46568(19)	
C20	0.2589(3)	0.8408(6)	0.43115(19)	
C21	-0.0822(3)	1.0977(6)	0.35629(18)	
C22	-0.0734(3)	1.1139(6)	0.42818(18)	
C23	-0.0833(3)	1.3202(6)	0.4507(2)	

C24	-0.1794(3)	1.3954(6)	0.4291(2)	
C25	-0.1868(3)	1.6042(7)	0.4519(2)	
C26	-0.2819(3)	1.6846(8)	0.4305(3)	
N1	-0.0747(2)	0.8998(4)	0.33500(16)	
H61	-0.411	0.3972	0.161	0.0345
H71	-0.561	0.4911	0.1167	0.0361
H81	-0.6114	0.7921	0.1361	0.0353
H91	-0.5149	1.0189	0.2055	0.0256
H161	0.2957	0.4036	0.3818	0.0316
H171	0.4443	0.4876	0.4369	0.0347
H181	0.4756	0.7829	0.4892	0.0328
H191	0.3613	1.0093	0.4877	0.0321
H211	-0.1395	1.1478	0.3337	0.0215
H212	-0.0362	1.174	0.3469	0.0215
H221	-0.1186	1.035	0.4377	0.0239
H222	-0.0155	1.0663	0.4508	0.0239
H231	-0.0645	1.3225	0.4963	0.0246
H232	-0.0457	1.4035	0.4345	0.0246
H241	-0.2171	1.313	0.4456	0.023
H242	-0.1984	1.3926	0.3835	0.023
H251	-0.1658	1.6055	0.4974	0.0367
H252	-0.1493	1.6851	0.4346	0.0367
H261	-0.2801	1.8133	0.4467	0.0363
H262	-0.3205	1.6072	0.4478	0.0363
H263	-0.304	1.6867	0.385	0.0363

Anisotropic displacement parameters, in Å²

Atom	**U_{11}**	**U_{22}**	**U_{33}**	**U_{12}**	**U_{13}**	**U_{23}**
S1	0.0207(5)	0.0166(5)	0.0166(4)	-0.0032(4)	0.0034(4)	-0.0041(4)
S2	0.0174(5)	0.0212(6)	0.0242(5)	0.0017(4)	0.0037(4)	0.0002(5)
S3	0.0204(5)	0.0163(5)	0.0203(4)	0.0043(4)	0.0053(3)	-0.0009(4)
S4	0.0169(4)	0.0201(5)	0.0220(5)	-0.0015(4)	0.0024(3)	-0.0058(4)
C1	0.0168(18)	0.020(2)	0.0158(18)	0.0014(15)	0.0040(15)	-0.0042(15)
C2	0.0113(17)	0.0199(19)	0.0127(17)	-0.0033(14)	-0.0006(14)	0.0008(15)
C3	0.0138(18)	0.0183(19)	0.0172(18)	0.0033(15)	0.0026(14)	-0.0020(15)
C4	0.0133(17)	0.022(2)	0.0135(17)	-0.0035(15)	0.0012(14)	-0.0013(15)
C5	0.0183(19)	0.027(2)	0.0121(18)	-0.0030(16)	0.0004(15)	0.0006(16)
C6	0.0231(19)	0.030(2)	0.0195(18)	-0.008(2)	0.0031(15)	-0.0047(19)
C7	0.0149(19)	0.050(3)	0.020(2)	-0.0114(18)	-0.0001(16)	0.005(2)
C8	0.016(2)	0.043(3)	0.028(2)	-0.0043(19)	0.0006(17)	0.005(2)
C9	0.0143(19)	0.027(2)	0.025(2)	0.0033(15)	0.0000(16)	0.0061(18)
C10	0.0129(19)	0.036(3)	0.021(2)	-0.0036(17)	0.0025(16)	0.0011(19)
C11	0.0186(19)	0.0117(17)	0.0207(19)	-0.0002(15)	0.0030(16)	-0.0028(15)

C12	0.0169(19)	0.022(2)	0.0116(17)	0.0068(15)	0.0015(14)	-0.0011(15)
C13	0.0168(18)	0.0144(18)	0.0161(18)	0.0013(15)	0.0048(14)	0.0028(15)
C14	0.0125(16)	0.0170(19)	0.0124(17)	-0.0018(14)	0.0011(13)	-0.0031(14)
C15	0.0134(18)	0.027(2)	0.0143(17)	0.0021(15)	0.0045(14)	0.0002(16)
C16	0.025(2)	0.024(2)	0.0247(19)	0.0050(19)	0.0075(15)	0.0010(19)
C17	0.025(2)	0.034(3)	0.022(2)	0.0091(17)	0.0068(17)	0.0061(18)
C18	0.0151(19)	0.034(3)	0.024(2)	-0.0018(18)	0.0010(16)	-0.0021(19)
C19	0.022(2)	0.031(2)	0.0173(19)	-0.0029(18)	0.0008(16)	-0.0034(17)
C20	0.0159(18)	0.022(2)	0.019(2)	-0.0021(16)	0.0028(15)	-0.0003(16)
C21	0.020(2)	0.0158(18)	0.0113(18)	0.0010(15)	0.0000(15)	-0.0042(14)
C22	0.032(2)	0.0168(19)	0.0131(18)	0.0063(17)	0.0014(16)	0.0013(15)
C23	0.026(2)	0.022(2)	0.023(2)	-0.0027(16)	0.0019(17)	-0.0113(17)
C24	0.028(2)	0.024(2)	0.019(2)	0.0014(17)	0.0127(17)	-0.0020(16)
C25	0.051(3)	0.020(2)	0.022(2)	0.0055(19)	0.017(2)	-0.0035(18)
C26	0.045(3)	0.032(3)	0.041(3)	0.011(2)	0.015(2)	-0.001(2)
N1	0.0133(15)	0.0126(15)	0.0203(17)	-0.0022(13)	0.0017(13)	-0.0049(13)

Selected geometric informations

Atoms 1,2	**d 1,2 [Å]**	**Atoms 1,2**	**d 1,2 [Å]**	**Atoms 1,2**	**d 1,2 [Å]**
S1-1	1.742(4)	C15-16	1.400(6)	C8-81	0.95
S1-4	1.746(4)	C15-20	1.408(6)	C9-10	1.398(5)
S2-3	1.746(4)	C16-17	1.389(5)	C9-91	0.95
S2-10	1.743(4)	C16-161	0.95	C11-12	1.396(5)
S3-11	1.748(4)	C17-18	1.381(6)	C12-13	1.423(5)
S3-14	1.748(4)	C17-171	0.95	C12-1	1.366(5)
S4-13	1.740(4)	C18-19	1.396(6)	C13-14	1.389(5)
S4-20	1.754(4)	C18-181	0.95	C14-15	1.439(5)
C1-2	1.395(6)	C19-20	1.409(5)	C24-241	0.95
C1-11	1.407(5)	C19-191	0.95	C24-242	0.95
C2-3	1.407(5)	C21-22	1.530(5)	C25-26	1.516(6)
C2-1	1.376(5)	C21-1	1.452(4)	C25-251	0.95
C3-4	1.395(5)	C21-211	0.95	C25-252	0.95
C4-5	1.424(5)	C21-212	0.95	C26-261	0.95
C5-6	1.423(5)	C22-23	1.522(6)	C26-262	0.95
C5-10	1.423(6)	C22-221	0.95	C26-263	0.95
C6-7	1.388(5)	C22-222	0.95	C7-71	0.95
C6-61	0.95	C23-24	1.516(6)	C8-9	1.420(6)
C7-8	1.380(7)	C23-231	0.95	C23-232	0.95
				C24-25	1.534(6)

Atoms 1,2,3	**Angle 1,2,3 [°]**	**Atoms 1,2,3**	**Angle 1,2,3 [°]**	**Atoms 1,2,3**	**Angle 1,2,3 [°]**

C1-1-4	90.00(19)	C16-17-18	120.7(4)	S3-11-1	140.4(3)
C3-2-10	91.1(2)	C16-17-171	120.1	S3-11-12	112.6(3)
C11-3-14	89.81(19)	C18-17-171	119.2	C1-11-12	107.1(3)
C13-4-20	90.57(19)	C17-18-19	122.0(4)	C11-12-13	112.6(3)
S1-1-2	112.4(3)	C17-18-181	119.4	C11-12-1	110.1(3)
S1-1-11	141.8(3)	C19-18-181	118.6	C13-12-1	137.2(4)
C2-1-11	105.7(3)	C18-19-20	117.4(4)	C12-13-4	136.7(3)
C1-2-3	112.9(3)	C18-19-191	121.4	C12-13-14	111.5(3)
C1-2-1	110.8(3)	C20-19-191	121.2	S4-13-14	111.8(3)
C3-2-1	136.2(4)	S4-20-19	125.4(3)	S3-14-13	113.5(3)
C2-3-2	136.6(3)	S4-20-15	113.7(3)	S3-14-15	131.7(3)
C2-3-4	111.7(3)	C19-20-15	120.8(4)	C13-14-15	114.7(3)
S2-3-4	111.7(3)	C22-21-1	113.5(3)	C14-15-16	130.8(4)
S1-4-3	113.0(3)	C22-21-211	108	C14-15-20	109.2(3)
S1-4-5	132.9(3)	N1-21-211	108.7	C16-15-20	120.0(4)
C3-4-5	114.0(3)	C22-21-212	108.5	C15-16-17	119.0(4)
C4-5-6	129.9(4)	N1-21-212	108.6	C15-16-161	120.5
C4-5-10	110.5(3)	H211-21-212	109.5	C17-16-161	120.5
C6-5-10	119.6(4)	C21-22-23	114.0(3)	C25-24-242	109
C5-6-7	118.2(4)	C21-22-221	108.4	H241-24-242	109.5
C5-6-61	121.3	C23-22-221	108.5	C24-25-26	113.3(4)
C7-6-61	120.5	C21-22-222	107.9	C24-25-251	108
C6-7-8	121.6(4)	C23-22-222	108.6	C26-25-251	109.7
C6-7-71	119.6	H221-22-222	109.5	C24-25-252	108.3
C8-7-71	118.8	C22-23-24	113.2(3)	C26-25-252	108
C7-8-9	122.1(4)	C22-23-231	108.7	H251-25-252	109.5
C7-8-81	118.4	C24-23-231	108	C25-26-261	107.5
C9-8-81	119.4	C22-23-232	108.5	C25-26-262	109.6
C8-9-10	116.8(4)	C24-23-232	108.9	H261-26-262	109.5
C8-9-91	121.4	H231-23-232	109.5	C25-26-263	111.3
C10-9-91	121.8	C23-24-25	111.9(4)	H261-26-263	109.5
C5-10-2	112.7(3)	C23-24-241	109.1	H262-26-263	109.5
C5-10-9	121.6(4)	C25-24-241	109.2	C21-1-2	126.3(3)
S2-10-9	125.7(4)	C23-24-242	108.2	C21-1-12	127.4(3)
				C2-1-12	106.3(3)

A10. bisbenzo[*b,b'*]thienocyclopenta [2,1-*b*:3,4-*b'*]dithiophene (32) (High temp.)

Atomic parameters

Atom	x / a	y / b	z / c	U [Å^2]
S1	0.35836(9)	0.22924(10)	0.37125(4)	
S99	0.22328(9)	0.2330(1)	0.21539(4)	
S3	0.22926(9)	0.50027(11)	0.47637(4)	

S4	-0.03762(9)	0.49081(11)	0.19159(4)	
C4	0.2530(3)	0.3065(3)	0.33437(15)	
C3	0.2041(3)	0.3075(3)	0.27820(15)	
C2	0.1216(3)	0.3962(3)	0.27550(14)	
C6	0.2493(3)	0.4041(3)	0.41927(14)	
C7	0.3339(3)	0.3204(4)	0.42932(15)	
C5	0.2013(3)	0.3961(3)	0.36506(15)	
C1	0.1101(3)	0.4633(3)	0.33091(15)	
C15	0.1177(3)	0.3216(4)	0.18467(15)	
C8	0.3873(3)	0.3293(4)	0.48373(15)	
C14	0.0712(3)	0.4032(3)	0.22153(15)	
C16	0.0667(4)	0.3261(4)	0.12954(17)	
C22	-0.0084(3)	0.4449(4)	0.35520(15)	
C28	0.1371(3)	0.6012(3)	0.32531(17)	
C13	0.3390(3)	0.4263(4)	0.51385(16)	
C21	-0.0201(4)	0.4138(5)	0.12766(16)	
C9	0.4757(3)	0.2615(4)	0.50860(18)	
C23	-0.0460(3)	0.3113(4)	0.35860(16)	
C25	-0.2011(3)	0.1610(5)	0.38250(17)	
C24	-0.1616(3)	0.2940(4)	0.38182(17)	
C10	0.5136(4)	0.2931(6)	0.5621(2)	
C12	0.3785(4)	0.4566(5)	0.56752(18)	
C29	0.2527(4)	0.6284(4)	0.30148(19)	
C30	0.2750(5)	0.7640(4)	0.2949(2)	
C17	0.0907(4)	0.2580(5)	0.08129(18)	
C19	-0.0613(7)	0.3669(8)	0.0333(3)	
C27	-0.3455(5)	0.0096(6)	0.4116(3)	
C26	-0.3124(4)	0.1428(6)	0.4079(2)	
C20	-0.0863(5)	0.4363(6)	0.0795(2)	
C18	0.0254(7)	0.2809(8)	0.0339(2)	
C11	0.4653(5)	0.3892(6)	0.5902(2)	
C31	0.3876(6)	0.7925(5)	0.2700(3)	
C33	0.494(1)	0.9653(10)	0.2480(6)	
C32	0.3939(8)	0.9395(9)	0.2670(5)	
H221	-0.0083	0.478	0.3919	0.1137
H222	-0.0622	0.4877	0.3323	0.1137
H281	0.1348	0.6378	0.3613	0.1208
H282	0.0811	0.6379	0.3015	0.1208
H91	0.5084	0.1945	0.4893	0.1373
H231	0.0076	0.2682	0.3815	0.1205
H232	-0.0465	0.2779	0.3219	0.1205
H251	-0.1461	0.1141	0.4029	0.1366
H252	-0.2055	0.1329	0.3449	0.1366
H241	-0.1602	0.3234	0.4192	0.1324

H242	-0.2146	0.3406	0.36	0.1324
H101	0.5746	0.2493	0.5795	0.1666
H121	0.3453	0.5229	0.5871	0.1591
H291	0.3095	0.5941	0.3256	0.1397
H292	0.2562	0.591	0.2657	0.1397
H301	0.2735	0.8004	0.331	0.1713
H302	0.2164	0.7981	0.2719	0.1713
H171	0.1504	0.1993	0.0818	0.1629
H191	-0.1042	0.3778	-0.0005	0.2148
H271	-0.4174	0.0015	0.4282	0.2298
H272	-0.2903	-0.0341	0.4333	0.2298
H273	-0.3492	-0.0232	0.3748	0.2298
H261	-0.3092	0.175	0.4448	0.1891
H262	-0.3681	0.1859	0.3863	0.1891
H201	-0.1453	0.4958	0.0788	0.1807
H181	0.0395	0.2363	0.0007	0.2079
H111	0.4929	0.4083	0.6268	0.1724
H311	0.4474	0.7597	0.2928	0.2157
H312	0.3902	0.7577	0.2337	0.2157
H331	0.4962	1.0527	0.247	0.3726
H332	0.5563	0.9356	0.2701	0.3726
H333	0.4983	0.9337	0.2111	0.3726
H321	0.3903	0.9721	0.3037	0.3356
H322	0.3322	0.9702	0.2448	0.3356

Anisotropic displacement parameters, in Å²

Atom	**U_{11}**	**U_{22}**	**U_{33}**	**U_{12}**	**U_{13}**	**U_{23}**
S1	0.0955(7)	0.0946(7)	0.0870(7)	0.0323(6)	0.0034(5)	-0.0041(6)
S99	0.1100(8)	0.0906(7)	0.0791(6)	0.0052(6)	0.0119(5)	-0.0143(5)
S3	0.0990(7)	0.1135(9)	0.0836(7)	0.0270(7)	-0.0091(5)	-0.0238(6)
S4	0.0925(7)	0.1008(8)	0.0907(7)	-0.0102(6)	-0.0127(5)	0.0167(6)
C4	0.083(2)	0.078(2)	0.079(2)	0.016(2)	0.0006(19)	-0.005(2)
C3	0.090(3)	0.079(2)	0.074(2)	0.009(2)	0.0048(19)	-0.0099(19)
C2	0.082(2)	0.076(2)	0.071(2)	0.000(2)	-0.0018(18)	-0.0056(19)
C6	0.077(2)	0.083(3)	0.073(2)	0.014(2)	0.0022(18)	-0.0102(19)
C7	0.079(2)	0.090(3)	0.073(2)	0.014(2)	0.0055(18)	-0.002(2)
C5	0.076(2)	0.077(2)	0.078(2)	0.0154(19)	-0.0015(18)	-0.0091(19)
C1	0.077(2)	0.076(2)	0.079(2)	0.0130(19)	-0.0052(18)	-0.0096(19)
C15	0.096(3)	0.087(3)	0.072(2)	-0.017(2)	0.006(2)	-0.002(2)
C8	0.075(2)	0.105(3)	0.076(2)	0.007(2)	0.0017(19)	0.010(2)
C14	0.078(2)	0.077(2)	0.077(2)	-0.0090(19)	-0.0015(19)	0.006(2)
C16	0.114(3)	0.103(3)	0.074(3)	-0.033(3)	0.004(2)	0.004(2)
C22	0.085(3)	0.094(3)	0.083(3)	0.023(2)	-0.005(2)	-0.014(2)

C28	0.095(3)	0.079(3)	0.102(3)	0.016(2)	-0.016(2)	-0.010(2)
C13	0.084(3)	0.113(3)	0.079(3)	0.014(2)	-0.003(2)	-0.004(2)
C21	0.116(4)	0.117(4)	0.072(3)	-0.037(3)	-0.011(2)	0.015(2)
C9	0.093(3)	0.128(4)	0.091(3)	0.019(3)	0.001(2)	0.013(3)
C23	0.082(3)	0.101(3)	0.089(3)	0.015(2)	0.007(2)	-0.008(2)
C25	0.086(3)	0.133(4)	0.092(3)	0.011(3)	0.013(2)	-0.003(3)
C24	0.089(3)	0.122(4)	0.090(3)	0.023(3)	0.010(2)	-0.005(3)
C10	0.107(4)	0.170(5)	0.096(3)	0.025(4)	-0.020(3)	0.016(3)
C12	0.117(4)	0.162(5)	0.087(3)	0.026(3)	-0.019(3)	-0.024(3)
C29	0.107(3)	0.080(3)	0.127(4)	0.003(2)	-0.016(3)	0.003(3)
C30	0.134(4)	0.078(3)	0.182(5)	0.002(3)	-0.029(4)	0.004(3)
C17	0.158(4)	0.137(4)	0.067(3)	-0.035(3)	0.006(3)	-0.003(3)
C19	0.206(8)	0.231(9)	0.082(4)	-0.040(6)	-0.039(5)	0.021(5)
C27	0.139(5)	0.163(6)	0.265(8)	-0.026(5)	0.061(5)	0.004(6)
C26	0.094(3)	0.164(6)	0.171(5)	0.000(4)	0.031(3)	0.006(4)
C20	0.147(5)	0.172(5)	0.090(3)	-0.028(4)	-0.027(3)	0.027(4)
C18	0.215(8)	0.202(8)	0.075(4)	-0.045(6)	-0.007(4)	-0.010(4)
C11	0.127(4)	0.188(6)	0.092(3)	0.027(4)	-0.021(3)	-0.007(4)
C31	0.164(6)	0.093(4)	0.226(7)	-0.017(4)	-0.020(5)	0.035(4)
C33	0.336(15)	0.222(11)	0.420(17)	-0.010(12)	0.070(14)	0.076(11)
C32	0.196(9)	0.195(9)	0.403(15)	-0.024(8)	0.056(9)	0.073(9)

Selected geometric informations

Atoms 1,2	**d 1,2 [Å]**	**Atoms 1,2**	**d 1,2 [Å]**	**Atoms 1,2**	**d 1,2 [Å]**
S1-4	1.724(4)	C25-26	1.476(5)	C16-17	1.407(6)
S1-7	1.737(4)	C25-251	0.95	C22-23	1.522(5)
S99-3	1.728(3)	C25-252	0.95	C22-221	0.95
S99-15	1.724(4)	C24-241	0.95	C22-222	0.95
S3-6	1.741(3)	C24-242	0.95	C28-29	1.522(5)
S3-13	1.751(4)	C10-11	1.374(6)	C28-281	0.95
S4-14	1.738(4)	C10-101	0.95	C28-282	0.95
S4-21	1.761(5)	C12-11	1.362(6)	C13-12	1.394(5)
C4-3	1.449(5)	C12-121	0.95	C21-20	1.398(6)
C4-5	1.374(4)	C29-30	1.506(6)	C9-10	1.388(6)
C3-2	1.371(5)	C29-291	0.95	C9-91	0.95
C2-1	1.522(4)	C29-292	0.95	C23-24	1.500(5)
C2-14	1.410(4)	C30-31	1.504(7)	C23-231	0.95
C6-7	1.368(4)	C30-301	0.95	C23-232	0.95
C6-5	1.405(4)	C30-302	0.95	C25-24	1.519(6)
C7-8	1.435(5)	C17-18	1.376(7)	C20-201	0.95
C5-1	1.520(5)	C17-171	0.95	C18-181	0.95
C1-22	1.543(5)	C19-20	1.377(8)	C11-111	0.95
C1-28	1.539(5)	C19-18	1.387(8)	C31-32	1.601(10)

C15-14	1.376(5)	C19-191	0.95	C31-311	0.95
C15-16	1.437(5)	C27-26	1.503(7)	C31-312	0.95
C8-13	1.406(5)	C27-271	0.95	C33-32	1.308(8)
C8-9	1.398(5)	C27-272	0.95	C33-331	0.95
C16-21	1.399(6)	C27-273	0.95	C33-332	0.95
C26-262	0.95	C26-261	0.95	C33-333	0.95
		C32-322	0.95	C32-321	0.95

Atoms 1,2,3	**Angle 1,2,3 [°]**	**Atoms 1,2,3**	**Angle 1,2,3 [°]**	**Atoms 1,2,3**	**Angle 1,2,3 [°]**
C4-1-7	89.94(18)	C26-25-252	108.6	S3-13-8	112.7(3)
C3-99-15	89.97(19)	H251-25-252	109.5	S3-13-12	126.0(4)
C6-3-13	90.70(19)	C25-24-23	114.0(3)	C8-13-12	121.2(4)
C14-4-21	89.7(2)	C25-24-241	107.9	S4-21-16	113.5(3)
S1-4-3	138.0(3)	C23-24-241	108.2	S4-21-20	123.8(5)
S1-4-5	113.4(3)	C25-24-242	108.3	C16-21-20	122.6(5)
C3-4-5	108.6(3)	C23-24-242	108.8	C8-9-10	118.8(4)
C4-3-99	138.2(3)	H241-24-242	109.5	C8-9-91	120.4
C4-3-2	108.3(3)	C9-10-11	120.8(5)	C10-9-91	120.8
S99-3-2	113.4(3)	C9-10-101	120.1	C22-23-24	114.2(3)
C3-2-1	112.0(3)	C11-10-101	119.1	C22-23-231	108.1
C3-2-14	111.3(3)	C13-12-11	118.1(5)	C24-23-231	108.8
C1-2-14	136.6(3)	C13-12-121	120.1	C22-23-232	108.1
S3-6-7	112.0(3)	C11-12-121	121.8	C24-23-232	108.1
S3-6-5	134.5(3)	C28-29-30	113.0(4)	H231-23-232	109.5
C7-6-5	113.4(3)	C28-29-291	108.8	C24-25-26	114.2(4)
S1-7-6	112.0(3)	C30-29-291	108.9	C24-25-251	108.1
S1-7-8	133.3(3)	C28-29-292	108.4	C26-25-251	108.7
C6-7-8	114.6(3)	C30-29-292	108.2	C24-25-252	107.8
C6-5-4	111.3(3)	H291-29-292	109.5	C12-11-111	119.1
C6-5-1	136.9(3)	C29-30-31	113.8(4)	C30-31-32	105.5(6)
C4-5-1	111.8(3)	C29-30-301	107.8	C30-31-311	110.3
C2-1-5	99.2(3)	C31-30-301	108.2	C32-31-311	111.5
C2-1-22	111.6(3)	C29-30-302	108.4	C30-31-312	109.4
C5-1-22	111.8(3)	C31-30-302	109.1	C32-31-312	110.7
C2-1-28	111.6(3)	H301-30-302	109.5	H311-31-312	109.5
C5-1-28	111.7(3)	C16-17-18	117.4(6)	C32-33-331	104.4
C22-1-28	110.5(3)	C16-17-171	120.6	C32-33-332	115.4
S99-15-14	112.5(3)	C18-17-171	122	H331-33-332	109.5
S99-15-16	133.8(4)	C20-19-18	122.3(6)	C32-33-333	108.4
C14-15-16	113.7(4)	C20-19-191	119.6	H331-33-333	109.5
C7-8-13	110.0(3)	C18-19-191	118.1	H332-33-333	109.5
C7-8-9	131.0(4)	C26-27-271	110.5	C31-32-33	105.8(10)
C13-8-9	119.0(4)	C26-27-272	109.7	C31-32-321	109.1

C2-14-4	134.2(3)	H271-27-272	109.5	C33-32-321	107.7
C2-14-15	112.7(3)	C26-27-273	108.1	C31-32-322	109.9
S4-14-15	113.1(3)	H271-27-273	109.5	C33-32-322	114.7
C15-16-21	110.0(4)	H272-27-273	109.5	H321-32-322	109.5
C15-16-17	130.3(5)	C27-26-25	113.0(5)	C29-28-281	107.8
C21-16-17	119.7(4)	C27-26-261	107.7	C1-28-282	108.6
C1-22-23	114.3(3)	C25-26-261	108.6	C29-28-282	108.1
C1-22-221	108.7	C27-26-262	109.3	H281-28-282	109.5
C23-22-221	107.8	C25-26-262	108.8	C19-18-181	118.7
C1-22-222	108.6	H261-26-262	109.5	C17-18-181	119.4
C23-22-222	107.8	C21-20-19	116.0(6)	C10-11-12	122.1(5)
H221-22-222	109.5	C21-20-201	121.8	C10-11-111	118.8
C1-28-29	114.3(3)	C19-20-201	122.2		
C1-28-281	108.5	C19-18-17	122.0(7)		

List of Publications

Publications

- **Gao, P.**; Cho, D.; Enkelmann, V.; Baumgarten, M.; Müllen, K. Conjugated Heteroheptacenes: Influence of the substituents on solid structures (IV) (In preparation)
- **Gao, P.**; Enkelmann, V.; Baumgarten, M.; Müllen, K. Synthesis of π-extended sulfur containing heteroacenes via sulfur extrution (In preparation)
- **Gao, P.**; Zhou, G.; Enkelmann, V.; Baumgarten, M.; Müllen, K. Conjugated Heteroheptacenes Bearing Thiophene and/or Pyrrole Rings (III) (In preparation)
- **Gao, P.**; Cho, D.; Yang, X. Y.; Enkelmann, V.; Baumgarten, M.; Müllen, K. Conjugated Ladder-Type Heteroheptacenes Bearing Thiophene and/or Pyrrole Rings (II) *Chemistry A European Journal*. (In preparation)
- **Gao, P.**; Beckmann, D.; Tsao, H. N.; Feng, X. L.; Enkelmann, V.; Pisula, W.; Müllen, K. Dithieno[2,3-*d*;2',3'-*d*']benzo[1,2-*b*;4,5-*b*']dithiophene (DTBDT) as semiconductor for high-performance, solution-processed organic field-effect transistors. *Advanced Materials.* **2009**, *21*, 213-216.
- **Gao, P.**; Feng, X. L; Yang, X. Y.; Enkelmann, V.; Baumgarten, M.; Müllen, K. Conjugated Ladder-Type Heteroacenes Bearing Pyrrole and Thiophene Ring Units: Facile Synthesis and Characterization. *Journal of Organic Chemistry*. **2008**, *73*, 9207-9213. (Featured Artical)
- **Gao, P.**; Beckmann, D.; Tsao, H. N.; Feng, X. L.; Enkelmann, V.; Pisula, W.; Müllen, K., Benzo[1,2-*b*:4,5-*b*']bis[*b*]benzothiophene as solution processible organic semiconductor for field-effect transistors. *Chemical Communications*. **2008**, *13*, 1548-1550.
- **Gao, P.**; Guo, X. X.; Xu, H. J.; Fang, J. H. Recent research development of fluorine-free sulfonated polymer proton exchange membrane for fuel cell. *Gaofenzi Tongbao* **2007**, *4*, 1-13.
- **Gao, P.**; Guo, X. X.; Xu, H. J.; Fang, J. H. Recent progress in development of sulfonated hydrocarbon polymers for fuel cell application (II). *Gaofenzi Tongbao* **2007**, *5*, 12-22.

Patents

- Klaus Müllen, **Peng Gao**, Dirk Beckmann, Dr. Hoi Nok Tsao, Xinliang Feng. High performance solution processable semiconductor based on Dithieno[2,3-*d*:2′,3′-*d*']benzo(1,2-*b*:4,5-*b*′)]dithiophene. Germany Patent. Apply Nr. AE20080382/MWa.